VORONOÏ'S IMPACT ON MODERN SCIENCE

Proceedings
of the Sixth International Conference
on Analytic Number Theory
and Spatial Tessellations

Volume 2

Dragomanov Ukrainian State University

VORONOÏ'S IMPACT ON MODERN SCIENCE

Proceedings
of the Sixth International Conference
on Analytic Number Theory
and Spatial Tessellations

In two volumes
Volume 2

Edited by Mykola Pratsiovytyi and Dmytro Karvatskyi
Compiled by Halyna Syta

Dragomanov Ukrainian State University Publ.
Kyiv ∘ 2025

UDC 511.32, 511.33, 511.41, 511.48, 511.52, 517.521.8
MSC2010 05C50, 05C82, 05C85, 11A67, 11J68, 11M732, 11M41, 14J20, 14G22, 14Q15, 26A30, 28A80, 51E24, 51M15, 52B55, 52C10, 60D20, 65D18, 65D99, 68Q25, 68U05, 68W30, 90C27

Voronoï's Impact on Modern Science. Proceedings of the Sixth International Conference on Analytic Number Theory and Spatial Tessellations : In two volumes / Mykola Pratsiovytyi and Dmytro Karvatskyi (Eds.) ; Halyna Syta (Compil.) ; Dragomanov Ukrainian State University — Kyiv : Dragomanov Ukrainian State University Publ., 2025. — Vol. 2. — xvi+219 p.

The papers in this book comprise the Part 2 of the Proceedings of the Sixth International Conference on Analytic Number Theory and Spatial Tessellations held in Kyiv (Ukraine) on September 24–28, 2018.

Affirmed to publication by the Scientific Council
of the Dragomanov Ukrainian State University
Minutes No. 13 of May 29, 2025

Вплив Вороного на сучасну науку. Праці Шостої міжнародної конференції з аналітичної теорії чисел і просторових мозаїк : У двох томах / Ред. : Микола Працьовитий, Дмитро Карвацький ; упоряд. Галина Сита ; Нац. пед. ун-т ім. М. П. Драгоманова. — Київ : Вид-во Нац. пед. ун-ту ім. М. П. Драгоманова, 2025. — Т. 2. — xvi+219 с.

Статті цієї книги складають другу частину праць Шостої міжнародної конференції з аналітичної теорії чисел і просторових мозаїк, що відбулася в Києві (Україна) з 24 по 28 вересня 2018 року.

Схвалено для публікації Вченою радою
Українського державного університету імені Михайла Драгоманова
протокол № 13 від 29 травня 2025 р.

ISBN 978-966-931-197-9
ISBN 978-966-931-333-1 (Vol. 2)

© Dragomanov Ukrainian State University, 2025

Contents

The Anniversary of Georgy Voronoï vii

Welcome Addresses ix

Conference Organization Structure xiii

Plenary Session 1

1 The Hausdorff dimension of sets of numbers defined by their Q-Cantor series expansions
Dylan Airey, Bill Mance

5 Recent developments on generalized Voronoi diagrams and their use in homotopy continuation
Francesc Antón Castro, Anthony Sebastian Ramos Cisneros, Fernando Patricio Zhapa Camacho, Oscar Vicente Guarnizo Cabezas

21 Zeta-functions and dimensions of a class of discrete self-affine subsets of $\mathbb{R}^2$.
Driss Essouabri

41 Correlations in a random universe
Vincent Icke

58 Computing optimal distance based clique relaxations in unit disk graphs
Sera Kahruman Anderoglu, Sergiy Butenko

69 Molecular geometry and its operating system: an emerging application of Voronoi diagrams
Deok-Soo Kim

71 Advantages of arc spline representations for various applications in computational geometry
Bastian Weiß

Section Voronoi Diagrams. Theoretical Aspects and Applications 87

87 Preface
Vasyl Tereshchenko

89 The dgeConflict predicate in the 3D Apollonius diagram
Manos Kamarianakis

108 Voronoi-based skeleton for segmenting the network of biological neurons
Dmytro Kotsur, Vasyl Tereshchenko

122 Topological characteristics of disordered carbon
Alexander Rud, Inna Kirian, Andrii Lakhnik

126 Voronoï random packing
Masaharu Tanemura

138 On small world Non-Sunada twins and cellular Voronoi diagrams
Vasyl Ustimenko

164 Voronoi congruences for Bernoulli numbers, Leopoldt's zeta functions and generalizations
Nikolaj Glazunov

Section Fractal Analysis and Fractal Geometry **185**

185 Preface
Dmytro Karvatskyi

186 A construction of real functions defined with quantities of digits occurrences in the Argument Representation
Oleksii Panasenko, Tetiana Kyrylaschuk

191 Evenly distributed sequences generated by shear transformations in a class $\boldsymbol{Q}_{\boldsymbol{s}}^{*}$-submit
Mykola Pratsiovytyi, Rostyslav Kryvoshyia, Oleg Makarchuk

199 Structural and self-similar properties of representations of one class of fractal functions and distributions of their values
Mykola Pratsiovytyi, Sofiia Ratushniak

208 Scale-invariant functions given by continued A_2-representation of numbers
Mykola Pratsiovytyi, Sofiia Ratushniak, Oxana Trebenko, Serhii Dmytrenko

Author Index **219**

The Anniversary of Georgy Voronoï

In this collection, the papers of participants of the Sixth International Conference on Analytic Number Theory and Spatial Tessellations are compiled.

This conference, like the previous five ones, was devoted to the development and generalization of the scientific heritage of Georgy Voronoï (1868–1908), a scientist whose mathematical achievements were highly appreciated by his contemporaries, but they have been widely used in our days.

Such conferences take place in Kyiv (once in five years), because G. Voronoï was a Ukrainian by origin, his motherland was here, he was buried here according to his last will, his archive is kept in the Institute of Manuscripts of the Vernadsky National Library of Ukraine. This idea was supported by our foreign participants in 1993.

April 28, 2018 was the 150th anniversary of Georgy Voronoï. In Ukraine, this event was celebrated at the national level (in accordance to the Resolution of the Verkhovna Rada (Parliament) of Ukraine "On Celebration of Memorial Dates and Anniversaries in 2018" No. 2287-VIII of February 8, 2018). A series of events devoted to this date were organized by the National Pedagogical Dragomanov University, National Academy of Sciences of Ukraine, Kyiv Mathematical Society, Shevchenko Scientific Society and others.

The Sixth International Conference on Analytic Number Theory and Spatial Tessellations was held at the Faculty of Physics and Mathematics of the National Pedagogical Dragomanov University on September 24–28, 2018. The conference was organized jointly with the Institute of Mathematics of the National Academy of Sciences of Ukraine; Taras Shevchenko National University of Kyiv; Ukrainian International Committee of Science and Culture, NAS of Ukraine; Voronoi Diagram Research Center, Hanyang University (Seoul, Korea); Institute of Mathematics of the Polish Academy of Sciences (Warsaw, Poland).

Over 70 scientists from 18 countries of the world (Austria, Belarus, Ecuador, France, Germany, Greece, Hungary, Japan, Korea, Lithuania, the Netherlands, Poland, Spain, Sweden, Thailand, Turkey, Ukraine, United States of America) participated in the conference.

During the conference, 14 plenary lectures were delivered by Francesc Antón Castro (Ecuador), Rikard Bøgvad (Sweden), Sergiy Butenko (United States of America), Driss Essouabri (France), Vincent Icke (the Netherlands), Deok-Soo Kim (Korea), Vichian Laohakosol (Thailand),

William Mance (Poland), Bogdana Oliynyk (Ukraine), Mykola Pratsiovytyi (Ukraine), Jörn Steuding (Germany), Grygoriy Torbin (Ukraine), László Tóth (Hungary), Bastian Weiß (Austria).

The conference talks were related to research interests of Georgy Voronoï mainly. The following four sections worked at the conference:

1. Number Theory,
2. Analysis,
3. Voronoi Diagrams (Theoretical Aspects and Applications),
4. Fractal Analysis and Fractal Geometry.

The following honored guests visited the opening ceremony of the conference: First Deputy Minister of Education and Science of Ukraine Volodymyr Kovtunets, Ambassador of the Republic of Korea to Ukraine Yang-Goo Lee, Head of Section for Cooperation in Science and Education at the Embassy of the Republic of Poland in Ukraine Emilia Jasiuk, Georgy Voronoï's great-granddaughters Maryna Kosenko (Kyiv) and Irina Voronaya (Vitebsk, Belarus).

The welcome addresses were sent to the organizers and participants of the conference by First Deputy Chair of the Committee on Science and Education of the Verkhovna Rada of Ukraine Oleksandr Spivakovsky and Director of the Section of Mathematical, Physical, and Technical Sciences of the Shevchenko Scientific Society in America Roman Brukh.

The working languages of the conference were English and Ukrainian. Most of the lectures were delivered in English.

On September 26, participants of the conference had a trip to Zhuravka in Chernihiv region, the native village of Voronoï. They held a memorial service on the grave of Georgy and Theodosiy Voronoïs and visited the school local lore museum.

November 2018

Professor Mykola Pratsiovytyi
Editor of the volume,
Chair of the Organizing Committee

Вітання від Верховної Ради

21 вересня 2018 року

Від імені Комітету з питань науки і освіти, а також від себе особисто вітаю учасників Шостої міжнародної конференції з аналітичної теорії чисел і просторових мозаїк, присвяченої 150-річному ювілею вченого-математика світового рівня Георгія Феодосійовича Вороного, українця з походження!

Георгій Вороний займає одне з почесних місць в історії математичної науки в світі, саме тому його ім'я увійшло до ювілейного календаря, затвердженого Постановою Верховної Ради України «Про відзначення пам'ятних дат і ювілеїв у 2018 році» № 2287-VIII від 8 лютого 2018 р.

Працюючи в області теорії чисел, Георгій Вороний своїми науковими працями заснував і розвинув основні напрямки досліджень в цій царині науки: аналітичну теорію чисел, алгебраїчну теорію чисел, став одним із засновників нової галузі знань — геометрії чисел. «Діаграми Вороного» — об'єкти, названі його ім'ям, дали поштовх для численних застосувань в різноманітних напрямках науки і практики: від молекулярної біології до космосу, у комп'ютерній графіці, у проблемах розпізнавання образів, штучного інтелекту тощо.

Той факт, що міжнародна конференція, присвячена розвитку наукових досягнень Вороного, проходить у Києві (а це вже шоста київська конференція) та поєднується з подорожжю до малої батьківщини Георгія Вороного і місця його поховання — села Журавка на Чернігівщині, додає вагомості вкладу українських вчених до світової наукової скарбниці, піднімає науковий рейтинг нашої країни у світі, що є важливим моментом у час становлення державності.

Коли ми говоримо про великих вчених, яких вже немає з нами, ми звертаємо особливу увагу на результати їхніх наукових розробок в довгостроковій перспективі. Пройшло вже 110 років з того часу, як професор Вороний помер у віці 40 років, але великі вчені і їхні наукові досягнення залишаються в колективній пам'яті, з цієї причини його ім'я буде тривати вічно в історії математики і природничих наук в цілому.

Маю надію, що наукова конференція, яка розпочинається тут, у Києві, 24 вересня, буде успішною і приверне пильну увагу не тільки з боку самих учасників зібрання, але і широкої громадськості.

З повагою

народний депутат Олександр Співаковський,
перший заступник голови Комітету Верховної Ради України
з питань науки і освіти

Welcome Address by the Parliament

September 21, 2018

On behalf of the Committee on Science and Education and on my own behalf, let me welcome the participants of the Sixth International Conference on Analytic Number Theory and Spatial Tessellations dedicated to the 150th anniversary of the prominent mathematician, Georgy Feodosiyovych Voronoï, a Ukrainian by origin!

G. Voronoï occupies one of the notable places in the history of mathematics in the world, and his name is in the calendar of celebrations approved by the Resolution of the Verkhovna Rada of Ukraine "On Celebration of Memorial Dates and Anniversaries in 2018" No. 2287-VIII of February 8, 2018.

Georgy Voronoï worked in the field of number theory. In his scientific works, he founded and developed the main directions of research in this field of science: the analytic number theory, the algebraic number theory, and became one of the founders of a new field of knowledge – the geometry of numbers. "Voronoi diagrams" are the objects named after him. They gave impetus to numerous applications in a variety of fields of science and practice, from molecular biology to cosmos, in computer graphics, in problems of pattern recognition, artificial intelligence, and so on.

This international conference devoted to the development of scientific achievements of Voronoï is taking place in Kyiv (this is the sixth Kyiv conference) and is combined with a trip to the small homeland of Georgy Voronoï and his burial place (it is the village Zhuravka in Chernihiv region). This fact adds value to the contribution of Ukrainian scholars to the world scientific treasure, raises scientific rating of our country in the world, which is an important moment for our state formation.

When we talk about the great scientists that are not already with us, we pay special attention to the results of their scientific developments in the long-term perspective. 110 years have passed since Professor Voronoï died at the age of 40, but great scholars and their scientific achievements remain in collective memory. For this reason, his name will last forever in the history of mathematics and the natural sciences as a whole.

I hope that the scientific conference opening here, in Kyiv, on September 24, will be successful and will attract attention not only of the participants of the meeting itself, but also of the wide public.

Sincerely,

Member of Parliament Oleksandr Spivakovskyi
First Deputy Chair of the Committee on Science and Education
of the Verkhovna Rada of Ukraine

Вітання від Наукового товариства ім. Шевченка в Америці (НТШ-А)

22 вересня 2018 року

Наукове товариство імені Шевченка в Америці, а особливо члени Математично-фізично-технічної секції НТШ-А, складають щирий привіт організаторам та учасникам Шостої міжнародної конференції з аналітичної теорії чисел та просторових мозаїк, що проходитиме 24–28 вересня 2018 року в Києві. Ми дуже раді, що ця конференція присвячена 150-річчю відомого українського математика Георгія Вороного.

Праці Г. Вороного відрізняються ретельністю та винятковою глибиною викладу. Майже кожна з них послужила основою і натхненням для розвитку нових напрямків наукових досліджень, що призводять до нових досягнень.

Ім'я Георгія Вороного відоме фахівцям усього світу, а його наукові роботи широко використовуються в багатьох галузях науки і прикладних дослідженнях. Крім того, ми пишаємося його українським походженням і хочемо поділитися цим з міжнародною спільнотою.

Ми віримо, що ця конференція зробить значний внесок у розвиток математики, посилення зв'язків у міжнародній математичній спільноті та поширення знань про Георгія Вороного як видатного математика, якого породила та дала світові Українська Земля.

Від імені Наукового товариства ім. Шевченка в Америці бажаю великих успіхів у роботі конференції.

Зі щирою повагою

д-р Роман Брух,
директор Секції математичних, фізичних та технічних наук
НТШ-А

Welcome Address by the Shevchenko Scientific Society in America (NTSh-A)

September 22, 2018

The Shevchenko Scientific Society in America and the members of the Mathematical, Physical, and Technical Section of the NTSh-A wish to extend a hearty congratulations to the organizers and participants of the Sixth International Conference on Analytic Number Theory and Spatial Tessellations, which will take place on September 24–28, 2018 in Kyiv. We are delighted that the conference is dedicated to the 150th anniversary of the renowned Ukrainian mathematician, Georgy Voronoï.

The works of Georgy Voronoï are revered because of their complexity and their tremendous scope. His work has also served as a foundation and inspiration for the development of new directions in scientific research leading to new advances.

Georgy Voronoï's reputation is known to professionals around the world, and his scientific works are widely used in many fields of science and applied research. Additionally, we are proud of his Ukrainian heritage, which we want to share with the international community.

We believe that this conference will make significant contributions to the development of mathematics, the strengthening of connections in the international mathematical community, and the dissemination of knowledge about Georgy Voronoï as an outstanding Ukrainian mathematician.

On behalf of the members of the Shevchenko Scientific Society in America, I wish the conference great success.

My sincerest regards,

Dr. Roman Brukh
Director of the Section of Mathematical, Physical, and Technical Sciences of NTSh-A

Conference Organization Structure

International Program Committee

Section of Pure Mathematics

Jean-Daniel Boissonnat	INRIA, France
Liliya Boytsun	Oles Honchar Dnipro National University, Ukraine
Johannes Buchmann	Technische Universität Darmstadt, Germany
Karma Dajani	Utrecht University, the Netherlands
Yuriy Drozd	Institute of Mathematics NAS of Ukraine, Ukraine
Driss Essouabri	Université Jean Monnet, France
Aleksandar Ivić	University of Belgrade, Serbia
Matti Jutila	University of Turku, Finland
Shigeru Kanemitsu	Kindai University, Japan
Khrystyna Kuchminska	Pidstryhach Institute for Applied Problems in Mechanics and Mathematics NAS of Ukraine, Ukraine
Vichian Laohakosol	Kasetsart University, Thailand
Antanas Laurinčikas	Vilnius University, Lithuania
Kohji Matsumoto	Nagoya University, Japan
Štefan Porubský	Institute of Computer Science of Academy of Sciences of the Czech Republic, Czech Republic
Mykola Pratsiovytyi	National Pedagogical Dragomanov University, Ukraine
Andrzej Schinzel	Institute of Mathematics PAN, Poland
Jörn Steuding	University of Würzburg, Germany
Jörg Thuswaldner	Montanuniversität Leoben, Austria
Robert Tichy	Technische Universität Graz, Austria
Grygoriy Torbin	National Pedagogical Dragomanov University, Ukraine
László Tóth	University of Pécs, Hungary
Pavel Varbanets	Mechnikov National University, Odesa, Ukraine

Section of Voronoi Diagrams

Franz Aurenhammer	Technische Universität Graz, Austria
Sergiy Butenko	Texas A&M University, USA
Sung Nok Chiu	Hong Kong Baptist University, Hong Kong
Christopher Gold	University of Glamorgan, UK

Bert Jüttler	Johannes Kepler Universität Linz, Austria
Deok-Soo Kim	Voronoi Diagram Research Center, Hanyang University, Korea
Igor Kovalenko	Institute of Cybernetics NAS of Ukraine, Ukraine
Ihor Mryglod	Institute for Condensed Matter Physics NAS of Ukraine, Ukraine
Atsuyuki Okabe	University of Tokyo, Japan
Evanthia Papadopoulou	Università della Svizzera italiana, Switzerland
Marjorie Senechal	Smith College, USA
Masaharu Tanemura	Institute of Statistical Mathematics, Tokyo, Japan
Vasyl Tereshchenko	Taras Shevchenko National University of Kyiv, Ukraine
Rien van de Weygaert	University of Groningen, the Netherlands
Yaroslav Yatskiv	Main Astronomical Observatory NAS of Ukraine, Ukraine
Ihor Yukhnovskii	Institute for Condensed Matter Physics NAS of Ukraine, Ukraine

Organizing Committee

Mykola Pratsiovytyi, Chair	National Pedagogical Dragomanov University
Halyna Syta, Secretary	National Pedagogical Dragomanov University
Oleksandr Baranovskyi	Institute of Mathematics NAS of Ukraine
Olga Bondarenko	National Pedagogical Dragomanov University
Yanina Goncharenko	National Pedagogical Dragomanov University
Tetiana Gulak	National Pedagogical Dragomanov University
Yevheniia Kalashnikova	National Pedagogical Dragomanov University
Vita Markitan	National Pedagogical Dragomanov University
Roman Nikiforov	National Pedagogical Dragomanov University
Roman Osaulenko	Institute of Mathematics NAS of Ukraine
Sofiia Ratushniak	Institute of Mathematics NAS of Ukraine
Ihor Savchenko	National Pedagogical Dragomanov University
Grygoriy Torbin	National Pedagogical Dragomanov University
Svitlana Vaskevych	Institute of Mathematics NAS of Ukraine
Natalya Vasylenko	Institute of Mathematics NAS of Ukraine
Irina Yehorchenko	Institute of Mathematics NAS of Ukraine

Conference Venue. The Sixth International Conference on Analytic Number Theory and Spatial Tessellations took place in Kyiv (Ukraine) on September 24–28. The sessions of the conference were held at the National Pedagogical Dragomanov University (9 Pyrohova St., Kyiv). On September 26, the participants of the conference had a small trip to the village Zhuravka, the place where Georgy Voronoï was born and where according to his last will, he was buried.

Our Sponsors and Supporters.



Voronoi Diagram Research Center, Hanyang University, Seoul, Korea



Ministry of Education and Science of Ukraine

The Organizing Committee of the Conference expresses the sincere gratitude to our sponsors. The organization of the conference would not have been possible without their funding and support.

We also would like to express the deep gratitude to Professor Jörn Steuding (University of Würzburg, Germany) and to Professor Deok-Soo Kim (Voronoi Diagram Research Center, Hanyang University, Seoul, Korea) for the large work during the conference preparation and to all the experts who reviewed the papers of the book.

Organizing Committee of the Conference

* * * * * * * * * * * * * * *

Note, that a reader can find here two spellings of the G. Voronoï's name: Voronoï and Voronoi. This established historically.

G. Voronoï himself used his name in such writing: Voronoï, so his followers in Pure Mathematics usually use his name in the author's spelling. But the term "Voronoi diagram" is used with the letter "i" at the end, and the experts in Voronoi diagrams applications hold on this spelling.

Voronoï's Impact on Modern Science, Book 6, Volume 2
Proceedings of the Sixth International Conference on Analytic Number Theory and Spatial Tessellations

THE HAUSDORFF DIMENSION OF SETS OF NUMBERS DEFINED BY THEIR Q-CANTOR SERIES EXPANSIONS

Dylan Airey (*USA*) and Bill Mance (*Poland*)

The study of normal numbers and other statistical properties of real numbers with respect to large classes of Cantor series expansions was first done by P. Erdős and A. Rényi in [3] and [4] and by A. Rényi in [9], [10], and [11] and by P. Turán in [12].

Denote by $N_n^b(B, x)$ the number of times a block B occurs with its starting position no greater than n in the b-ary expansion of x.

Definition 0.1. A real number x is *normal in base* b if for all k and blocks B in base b of length k, one has

$$\lim_{n\to\infty} \frac{N_n^b(B,x)}{n} = b^{-k}. \tag{0.1}$$

A number x is *simply normal in base* b if (0.1) holds for $k = 1$.

Borel introduced normal numbers in 1909 and proved that almost all (in the sense of Lebesgue measure) real numbers are normal in all bases. The best known example of a number that is normal in base 10 is due to Champernowne [2]. The number

$$H_{10} = 0.1\ 2\ 3\ 4\ 5\ 6\ 7\ 8\ 9\ 10\ 11\ 12\ldots,$$

formed by concatenating the digits of every natural number written in increasing order in base 10, is normal in base 10. Any H_b, formed similarly to H_{10} but in base b, is known to be normal in base b. Since then, many examples have been given of numbers that are normal in at least one base.

We wish to mention one of the most fundamental and important results relating to normal numbers in base b. The following is due to D. D. Wall in his Ph.D. dissertation [13].

Theorem 0.2 (D. D. Wall)**.** *A real number x is normal in base b if and only if the sequence $(b^n x)$ is uniformly distributed mod* 1.

The Q-Cantor series expansions, first studied by G. Cantor in [1], are a natural generalization of the b-ary expansions. G. Cantor's motivation to study the Cantor series expansions was to extend the well known proof of the irrationality of the number $e = \sum 1/n!$ to a larger class of numbers. Let $\mathbb{N}_k := \mathbb{Z} \cap [k, \infty)$. If $Q \in \mathbb{N}_2^{\mathbb{N}}$, then we say that Q is a *basic sequence*. Given a basic sequence $Q = (q_n)_{n=1}^{\infty}$, the *Q-Cantor series expansion* of a real number x is the (unique) expansion of the form

$$x = E_0 + \sum_{n=1}^{\infty} \frac{E_n}{q_1 q_2 \cdots q_n} \tag{0.2}$$

where $E_0 = \lfloor x \rfloor$ and E_n is in $\{0, 1, \ldots, q_n - 1\}$ for $n \geq 1$ with $E_n \neq q_n - 1$ infinitely often. We abbreviate (0.2) with the notation $x = E_0.E_1E_2E_3\ldots$ w.r.t. Q.

A *block* is an ordered tuple of non-negative integers, a *block of length k* is an ordered k-tuple of integers, and *block of length k in base b* is an ordered k-tuple of integers in $\{0, 1, \ldots, b-1\}$. Let $N_n^Q(B, x)$ denote the number of occurrences of the block B in the digits of the Q-Cantor series expansion of x up to position n.

Let

$$Q_n^{(k)} := \sum_{j=1}^{n} \frac{1}{q_j q_{j+1} \cdots q_{j+k-1}} \text{ and } T_{Q,n}(x) := \left(\prod_{j=1}^{n} q_j \right) x \pmod 1.$$

A. Rényi [10] defined a real number x to be *normal* with respect to Q if for all blocks B of length 1,

$$\lim_{n\to\infty} \frac{N_n^Q(B, x)}{Q_n^{(1)}} = 1. \tag{0.3}$$

If $q_n = b$ for all n and we restrict B to consist of only digits less than b, then (0.3) is equivalent to *simple normality in base b*, but not equivalent to *normality in base b*. A basic sequence Q is *k-divergent* if $\lim_{n\to\infty} Q_n^{(k)} = \infty$, *fully divergent* if Q is k-divergent for all k, and *k-convergent* if it is not k-divergent. A basic sequence Q is *infinite in limit* if $q_n \to \infty$.

Motivated by Theorem 0.2, we make the following definitions of normality for Cantor series expansions.

Definition 0.3. A real number x is *Q-normal of order k* if for all blocks B of length k,

$$\lim_{n\to\infty} \frac{N_n^Q(B, x)}{Q_n^{(k)}} = 1.$$

We let $\mathcal{N}_k(Q)$ be the set of numbers that are Q-normal of order k. The real number x is *Q-normal* if $x \in \mathcal{N}(Q) := \bigcap_{k=1}^{\infty} \mathcal{N}_k(Q)$.

Definition 0.4. A real number x is *Q-ratio normal of order k* (here we write $x \in \mathcal{RN}_k(Q)$) if for all blocks B_1 and B_2 of length k

$$\lim_{n\to\infty} \frac{N_n^Q(B_1, x)}{N_n^Q(B_2, x)} = 1.$$

We say that x is *Q-ratio normal* if $x \in \mathcal{RN}(Q) := \bigcap_{k=1}^{\infty} \mathcal{RN}_k(Q)$.

Definition 0.5. A real number x is *Q-distribution normal* if the sequence $(T_{Q,n}(x))_{n=0}^{\infty}$ is uniformly distributed mod 1. Let $\mathcal{DN}(Q)$ be the set of Q-distribution normal numbers.

We note that by Theorem 0.2, the analogous versions of the above definitions are equivalent for the b-ary expansions.

It was proven in [7] that the directed graph in Figure 1 gives the complete containment relationships between these notions when Q is infinite in limit and fully divergent. The vertices are labeled with all possible intersections of one, two, or three choices of the sets $\mathcal{N}(Q)$, $\mathcal{RN}(Q)$, and $\mathcal{DN}(Q)$, where we know that $\mathcal{N}(Q) = \mathcal{N}(Q) \cap \mathcal{RN}(Q)$ and $\mathcal{N}(Q) \cap \mathcal{DN}(Q) = \mathcal{N}(Q) \cap \mathcal{DN}(Q) \cap \mathcal{RN}(Q)$. The set labeled on vertex A is a subset of the set labeled on vertex B if and only if there is a directed path from A to B. For example, $\mathcal{N}(Q) \cap \mathcal{DN}(Q) \subseteq \mathcal{RN}(Q)$, so all numbers that are Q-normal and Q-distribution normal are also Q-ratio normal.

FIGURE 1.

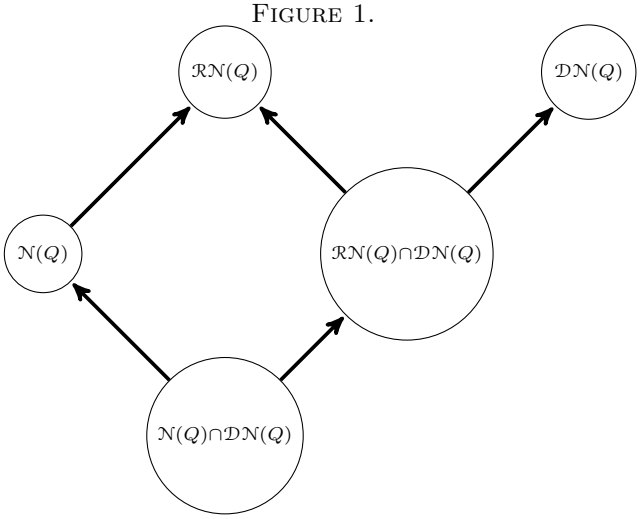

We remark that all inclusions suggested from Figure 1 are either easily proven ($\mathcal{N}(Q) \subseteq \mathcal{RN}(Q)$) or are trivial. The difficulty comes in showing a lack of inclusion. The most challenging of these is to prove that there is a basic sequence Q where $\mathcal{RN}(Q) \cap \mathcal{DN}(Q) \backslash \mathcal{N}(Q) \neq \emptyset$. Moreover, when Q is infinite in limit and fully divergent, the sets $\mathcal{N}(Q), \mathcal{RN}(Q)$, and $\mathcal{DN}(Q)$ all have full Lebesgue measure [6].

It is natural to ask for the Hausdorff dimension of the difference sets. It was proven in [8] that for every basic sequence Q that is infinite in limit

$$\dim_{\mathrm{H}} (\mathcal{DN}(Q) \backslash \mathcal{N}(Q)) = \dim_{\mathrm{H}} (\mathcal{DN}(Q) \backslash \mathcal{RN}(Q)) = 1.$$

Using different methods we will prove the following theorem.

Theorem 0.6. *Every non-empty set formed by taking the difference of two sets listed in Figure 1 has full Hausdorff dimension for every Q that is infinite in limit, except possibly the set $\mathcal{N}(Q) \setminus \mathcal{DN}(Q)$. That is, the following sets have full Hausdorff dimension for every Q that is infinite in limit*

$$\begin{array}{lll} \mathcal{N}(Q) \setminus \mathcal{DN}(Q) & \mathcal{RN}(Q) \setminus \mathcal{N}(Q) & \mathcal{RN}(Q) \setminus \mathcal{DN}(Q) \\ \mathcal{DN}(Q) \setminus \mathcal{N}(Q) & \mathcal{RN}(Q) \cap \mathcal{DN}(Q) \setminus \mathcal{N}(Q) & \mathcal{DN}(Q) \setminus \mathcal{RN}(Q) \\ & \mathcal{RN}(Q) \setminus (\mathcal{N}(Q) \cap \mathcal{DN}(Q)) & \end{array}$$

except for $\mathcal{N}(Q) \setminus \mathcal{DN}(Q)$, which has full Hausdorff dimension for a subset of those Q which are infinite in limit.

A surprising property of Q-normality of order k is that we may not conclude that $\mathcal{N}_k(Q) \subseteq \mathcal{N}_j(Q)$ for all $j < k$ like we may for the b-ary expansions. In fact, it was shown in [5] that for every k there exists a basic sequence Q and a real number x such that $\mathcal{N}_k(Q) \backslash \bigcup_{j=1}^{k-1} \mathcal{N}_j(Q)$ is non-empty. Thus, we will have to be more careful in stating exactly what our theorems prove since lack of Q-normality of order 2 does not imply lack of Q-normality of order 338, for example. Furthermore, we will greatly expand on this result by showing that for each natural number ℓ we exhibit a class of

basic sequences such that

$$\dim_{\mathrm{H}} \left(\bigcap_{j=\ell}^{\infty} \mathcal{N}_j(Q) \Big\backslash \bigcup_{j=1}^{\ell-1} \mathcal{N}_j(Q) \right) = 1.$$

References

1. G. Cantor, *Über die einfachen Zahlensysteme*, Zeitschrift für Math. und Physik **14** (1869), 121–128.
2. D. G. Champernowne, *The construction of decimals normal in the scale of ten*, Journal of the London Mathematical Society **8** (1933), 254–260.
3. P. Erdős and A. Rényi, *On Cantor's series with convergent* $\sum 1/q_n$, Annales Universitatis L. Eötvös de Budapest, Sect. Math. **2** (1959), 93–109.
4. ———, *Some further statistical properties of the digits in Cantor's series*, Acta Math. Acad. Sci. Hungar **10** (1959), 21–29.
5. B. Li and B. Mance, *Number theoretic applications of a class of Cantor series fractal functions, II*, Int. J. Number Theory **11** (2015), no. 02, 407–435.
6. B. Mance, *Typicality of normal numbers with respect to the Cantor series expansion*, New York J. Math. **17** (2011), 601–617.
7. ———, *Number theoretic applications of a class of Cantor series fractal functions, I*, Acta Math. Hungar. **144** (2014), no. 2, 449–493.
8. ———, *On the Hausdorff dimension of countable intersections of certain sets of normal numbers*, J. Théor. Nombers de Bordeaux **27** (2015), no. 1, 199–217.
9. A. Rényi, *On a new axiomatic theory of probability*, Acta Math. Acad. Sci. Hungar. **6** (1955), 329–332.
10. ———, *On the distribution of the digits in Cantor's series*, Mat. Lapok **7** (1956), 77–100.
11. ———, *Probabilistic methods in number theory*, Shuxue Jinzhan **4** (1958), 465–510.
12. P. Turán, *On the distribution of "digits" in Cantor systems*, Mat. Lapok **7** (1956), 71–76.
13. D. D. Wall, *Normal numbers*, Ph.D. thesis, Univ. of California, Berkeley, Berkeley, California, 1949.

The paper in full form with all the proofs of the statements is already published. See: D. Airey and B. Mance, *The Hausdorff dimension of sets of numbers defined by their Q-Cantor series expansions,* J. Fractal Geom. **3** (2016), no. 2, 163–186.

(Dylan Airey) Department of Mathematics, Princeton University, Fine Hall, Washington Road, Princeton, NJ 08544-1000, USA
Email: dairey(at)math(dot)princeton(dot)edu

(Bill Mance) Uniwersytet im. Adama Mickiewicza w Poznaniu, Collegium Mathematicum, ul. Umultowska 87, 61-614 Poznań, Poland
Email: william(dot)mance(at)amu(dot)edu(dot)pl

Voronoï's Impact on Modern Science, Book 6, Volume 2
Proceedings of the Sixth International Conference on Analytic Number Theory and Spatial Tessellations

RECENT DEVELOPMENTS ON GENERALIZED VORONOI DIAGRAMS AND THEIR APPLICATIONS IN HOMOTOPY CONTINUATION

Francesc Antón Castro, Anthony Sebastian Ramos Cisneros,
Fernando Patricio Zhapa Camacho,
and Oscar Vicente Guarnizo Cabezas (*Ecuador*)

Abstract. In this paper, we will present our ongoing work on the generalized offset of quadrics and their application to homotopy continuation using barycentric coordinates. The formulation of the loci involved in the computation of these generalized offsets is done by applying algebraic techniques (Wu's algorithm) in order to determine automatically (or mechanically) all the geometric, geometric topology and topological invariants involved in the computation of these generalized offsets. Finally, we will present our work on the application of generalized offsets of quadrics to homotopy continuation.

Introduction

Voronoi diagrams have been a central topic in research in computational geometry since their inception [12, 9, 6, 7, 15], and they have many applications in different scientific and engineering disciplines [19, 24, 16]. However, generalized Voronoi diagrams, and especially the Voronoi diagram of quadrics have not been explored sufficiently [18]. With applications in biology and geodesy, Voronoi diagrams of quadrics (especially of ellipsoids) are important for representing and analysing the 3D positioning and trajectories of planets and the molecular 3D structure and surface [25] of proteins [17], etc.

Research works have concentrated on the easiest quadrics (spheres). Gavrilova provided an early work on generalised Voronoi diagrams in her doctoral thesis [11] and subsequent work by Gavrilova and Rokne

Received January 20, 2020.
2010 *Mathematics Subject Classification.* Primary 14Q15; Secondary 51M15, 65H20.
Key words and phrases. Generalized offsets of quadrics, geometric invariants, topological invariants, Ritt-Wu's characteristic set method, homotopy continuation, natural neighbor interpolation.

on topology updating of the kinematic Voronoi diagram of hyperspheres [10]. Nishida and Sugihara [22] and Nishida et al. [23] extended the results of Gavrilova and Rokne [10] by providing the topological structure of the Voronoi diagram of hyperspheres in $d-$dimensional space using finite precision arithmetic (double).

The use of generalized Voronoi diagrams in the so-called natural neighor coordinates and interpolation has been limited to sites being points, points and straight line segments and points and open oriented straight line segments [2]. In this paper, we extend the use of generalized Voronoi diagrams in natural neighbor coordinates and interpolation using homotopy continuation to quadrics.

For this purpose, we are also addressing the geometric and topological invariants that arise in the exact computation of the generalized offset (the smallest algebraic surface that is a super-set of the true semi-algebraic offset) of a quadric using Ritt-Wu's algorithm rather than Gröbner bases, because the complexity of Ritt-Wu's algorithm is simply exponential [20], while the complexity of Gröbner bases is doubly exponential. To this extent, our main contribution is a methodology for automated derivation of geometric and topological invariants of the generalized offset using Wu's algortihm.

The exact knowledge of the generalized offset of a quadric may sound like a purely theoretical knowledge, but in fact, it is central in astronomy, where the closest mathematical surface to a planet is the ellipsoid and the trajectories of the planets according to Kepler laws is also an ellipsoid. Finally, the exact computation of the generalized offset of quadrics participates to the recent move in the development of numerical and simulation software as well as computer algebra systems to exact systems [8].

This paper is organised as follows. In Section 1, we review the preliminaries: the generalized offset of quadrics, the generalized bisector of quadrics, the Dealaunay graph of quadrics and its empty Delaunay circumsphere criterion for quadrics, the natural neighbor coordinates and interpolation and the homotopy continuation. In Section 2, we present Wu's method. In Section 3, we present a novel method of computation of the topological and geometric invariants of the generalized offset of quadrics using Wu's method and its use in the exact Delaunay empty circumsphere criterion. Section 4 is devoted to the application of the

generalized Voronoi diagrams to homotopy continuation through functions on quadrics. Finally, in Section 5, we conclude the paper.

1. Preliminaries

1.1. **Voronoi diagrams and Delaunay graphs.** Voronoi diagrams are irregular tessellations of space, where space is continuous and structured by discrete objects [24]. The Voronoi tessellation of a set of sites is a decomposition of the space into proximal regions (one for each site). Sites were points for the first historical Voronoi diagrams [27, 28, 29], but in this paper we will explore sets of hyperspheres in $\mathbb{R}^N$. The proximal region corresponding to one site (i.e. its Voronoi region) is the set of points of the space that are closer to that site than to any other site of the set of sites [24]. We will recall now the formal definitions of the Voronoi diagram and of the Delaunay graph. For this purpose, we need to recall some basic definitions.

Definition 1. (Metric) Let M be an arbitrary set. A *metric* on M is a mapping $\mathrm{d} : M \times M \to \mathbb{R}_+$ such that for any elements a, b, and c of M, the following conditions are fulfilled: $\mathrm{d}(a,b) = 0 \Leftrightarrow a = b$, $\mathrm{d}(a,b) = \mathrm{d}(b,a)$, and $\mathrm{d}(a,c) \leq \mathrm{d}(a,b) + \mathrm{d}(b,c)$. (M, d) is then called a *metric space*, and $\mathrm{d}(a,b)$ is the distance between a and b.

Let $M = \mathbb{R}^N$, and δ denote a distance between points. Let $\mathcal{S} = \{s_1, ..., s_m\}, m \geq 2$ be a set of m different subsets of M, which we call *sites*. The distance between a point x and a site $s_i \in \mathcal{S}$ is defined as $d(x, s_i) = \inf_{y \in s_i} \{\delta(x,y)\}$.

Definition 2. (Bisector) For $s_i, s_j \in \mathcal{S}, s_i \neq s_j$, the *bisector* $\mathrm{B}(s_i, s_j)$ of s_i with respect to s_j is: $\mathrm{B}(s_i, s_j) = \{x \in M | d(x, s_i) = d(x, s_j)\}$.

Definition 3. (Influence zone) For $s_i, s_j \in \mathcal{S}, s_i \neq s_j$, the *influence zone* $\mathrm{D}(s_i, s_j)$ of s_i with respect to s_j is: $\mathrm{D}(s_i, s_j) = \{x \in M | d(x, s_i) < d(x, s_j)\}$.

Definition 4. (Voronoi region) The *Voronoi region* $\mathrm{V}(s_i, \mathcal{S})$ of $s_i \in \mathcal{S}$ with respect to the set $\mathcal{S}$ is: $\mathrm{V}(s_i, \mathcal{S}) = \bigcap_{s_j \in \mathcal{S}, s_j \neq s_i} \mathrm{D}(s_i, s_j)$.

Definition 5. (Voronoi diagram) The *Voronoi diagram* of $\mathcal{S}$ is the union $\mathrm{V}(\mathcal{S}) = \bigcup_{s_i \in \mathcal{S}} \partial \mathrm{V}(s_i, \mathcal{S})$ of all region boundaries.

Definition 6. (Delaunay graph) The *Delaunay graph* $\mathrm{DG}(\mathcal{S})$ of $\mathcal{S}$ is the dual graph of $\mathrm{V}(\mathcal{S})$ defined as follows:

- the set of vertices of $\mathrm{DG}(\mathcal{S})$ is $\mathcal{S}$,
- for each $(N-1)-$dimensional facet of $\mathrm{V}(\mathcal{S})$ that belongs to the common boundary of $\mathrm{V}(s_i, \mathcal{S})$ and of $\mathrm{V}(s_j, \mathcal{S})$ with $s_i, s_j \in \mathcal{S}$ and $s_i \neq s_j$, there is an edge of $\mathrm{DG}(\mathcal{S})$ between s_i and s_j and reciprocally,
- for each vertex of $\mathrm{V}(\mathcal{S})$ that belongs to the common boundary of $\mathrm{V}(s_{i_1}, \mathcal{S}), \ldots, \mathrm{V}\left(s_{i_{N+2}}, \mathcal{S}\right)$, with $\forall k \in \{1, ..., N+2\}, s_{i_k} \in \mathcal{S}$ all distinct, there exists a complete graph K_{N+2} between the $s_{i_k}, k \in \{1, ..., N+2\}$, and reciprocally.

The Delaunay graph satisfies the Delaunay empty circumsphere criterion: since a Voronoi vertex has at least $N+1$ nearest neighbors, it must be the center of an hypersphere, that is tangent to its nearest neighboring quadrics, and whose interior does not contain any point of any nearest neighboring quadrics. Notice that the Delaunay empty circumsphere might be externally tangent to all the neighboring quadrics or internally tangent to all the neighboring quadrics or internally tangent to some of them and externally tangent to the other nearest neighbors.

1.2. **Homotopy continuation.** Homotopy is concerned with identification of paths between objects that can be continuously deformed into each other. The history of study of homotopy dates back in the late 1920's when the the homotopy theory was formalized.

Definition 7. Let $f : X \to Y$ and $g : X \to Y$ be two continuous maps between topological spaces X and Y. These maps are called *homotopic*, $f \simeq g$, if there is a *homotopy* or a continuous map $\mathcal{H} : X \times [0,1] \to Y$ between them, such that $\mathcal{H}(x,0) = f(x)$ and $\mathcal{H}(x,1) = g(x)$ for all $x \in X$.

Therefore, we can write the homotopy $\mathcal{H}_\lambda : X \to Y$ as

$$\mathcal{H}_\lambda(x) = \mathcal{H}(x, \lambda), \tag{1}$$

and thus, $\mathcal{H}_0 = f$ and $\mathcal{H}_1 = g$. One can visualize how the deformation h continuously takes f to g (see Fig. 1) by varying the parameter λ.

One can impose additional constraints on the deformation path. For example, a specific constraint on fixed endpoints leads to homotopy of paths. For two pairs of homotopic maps $X \underset{f \simeq g}{\longrightarrow} Y \underset{\bar{f} \simeq \bar{g}}{\longrightarrow} Z$, the compositions $\bar{f} \circ f$ and $\bar{g} \circ g$ are also homotopic via the composition $\bar{\mathcal{H}}_\lambda \circ \mathcal{H}_\lambda$. Further, for two pairs of homotopic maps $f_i \simeq g_i : X_i \to Y_i, i = 1, 2$, the maps $f_1 \times f_2$ and $g_1 \times g_2$ from $X_1 \times X_2$ into $Y_1 \times Y_2$ are also homotopic via $\mathcal{H}_\lambda^{(1)} \times \mathcal{H}_\lambda^{(2)}$, in which case it is called a *product homotopy* [14].

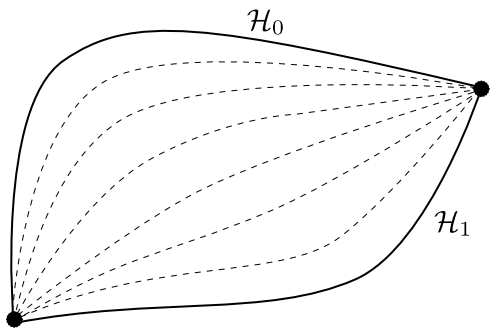

FIGURE 1. Continuous deformation.

Continuous deformations have been successfully used to solve non-linear system of equations that are otherwise hard to solve. A homotopy tries to solve a difficult problem with unknown solutions by starting with a simple problem with known solutions. Stable predictor-corrector and piecewise-linear methods for solving such problems exist (see Allgower and Georg [1]). The system $\mathcal{H}(x, \lambda) = 0$ implicitly defines a curve or 1-manifold of solution points as λ varies in $[0, 1]$ and x is fixed.

Given smooth $\mathcal{H}$ and existence of $u_0 \in \mathbb{R}^{N+1}$ such that $\mathcal{H}(u_0) = 0$ and $\text{rank}(\mathcal{H}'(u_0)) = N$, there exists a smooth curve $c : \alpha \in J \mapsto c(\alpha) \in \mathbb{R}^{N+1}$ for some open interval J containing zero such that for all $\alpha \in J$ (Allgower and Georg [1])

(1) $c(0) = u_0$,
(2) $\mathcal{H}(c(\alpha)) = 0$,
(3) $\text{rank}(\mathcal{H}'(c(\alpha))) = N$,
(4) $c'(\alpha) \neq 0$.

1.3. **Barycentric Coordinates.** It is natural to consider barycentric coordinates of a polygon as homotopy variables because of the two useful properties that they offer. Barycentric coordinates span a complete polygon and are a partition of unity. Traditional barycentric coordinates for triangles (and simplices in general) are defined by its vertices. Relevant generalizations of barycentric coordinates to n-sided polygons were provided by Wachspress [30] and later by Meyer et al.[21]. In the current context, we define barycentric coordinates in terms of the edges of a polygon rather than the vertices. Such a definition allows us to apply the concepts developed so far to associate a suitable homotopy to a polygon. We define Voronoi diagram based barycentric coordinates of edges for an n-sided polygon.

An interesting class of barycentric coordinates can be derived from Voronoi diagram of line segments and a point. Consider again a polygon $\mathcal{G}$ and a point p inside it. The Voronoi region of a point inside a polygon is a closed region of piecewise parabolic arcs as shown in Fig. 2. From the Voronoi diagram of the edges $\{e_i\}$ in a polygon, introduction of a point p steals an area from two or more existing Voronoi regions. If the stolen area for any edge e_i and p is denoted by $\mathcal{A}_i$, the barycentric coordinates for the edge can be written as

$$\lambda_i = \frac{\mathcal{A}_i}{\sum_{j=0}^{s-1} \mathcal{A}_j}, i \in [0, s-1], \tag{2}$$

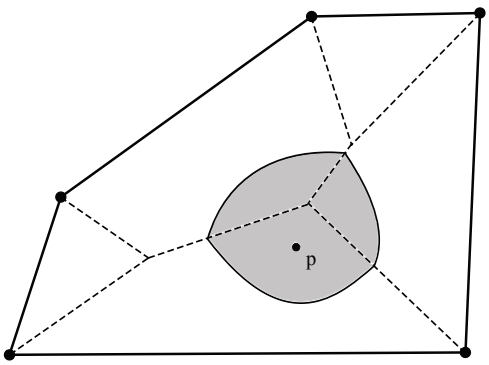

FIGURE 2. Voronoi diagram of a polygon $\mathcal{G}$ and a point p inside.

Area $\mathcal{A}_i$ can be computed as the area between the parabolic arc and the involved angle bisectors. Again, the barycentric coordinates defined in this way satisfy positivity, partition of unity and continuity. In the limiting case as p approaches one of the sides e_k, the stolen area $\mathcal{A}_k$ becomes very small, but simultaneously areas $\mathcal{A}_{i,i\neq k}$ become smaller (and eventually zero) by a rate higher than that of the former. Thus as p approaches e_k, $\lambda_k \to 1$, and $\lambda_{i,i\neq k} \to 0$.

We will use these barycentric coordinates in Sections 1.4 and 4.

1.4. **Homotopy continuation based on barycentric coordinates.** We call an *edge map* whichever function that is defined along an edge of a closed region of the Euclidean affine plane using the arc length of a point on that edge as only variable.

Equipped with the above defined edge maps and barycentric coordinates for any polygon $\mathcal{G}_k$, we define a homotopy $\mathcal{H}_k$ in s_k variables, where

s_k is the number of variables used in the k-th homotopy as

$$\mathcal{H}_k(p) = \sum_{i=0}^{s_k-1} f_i\left(d_i(p)\right)\lambda_i(p), \tag{3}$$

where $d_i(p)$ is the arc length along line $\mathcal{L}_k$ from a chosen origin O_k on it until the foot of the perpendicular from point p . We can write

$$d_i(p) = ||O_k - p_i|| + (p - p_i)^T \frac{(p_{i+1} - p_i)}{l_i}, \tag{4}$$

where p_{i+1} and p_i are two end points of an edge e_i of $\mathcal{G}_k$ lying on $\mathcal{L}_k$, and $||\mathbf{x}||$ denotes the length of a vector $\mathbf{x}$. Homotopy (3) continuously deforms edge maps f_i within the polygon and thus generates a smooth field. It can be seen as a linear combination of edge maps f_i with barycentric coordinates λ_i. We can further extend this so called *linear homotopy* to a *non-linear homotopy* as

$$\mathcal{H}_k(p,\eta) = \sum_{i=0}^{s_k-1} f_i\left(d_i(p)\right)\lambda_i(p)^\eta, \tag{5}$$

with η as the power of the non-linear homotopy.

Across polygons, the homotopy (3) is continuous and is at least C^1 smooth (see Appendix A for the proof). However, at all the intersection points $\mathcal{Q} = \{\mathcal{Q}_{i,j} : \mathcal{Q}_{i,j} \in \mathcal{L}_i \bigcap \partial\mathcal{O}\}$ of the lines $\{\mathcal{L}_i\}$ and the boundary $\partial\mathcal{O}$ of the object $\mathcal{O}$, the generated curve $\mathcal{H}^{-1}(0)$ is orthogonal to any line in $\{\mathcal{L}_i\}$. Therefore, the resulting reconstruction is somewhat unnatural. Given normals at the intersection points $\mathcal{Q}$ (which is the case with many range scanning physical devices), we propose a tangent alignment scheme for the resulting curve by locally warping the domain of the homotopies in [26].

2. Wu's algorithm

Let $\mathcal{K} = \mathbb{Q}$ be the field of rational numbers, $\mathbb{X} = \{x_1, \cdots, x_n\}$ a set of variables, $\mathcal{K}[\mathbb{X}]$ be the set of *polynomials* in the variables of $\mathbb{X}$, with coefficients in $\mathcal{K}$. If not otherwise stated the order of the monomials composing a polynomial will be taken as the lexicographic monomial ordering where $1 \prec x_1 \prec x_2 \prec \cdots \prec x_n$. The *universal field* $\mathcal{E}$ over $\mathcal{K}$ is an algebraically closed field containing an infinite number of indeterminates, or more simply a projective space over an algebraically closed field.

Definition 8. (from [31]) For any set of polynomials $\mathbb{P} \subset \mathcal{K}[\mathbb{X}]$, Zero $(\mathbb{P}) = \{x \in \mathcal{E}^n | \forall P \in \mathbb{P}, P(x) = 0\}$ is called a *variety*. For a set of polynomials

$\mathbb{P}$ and a polynomial D, we define $\text{Zero}(\mathbb{P}/D) = \text{Zero}(\mathbb{P}) \setminus \text{Zero}(\{D\})$, called a *quasi-algebraic variety*.

The aim of Wu's method is to determine the decomposition of quasi-algebraic varieties into irreducible components and the dimensions of these irreducible components. For example $\text{Zero}(\{xy\})$ in the three-dimensional projective space corresponds to the union of two irreducible components of dimension 2: the projective plane $\text{Zero}(\{x\})$ and the projective plane $\text{Zero}(\{y\})$. Likewise, Wu's method allowed us to prove that the *generalized* $v-$*offset* to a sphere of center Π and of radius r (i.e., the set of centers of spheres of radius v that are tangent to that sphere) is the union of two irreducible components of dimension 2: the sphere of center Π and of radius $r+v$, and the sphere of center Π and of radius $|r-v|$. The difference between the generalized $v-$offset and the true $v-$offset to a given sphere is that the true $v-$offset is the set of centers of circles of radius v that are externally tangent to that given sphere while the generalized $v-$offset is the set of centers of circles of radius v that are internally or externally tangent to that given sphere. If $v \leq r$, than the generalized and the true offsets coincide while otherwise ($v > r$), the true offset includes only the bigger sphere of radius $r+v$.

Definition 9. (from [31]) Let $P \in \mathcal{K}[\mathbb{X}]$ be a polynomial. The *class* of P, denoted by $\text{cls}(P)$ is the c such that x_c is the largest variable that occurs in P. If $\text{cls}(P) = c$, then x_c is called the *leading variable* and denoted by $\text{lvar}(P)$, the highest degree monomial of P as a univariate polynomial in $\text{lvar}(P)$ is called the *leading monomial*, and its coefficient is called the *initial* of P and denoted by $\text{init}(P)$.

Typically, the polynomial D whose variety is subtracted from a polynomial set will be a product of initials corresponding to geometric invariants that correspond to special cases of the geometric problem at hand. In all this paper, we mean by geometric invariant a quantity that is invariant under some geometric transformation, and we mean by topological invariant a quantity or a quality that is invariant by any continuous transformation.

Definition 10. (from [31]) A polynomial P_1 has higher *ordering* than a polynomial P_2, denoted as $P_2 \prec P_1$, if either $\text{cls}(P_1) > \text{cls}(P_2)$, or $c = \text{cls}(P_1) = \text{cls}(P_2)$ and $\deg(P_1, x_c) > \deg(P_2, x_c)$ (where deg denotes the degree of the polynomial). If none of two polynomials has higher ordering than the other, they are said to have the same rank, denoted as $P_1 \sim P_2$.

Definition 11. (from [31]) A polynomial Q is *reduced* with respect to P, if $\mathrm{cls}(P) = c > 0$ and $\deg(Q, x_c) < \deg(P, x_c)$. A sequence of non-zero polynomials $\mathcal{A} : A_1, A_2, \cdots, A_r$ is a *triangular set* if either $r = 1$ or $\mathrm{cls}(A_1) < \mathrm{cls}(A_2) < \cdots < \mathrm{cls}(A_r)$. A triangular set is called an *ascending chain*, or simply a chain, if A_j is reduced with respect to A_i for $i < j$. For a chain $\mathcal{A}$, we denote $\mathbb{I}_{\mathcal{A}}$ as the product of the initials of the polynomials in $\mathcal{A}$.

Definition 12. (from [31]) Let $\mathcal{A}' : A'_1, A'_2, \cdots, A'_{r'}$ and $\mathcal{A}'' : A''_1, A''_2, \cdots, A''_{r''}$ be two (ascending) chains. $\mathcal{A}'$ is said to be of lower ordering than $\mathcal{A}''$, denoted as $\mathcal{A}' \prec \mathcal{A}''$, if either there is some k such that $A'_1 \sim A''_1 \cdots A'_{k-1} \sim A''_{k-1}$, while $A'_k \prec A''_k$; or $r' > r''$ and $A'_1 \sim A''_1 \cdots A'_{r''} \sim A''_{r''}$.

Lemma 1. *(from [31]) A sequence of (ascending) chains steadily lower in ordering is finite.*

Definition 13. (from [31]) A *basic set* of a polynomial set $\mathbb{P}$ is any chain of lowest ordering contained in $\mathbb{P}$. A polynomial Q is called *reduced* with respect to a chain $\mathcal{A}$ if Q is reduced with respect to all the polynomials in $\mathcal{A}$.

Lemma 2. *(from [31]) Let $\mathcal{A}$ be a basic set of a polynomial set $\mathbb{P}$. If P is reduced with respect to $\mathcal{A}$, then a basic set of $\mathbb{P} \cup P$ is of lower ordering than that of $\mathbb{P}$.*

Let F and G be non-zero polynomials with $c = cls(F)$ and $I = \mathrm{init}(F)$. Either G is reduced with respect to F (which means that $\deg(G, x_c) < \deg(F, x_c)$), or $\deg(G, x_c) \geq \deg(F, x_c)$, and then it is possible to divide G by F as univariate polynomials in x_c. Indeed, let $k = \deg(G, x_c) - \deg(F, x_c)$, $k' = \deg(G, x_c)$, and I' be the coefficient of $x_c^{k'}$ in G, then $\deg\left(IG - I'x_c^k F\right) < k'$. Therefore in a finite number of steps $s \leq k + 1$, we get that $I^s G = QF + R$ where Q and R are polynomials in $\mathcal{K}[\mathbb{X}]$ with R reduced with respect to F. R is uniquely determined and called the *pseudo-remainder* of G with respect to F and denoted as $R = \mathrm{prem}(G, F)$.

It is therefore trivial to generalize this Euclidean division to the case of a triangular system: the result of the division of a polynomial G with respect to the polynomials of the triangular set $\mathcal{A} : A_1, A_2, \cdots, A_r$ is obtained by repeated division of G by A_1, A_2, $\cdots$, A_r. Thus, we get the *division formula*: $JG = \sum_i Q_i A_i + R$, where J is a polynomial in $\mathcal{K}[\mathbb{X}]$, R is reduced with respect to all the polynomials in the triangular set $\mathcal{A}$, the polynomials Q_i are in $\mathcal{K}[\mathbb{X}]$ and R is called the pseudo-remainder of

G with respect to $\mathcal{A}$, and denoted as $R = \text{prem}(G, \mathcal{A})$ [31].

This leads to Wu's algorithm for producing the decomposition of a variety into irreducible varieties (corresponding to irreducible polynomial sets). Starting with a polynomial set $\mathbb{P}_0 = \mathbb{P}$, one should select a basis $\mathcal{B}_0$ of $\mathbb{P}_0$, and then compute the set $\mathbb{R}_0$ of non-zero pseudo-remainders of polynomials of $\mathbb{P}_0 \setminus \mathcal{B}_0$ with respect to $\mathcal{B}_0$. Then, let $\mathbb{P}_1 = \mathbb{P}_0 \cup \mathbb{R}_0$. Then, one should compute a basis set $\mathbb{B}_1$ in $\mathbb{P}_1$. By Lemma 2, $\mathcal{B}_1$ is of lower ordering than $\mathcal{B}_0$. After this, one should compute the set $\mathbb{R}_1$ of non-zero pseudo-remainders of polynomials of $\mathbb{P}_1 \setminus \mathcal{B}_1$ with respect to $\mathcal{B}_1$. Therefore, such a process has a finite number of steps, and the final result is a basic set $\mathcal{B}_m = \mathcal{C}$, such that the corresponding set of non-zero pseudo-remainders $\mathbb{R}_m$ is the empty set and $\text{prem}(\mathbb{P}, \mathcal{C}) = \{0\}$. Thus, for each chain that can be obtained in such a way, $\text{Zero}(\mathbb{P}) \subseteq \text{Zero}(\mathcal{C})$. Therefore, one can obtain the variety of $\mathbb{P}$ as a union of quasi-projective varieties, where each algebraic variety is irreducible and the algebraic varieties being subtracted correspond to degenerate cases expressed as geometric invariants. Any chain $\mathcal{C}$ obtained by applying Wu's algorithm is called *a characteristic set* [31].

3. Generalized offset of quadrics

We can state that a point on the generalized offset to a quadric Q is a zero of the following polynomial set (i.e. a point on which all the polynomials in the following polynomial set $\mathcal{I}$ evaluate to 0):

$$\mathcal{I}: \begin{cases} ax^2 + bxy + cxz + dy^2 + eyz + fz^2 + gx + hy + iz + j \\ X - x - \lambda(2ax + by + cz + g) \\ Y - y - \lambda(bx + 2dy + ez + h) \\ Z - z - \lambda(cx + ey + 2fz + i) \\ (X - x)^2 + (Y - y)^2 + (Z - z)^2 - o^2 \end{cases},$$

where the variables a to j are the coefficients of the second degree polynomial in the variables x, y and z defining a general quadric in the three-dimensional affine Euclidean space (x, y and z are the coordinates of a point on the quadric), X, Y and Z are the coordinates of the point on the generalized offset to the quadric and o is the generalized offset parameter.

By computing the characterisitic set using Wu's algorithm, we obtain at the different steps the formal coeffcients corresponding to geometric, topological and geometric topology invariants of the generalised offset of

quadrics (see the files CoeffsStepi.txt, where i corresponds to the sequential steps of computation of the carateristic set through different ascending chains in https://drive.google.com/drive/folders/1bWtfqD-1V72EfKimNsTSzcMxl9KTc4Jf?usp=sharing).

The first round of formal coefficients are algebraic combinations (also called syzzygies) of the formal coefficients defining the quadrics. The first invariants are those coefficients of the monomials of total degree 2 that define the classification of quadrics into reducible (special case of the product of the affine equations of two infinite straight lines or quadric degenerated into a point of multiplicity 2) or irreducible (all other cases) and the presence of points at infinity of the projective quadric corresponding to the homogeneization of the polynomial that defines the quadric.

For the next steps, the formal coefficients need to be factorized. The invariants obtained are the invariants of the group of isometries or positive isometries as well as the geometric, topological and geometric topology invariants of the quadric, whose generalized offset is being computed.

For example, we would obtain the geometric invariants that make that $2ax + by + cz + g$, $bx + 2dy + ez + h$ and $cx + ey + 2fz + i$ vanish, and these geometric invariants will be replaced as new coefficients. They correspond to the special configurations of normals to the quadric that are respectively contained in planes of equations $x = X$, $y = Y$ and $z = Z$ or are one of the infinite straight lines that are the intersections of two of these planes, which are obtained when the point on the quadric also belongs to one of the hyperplanes of equations $2ax + by + cz + g$, $bx + 2dy + ez + h$ and $cx + ey + 2fz + i$ or to one of their intersections.

The structure of the polynomials corresponding to the invariants (symbolic coefficients) in terms of monomials is analogous with all monomials being of the same degree. The polynomials are either constant or homogeneous and composed of only quadratic monomials (repeated or not). Since constant symbolic coefficients correspond to previous invariants, all formal coefficients with more than one term are homogeneous. We can further simplify the expressions by considering the quadratic forms as invariants. In such a way, we can automatically exhibit the relationship between quadrics and quadratic forms and their generalized offset. Finally, we show two examples of computation of the generalized offsets of quadrics in Figures 3 and 4.

Each time a new pseudo-remainder is computed, the formal coefficients for each monomial in the class variable are gathered and stored in the file CoeffsStepi.txt, where i is the index of the step of computation of

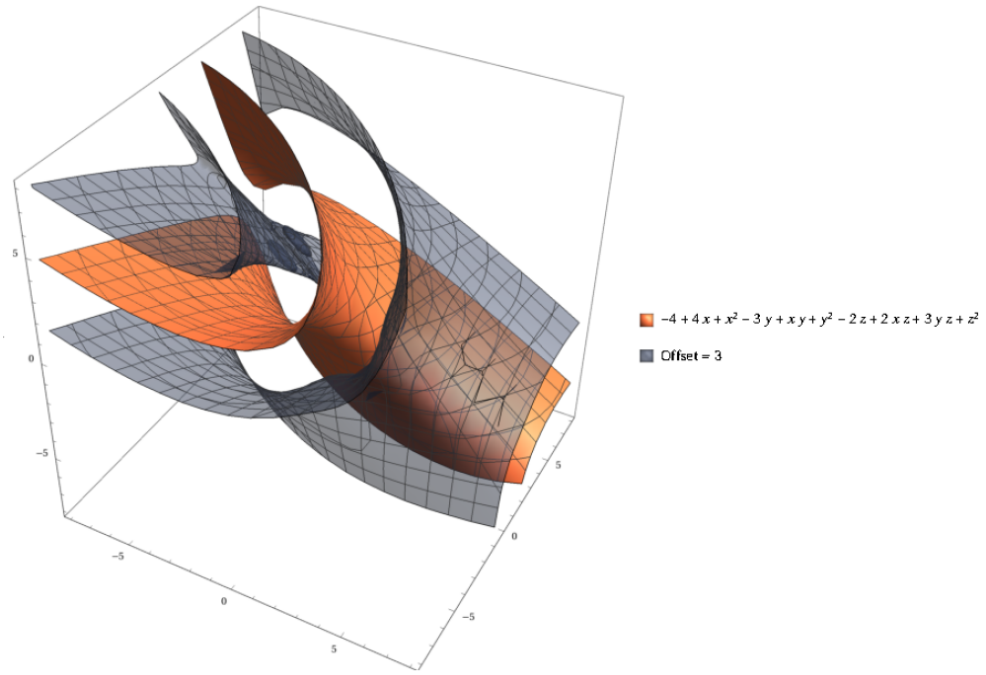

FIGURE 3. Generalized offset of a quadric

the ascending chains. Ecah ascending chain is stored in the file AscChainStepi.txt, where i is the same ascending chain index. Each new set of polynomilas to be processed after each step of computation of ascending chains is stored in the file NewSetStepi.txt and uses the formal coefficients de?ned in the file CoeffsStepi.txt. The next step of computation of ascending chains generates a new ascending chain stored in the file AscChainStepj.txt, where j = i + 1. At the first step of computation of the first ascending chain, i = 0.

4. Homotopy continuation defined on quadrics

The homotopy continuation based on quadrics corresponds to the homotopy parameter λ being the offset distance o_i of the interpolation point with respect to each one of the neighboring quadrics over the sum of the offsets to the neighboring quadrics, thus realizing the partition of unity. This is clearly the application of the barycentric coordinates and their use in homotopy continuation. Indeed, each quadric enclosing the interpolation point has associated an "edge map" $f_i(x, y, z)$ of the coordinates x, y, z of its point. The homotopy continuation computes the closest point of each one of the enclosing quadrics $\pi_i(x, y, z)$ from

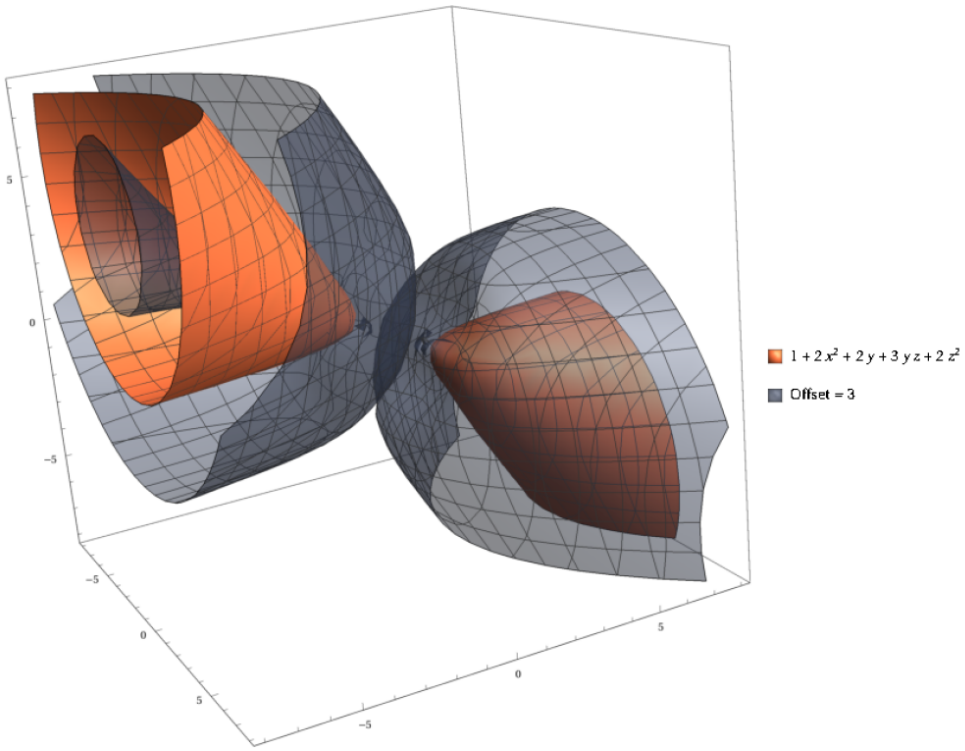

FIGURE 4. Generalized offset of another quadric

the interpolating point (x, y, z) and the "orthogonal" (or smallest) distance $o_i\,(x, y, z)$ from the point to the quadric, i.e., the distance between $\pi_i\,(x, y, z)$ and (x, y, z).

The total number of quadrics enclosing the interpolation is denoted by s in Eqs. 6 and 7, which express respectively the homotopy parameter associated with the i-th quadric enclosing the interpolation point and the homotopy of the interpolation point and the homotopy parameter vector $(\lambda = (\lambda_1 \ldots \lambda_s)$ associated with the interpolation point.

$$\lambda_i = \frac{o_i\,(x, y, z)}{\sum_{j=0}^{s-1} o_j\,(x, y, z)}, i \in [0, s-1]\,, \tag{6}$$

$$\mathcal{H}(x, y, z, \lambda) = \sum_{i=0}^{s-1} \lambda_i f_i(x, y, z) \tag{7}$$

5. CONCLUSIONS

We have shown how homotopy continuation can be extended by considering barycentric coordinates defined by the smallest distance to the

closest quadric over the sum of the smallest distances to the neighboring quadrics, obtained thanks to the equation of the generalized offset to a quadric, we obtained using Wu's algorithm. In this process of the computation of the characteristic set, we obtained all the geometric, geometric topology and topological invariants of the generalized offset to a quadric. This has potential applications in prediction of collisions in astronomy, where the trajectories of the planets of the solar system are quadrics and the trajectories of the possible sources of collisions are also quadrics.

References

[1] Allgower, E.L., Georg, K.: Numerical continuation methods: an introduction. Springer-Verlag New York, Inc. New York, NY, USA 1990.

[2] Antón Castro, F., Gold, C., Mioc, D.: Local coordinates and interpolation in a voronoi diagram for a set of points and line segments. In: Proceedings of the 2nd Voronoi Conference on Analytic Number Theory and Space Tillings. pp. 9–12, 1998.

[3] Francois Anton, *Voronoi diagrams of semi-algebraic sets*, Ph.D. thesis, The University of British Columbia (UBC), Vancouver, Canada, 2004.

[4] Francois Anton, *A certified delaunay graph conflict locator for semi-algebraic sets*, Computational Science and Its Applications - ICCSA 2005, International Conference, Singapore, May 9-12, 2005, Proceedings, Part I, pp. 669–682,2005

[5] F. Anton, D. Mioc, and M. Santos, *Exact computation of the topology and geometric invariants of the Voronoi diagram of spheres in 3D*, Journal of Computer Science and Technology, Vol. **28**, No. 2, pp. 255–266.

[6] F. Aurenhammer, *Gewichtete Voronoi Diagramme: Geometrische Deutung und Konstruktions-Algorithmen*, Ph.D. thesis, IIG-TU Graz, Austria, 1984, Report B53.

[7] F. Aurenhammer and R. Klein, *Voronoi diagrams*, Handbook of Computational Geometry, Chapter V (J. Sack and G. Urrutia, eds.), Elsevier Science Publishing, 2000, pp. 201–290.

[8] Lenore Blum, Felipe Cucker, Michael Shub, and Steve Smale, *Complexity and real computation*, Springer-Verlag, New York, 1998, With a foreword by Richard M. Karp. MR 99a:68070

[9] K. Q. Brown, *Voronoi diagrams from convex hulls*, Information Processing Letters **9** (1979), no. 5, pp. 223–228.

[10] M. L. Gavrilova and J. Rokne, *Updating the topology of the dynamic voronoi diagram for spheres in euclidean d-dimensional space*, Comput. Aided Geom. Des. **20** (2003), pp. 231–242.

[11] Marina Gavrilova, *Proximity and applications in general metrics*, Ph.D. thesis, University of Calgary, Calgary, Alberta, Canada, 1998.

[12] P.J. Green and R. Sibson, *Computing dirichlet tessellations in the plane*, The Computer Journal **21**, 1977, no. 2, pp. 168–173.

[13] Gert-Martin Greuel and Gerhard Pfister, *A* **singular** *introduction to commutative algebra*, Springer-Verlag, Berlin, 2002, With contributions by Olaf Bachmann, Christoph Lossen and Hans Schönemann, With 1 CD-ROM (Windows, Macintosh, and UNIX). MR 1 930 604

[14] Klaus Jänich, *Topology*, Undergraduate texts in mathematics, Springer, 1984.

[15] Leonidas J. Guibas, Donald E. Knuth, and Micha Sharir, *Randomized incremental construction of delaunay and voronoi diagrams*, ICALP '90: Proceedings of the 17th International Colloquium on Automata, Languages and Programming (London, UK), Springer-Verlag, 1990, pp. 414–431.

[16] Deok-Soo Kim, Youngsong Cho, and Donguk Kim, *Euclidean voronoi diagram of 3d balls and its computation via tracing edges.*, Computer-Aided Design, 2005, pp. 1412–1424.

[17] Deok-Soo Kim, Youngsong Cho, Donguk Kim, Sangsoo Kim, Jonghwa Bhak, and Sung-Hoon Lee, *Euclidean voronoi diagrams of 3d spheres and applications to protein structure analysis*, Japan Journal of Industrial and Applied Mathematics **22**, 2005, pp. 251–265, 10.1007/BF03167441.

[18] Donguk Kim and Deok-Soo Kim, *Region-expansion for the voronoi diagram of 3d spheres*, Comput. Aided Des. **38**, 2006, pp. 417–430.

[19] A. Kolmogorov, *A statistical theory for the recrystallization of metals*, Akad. nauk SSSR, Izv., Ser. Matem., No. **3**, pp. 355–359, 1937.

[20] Meng Lin, Xiaoliang Li, and Donming Wang, *A new algorithmic scheme for computing characteristic sets*, Journal of Symbolic Computation **50**, 2013, pp. 431–449.

[21] Meyer M., Lee H. Barr A., and Desbrun, M.,Generalized Barycentric Coordinates on Irregular Polygons, *Journal of graphics, gpu, and game tools*, Vol. **7**, No. **1**, 2002, pp. 13-22.

[22] Tetsushi Nishida and Kokichi Sugihara, *Precision necessary for d−dimensional Sphere Voronoi Diagrams*, Proceedings of the Fifth International Symposium on Voronoi Diagrams in Science and Engineering (ISVD 2008), 2008, pp. 157–167.

[23] Tetsushi Nishida, Yoshiaki Tanaka, and Kokichi Sugihara, *Evaluation of the Precision for Exact Computation of a Circle Voronoi Diagram*, Tech. Report UW-CS-TR-1481, Department of Mathematical Informatics, Graduate School of Information Science and Technology, The University of Tokyo, Bunkyo-Ku, Tokyo 113-8656, Japan, October 2007.

[24] Atsuyuki Okabe, Barry Boots, and Kōkichi Sugihara, *Spatial tessellations: concepts and applications of Voronoï diagrams*, John Wiley & Sons Ltd., Chichester, 1992, With a foreword by D. G. Kendall. MR 94a:52033

[25] Joonghyun Ryu, Donguk Kim, Youngsong Cho, Rhohun Park, and Deok soo Kim, *D-s, Scomputation of molecular surface using euclidean voronoi diagram*, Computer-Aided Design and Applications, Vol. **2**, Nos. **1-4**, 2005.

[26] O. Sharma and F. Anton., Homotopic object reconstruction using natural neighbor barycentric coordinates. In *Seventh International Symposium on Voronoi Diagrams in Science and Engineering (ISVD)*, 2010.

[27] G. F. Voronoï, *Nouvelles applications des paramètres continus à la théorie des formes quadratiques. premier mémoire. sur quelques propriétés des formes quadratiques positives parfaites.*, Journal für die reine und angewandte Mathematik **133**, 1907, pp. 97–178.

[28] ———, *Nouvelles applications des paramètres continus à la théorie des formes quadratiques. deuxième mémoire. recherches sur les parallélоèdres primitifs. première partie. partition uniforme de l'espace analytique à n dimensions à l'aide des translations d'un même polyèdre convexe.*, Journal für die reine und angewandte Mathematik **134**, 1908, pp. 198–287.

[29] _____, *Nouvelles applications des paramètres continus à la théorie des formes quadratiques. deuxième mémoire. recherches sur les paralléloèdres primitifs. seconde partie. domaines de formes quadratiques correspondant aux différents types de paralléloèdres primitifs.*, Journal für die reine und angewandte Mathematik **136**, 1910, pp. 67–181.

[30] Wachspress, E. L.,*A rational finite element basis*,1975,Academic Press.

[31] Wen-Tsun Wu and Xiao-Shan Gao, *Automated reasoning and equation solving with the characteristic set method*, J. Comput. Sci. & Technol. **21**, No. **5**, 2006, pp. 756–764.

(F. Antón Castro) Department of Computational sciences, School of Mathematical and Computational Sciences, Yachay Tech University
Email: fcastro(at)yachaytech(dot)edu(dot)ec

(A. S. Ramos Cisneros) Department of Computational sciences, School of Mathematical and Computational Sciences, Yachay Tech University
Email: anthonyramos(at)yachaytech(dot)edu(dot)ec

(F. P. Zhapa Camacho) Department of Computational sciences, School of Mathematical and Computational Sciences, Yachay Tech University
Email: fernandozhapa(at)yachaytech(dot)edu(dot)ec

(O. V. Guarnizo Cabezas) Department of Computational sciences, School of Mathematical and Computational Sciences, Yachay Tech University, Ecuador
Email: oscarguarnizo(at)yachaytech(dot)edu(dot)ec

ZETA-FUNCTIONS AND DIMENSIONS OF A CLASS OF DISCRETE SELF-AFFINE SUBSETS OF $\mathbb{R}^2$.

Driss Essouabri (*France*)

Abstract. In this paper we study a class of discrete subsets of $\mathbb{R}^2$ that are "self-affine" with respect to a finite set of affine transformations. Any such set can be interpreted as having a fractal structure. We introduce a zeta function for these sets, and derive basic analytic properties of this "fractal" zeta function. By using in addition the classical Baker's theorem on the lower bound for linear forms in logarithms, we obtain a simple formula for the fractal dimension for this class of self-affine sets.

1. Introduction

First we recall the following classical definition from ([Fa], §9.4):

Definition 1. A subset $\mathcal{F}$ of $\mathbb{R}^n$ is said to be self-affine if there exists a finite set $\mathbf{f} = \{f_i\}_{i=1}^d$ of affine transformations[1] such that $\mathcal{F} = \cup_{i=1}^d f_i(\mathcal{F})$.

Self-affine sets form an important class of fractals sets, which includes self-similar sets as a particular case. Thus, it is natural to study their geometry and in particular to look to a formula for the dimension of self-affine sets that generalizes the known formula for self-similar sets. Unfortunately, as it was remarked by K. Falconer in ([Fa], §9.4), the situation is much more complicated than the self-similar case.

Let $\mathcal{F}$ be a discrete unbounded self-affine subset of $\mathbb{R}^n$. We next recall the notion of dimension that suffices for our purposes.

Received September 4, 2019.

2010 *Mathematics Subject Classification.* 11M41, 28A80, 52C10, 11J69, 11M32.

Key words and phrases. Self-affine discrete sets, self-similar discrete sets, fractals, zeta functions, meromorphic continuation, fractal dimensions.

The author expresses his thanks to the organizers of the Voronoi Memorial Conference for all they did to make participation in this Conference so easy, pleasurable and rewarding. The author also expresses his thanks to an anonymous referee for careful reading of the paper and for his comments which improved the exposition.

[1]An affine transformation is a map $f : \mathbb{R}^n \to \mathbb{R}^n$ of the form $f(\mathbf{x}) = T(\mathbf{x}) + \mathbf{b}$, where T is a linear transformation of $\mathbb{R}^n$ and $\mathbf{b}$ is a vector of $\mathbb{R}^n$.

Definition 2. The upper Minkowski dimension of $\mathcal{F}$ equals:

$$e_{\mathcal{F}} := \limsup_{R\to\infty} \frac{\ln\left[\#\mathcal{F}(R)\right]}{\ln R} \in [0,\infty]$$

where

$$\mathcal{F}(R) := \mathcal{F} \cap B(R) = \{\mathbf{m} \in \mathcal{F};\ \|\mathbf{m}\| \leq R\}\,.$$

Note. *We will subsequently restrict attention here to discrete $\mathcal{F}$ whose upper Minkowski dimension is finite.* □

We also attache to $\mathcal{F}$ the following zeta function defined formally by

$$\zeta_{\mathcal{F}}(s) := \sum_{\mathbf{m}\in\mathcal{F}'} \|\mathbf{m}\|^{-s} \qquad \text{where} \quad \mathcal{F}' := \mathcal{F} - \{\mathbf{0}\}, \tag{1}$$

where $\|\mathbf{x}\| = \sqrt{x_1^2 + \cdots + x_n^2}$ is the Euclidean norm of $\mathbb{R}^n$.

It follows from an elementary estimation (see [EL1]) that

$$\begin{aligned}&\zeta_{\mathcal{F}}(s) \textit{converges absolutely in the half-plane } \{\Re(s) > e_{\mathcal{F}}\} \text{ and}\\ &e_{\mathcal{F}} \text{ is its abscissa of convergence.}\end{aligned} \tag{2}$$

In light of earlier results, in particular ([BT1], [BT2], [DGLMM]), [Fa], [LF], [St],...), it is natural to interpret the abscissa of convergence $e_{\mathcal{F}}$ of $\zeta_{\mathcal{F}}(s)$ as the "fractal dimension" of $\mathcal{F}$. Moreover, in the case where $\zeta_{\mathcal{F}}(s)$ has meromorphic continuation beyond its domain of convergence, its singularities and in particular those located in the line $\Re(s) = e_{\mathcal{F}}$ contain important information about the geometry of the fractal set $\mathcal{F}$.

In a series of joint works with B. Lichtin ([EL1], [EL3], [EL6],...), we have studied the analytic properties of the zeta functions associated to discrete self-similar sets, and obtained as application several results concerning the geometry of these sets. Section §2 below will give a brief survey of some of these results.

In section §3, we will introduce a class of discrete self-affine subsets of $\mathbb{R}^2$ that are neither self-similar nor automatic in the sens of Allouche-Salon. Our main result in this paper (see Theorem 2 in §3 below) shows that the fractal zeta functions of these self-affine sets extend beyond their domains of convergence and gives a fairly precise description of the set of their possible singularities on the line of convergence. By using in addition the classical Baker's theorem on the lower bound for linear forms in logarithms, we also obtain (see Corollary 1 below) a simple formula for the fractal dimension for this class of self-affine sets.

Self-similar or automatic sets have some kinds of periodicity, which make it possible to use shifting methods to obtain meromorphic continuation of their zeta functions. Unfortunately, self-affine sets do not have

such types of periodicity and therefore their zeta functions cannot be analyzed by the shifting methods developed in [APM], [E], [EL1], [EL3], [EL6], etc. In order, to obtain our Theorem 2, we developed instead an other approach based on the classical Mellin-Barnes formula.

In this paper we restrict ourself to the case of self-affine sets which are a product of $r = 2$ digits sets associated to pairs of independent irrational numbers (see (11) below). For $r \geq 2$, the part of our argument based on Mellin Barnes formula became rather intricate. Nonetheless, since Baker's theorem holds for $r \geq 2$ independent irrational number, the foundation of the most significant part of Theorem 2, i.e. part (2), is available and ought to be applicable to prove Theorem 2 in most general context. We will treat this more general case in a separate work in progress.

Notations: Some notations of use in this paper are as follows:

(1) $\mathbb{N} = \{1, 2, \dots\}$, $\mathbb{N}_0 = \mathbb{N} \cup \{0\}$, $\mathbb{Z} = \{\dots, -2, -1, 0, 1, 2, \dots\}$ and $\mathbb{Z}^* = \mathbb{Z} \setminus \{0\}$.

(2) For a vector $\mathbf{b} = (b_1, \dots, b_n) \in \mathbb{N}_0^n$, set $|\mathbf{b}| = b_1 + \cdots + b_n$; and $\mathbf{y}^{\mathbf{b}} = \prod_j y_j^{b_j}$ for any $\mathbf{y} = (y_1, \dots, y_n) \in \mathbb{R}^n$.

(3) Given an unbounded variable $\mathbf{x} \in X$ and parameter $\mathbf{y} \in Y$, the expression

$$f(\mathbf{y}, \mathbf{x}) \ll_{\mathbf{y}} g(\mathbf{x}) \quad \textit{uniformly in } \mathbf{x} \in X$$

means that for any $\mathbf{y} \in Y$ there exists a constant $C = C(\mathbf{y}) > 0$, such that for each $\mathbf{x} \in X$ $|f(\mathbf{y}, \mathbf{x})| \leq C\ g(\mathbf{x})$.

(4) Let U a subset of $\mathbb{C}$ and $a \in \mathbb{C}$. We define the distance of the point a to the set U by $d(a, U) := \inf_{z \in U} |a - z|$.

(5) Let $F(s)$ be a meromorphic function on a domain $\mathcal{D}$ of $\mathbb{C}$ and let $\mathcal{P}$ be the set of its poles. We define $(Re\, s, Im\, s) = (\sigma, t)$. In addition, we say that F has moderate growth on $\mathcal{D}$ if there exists $a, b > 0$ such that $\forall \sigma_1, \sigma_2 \in \mathbb{R}$ verifying $\sigma_1 \leq \sigma_2$ and $\forall \theta > 0$, $F(s) \ll_{\sigma_1, \sigma_2, \theta} (1 + |t|)^{a|\sigma| + b}$ uniformly in $s = \sigma + it \in \mathcal{D}$ such that $\sigma_1 \leq \sigma \leq \sigma_2$ and $d(s, \mathcal{P}) \geq \theta$.

2. A a brief survey on self-similar sets

Definition 3. A similarity on the Euclidean space $\mathbb{R}^n$ is an affine transform $f : \mathbb{R}^n \to \mathbb{R}^n$ of the form $f(\mathbf{x}) = c\, T(\mathbf{x}) + \mathbf{b}$, where

(1) $c = c(f) > 0$ is the scale factor of f;

(2) $T = T(f)$ is an orthogonal linear transformation of $\mathbb{R}^n$ with respect to the quadratic form $\|\mathbf{x}\|^2 = \sum_i x_i^2$.

Self-similarity is typically defined in terms of a finite family of "similarity transformations". For the classical case of compact fractals, each such transformation is contractive. We recall the following two classical results on compact self-similar sets, the first due originally to Hutchinson [H]. The second goes back, apparently, to Moran [Mor].

Theorem.([Fa], th 2.7, p. 36).
Let $f_1, \ldots, f_m$ be a family of contractive similarity transformations of $\mathbb{R}^n$; that is the scale factor c_i of each f_i belongs to $(0,1)$. Then there exists a unique non-empty compact set K such that $K = \cup_{i=1}^m f_i(K)$.

(K is called a self-similar compact set.)

Next, assume the *Open Set Condition* holds.
There exists a bounded open set U such that

$$\cup_{i=1}^m f_i(U) \subset U \text{ and } f_i(U) \cap f_j(U) = \emptyset \text{ if } i \neq j. \tag{3}$$

Then *the Hausdorff dimension of K is the unique positive solution of the equation* $\sum_{i=1}^{m} c_i^s = 1$.

Example: With $f_1, f_2 : \mathbb{R} \to \mathbb{R}$ given by $f_1(x) = \frac{1}{3}x$ and $f_2(x) = \frac{1}{3}x + \frac{2}{3}$, the set K is the middle-third Cantor set, and its Hausdorff dimension is the positive solution of the equation $2\left(\frac{1}{3}\right)^s = 1$, that is, $\frac{\ln 2}{\ln 3}$.



In a series of joint works with B. Lichtin ([EL1], ,[EL2], [EL3],[EL4], [EL5] and [EL6]) we analyze countable and discrete subsets of a Euclidean space that exhibit the property of "self-similarity". This is a natural analogue of that used to define a compact self-similar set, a core subject of interest in classical fractal analysis. For the classical case of compact fractals, each transformation f_i is contractive. In the discrete case, however, each such transformation is expansive and it is natural to think of these unbounded discrete sets as exhibiting a fractal structure at infinity. Because of the discrete structure, they often arise from an arithmetic or combinatorial construction. A basic example of such set is the pascal triangle modulo a fixed prime p defined by $Pascal(p) = \left\{(m_1, m_2) \in \mathbb{N}_0^2; \binom{m_1}{m_2} \not\equiv 0 \pmod{p}\right\}$.

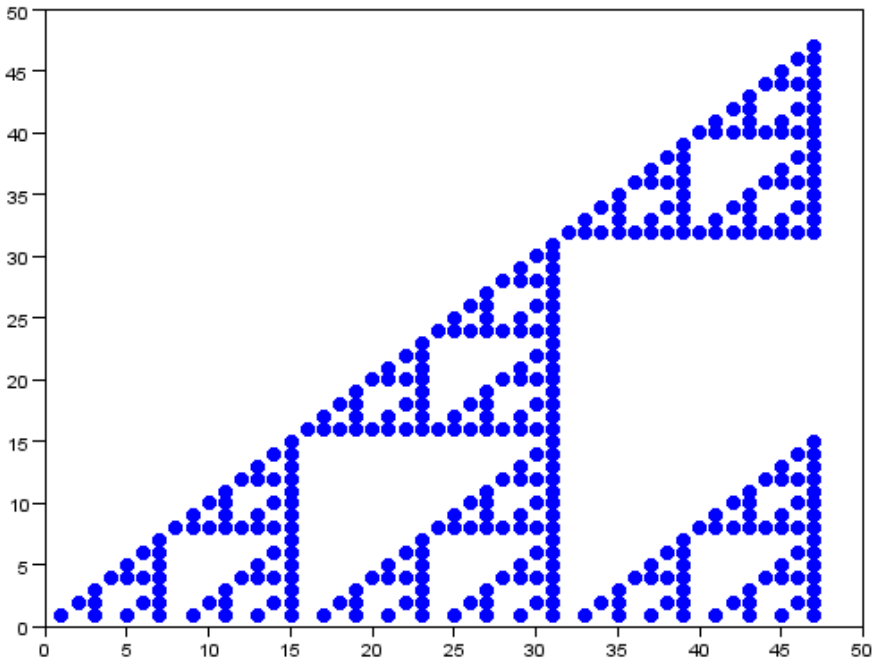

Figure above shows the first 48 lines of Pascal's triangle mod 2.

It is known (see for example [E]) that the fractal dimension of $Pascal(p)$ is $\theta_p = \log(\frac{p(p+1)}{2})\,(\log p)^{-1}$. Moreover, it is easy to see that

$$Pascal(p) = \bigsqcup_{\substack{\mathbf{r}=(r_1,r_2)\in\{0,\dots,p-1\}^2 \\ r_2\le r_1}} (pId_{\mathbb{R}^2} + \mathbf{r})\,(Pascal(p))\,.$$

Thus, $Pascal(p)$ is a natural example[2] of self-similar set with expansive similarities. This example belongs to the class of discrete self-similar sets defined as follows:

Throughout this paper, we restrict attention to unbounded discrete subsets of $\mathbb{R}^n$ $(n \ge 1)$*, and will always denote such a set by* $\mathcal{F}$*.*

[2] $Pascal(p)$ also belongs to the important class of automatic sequences in the sense of Allouche-Salon (see §14.6 of [AS]) and it has been studied from this perspective in several works [S], [AB], [AHPPS], [APM], [BG], etc.

Definition 4. $\mathcal{F}$ is a discrete self-similar set if there exists a finite set $\mathbf{f} = \{f_i = c_i T_i + \mathbf{b}_i\}_{i=1}^{d}$ of affine similarities such that each scale factor $c_i > 1$ and[3] $\mathcal{F} \equiv \cup_{i=1}^{d} f_i(\mathcal{F})$.

By specifying the sizes of overlaps of the sets invariant under the individual f_i, two distinct possibilities occur for any self similar set.

Definition 5. We say that

(1) $\mathcal{F}$ satisfies the "finite overlap" condition if

$$f_i(\mathcal{F}) \cap f_j(\mathcal{F}) \text{ is finite if } i \neq j. \tag{4}$$

(2) $\mathcal{F}$ satisfies the "normal overlap" condition if

$$e'_{\mathcal{F}} := max \left\{ e_{\left(f_i(\mathcal{F}) \cap f_j(\mathcal{F})\right)} \mid i \neq j \right\} < e_{\mathcal{F}}. \quad \square \tag{5}$$

Remark 1. The finite overlap condition (4) can be understood to be a reasonable analogue of the open set condition for compact fractals due to Moran [Mor] since outside a bounded subset the different invariant subsets must be disjoint.

Of course, many other possibilities can occur for the density of overlaps of different invariant subsets. We have chosen these two since they reflect opposite extremes of what can happen in general. In addition, it is worth emphasizing that the zeta function method appears to be useful not only for these two cases but for others as well, though we do not address this point here.

Recall that the zeta function of $\mathcal{F}$ is the Dirichlet series defined formally by

$$\zeta_{\mathcal{F}}(s) := \sum_{\mathbf{m} \in \mathcal{F}'} \|\mathbf{m}\|^{-s} \qquad \text{where} \qquad \mathcal{F}' := \mathcal{F} - \{\mathbf{0}\}. \tag{6}$$

We need also the following construction:

Definition 6. Let $\mathbf{f} = \{f_j = c_j T_j + \mathbf{b}_j\}_{j=1}^{d}$ be a finite set of affine expansive similarities.
Let $r \in \mathbb{N}_0$. Set $N_r = \binom{n+r-1}{n-1}$ and denote by $\boldsymbol{\alpha}_1, \ldots, \boldsymbol{\alpha}_{N_r}$ the elements $\boldsymbol{\alpha}_i = (\alpha_{1,i}, \ldots, \alpha_{n,i}) \in \mathbb{N}_0^n$ of weight r and ordered lexicographically.
The transformation $\mathbf{y} = (y_1, \ldots, y_n) \to \mathbf{x} = T_j(\mathbf{y})$ induces a linear map on the vector space of monomials of degree r

$$\mathbf{x}^{\boldsymbol{\alpha}_u} = \sum_{v=1}^{N_r} g_{(u,v)}^{(j)} \, \mathbf{y}^{\boldsymbol{\alpha}_v}. \tag{7}$$

[3]The notation $F \equiv G$ means that $(F \setminus G) \cup (G \setminus F)$ is a finite set.

We define the $N_r \times N_r$ matrix $\mathcal{M}_r(s)$ $(s \in \mathbb{C})$, where

$$\mathcal{M}_r(s)_{(u,v)} = \sum_{j=1}^{d} g_{(u,v)}^{(j)}\ c_j^{-s};$$

and set

$$\delta_r(s) := det\big(I_{N_r} - \mathcal{M}_r(s)\big)\,. \tag{8}$$

Remark 2. If $r = 0$, then $\delta_0(s) = 1 - \sum_{j=1}^{d} c_j^{-s}$ is the "Dirichlet polynomial" for $\mathcal{F}$. Its roots are fairly easy to understand since the coefficient of each c_j^{-s} has the same sign. When $r \geq 1$, however, this property will not in general occur for $\delta_r(s)$. As a result, it is more difficult to study its roots. □

In our joint work with Lichtin [EL6], We prove the following theorem which describes the behavior of $\zeta_{\mathcal{F}}(s)$ outside the half-plane $\{\sigma > e_{\mathcal{F}}\}$ of absolute convergence and gives in particular a simple description of the fractal dimension of $\mathcal{F}$.

Theorem 1. *([EL6], Theorem 1).*
Let $\mathcal{F} \subset \mathbb{R}^n$ be a discrete self-similar set, determined by a set of expansive similarities **f** *as in Definition 4. Then the following properties are satisfied.*

(1) The fractal dimension $e_{\mathcal{F}}$ of $\mathcal{F}$ is the abscissa of convergence of $\zeta_{\mathcal{F}}(s)$, and equals the unique real solution of the equation $\delta_0(s) = 1 - \sum_{j=1}^{d} c_j^{-s} = 0$.

(2) If the finite overlap condition (4) holds, then $\zeta_{\mathcal{F}}(s)$ has a meromorphic extension with moderate growth to the whole complex plane $\mathbb{C}$.

(3) If the normal overlap condition (5) holds, then $\zeta_{\mathcal{F}}(s)$ has a meromorphic extension with moderate growth to the half-plane $\{\sigma > e'_{\mathcal{F}}\}$.

(4) In each case:

(a) the polar locus $\mathcal{P}ol_{\mathcal{F}}$ of $\zeta_{\mathcal{F}}(s)$ is a subset of

$$\{\sigma \leq e_{\mathcal{F}}\} \cap \bigcup_{r \in \mathbb{N}_0} \bigcup_{\substack{k \leq r \\ k \in \mathbb{Z}}} \big\{s + k : \delta_r(s) = 0\big\}; \tag{9}$$

(b) $s \mapsto \delta_0(s) \cdot \zeta_{\mathcal{F}}(s)$ is holomorphic and has moderate growth in the half-plane $\{\sigma > e''_{\mathcal{F}}\}$, where $e''_{\mathcal{F}} = e_{\mathcal{F}} - 1$ if (4) holds, and $e''_{\mathcal{F}} = \max\left(e_{\mathcal{F}} - 1, e'_{\mathcal{F}}\right)$ if (5) holds.

(c) $e_{\mathcal{F}}$ is a simple pole of $\zeta_{\mathcal{F}}(s)$.

Remark 3. Theorem 1 gives a precise description of the meromorphic extension of the zeta function of a discrete self-similar set $\mathcal{F}$ beyond its domain of convergence. This description makes it possible to understand the geometry of $\mathcal{F}$ and not only its dimension. The combination of this theorem with two multivariate Tauberian theorems that we established in our joint works with Lichtin [EL3] and [EL6], allowed us to solve a variety of Point Configuration and Sum-Product type problems for discrete self-similar sets. The same results also follow immediately for the self-affine set studied in §3 and §4 below.

3. A class of Self-affine discrete sets, their zeta functions and dimensions

Let $\mathbf{q} = (q_1, q_2) \in \mathbb{N}^2$ be a pair of positive integers satisfying $q_1, q_2 \geq 2$. We fix two sets of digits $I_j \subset \{0, \ldots, q_j - 1\}$ such that $0 \in I_j$ $(j = 1, 2)$. We set also $\mathcal{I} = I_1 \times I_2$.
We define for $j = 1, 2$, the set

$$\mathcal{D}(q_j, I_j) \text{ as the set of non negative integers such that all their digits in base } q_j \text{ are in } I_j. \tag{10}$$

We define now the discrete fractal set $\mathcal{F}(\mathbf{q}, \mathcal{I})$ by

$$\mathcal{F}(\mathbf{q}, \mathcal{I}) := \mathcal{D}(q_1, I_1) \times \mathcal{D}(q_2, I_2). \tag{11}$$

First we remark that $\mathcal{F}(\mathbf{q}, \mathcal{I})$ is a discrete self-affine subset of $\mathbb{R}^2$. More precisely, we have:

Lemma 1.

$$\mathcal{F}(\mathbf{q}, \mathcal{I}) = \bigsqcup_{\mathbf{r} \in \mathcal{I}} f_{\mathbf{q},\mathbf{r}} \left(\mathcal{F}(\mathbf{q}, \mathcal{I}) \right) \qquad \textit{(disjoint union)},$$

where for $\mathbf{r} = (r_1, r_2) \in \mathcal{I}$, $f_{\mathbf{q},\mathbf{r}}$ *is the affine transformation of* $\mathbb{R}^2$ *defined by*
$f_{\mathbf{q},\mathbf{r}}(x_1, x_2) = (q_1 x_1 + r_1, q_2 x_2 + r_2)$ *for all* $(x_1, x_2) \in \mathbb{R}^2$.

Proof of Lemma 1: The proof is a simple consequence of the uniqueness of the q-ary expansion in basis q. □

In order to avoid the trivial cases, we assume here that

$$2 \leq |I_j| \leq q_j - 1 \quad \forall j = 1, 2. \tag{12}$$

We assume also that q_1 and q_2 are multiplicatively independent. That is,

$$q_1^{k_1} q_2^{k_2} \neq 1 \quad \forall (k_1, k_2) \in \mathbb{Z}^2 \setminus \{(0, 0)\}. \tag{13}$$

The main result of this paper is the following theorem:

Theorem 2. *Set*

$$e_1 := \frac{\ln|I_1|}{\ln q_1}, \quad e_2 := \frac{\ln|I_2|}{\ln q_2} \quad \text{and} \quad \sigma_0(\mathbf{q},\mathcal{I}) := e_1 + e_2.$$

Assume that (12) and (13) hold. Then, the zeta function

$$s \mapsto \zeta_{\mathcal{F}(\mathbf{q},\mathcal{I})}(s) = \sum_{(m_1,m_2)\in\mathcal{F}(\mathbf{q},\mathcal{I})'} \frac{1}{(m_1^2+m_2^2)^{s/2}}$$

satisfies the following properties:

(1) $\zeta_{\mathcal{F}(\mathbf{q},\mathcal{I})}(s)$ *converges absolutely in the half-plane* $\{\Re(s) > 2\}$*;*

(2) $\zeta_{\mathcal{F}(\mathbf{q},\mathcal{I})}(s)$ *has holomorphic continuation to the domain* $\{\Re(s) > \sigma_1(\mathbf{q},\mathcal{I})\} \setminus \mathcal{S}$ *where*

(a) $\sigma_1(\mathbf{q},\mathcal{I}) = \max(e_1,e_2) < \sigma_0(\mathbf{q},\mathcal{I})$ *and;*

(b) $$\mathcal{S} := \left\{ \sigma_0(\mathbf{q},\mathcal{I}) + 2\pi i \left(\frac{k_1}{\ln q_1} + \frac{k_2}{\ln q_2} \right) \mid (k_1,k_2) \in \mathbb{Z}^2 \right\};$$

(3) There exists a positive constant $C > 0$ *such that*

$$\zeta_{\mathcal{F}(\mathbf{q},\mathcal{I})}(\sigma) \sim \frac{C}{\sigma - \sigma_0(\mathbf{q},\mathcal{I})} \quad \text{as } \sigma \to \sigma_0(\mathbf{q},\mathcal{I}) \quad (\sigma > \sigma_0(\mathbf{q},\mathcal{I})).$$

In particular, $\sigma_0(\mathbf{q},\mathcal{I})$ *is a singular point of* $\zeta_{\mathcal{F}(\mathbf{q},\mathcal{I})}$*.*

Remark 4. Let $j \in \{1,2\}$. We will prove in Lemma 2 below that e_j is a simple pole with positive residue of the zeta function $\zeta_{\mathcal{D}(q_j,I_j)}$ associated to the discrete set $D(q_j,I_j)$. We will also establish in the proof of Theorem 2 that the constant C is given explicitly by

$$C := \frac{\Gamma\left(\frac{e_1}{2}\right)\Gamma\left(\frac{e_2}{2}\right)}{2\Gamma((e_1+e_2)/2)}\ Res_{z=e_1}\zeta_{\mathcal{D}(q_1,I_1)}\ Res_{z=e_2}\zeta_{\mathcal{D}(q_2,I_2)} > 0.$$

As a consequence of Theorem 2, we obtain

Corollary 1. $\zeta_{\mathcal{F}(\mathbf{q},\mathcal{I})}(s)$ *converges absolutely in the half-plane* $\{\Re(s) > \sigma_0(\mathbf{q},\mathcal{I})\}$ *and* $\sigma_0(\mathbf{q},\mathcal{I})$ *is its abscissa of convergence.*

In particular, the fractal dimension (see Definition 2 above) of the self-affine set $\mathcal{F}(\mathbf{q},\mathcal{I})$ *is equal to*

$$\sigma_0(\mathbf{q},\mathcal{I}) = \frac{\ln|I_1|}{\ln q_1} + \frac{\ln|I_2|}{\ln q_2}.$$

Remark 5. As we will see in §4.1 below, for $j = 1,2$ the set $\mathcal{D}(q_j,I_j)$ is a discrete self-similar subset of $\mathbb{R}$ of dimension $e_j = \frac{\ln|I_j|}{\ln q_j}$. So, Corollary 1 implies that the product formula

$$dim\mathcal{F}(\mathbf{q},\mathcal{I}) = dim\left(\mathcal{D}(q_1,I_1)\times\mathcal{D}(q_2,I_2)\right) = dim\mathcal{D}(q_1,I_1) + dim\mathcal{D}(q_2,I_2)$$

holds. Note that this result is not a priori obvious because, unlike the "smooth" situation, the product formula is not always valid for fractal dimensions (see [Fa], chap. 7, §7.1).

4. Proofs of Theorem 2 and Corollary 1

4.1. **Zeta function of $\mathcal{D}(q_j, I_j)$.** Let $j \in \{1, 2\}$. We will first derive from Theorem 1 the basic properties of zeta function of $\mathcal{D}(q_j, I_j)$.
First we remark that the following identity holds.

$$\mathcal{D}(q_j, I_j) = \bigsqcup_{r \in I_j} g_r^j \left(\mathcal{D}(q_j, I_j)\right), \qquad \text{where} \qquad g_r^j = q_j Id_{\mathbb{R}} + r \quad \forall r \in I_j. \tag{14}$$

Thus, $\mathcal{D}(q_j, I_j)$ is a discrete self-similar subset of $\mathbb{R}$.

$$\text{Set} \quad \delta_0^j(s) := \sum_{r \in I_j} q_j^{-s} - 1 = |I_j|\, q_j^{-s} - 1 = q_j^{e_j - s} - 1, \quad \text{where } e_j := \frac{\ln |I_j|}{\ln q_j}. \tag{15}$$

Since e_j is the unique real solution of the equation $\delta_0^j(s) = 0$, it is easy to see from Theorem 1 above and the simple form of the exponential polynomial $\delta_0^j(s)$ that the following lemma holds:

Lemma 2. *The zeta function*

$$s \mapsto \zeta_{\mathcal{D}(q_j, I_j)}(s) = \sum_{m \in \mathcal{D}(q_j, I_j)'} \frac{1}{m^s}$$

converges absolutely in the half-plane $\{\Re(s) > e_j\}$ and e_j is its abscissa of convergence. Moreover, the following properties are satisfied.

(1) $s \mapsto W_j(s) := \delta_0^j(s) \cdot \zeta_{\mathcal{D}(q_j, I_j)}(s)$ has holomorphic continuation with moderate growth to the half-plane $\{\Re(s) > e_j - 1\}$;
(2) $s \mapsto \zeta_{\mathcal{D}(q_j, I_j)}(s)$ has meromorphic continuation with moderate growth to the half-plane $\{\Re(s) > e_j - 1\}$;
(3) The poles of $\zeta_{\mathcal{D}(q_j, I_j)}(s)$ in the half-plane $\{\Re(s) > e_j - 1\}$ are located in the set $\mathcal{S}_j := \left\{ e_j + \frac{2\pi i k}{\ln q_j} \mid k \in \mathbb{Z} \right\}$ and are simple poles.
(4) e_j is a simple pole of $\zeta_{\mathcal{D}(q_j, I_j)}(s)$ and $Res_{s=e_j} \zeta_{\mathcal{D}(q_j, I_j)} > 0$.

4.2. **Proof of Theorem 2.** We will use in the sequel the notations of Lemme 2.

First we remark that if $\Re(s) > 2$, then

$$\sum_{\substack{(m_1,m_2)\in\mathcal{F}(\mathbf{q},\mathcal{I})\\ m_1,m_2\geq 1}} \left|\frac{1}{(m_1^2+m_2^2)^{s/2}}\right| \leq \sum_{(m_1,m_2)\in\mathbb{N}^2} \frac{1}{(m_1^2+m_2^2)^{\Re(s)/2}}$$

$$\leq \; 2^{-\Re(s)/2} \sum_{(m_1,m_2)\in\mathbb{N}^2} \frac{1}{(m_1 m_2)^{\Re(s)/2}} = 2^{-\Re(s)/2}\zeta\left(\Re(s)/2\right)^2 < +\infty.$$

It follows that the Dirichlet series defined by

$$\mathcal{G}(s) := \zeta_{\mathcal{F}(\mathbf{q},\mathcal{I})}(s) - \zeta_{\mathcal{D}(q_1,I_1)}(s) - \zeta_{\mathcal{D}(q_2,I_2)}(s) = \sum_{\substack{(m_1,m_2)\in\mathcal{F}(\mathbf{q},\mathcal{I})\\ m_1,m_2\geq 1}} \frac{1}{(m_1^2+m_2^2)^{s/2}} \tag{16}$$

converges absolutely in the half-plane $\{\Re(s) > 2\}$.

We deduce that $s \mapsto \zeta_{\mathcal{F}(\mathbf{q},\mathcal{I})}(s)$ also converges absolutely in the half-plane $\{\Re(s) > 2\}$, since the abscissa of absolute convergence e_j of $\zeta_{\mathcal{D}(q_j,I_j)}$ is in $(0,1)$ $\forall j = 1,2$. This ends the proof of point 1 of Theorem 2.

Recall now the Mellin-Barnes integral formula:

$$(1+\lambda)^{-s} = \frac{1}{2\pi i}\int_{(c)} \frac{\Gamma(s+z)\Gamma(-z)}{\Gamma(s)}\lambda^z dz, \tag{17}$$

where $s,\lambda \in \mathbb{C}$, $\Re s > 0$, $\lambda \neq 0$, $|\arg\lambda| < \pi$ (the principal branch), $-\Re s < c < 0$, and the path of the integral is the vertical line $\Re z = c$ (see [WW]).

Fix temporarily $s \in \mathbb{C}$ such that that $\Re(s) > 2$. Choose a real c verifying

$$\frac{e_1}{2} - \frac{\Re(s)}{2} < c < -\frac{e_2}{2}, \qquad \text{where} \qquad e_j = \frac{\ln|I_j|}{\ln q_j} \in (0,1)\ \forall j = 1,2. \tag{18}$$

Mellin-Barnes formula (17) implies then that for $m_1, m_2 \in \mathbb{N}$,

$$(m_1^2+m_2^2)^{-s/2} = m_1^{-s}\left(1+\frac{m_2^2}{m_1^2}\right)^{-s/2}$$

$$= \frac{1}{2\pi i}\int_{(c)} \frac{\Gamma(s/2+z)\Gamma(-z)}{\Gamma(s/2)} m_2^{2z} m_1^{-s-2z}\, dz. \tag{19}$$

Lemma 2 and (18) imply that the series $\zeta_{\mathcal{D}(q_1,I_1)}(s+2z)$ and $\zeta_{\mathcal{D}(q_2,I_2)}(-2z)$ converge absolutely for $z \in \mathbb{C}$ verifying $\Re(z) = c$. Substituting (19) into (16) and changing the order of integration and summation, implies then

that

$$\mathcal{G}(s) = \frac{1}{2\pi i}\int_{(c)} \frac{\Gamma(s/2+z)\Gamma(-z)}{\Gamma(s/2)} \sum_{\substack{(m_1,m_2)\in\mathcal{F}(\mathfrak{q},\mathcal{I})\\ m_1,m_2\geq 1}} m_2^{2z} m_1^{-s-2z}\, dz$$

$$= \frac{1}{2\pi i}\int_{(c)} \frac{\Gamma(s/2+z)\Gamma(-z)}{\Gamma(s/2)}\, \zeta_{\mathcal{D}(q_1,I_1)}(s+2z)\, \zeta_{\mathcal{D}(q_2,I_2)}(-2z)\, dz. \quad (20)$$

Let $\kappa \in \left(0, \dfrac{1-e_2}{2}\right)$. Now we shift the path of integration to the right to $\Re z = \kappa$. We claim that *this shifting is possible*. In fact, in the strip $c \leq \Re z \leq \kappa$, by Stirling's formula we have

$$\Gamma(s/2+z)\Gamma(-z) \ll e^{(\pi/4)|\Im s|-\pi|\Im z|}(|\Im s|+|\Im z|+1)^{\Re(s/2)+\Re z-1/2} \times(|\Im z|+1)^{-\Re z-1/2} \quad (|z|\gg 1).$$

The factor $\zeta_{\mathcal{D}(q_1,I_1)}(s+2z)$ is $O(1)$, because it is in the domain of absolute convergence.

Moreover, Lemma 2 implies that $\zeta_{\mathcal{D}(q_2,I_2)}$ is of moderate growth and therefore there exists a constant $A = A(\kappa) > 0$ such that if we set $\mathcal{L}_2 := \left\{-\frac{e_2}{2} + \frac{\pi i k}{\ln q_2} \mid k \in \mathbb{Z}\right\}$, then for any $\varepsilon > 0$

$$\zeta_{\mathcal{D}(q_2,I_2)}(-2z) \ll_\varepsilon (|\Im z|+1)^A \quad (21)$$

uniformly in z such that $c \leq \Re z \leq \kappa$ and $d(z,\mathcal{L}_2) \geq \varepsilon$.

These estimates imply that for $\varepsilon > 0$ small enough, we have uniformly in z such that $c \leq \Re z \leq \kappa$ and $d(z, \mathcal{L}_2 \cup \{0\}) \geq \varepsilon$:

$$\Gamma(s/2+z)\Gamma(-z)\zeta_{\mathcal{D}(q_2,I_2)}(-2z) \ll_\varepsilon \quad (22)$$
$$e^{(\pi/4)|\Im s|-\pi|\Im z|}(|\Im s|+|\Im z|+1)^{\Re(s/2)+\Re z-1/2}(|\Im z|+1)^{A-\Re z-1/2}.$$

Therefore, we see that the integrand on the right-hand side of (20) is of exponential decay. This implies that the integral is absolutely convergent, and the indicated shifting of the path of integral is possible. The proof of the claim is complete.

Carrying out this shifting, we find that the relevant poles are $z = 0$ (from $\Gamma(-z)$) and $z = -\frac{e_2}{2} + \frac{\pi i k}{\ln q_2}$ ($k \in \mathbb{Z}$) (from the zeta factor $\zeta_{\mathcal{D}(q_2,I_2)}(-2z)$). Counting the residues, we obtain from (20) that for $s \in \mathbb{C}$ such that $\Re(s) > 2$ we have

$$\mathcal{G}(s) = \zeta_{\mathcal{D}(q_1,I_1)}(s)\zeta_{\mathcal{D}(q_2,I_2)}(0) + \frac{1}{2}\mathcal{V}(s) + \mathcal{R}_\kappa(s), \quad (23)$$

where

$$\mathcal{V}(s) := \sum_{k\in\mathbb{Z}} \frac{\Gamma\left(\frac{s}{2}-\frac{e_2}{2}+\frac{\pi ik}{\ln q_2}\right)\Gamma\left(\frac{e_2}{2}-\frac{\pi ik}{\ln q_2}\right)}{\Gamma(s/2)} \times\zeta_{\mathcal{D}(q_1,I_1)}\left(s-e_2+\frac{2\pi ik}{\ln q_2}\right) \; Res_{z=e_2-\frac{2\pi ik}{\ln q_2}}\zeta_{\mathcal{D}(q_2,I_2)}, \quad (24)$$

and

$$\mathcal{R}_\kappa(s) = \frac{1}{2\pi i}\int_{(\kappa)} \frac{\Gamma(s/2+z)\Gamma(-z)}{\Gamma(s/2)}\; \zeta_{\mathcal{D}(q_1,I_1)}(s+2z)\; \zeta_{\mathcal{D}(q_2,I_2)}(-2z)\; dz. \quad (25)$$

In order to conclude we need the following two lemmas:

Lemma 3. *(1) The function $s\mapsto \mathcal{R}_\kappa(s)$ has holomorphic continuation to the half-plane $\{\Re(s) > e_1 - 2\kappa\}$;*

(2) The function $s\mapsto \mathcal{V}(s)$ is holomorphic in the domain $\{\Re(s) > e_1+e_2-1\}\setminus\mathcal{S}$, where

$$\mathcal{S} := \left\{ e_1+e_2+2\pi i\left(\frac{k_1}{\ln q_1}+\frac{k_2}{\ln q_2}\right) \mid (k_1,k_2)\in\mathbb{Z}^2\right\};$$

Lemma 4. *(1) For $k\in\mathbb{Z}^* = \mathbb{Z}\setminus\{0\}$, the function $s\mapsto \zeta_{\mathcal{D}(q_1,I_1)}\left(s-e_2+\frac{2\pi ik}{\ln q_2}\right)$ is regular in the point $s=e_1+e_2$;*

(2) There exists a constant $D = D(q_1,q_2) > 0$ such that

$$\zeta_{\mathcal{D}(q_1,I_1)}\left(e_1+x+\frac{2\pi ik}{\ln q_2}\right) \ll |k|^D$$

uniformly in $k\in\mathbb{Z}^*$ and $x\in[0,1]$.

(3) e_1+e_2 is a singular point of $\mathcal{V}(s)$. More precisely, we have

$$\mathcal{V}(e_1+e_2+x) \sim \frac{B}{x} \quad \text{as } x\to 0 \ (x>0),$$

where

$$B := \frac{\Gamma\left(\frac{e_1}{2}\right)\Gamma\left(\frac{e_2}{2}\right)}{\Gamma((e_1+e_2)/2)}\; Res_{z=e_1}\zeta_{\mathcal{D}(q_1,I_1)}\; Res_{z=e_2}\zeta_{\mathcal{D}(q_2,I_2)} > 0. \quad (26)$$

4.2.1. *Proof of Lemma 3.* • **Proof of point 1 of Lemma 3:** Since $0 > -2\kappa > e_2-1$, it is easy to see that the following two properties hold:

(1) $(s,z)\mapsto \frac{\Gamma(s/2+z)\Gamma(-z)}{\Gamma(s/2)}\; \zeta_{\mathcal{D}(q_1,I_1)}(s+2z)\; \zeta_{\mathcal{D}(q_2,I_2)}(-2z)$ is a continuous function in the set $\{\Re(s) > e_1-2\kappa\}\times\{\Re(z)=\kappa\}$ and;

(2) for $z \in \mathbb{C}$ such that $\Re(z) = \kappa$, the function $s \mapsto \frac{\Gamma(s/2+z)\Gamma(-z)}{\Gamma(s/2)}\, \zeta_{\mathcal{D}(q_1,I_1)}(s+2z)\, \zeta_{\mathcal{D}(q_2,I_2)}(-2z)$ is holomorphic in the domain $\{\Re(s) > e_1 - 2\kappa\}$.

Furthermore, for any compact $K \subset \{\Re(s) > e_1 - 2\kappa\}$, we have

$$\zeta_{\mathcal{D}(q_1,I_1)}(s+2z) \leq \zeta_{\mathcal{D}(q_1,I_1)}\left(\min_{s\in K} Re(s) + 2\kappa\right) \ll_K 1,$$

uniformly in $s \in K$ and z such that $\Re(z) = \kappa$.

Combining this with the estimate (22) implies that for any compact $K \subset \{\Re(s) > e_1 - 2\kappa\}$, we have uniformly in $(s,z) \in K \times \{\Re(z) = \kappa\}$

$$\frac{\Gamma(s/2+z)\Gamma(-z)}{\Gamma(s/2)}\, \zeta_{\mathcal{D}(q_1,I_1)}(s+2z)\, \zeta_{\mathcal{D}(q_2,I_2)}(-2z) \ll_K e^{-\pi|\Im z|}(|\Im z|+1)^{A+B-1},$$

where $B = \frac{1}{2}\max_{s\in K} \Re(s)$. Point 1 of Lemme 3 follows then from the theorem of differentiation under the integral signs. □

• **Proof of point 2 of Lemma 3:**

Recall that the sets $\mathcal{S}_1$ and $\mathcal{S}$ are defined by

$$\mathcal{S}_1 := \left\{ e_1 + \frac{2\pi i k}{\ln q_1} \mid k \in \mathbb{Z} \right\}$$

and

$$\mathcal{S} := \left\{ e_1 + e_2 + 2\pi i \left(\frac{k_1}{\ln q_1} + \frac{k_2}{\ln q_2} \right) \mid (k_1,k_2) \in \mathbb{Z}^2 \right\}.$$

Let $\varepsilon > 0$. Let K be a compact subset of $\{\Re(s) > e_1 + e_2 - 1\} \bigcap \{s \in \mathbb{C} \mid d(s,\mathcal{S}) > \varepsilon\}$.

First we remark that if $s \in \mathbb{C}$ verifies $d(s,\mathcal{S}) = \inf_{u\in\mathcal{S}} |s-u| \geq \varepsilon$, then $d\left(s - e_2 + \frac{2\pi i k}{\ln q_2}, \mathcal{S}_1\right) \geq \varepsilon$ for all $k \in \mathbb{Z}$. It follows then from the moderate growth of $\zeta_{\mathcal{D}(q_1,I_1)}$ that there exists a positive constant α such that

$$\zeta_{\mathcal{D}(q_1,I_1)}\left(s - e_2 + \frac{2\pi i k}{\ln q_2}\right) \ll_K (1+|k|)^{\alpha} \quad \text{uniformly in } s \in K \text{ and } k \in \mathbb{Z}. \tag{27}$$

Set $\theta = \inf\left(\frac{\pi}{\ln q_2}, \frac{1}{2}\right)$ and $\mathcal{S}_2 := \left\{ e_2 + \frac{2\pi i k}{\ln q_2} \mid k \in \mathbb{Z} \right\}$. The moderate growth of $\zeta_{\mathcal{D}(q_2,I_2)}$ and points 2 and 3 of lemma 2 imply then that there exists $\beta > 0$ such that

$$\zeta_{\mathcal{D}(q_2,I_2)}(s) \ll (1+|s|)^{\beta}$$

uniformly in $s \in \mathbb{C}$ such that $e_2 - \frac{1}{2} \leq \Re(s) \leq e_2 + \frac{1}{2}$ and $d(s,S_2) \geq \theta$.

Let $k \in \mathbb{Z}$ and $z_k := e_2 - \frac{2\pi i k}{\ln q_2}$.

Since $|s-z_k|=\theta$ implies that $e_2-\frac{1}{2}\leq\Re(s)\leq e_2+\frac{1}{2}$ and $d(s,S_2)\geq\theta$, we deduce from Cauchy formula and the previous estimate that

$$Res_{s=z_k}\zeta_{\mathcal{D}(q_2,I_2)}=\frac{1}{2\pi i}\int_{|s-z_k|=\theta}\frac{\zeta_{\mathcal{D}(q_2,I_2)}(s)}{s-z_k}\,ds\ll\max_{|s-z_k|=\theta}(1+|s|)^{\beta}\ll(1+|k|)^{\beta}.$$

Thus, we have proved that

$$Res_{z=e_2-\frac{2\pi ik}{\ln q_2}}\zeta_{\mathcal{D}(q_2,I_2)}\ll(1+|k|)^{\beta}\quad\text{uniformly in } k\in\mathbb{Z}. \tag{28}$$

Furthermore, Stirling's formula implies that

$$\frac{\Gamma\left(\frac{s}{2}-\frac{e_2}{2}+\frac{\pi ik}{\ln q_2}\right)\Gamma\left(\frac{e_2}{2}-\frac{\pi ik}{\ln q_2}\right)}{\Gamma(s/2)}\ll_K(1+|k|)^{M/2-1}\,e^{-\frac{\pi^2|k|}{\ln q_2}} \tag{29}$$

uniformly in $s\in K$ and $k\in\mathbb{Z}$, where $M=\max_{s\in K}\Re(s)$.

Combining (27), (28) and (29) implies that the series defining the function $\mathcal{V}$ (see (24)) converges uniformly in the compact K. Since in addition each term of this series is holomorphic in the domain $\{\Re(s)>e_1+e_2-1\}\bigcap\{s\in\mathbb{C}\mid d(s,\mathcal{S})>\varepsilon\}$, we conclude by letting $\varepsilon\to 0$ that the function $s\mapsto\mathcal{V}(s)$ is holomorphic in the domain $\{\Re(s)>e_1+e_2-1\}\setminus\mathcal{S}$. This ends the proof of the point 2 and of Lemma 3. □

4.2.2. *Proof of Lemma 4.* • **Proof of point 1 of Lemma 4:**
Let $k\in\mathbb{Z}^*=\mathbb{Z}\setminus\{0\}$. Assume, for the sake of contradiction, that the function $s\mapsto\zeta_{\mathcal{D}(q_1,I_1)}\left(s-e_2+\frac{2\pi ik}{\ln q_2}\right)$ is not regular in $s=e_1+e_2$. It follows that there exists $k'\in\mathbb{Z}$ such that $e_1+\frac{2\pi ik}{\ln q_2}=e_1+\frac{2\pi ik'}{\ln q_1}$ and therefore that $q_1^k=q_2^{k'}$. This is a contradiction, since q_1 and q_2 are multiplicatively independent (see (13)). This ends the proof of point 1 of Lemma 4. □

• **Proof of point 2 of Lemma 4:**
Point 1 of Lemma 2 and point 1 of Lemma 4 imply that for $k\in\mathbb{Z}^*$ and $x\in[0,1]$, we have

$$\zeta_{\mathcal{D}(q_1,I_1)}\left(e_1+x+\frac{2\pi ik}{\ln q_2}\right)=\frac{W_1\left(e_1+x+\frac{2\pi ik}{\ln q_2}\right)}{\delta_0^1\left(e_1+x+\frac{2\pi ik}{\ln q_2}\right)}, \tag{30}$$

where $s\mapsto W_1(s)$ is a holomorphic function with moderate growth in $\{\Re(s)>e_1-1\}$ and

$$\delta_0^1(s)=|I_1|q_1^{-s}-1=q_1^{e_1-s}-1.$$

Set $\gamma := \frac{\ln q_1}{\ln q_2}$. We have uniformly in $k \in \mathbb{Z}^*$ and $x \in [0,1]$:

$$\begin{aligned}\left|\delta_0^1\left(e_1 + x + \frac{2\pi i k}{\ln q_2}\right)\right| &= |q_1^{-x}e^{-2\pi i k\gamma} - 1| \\ &\geq \max\left(|q_1^{-x}\cos(2\pi k\gamma) - 1|, |q_1^{-x}\sin(2\pi k\gamma)|\right) \\ &\geq \max\left(|q_1^{-x}\cos\left(2\pi\langle k\gamma\rangle\right) - 1|, |q_1^{-x}\sin\left(2\pi\langle k\gamma\rangle\right)|\right),\end{aligned} \tag{31}$$

where we denote here by $\langle t\rangle \in [-1/2, 1/2]$ the difference between t and its nearest integer.

Let $k \in \mathbb{Z}^*$. We have necessarily $|\langle k\gamma\rangle| \leq \frac{1}{4}$ or $\frac{1}{4} \leq |\langle k\gamma\rangle| \leq \frac{1}{2}$. Furthermore,

(1) If $|\langle k\gamma\rangle| \leq \frac{1}{4}$, then $0 \leq 2\pi|\langle k\gamma\rangle| \leq \frac{\pi}{2}$ which implies (by concavity of sin over $[0, \pi/2]$) that

$$|\sin\left(2\pi\langle k\gamma\rangle\right)| = \sin\left(2\pi|\langle k\gamma\rangle|\right) \geq \frac{2}{\pi} \times 2\pi|\langle k\gamma\rangle| \geq |\langle k\gamma\rangle|;$$

(2) If $\frac{1}{4} \leq |\langle k\gamma\rangle| \leq \frac{1}{2}$, then $\frac{\pi}{2} \leq 2\pi|\langle k\gamma\rangle| \leq \pi$ and therefore $\cos\left(2\pi|\langle k\gamma\rangle|\right) \leq 0$.

Combining these two points and (31) implies that we have uniformly in $k \in \mathbb{Z}^*$ and $x \in [0,1]$:

$$\left|\delta_0^1\left(e_1 + x + \frac{2\pi i k}{\ln q_2}\right)\right| = |q_1^{-x}e^{-2\pi i k\gamma} - 1| \geq q_1^{-x}|\langle k\gamma\rangle| \geq q_1^{-1}|\langle k\gamma\rangle|. \tag{32}$$

We will now use Baker's deep result ([Ba], Theorem 3.1) on the lower bound for linear forms in logarithms, to precise our estimate (32).
Since q_1 and q_2 are multiplicatively independent, its follows that for any $(a,b) \in \mathbb{Z}^2 \setminus \{(0,0)\}$ $a\ln q_1 + b\ln q_2 \neq 0$. Baker's Theorem ([Ba], Theorem 3.1) implies then that there exists a positive constant $c = c(q_1, q_2) > 0$ such that

$$|a\ln q_1 + b\ln q_2| \gg (\max(|a|, |b|))^{-c} \tag{33}$$

uniformly in $(a,b) \in \mathbb{Z}^2 \setminus \{(0,0)\}$.
Let $k \in \mathbb{Z}^*$. There exists $n_k \in \mathbb{Z}$ such that $\langle k\gamma\rangle = k\gamma - n_k$ and (33) implies that

$$|\langle k\gamma\rangle| = |k\gamma - n_k| = \frac{1}{\ln q_2}|k\ln q_1 - n_k\ln q_2| \gg (\max(|k|, |n_k|))^{-c} \gg |k|^{-c}.$$

We deduce then from (32) that there exists a constant $c = c(q_1, q_2) > 0$ such that

$$\left|\delta_0^1\left(e_1 + x + \frac{2\pi i k}{\ln q_2}\right)\right| \gg |k|^{-c}, \tag{34}$$

uniformly in $k \in \mathbb{Z}^*$ and $x \in [0,1]$.

By using in addition the fact that W_1 is holomorphic and has moderate growth in $\{\Re(s) > e_1 - 1\}$, we deduce from (30) and (34) that there exists a constant $D = D(q_1, q_2) > 0$ such that

$$\zeta_{\mathcal{D}(q_1,I_1)}\left(e_1 + x + \frac{2\pi i k}{\ln q_2}\right) \ll |k|^D, \tag{35}$$

uniformly in $k \in \mathbb{Z}^*$ and $x \in [0,1]$. This ends the proof of point 2 of Lemma 4. □

• **Proof of point 3 of Lemma 4:**
Stirling's formula implies that

$$\frac{\Gamma\left(\frac{e_1+x}{2} + \frac{\pi i k}{\ln q_2}\right)\Gamma\left(\frac{e_2}{2} - \frac{\pi i k}{\ln q_2}\right)}{\Gamma((e_1+e_2+x)/2)} \ll (1+|k|)^{\frac{e_1+e_2-1}{2}}\ e^{-\frac{\pi^2|k|}{\ln q_2}} \tag{36}$$

uniformly in $x \in [0,1]$ and $k \in \mathbb{Z}$.
Combining (28), (35) and (36) implies that the series

$$x \mapsto T(x) \ := \sum_{k\in\mathbb{Z}^*} \frac{\Gamma\left(\frac{e_1+x}{2} + \frac{\pi i k}{\ln q_2}\right)\Gamma\left(\frac{e_2}{2} - \frac{\pi i k}{\ln q_2}\right)}{\Gamma((e_1+e_2+x)/2)} \times \zeta_{\mathcal{D}(q_1,I_1)}\left(e_1 + x + \frac{2\pi i k}{\ln q_2}\right)\ Res_{z=e_2-\frac{2\pi i k}{\ln q_2}} \zeta_{\mathcal{D}(q_2,I_2)}$$

converges uniformly in the interval $[0,1]$ and therefore defines a continuous function in $[0,1]$.

Moreover, point 2 of Lemma 3 implies that the function $\mathcal{V}$ defined by (24) is holomorphic in the half-plane $\{\Re(s) > e_1 + e_2\}$ and that for all $x \in (0,1)$,

$$\mathcal{V}(e_1+e_2+x) = \frac{\Gamma\left(\frac{e_1+x}{2}\right)\Gamma\left(\frac{e_2}{2}\right)}{\Gamma((e_1+e_2+x)/2)}\ \zeta_{\mathcal{D}(q_1,I_1)}\,(e_1+x)\ Res_{z=e_2}\zeta_{\mathcal{D}(q_2,I_2)} + T(x).$$

Since the function T is continuous in $[0,1]$, it follows then from point 4 of Lemma 2 that

$$\mathcal{V}(e_1+e_2+x) \sim \frac{B}{x} \quad \text{as } x \to 0\ (x>0),$$

where

$$B := \frac{\Gamma\left(\frac{e_1}{2}\right)\Gamma\left(\frac{e_2}{2}\right)}{\Gamma((e_1+e_2)/2)}\ Res_{z=e_1}\zeta_{\mathcal{D}(q_1,I_1)}\ Res_{z=e_2}\zeta_{\mathcal{D}(q_2,I_2)} > 0.$$

We deduce in particular that $s = e_1 + e_2$ is a singular point of the function $\mathcal{V}$. This ends the proof of Lemma 4. □

4.2.3. *End of the proof of Theorem 2.* We will now carry out the proof of Theorem 2 by using lemmas 2, 3 and 4 that we have established above. We will also continue to use the notations introduced in the statement of Theorem 2.

Fix $\kappa \in \left(0, \dfrac{1-e_2}{2}\right)$. Combining (16) and (23) imply that for $s \in \mathbb{C}$ such that $\Re(s) > 2$, we have

$$\zeta_{\mathcal{F}(\mathbf{q},\mathcal{I})}(s) = \left(1 + \zeta_{\mathcal{D}(q_2,I_2)}(0)\right) \zeta_{\mathcal{D}(q_1,I_1)}(s) + \zeta_{\mathcal{D}(q_2,I_2)}(s) + \frac{1}{2}\mathcal{V}(s) + \mathcal{R}_\kappa(s). \tag{37}$$

It follows then from lemmas 2 and 3 that $s \mapsto \zeta_{\mathcal{F}(\mathbf{q},\mathcal{I})}(s)$ has holomorphic continuation to the domain $\{\Re(s) > \sigma_1(\mathbf{q},\mathcal{I})\} \setminus \mathcal{S}$, where

$$\sigma_1(\mathbf{q},\mathcal{I}) := \max(e_1, e_2) < \sigma_0(\mathbf{q},\mathcal{I}) = e_1 + e_2.$$

Moreover, since the functions $\zeta_{\mathcal{D}(q_1,I_1)}$, $\zeta_{\mathcal{D}(q_2,I_2)}$ and $\mathcal{R}_\kappa$ are regular in the point $s = \sigma_0(\mathbf{q},\mathcal{I}) = e_1 + e_2$, it follows from (37) and point 3 of Lemme 4 that

$$\zeta_{\mathcal{F}(\mathbf{q},\mathcal{I})}(\sigma) \sim \frac{(B/2)}{\sigma - \sigma_0(\mathbf{q},\mathcal{I})} \quad \text{as } \sigma \to \sigma_0(\mathbf{q},\mathcal{I}) \quad (\sigma > \sigma_0(\mathbf{q},\mathcal{I}))\,, \tag{38}$$

where the positive constant B is defined by (26).
This ends the proof of Theorem 2. □

4.3. **Proof of Corollary 1.** We will continue to use notations of Theorem 2.

On the one hand, we remark that

$$\{\Re(s) > \sigma_0(\mathbf{q},\mathcal{I})\} \subset \{\Re(s) > \sigma_1(\mathbf{q},\mathcal{I})\} \setminus \mathcal{S}.$$

Points 2 and 3 of Theorem 2 imply then that $s \mapsto \zeta_{\mathcal{F}(\mathbf{q},\mathcal{I})}(s)$ has holomorphic continuation to the half-plane $\{\Re(s) > \sigma_0(\mathbf{q},\mathcal{I})\}$ and that $\sigma_0(\mathbf{q},\mathcal{I})$ is a singular point of $\zeta_{\mathcal{F}(\mathbf{q},\mathcal{I})}$. Thus,

$$\sigma_0(\mathbf{q},\mathcal{I}) \text{ is the largest real singular point of } \zeta_{\mathcal{F}(\mathbf{q},\mathcal{I})}. \tag{39}$$

On the other hand, a classical theorem of Landau (see [La], [HR]) states that, if a Dirichlet series has non-negative coefficients, then it has a singularity on the real line at its abscissa of convergence. Combining Landau's result and (39) implies then that $\sigma_0(\mathbf{q},\mathcal{I})$ is equal to the the abscissa of convergence of the Dirichlet with non-negative coefficients $\zeta_{\mathcal{F}(\mathbf{q},\mathcal{I})}(s)$. This ends the proof of Corollary 1. □

References

[AB] **J.-P. Allouche,V. Berthé**. *Triangle de Pascal, complexité et automates*. Bull. Belg. Math. Soc. 4 (1997) 1-23.

[AHPPS] **J.-P. Allouche, F.v. Haeseler, H.-O. Peitgen, A. Petersen, G. Skordev**. *Automaticity of double sequences generated by one-dimensional linear cellular automata*. Theoret. Comput. Sci. 188 (1997) 195-209.

[APM] **J.-P. Allouche, J. Peyrière, and M. Mendès France**. *Automatic Dirichlet series*. J. Number Theory 81 (2000), 359-373.

[AS] **J.-P. Allouche, J. Shallit**. *Automatic Sequences: Theory, Applications, Generalizations*. Cambridge University Press, Cambridge, 2003.

[Ba] **A. Baker**. *Transcendental Number Theory*. Cambridge University Press, 1975.

[BG] **D. Barbolosi, P.J. Grabner**. *Distribution des coefficients multinomiaux et q-binomiaux modulo p*. Indag. Math.(N.S.) 7 (1996) 129-135.

[BT1] **M. Barlow and S.J. Taylor**. *Fractal Dimension of sets in Discrete Spaces*. J. Phys. A., 22 (1989) 2621-2626.

[BT2] **M. Barlow and S.J. Taylor**. *Defining Fractal Subsets of* $\mathbb{Z}^d$. Proc. London Math. Soc., 64 (1992) 125-152.

[DGLMM] **D. Doty, X. Gu, J. H. Lutz, E. Mayordomo, and P. Moser**. *Zeta-dimension*, in Proceedings of the 30th International Symposium on Mathematical Foundations of Computer Science. Springer-Verlag (2005) 283-294.

[E] **D. Essouabri**. *Zeta Functions associated to Pascal's Triangle mod p*. Jap. J. Math. 31 (2005) 157-174.

[EL1] **D. Essouabri and B. Lichtin**. *Zeta functions of discrete self-similar sets*. Adv. Math. 232 (2013) 142-187.

[EL2] **D. Essouabri and B. Lichtin**. *$k-$point configurations of discrete self-similar sets. Contemporary Mathematics* 600 (2013) 21-50.

[EL3] **D. Essouabri and B. Lichtin**. *Zeta functions and solutions of Falconer-type problems for self-similar subsets of* $\mathbb{Z}^n$. *Proc. Lond. Math. Soc.(3)* 111 (2015) 1163-1205.

[EL4] **D. Essouabri and B. Lichtin** *Sum-product estimates for self similar subsets of* $\mathbb{Z}$ *and Fractal zeta functions. Proceedings of the RIMS conference "Analytic Number Theory and Related Areas" Kyoto, 2015. RIMS Kôkyûroku No. 2014.*

[EL5] **D. Essouabri and B. Lichtin**. *Thick self similar sets are asymptotically generic. Annales Academiæ Scientiarum Fennicæ Mathematica*. Volumen 43, 2018, 835-857.

[EL6] **D. Essouabri and B. Lichtin**. *Zeta functions of discrete self similar sets and applications to Point Configuration and Sum-Product type problems. To appear in IMRN.*

[Fa] **K. J. Falconer**. *Fractal Geometry-Mathematical Foundations and Applications*. Wiley & Sons, 1990.

[HR] **G.H. Hardy and M. Reisz**. *The General Theory of Dirichlet's Series*. Hafner Publishing, New York (1972).

[H] **J.E. Hutchinson**. *Fractals and Self-Similarity*. Indiana University Math. J., 30 (1981) 713-747.

[La] **E. Landau**. *Handbuch der Lehre von der Verteilung der Primzahlen*, Volume II, Druck und Verlag von B.G. Teubner, Leipzig and Berlin, 1909.

[LF] **M.L. Lapidus and M. van Frankenhuysen**. *Fractal Geometry, Complex Dimensions, and Zeta Functions: Geometry and Spectra of Fractal Strings* . Springer-Verlag (2006).

[Mor] **P.A.P. Moran** *Additive functions of intervals and Hausdorff dimension.* Proc. Cambridge Phil. Soc., 42 (1946) 15-23.

[S] **O. Salon**. *Suites automatiques à multi-indices et algébricité.* C. R. Acad. Sci. Paris Ser. I Math., 305(12):501–504, 1987.

[St] **R. Strichartz**. *Fractals in the large.* Canad. J. Math., 50 (1996) 638-657.

[WW] **E. T. Whittaker and G. N. Watson**. *A Course of Modern Analysis*, 4th ed., Cambridge Univ. Press, 1927.

Univ. Lyon, UJM-Saint-Etienne, CNRS, Institut Camille Jordan UMR 5208, Faculté des Sciences et Techniques, 23 rue du Doc. Paul Michelon, F-42023, Saint-Etienne, France

Email: driss(dot)essouabri(at)univ-st-etienne(dot)fr

URL: https://perso.univ-st-etienne.fr/esdr9935/Page_D.Essouabri.htm

Voronoï's Impact on Modern Science, Book 6, Volume 2
Proceedings of the Sixth International Conference on Analytic Number Theory and Spatial Tessellations

CORRELATIONS IN A RANDOM UNIVERSE

Vincent Icke (*The Netherlands*)

Abstract. This is a very brief summary of some key stations along my path through the theory and applications of the Voronoi Tessellation, and its dual, the Delaunay Triangulation. I show in some detail why cosmic structures on the scale above a hundred million light years should show Voronoi-Delaunay patterns, which have become known as the 'cosmic web'. This exposition is followed by applications of tessellation techniques to stellar seismology and radiative transfer. I conclude by showing a few results of exotic Voronoi tessellations in graphic art.

Introduction

I feel honoured by the organisers of this conference for having invited me to present a contribution in the memory of Georgy Voronoi. I am grateful for the distinguished opportunity they have offered me. My intention is to show a little bit of my work from the past to the present, insofar as it is related to Voronoi's mathematics. The main subjects of the presentation are: first, the formation of the largest structures in the Universe; second, some applications of Voronoi tessellations and their dual Delaunay networks, in particular a novel Markov-process approach to radiative transfer; third, a few examples of Voronoi techniques from my studio as a visual artist.

Received August 2, 2020.

2010 *Mathematics Subject Classification.* Primary 01A23; Secondary 45B67, 89C10.

Key words and phrases. Cosmology, astrophysics, visual art.

I am endebted to my colleagues Bernard Jones, Joan Centrella, and Adrian Melott, for candid and lively discussions about cosmic structure formation, which put me on the trail that led me to Voronoi's work. I am grateful to my teachers at the Gerrit Rietveld Academy of Art for the time and energy they invested in my education there. I am delighted by the unfailing enthusiasm of the members of my Astrophysics Theory Group at Sterrewacht Leiden, in particular the 'Voronoi Platoon' Garrelt Mellema, Jelle Ritzerveld, Jan-Pieter Paardekooper, Chael Kruip and Nicola Clementel. Furthermore, I thank the referee for pertinent criticism of an earlier version of this paper, which has led to significant improvements. A word of special thanks to Rien van de Weygaert, who has been, and still is, a trusted comrade in the cosmological jungle.

1. The Cosmic Web

Looking out in space is looking back in time. Some of the galaxies we see in the deep Universe have just been born. But at the time when we receive their light, they are already 10 billion years older. How do these structures form? Gravity compresses matter. Today's calculations use supercomputers, but thirty years ago the basics were much simpler. We knew already that matter in the early Universe was not distributed smoothly, but had small fluctuations, with a mean amplitude of 10^{-5}. Therefore, if in the beginning there is matter with a density that happens to be a little above average, that region will start to contract. But elsewhere the matter density is below average. Therefore such regions expand a little faster than the average Universe. Matter then flows away from those low-density regions.

Consider what happens when regions with above-average density contract, and regions with lower density expand. The shape of self-gravitating matter on cosmological scales must be highly asymmetrical, because of the an effect described in a nice paper by Lin, Mestel & Shu [7], which I generalized in my PhD Thesis [4]. The potential Φ near any point (x, y, z) of a self-gravitating medium can be written as

$$\Phi = \sum_{ijk} a_{ijk} x^i y^j z^k \tag{1}$$

Near a density maximum, the leading terms are the quadratic ones, which, by a suitable orientation of Cartesian coordinates, can be written as

$$\Phi = Ax^2 + By^2 + Cz^2 + \cdots \tag{2}$$

Neglecting terms of higher than second order, this is the potential of a homogeneous ellipsoid. That should be no surprise: the smallest closed contours in any topographical map are ellipses.

The collapse of high-density regions can thus be approximated by considering the homologous motion of ellipsoids. Consider, then, the Newtonian collapse of a homogeneous ellipsoid. Suppose that a particle within such a mass distribution were initially located at (a, b, c), and that at some later time t it had moved to the point $(aX(t), bY(t), cZ(t))$. Then the density ρ would evolve according to

$$\rho(t) = \rho_0 / XYZ \tag{3}$$

The equations of motion for the scaling functions X, Y, and Z are found as follows. The potential Φ obeys

$$\Phi = k(\alpha x^2 + \beta y^2 + \gamma z^2) + \cdots \simeq k(\alpha a^2 X^2 + \beta b^2 Y^2 + \gamma c^2 Z^2) \tag{4}$$

and Poisson's Equation demands that

$$k(\alpha + \beta + \gamma) = 2\pi G\rho \tag{5}$$

The components of the gravitational force are $-\partial\Phi/\partial x = -\frac{1}{X}\partial\Phi/\partial a$ *et cycl.*, so that the equations of motion become

$$-\frac{1}{X}\frac{d^2X}{dt^2} = 2\pi G\rho\alpha \ ; \quad -\frac{1}{Y}\frac{d^2Y}{dt^2} = 2\pi G\rho\beta \ ; \quad -\frac{1}{Z}\frac{d^2Z}{dt^2} = 2\pi G\rho\gamma \tag{6}$$

where the functions α, β, and γ are defined as

$$\alpha = abc\int_0^\infty \frac{ds}{(a^2+s)\Delta} \quad \text{et cycl.} \tag{7}$$

in which

$$\Delta^2 \equiv (a^2+s)(b^2+s)(c^2+s) \tag{8}$$

Here a, b, and c are identified with the axes of the ellipsoid.

Now comes a crucial observation: without loss of generality, one may order the axes according to $a > b > c$, in which case $\alpha < \beta < \gamma$, so that

$$-\frac{1}{X}\frac{d^2X}{dt^2} < -\frac{1}{Y}\frac{d^2Y}{dt^2} < -\frac{1}{Z}\frac{d^2Z}{dt^2} \tag{9}$$

Consequently, the axial ratios $a : b : c$ always increase with time, and *slight initial asphericities are amplified during the collapse.* This secular increase of aspherical perturbations provides an explanation for the filamentary appearance of megaparsec structures (i.e. larger than a few million light years). Although the authors [7] did not look beyond galactic scales, their theorem was eminently suited for megaparsec structures. For the contraction described, the velocities inside the ellipsoid are linear functions of position: *the collapse produces a Hubble-type velocity field.* Moreover, Poisson's Equation (5) implies that the potential function is always smoother than the corresponding density distribution (in Fourier terms: the difference is two powers of the wave number), so that the supposition in Eq. (4) is even better than one might think.

2. The Voronoi Surprise

Throughout these events, it had been obvious to me (because of Eqs. (3), (9)) that there should be enormous empty regions in between the galaxy filaments. After all, the Oort constants of the Universe showed that there must be zones of super-Hubble expansion; and the galactic matter must have come from somewhere.

Mountains can grow indefinitely. But valleys in the cosmic density field can never be deeper than zero, wherefore these regions allow a linear approximation for much longer than high-density matter concentrations.

So the best thing to do, if one wants to understand cosmic structure on extremely large scales, is to look at the low-density regions. That makes things very simple. In regions where the density is below average, the motion of the cosmic gas is an expansion, as if gravity were negative. The net effect is a repulsion of matter away from the low-density regions. Therefore we expect that the structure of cosmic matter is a bubble structure.

I am not a mathematician, and I did not know about Voronoi tessellations. It was not until 1983 that I finally wrote this up [5]. During a meeting of the American Astronomical Society in that year, I was talking with my colleagues Bernard Jones, Joan Centrella, and Adrian Melott. The latter two had just completed [3] the first three-dimensional hydrodynamic simulation of dark-matter-dominated structure formation. They were puzzled that the low density regions were so spherical, whereas the collapsing structures were long filaments. Of course they knew that Ya. B. Zel'dovich had emphasized the formation of 'pancakes' (in Russian: *blini*), but these turned out to be hard to find in their results.

And so, during coffee break, I said that it was obvious: in order to avoid nonlinearities and other complications that always occur in high-density regions, we should view the development of structure in a selfgravitating pressure-free medium by considering the evolution of the *low*-density regions. These are the progenitors of the observed voids. The arguments presented by Lin *et al.* [7] can still be applied, except that the sense of the final effect is reversed: the $<$ sign in Eq. (9) must be replaced by $>$ if a, b, c are the axes of a void.

Because a void is effectively a region of negative density in a uniform background, the voids expand slightly faster than the average Universe, as a 'superHubble bubble' while the overdense regions collapse. In the process, *slight asphericities of the voids decrease as the voids become larger*. This I called the 'Bubble Theorem', which explained the numerical findings of Centrella & Melott [3], and Joan and Bernard persuaded me to write it up [5]. The proof holds strictly only on a non-expanding background, though this should be no objection for structures which are much smaller than the region where the collapse speed is approximately equal to the speed of the overall cosmic expansion across the void. Because $|\delta\rho/\rho|$ does not exceed unity in a void, the approximation will remain good for a longer period, except, of course, near the outer parts of the voids, where the matter gets swept up. That is precisely why the present approximation is so good: it treats specifically the regions where the motion is simple, rather than the chaos expected in the high-density regions.

According to the above, voids are the dominant geometric component of the inhomogeneous Universe. One may think of the megaparsec structure as a close packing of spheres of different sizes, out of which matter flows in a slightly super-Hubble expansion towards the interstices of the spheres. Thus, *the importance of the Bubble Theorem is that it provides a specific physical mechanism for producing the non-Poissonian matter distribution in the large scale Universe.* Moreover, it dictates a specific spatial arrangement, and predicts that matter should ultimately collect only in the regions where the filaments meet.

Back in Leiden, I was fortunate to get a brilliant young graduate student, Rien van de Weygaert, interested in this problem. Since Rien was graduating in mathematics as well as astronomy, he was very well placed for the next step. I asked him to find out what such a collection of super-Hubble bubbles would look like. In no time at all, he unearthed Voronoi's paper, almost a century old [17], that provided the answer: a collection of expanding spheres produces a unique partitioning of space, the *Voronoi tessellation.* Rien proceeded to give an extremely complete treatment of this, including some remarkable 'experimental mathematics' [15].

Together, we studied the properties of this type of tessellation [6]. We called it 'Voronoi foam', which was perhaps an unfortunate choice because it led some people to think that the walls of this tessellation join at angles of 120°, which is not the case at all.

The really special thing about the Voronoi model is, that it reveals a specific topological arrangement of the matter distribution. There can be *four and only four elements*: voids (the superHubble bubbles), walls, filaments, and nodes [15]. This arrangement has since become known as the *Cosmic Web.* Although nobody specifically refers to our introduction of the words, these four elements are now completely standard in cosmology (sometimes people use 'sheet' instead of 'wall' and 'cluster' for 'node').

When Rien and I calculated the two-point correlation function of the 'galaxies' in a Voronoi model in which points were allowed to migrate from voids, via walls and filaments, to nodes, we found that the result looked remarkably like the results found from observed galaxy counts by Peebles [10] and others.

That was the first application of a dynamical Voronoi tessellation in cosmology. At the meeting in 2018, I presented a movie that shows how this works. Here the reader will have to make do with a snapshot (Fig. 1). Statistically, this distribution matches the observed matter in the Universe quite well. Rien van de Weygaert studied the correlation properties

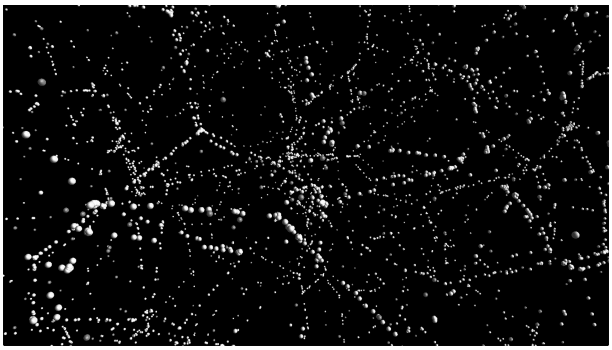

FIGURE 1. Cosmic web formed by an evolving Voronoi tessellation in 3-space. In order to be clear in this black-and-white image, the time of the evolution was chosen such that most of the matter is in the filaments (white dots, corresponding to $\theta = 1$ in Fig. 4)

of Voronoi tessellations in great detail, beginning with the two-point correlation function of the Voronoi nodes (Fig. 2), which we supposed to correspond to the galaxy clusters. This showed two remarkable things: first, that the amplitude of this correlation was larger than that of the galaxies, as had indeed been seen in galaxy surveys but was not understood at the time; second, that this function was a power law over a large range of its argument, with an exponent of the order of -2, close to the value of -1.88 that was observed. So *we had found a way to make correlations from totally uncorrelated initial conditions, namely the distribution of nuclei* (centres of initial low-density regions). Furthermore, the rise and fall of the Voronoi features can be calculated exactly. The effective excess Hubble parameter H^* in a Voronoi structure is *the same* in all topological features. This is one of the elegant properties of the Voronoi model. Because the model is analytic, it is not difficult to give algebraic expressions for the amount of mass in each Voronoi feature when the Universe grows older.

Let N be a nucleus, let P be the point where a *Delaunay line* (that is a line connecting two nuclei, perpendicular to a wall) intersects a wall, let W be a point in the wall, and let the angle WNP be called ϕ (Fig. 3). If we indicate the distance NP by a, the distance PW by b, and NW by c, then the velocity at W is cH^*. The components perpendicular and parallel to the wall are

$$cH^* \cos\phi = aH^*; \qquad cH^* \sin\phi = bH^* \tag{10}$$

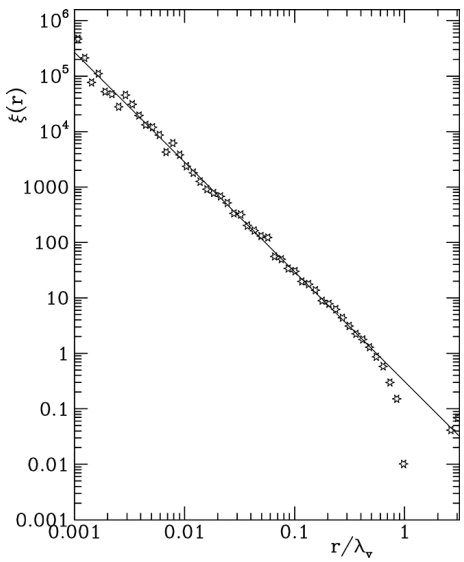

FIGURE 2. Two-point correlation of Voronoi vertices using the Pythagoras distance recipe. Drawn line is a least-squares power law with exponent -2, fitted to a numerical simulation (stars) from Van de Weygaert, 2000 (priv. comm.)

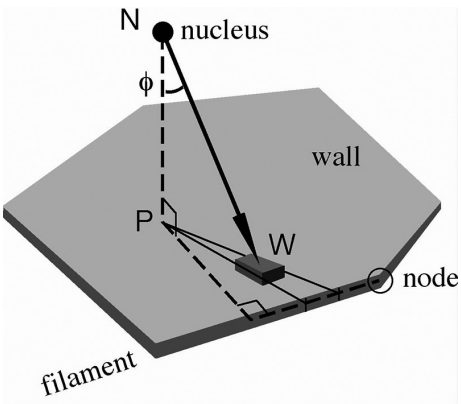

FIGURE 3. Geometry of the mass flow in a three-dimensional Voronoi tessellation

Thus, *the excess velocity in any Voronoi feature is simply found by multiplying H^* with the length along the feature.* This allows us to use the above formula for $N = 3$, 2, 1, and 0.

It is then easy to determine how matter is transferred from one Voronoi feature to another. In the quasi-linear case, the Hubble parameter H^*

is proportional to $t^{-1/3}$, because the excess velocity increases as $H^*ax = v \propto t^{1/3}$, and in the Einstein-De Sitter case the Universe's scale factor $a \propto t^{2/3}$. The power law dependence means that one may absorb H^* into the time by defining $d\theta \equiv H^* dt$. Consequently,

$$\theta = \theta_r (t/t_r)^{2/3} \tag{11}$$

where t_r is the time at which the Universe becomes transparent to radiation and may begin to fragment. The constant θ_r is related to the amplitude δ_r of the voids at the time when radiation and matter decoupled. One readily finds that

$$3\theta_r = \delta_r \tag{12}$$

The amount dm of mass lost in a dimensionless time interval $d\theta$, in N dimensions, is then

$$dm = -Nm\, d\theta \tag{13}$$

The mass gain is found simply by reversing the sign of the loss term of the feature higher in the hierarchy. This gives the following equations for the mass in voids, walls, filaments and nodes:

$$\frac{dm_v}{d\theta} = \quad -3m_v \tag{14}$$

$$\frac{dm_w}{d\theta} = 3m_v - 2m_w \tag{15}$$

$$\frac{dm_f}{d\theta} = 2m_w - m_f \tag{16}$$

$$\frac{dm_n}{d\theta} = m_f \tag{17}$$

By summing over the equations, it is obvious that mass is conserved. These equations are simply solved by noting that the N-dimensional mass loss equation has a solution of the type $\psi \exp(-N\theta)$:

$$m_v = \mathrm{e}^{-3\theta} \tag{18}$$

$$m_w = 3\mathrm{e}^{-2\theta}(1 - \mathrm{e}^{-\theta}) \tag{19}$$

$$m_f = 3\mathrm{e}^{-\theta}(1 - \mathrm{e}^{-\theta})^2 \tag{20}$$

$$m_n = (1 - \mathrm{e}^{-\theta})^3 \tag{21}$$

If we call $m_h = m_w + m_f + m_n$ the total mass of the high density regions, while $m_l = m_v + m_w + m_f$ is the mass in low density features, I find that

$$m_h/m_v = \exp(3\theta^{2/3}) - 1 \tag{22}$$

$$m_l/m_n = \left(1 - \exp(-\theta^{2/3})\right)^{-3} - 1 \tag{23}$$

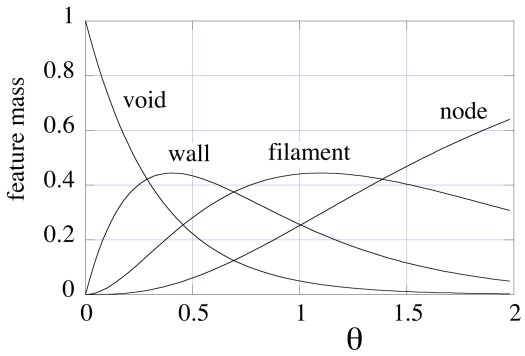

FIGURE 4. Growth and decline of the mass in the four types of Voronoi features. The voids steadily (and quickly) lose mass, which ultimately ends up in the nodes. Notice that, if we could observe the mass in the various cosmological mass concentrations, we could determine the age of the Universe by means of this graph

The time scale of the Voronoi growth can be related to the initial amplitude of the perturbations. Both mass ratios can then be compared with published galaxy surveys. This gives us a way to determine 'what time it is' in the simulations and in the Universe (Fig. 4). The equations allow one to relate the dimensionless time parameter θ to the cosmic time and to the redshift z at decoupling:

$$\theta = \frac{1}{3}\delta_r(t_0/t_r)^{2/3}(t/t_0)^{2/3} = \frac{1+z}{3}\,\delta_r(t/t_0)^{2/3} = \frac{1+z}{3}\,\delta_r\tau^{2/3} \qquad (24)$$

The scaling of the time is given by the initial amplitude of the perturbations. To my knowledge, this time-keeping method has not yet been applied to the cosmological data.

After four decades, my 'discovery in the mathematics library' is at most of historical interest, even though my analysis has shown that fairly straightforward considerations can lead to far-reaching conclusions. The advent of large-scale three-dimensional cosmic hydrodynamics, the descendant of the pioneering Centrella-Melott computations [3], has superseded my early analytic work [13]. It is interesting that the Voronoi approximation works quite well, because the matter density in a void cannot become less than zero, whereas the density in the other features (especially the filaments and the nodes) can grow almost without limit. The volume occupied by these high-density regions is negligible compared with the voids, but their gravitational influence can be considerable [12].

Consequently, the contemporary images of the cosmic web show many more small-scale structures than the original Voronoi foam.

By presenting the above in some detail, I have emphasized how Voronoi methods found their way in cosmology. Since then, the power of this beautiful branch of mathematics has been applied much more extensively, especially through the work of Volker Springel and his collaborators [14]. In present-day cosmological simulations, the initial conditions of the primordial cosmic noise are much more realistic than in the original Voronoi model. Moreover, extreme nonlinearities in the higher density regions due to star formation and its radiative consequences are included. But the original overall picture of the Cosmic Web remains [2].

3. Trembling Stars

Having discovered Voronoi's work and its power, I found other things to do with the same formalism. Just briefly, I will mention two more applications. The first is a model of the oscillations of giant stars. In these objects, especially the so-called 'yellow supergiants', the star's radius is enormous, comparable with the size of Earth's orbit, occasionally as large as the orbit of Mars. The outer layers of the star are in convective motion, with only a small number of convective cells (for a detailed review, see [1]).

I have modelled this arrangement by constructing a Voronoi tessellation that represents the convection cells in a supergiant star. A small number of nuclei, typically somewhere between 10 and 20, is placed on a sphere. The positions of the nuclei may be entirely random, or - more realistically - slightly anticorrelated. The Voronoi tiles corresponding to these nuclei represent the convective cells of the stellar mantle (Fig. 5). The oscillation frequency assigned to each cell depends on the size of the

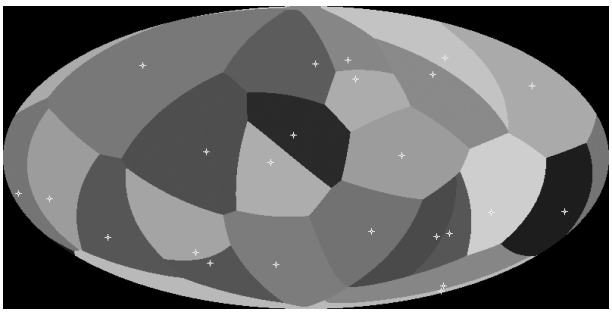

Figure 5. Aitoff projection of a Voronoi tessellation around 24 nuclei (white stars) randomly distributed on a sphere

Voronoi tile. To a first approximation the frequency is inversely proportional to the size, assuming that the stellar temperature at the surface is roughly constant so that the speed of sound does not vary much. The nuclei of Voronoi cells that have an edge in common are connected by the Delaunay triangulation. Cells that share an edge are supposed to be dynamically coupled. In this way, the spherical terssellation acts as a system of coupled oscillators.

Their motions can be solved numerically. A sample solution for Voronoi cells around 24 randomly distributed nuclei is shown in Fig. 6. What we observe with a telescope is the total signal of all these oscillators together. The signal is recorded by means of stellar photometry. The noise spectrum of the observed signal can be compared with the theoretical results. Comparison with actual observations indicate that the number of convective cells probably lies in the range 6-20. Although this type of model is

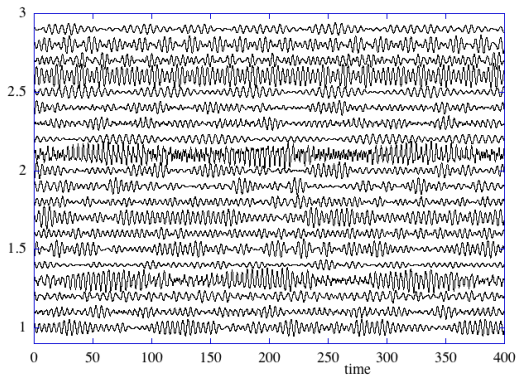

FIGURE 6. Amplitudes of the 24 Voronoi oscillators shown in Fig. 5, as a function of time

quite limited, given the fact that the internal structure of the oscillating star is not explicitly modeled, it describes how giant stars exhibit multifrequency oscillations. Recent observations of yellow hypergiants appear to show some support for this view [16].

4. Voronoi-Delaunay-Markov Radiative Transfer

My second application of the Voronoi formalism is a numerical treatment of radiative transfer. The algorithm is based on a Markov process on a Voronoi-Delaunay grid, a nonperiodic lattice which is derived from a random point process that is chosen to optimally represent certain properties of the medium through which the radiation flows. The grid is locally translation and rotation invariant in the mean; the word 'grid' in

this case is a little misleading, because one might assume that it refers to a periodic lattice. Transport is defined as simply moving photons from one nucleus to the next, along the Delaunay lines. At each nucleus, the arriving radiation is redistributed to the neighbouring nuclei.

This prescription generates a Markov process that describes the flow of radiation between the nuclei [8]. A given radiative state of the system – that is the vector R_i containing the number of photons present at each of the n nuclei – evolves into the next state by multiplication with a Markov matrix M_{ij}. If all Delaunay lines have equal weight, $M_{ij} = 1/n$. The steady state corresponds to the unique eigenvector S_i of M with eigenvalue 1. At first sight, this may seem trivial, because it is easy to prove that S_i is proportional to the number of Delaunay lines attached to nucleus i. However, in a practical case some nuclei are sources and others are sinks of radiation. At a source, the Delaunay lines are 'outgoing' lines, such that photons may only move away from the source node. At a sink, the Delaunay lines are 'incoming' lines, such that photons may only move towards the sink node. To conserve photons, all sinks are connected to all sources by means of 'outgoing' lines that equally redistribute the sink-photons over all the source nodes.

The corresponding eigenvector is no longer trivial. Because the speed of light is extremely large compared with the possible motions of the nuclei, we must find the stationary state of this process, that is to say, the equilibrium number of photons that are present at every nucleus. This amounts to diagonalization of M_{ij}, which is an $n \times n$ matrix. In a practical case, n may be of the order of several million or more. That might be a problem in an astrophysical application, because the matter that scatters the photons is almost always in motion, so that S_i must be calculated at every step of the computation that describes the motion of the matter (and therefore the motion of the nuclei).

The great virtue of the Voronoi-Delaunay method is, that the Markov matrix M_{ij} is very sparse: every row is filled with zeroes, except for those locations that correspond to a Delaunay line connecting nucleus i with nucleus j. This allows a quick diagonalization, so that my method is very efficient in applications to radiation hydrodynamics. In Fig. 7 I show the results for radiation starting at the centre of a homogeneous sphere, to show that the Voronoi-Delaunay method works as it should. Using the statistical properties of such lattices and their limiting behaviour, interactions may be incorporated as global coefficients. The whole procedure is carried out in such a way that the point process used to place the nuclei optimizes the solution (the *SimpleX* algorithm; see [11] and [9]).

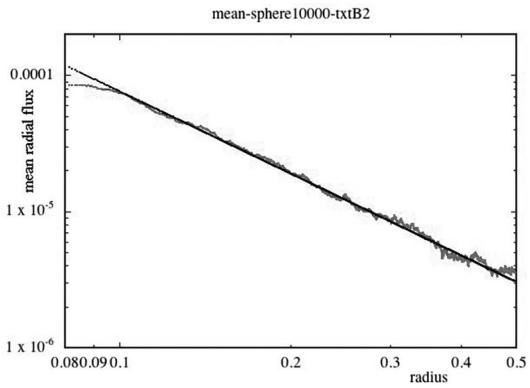

FIGURE 7. Mean radiative flux from the centre of a homogeneous sphere. The wiggly line is the result of the numerical Voronoi-Delaunay-Markov process, the smooth line is the analytical solution. Note that this case is highly contrived, and serves only to show that the method works as it should. In general, there are no analytical solutions for realistic applications of radiative transfer

In a Voronoi-Delaunay construction one may prescribe the distance recipe in the space of the nuclei, and the distribution of the nuclei themselves. In the application to radiative transfer, I use the placement of the nuclei rather than the distance recipe, because the average spatial isotropy – one of the key advantages of this construction – must not be broken. Thus, the point process that generates the nuclei is a representation of the optical properties of the matter.

If the density of the nuclei is proportional to the matter density, every nucleus represents a scattering centre, or an average over many such centres. But other choices are possible, and often useful. For example, if the expectation value of the length of a Delaunay grid line corresponds to the local mean free path, the lattice is a direct representation of the 'free path space' of the medium. In Fig. 8 I show a more realistic result, namely two colliding galaxies, each of which has a source of radiation at its centre.

Extensive experimentation with and testing of this method show that it is quick and robust, while the systematic errors are modest. Ironically, the main drawback is a consequence of its main advantage: namely, that the Delaunay lines connect nearby nuclei, by definition. Thus, there are only a dozen or so lines per nucleus, so that the Markov matrix is nice and sparse. On the other hand, a bunch of photons must hop via many

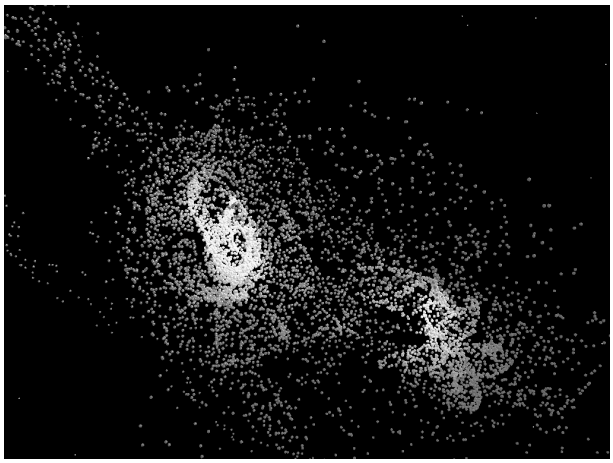

FIGURE 8. Static solution of the radiative transfer in two colliding galaxies. The two sources of the radiation are the galactic nuclei. The radiative intensity is coded by the print density: white for the largest specific intensity, dark for the smallest

nuclei to cover a large distance. Therefore, regions of very low optical depth are not easily modeled, and require extra attention [11].

5. Voronoi in Art

Mathematics and art have some things in common. One of these is: imagination. Having had the privilege of working with Voronoi tessellations in my job as an astrophysicist, I have had the opportunity of using these wonderful constructs in my capacity as a visual artist. In doing so, I may have stretched Voronoi tessellations beyond their mathematical limits. I make no apologies for this, because of Vincent's No-Limit Theorem: *Once you have started with Voronoi techniques, there is no limit to their applications.*

The images produced by means of my Voronoi methods might be called *algorithmic art*. In these productions, I have systematically explored the three primary degrees of freedom that the Voronoi tessellation allows: namely, first, the dimension of the space to be tessellated; second, the placement of the nuclei in this space; third, the distance recipe in that space. Because paper is two-dimensional, I will restrict myself here to giving a few examples of 2D Voronoi art (the cosmological 3D mass distribution in Fig. 1 gives a brief impression of what is possible in higher dimensions). But even two dimensions are very rich. Consider the prescription for the distance d. Normally, that is the 'Pythagoras recipe'



FIGURE 9. Left: Tessellation with 8 nuclei using the Manhattan distance recipe Eq. (25). The colours (not reproduced here) were chosen to give a balanced image, deliberately similar to the work by e.g. the artists Mondriaan or Van Doesburg. Right: tessellation with 10 correlated nuclei using the distance recipe of Eq. (28) with $n = 1/2$ which does not obey the triangle inequality

$d^2 = x^2 + y^2$. A different recipe might be

$$d = |x| + |y| \tag{25}$$

which is sometimes called the 'Manhattan distance': it is the distance produced by an infinitely fine mesh of perpendicular streets-and-avenues. Because d is anisotropic, the resulting tessellations have a distinct 'graphical' appearance (Fig. 9, left). The cell walls occur only at integral multiples of half a right angle. Distance prescriptions that are isotropic, but more general than Eq. (25), include

$$d = g(x^2 + y^2) = f(r) \tag{26}$$

This may seem uninteresting because they produce a regular Voronoi tessellation. However, in artistic applications, the function $f(r)$ is isotropic but need not be monotonic, for example

$$d = \frac{r}{1 + r^2} \tag{27}$$

which produces tessellations such as shown in Fig. 10. An even wilder possibility is, to use distance formulas that do not obey the Triangle Inequality, such as

$$d = |x|^n + |y|^n \tag{28}$$

in the case that $n < 1$. An example of such a tessellation with $n = 1/2$ is shown on the right hand side of Fig. 9. Note that using $d = |x|^n + |y|^m$ produces even wilder results if $n \neq m$, which - for brevity's sake - I will not show here. Suffice it to say that the patterns obtained with non-Triangle

distances are a very big inspiration for using Voronoi tessellations in my art.

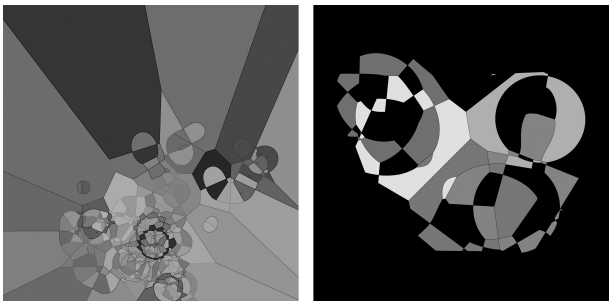

FIGURE 10. Left: Voronoi tessellation with 50 correlated nuclei, using the isotropic but non-monotonic distance recipe of Eq. (27) (this work is part of a private collection in Poland). Right: selection of five Voronoi tiles, hand-picked from the image on the left, and re-coloured

6. Conclusion

I thank the organisers of this Conference for their invitation and their support, and the people of Ukraine for their generous hospitality. I have found great benefit and inspiration in the work of Georgy Voronoi, even in a more general sense than just physics and mathematics.

Making a Voronoi-Delaunay diagram is a matter of connecting the dots. As I have shown, we can use these connections to understand the structure of our Universe. We can make connections on a sphere, as I did in my research on supergiant stars. But let us finally return to our home planet. Allow me to conclude by saying that to me, these connections are symbolic. Because science is universal, we can extend these scientific patterns, and imagine them to be connections all over the sphere of Earth. In this way, our Voronoi network brings everybody together. First in science, but then, I hope, all over the world.

References

[1] Aerts, C., Christensen-Dalsgaard, J. and Kurtz, D.W., *Asteroseismology*, Springer, Heidelberg (2010), ISBN 978-1-4020-5803-5.

[2] Cautun, M., Van de Weygaert, R., Jones, B.J.T. and Frenk, C.S., *Understanding the Cosmic Web*, arXiv:1501.01306v1 (2015).

[3] Centrella, J. and Melott, A.L., *Three-dimensional simulation of large-scale structure in the Universe*, Nature **305** (1983), 196.

[4] Icke, V., *Formation of Galaxies inside Clusters*, Astron. & Astrophys. **27** (1973), 1.
[5] Icke, V., *Voids and Filaments*, Monthly Notices Roy. astron. Soc. **206** (1984), 1P.
[6] Icke, V. and Van de Weygaert, R., *Fragmenting the universe*, Astron. & Astrophys. **184** (1987), 16.
[7] Lin, C.C., Mestel, L. and Shu, F.H., *Homologous Gravitational Collapse in Lagrangian Coordinates*, Astrophys. J. **142** (1965), 1431-1446.
[8] Norris, J.R., *Markov Chains*, Cambridge U. Press (2012), ISBN 9780511810633.
[9] Paardekooper, J.-P., Kruip, C.J.H. and Icke, V., *SimpleX2: radiative transfer on an unstructured, dynamic grid*, Astron. & Astrophys. **515** (2010), A79.
[10] Peebles, P.J.E., *The large-scale structure of the universe*, Princeton Univ. Press, Princeton (1980).
[11] Ritzerveld, N.G.H., *The Simplicity of Transport*, PhD Thesis, Universiteit Leiden (2007).
[12] Sheth, R.K. and Van de Weygaert, R., *A hierarchy of voids*, Monthly Notices Roy. Astron. Soc. **350** (2004), 517P538.
[13] Springel, V., *Hydrodynamic simulations on a moving Voronoi mesh*, arXiv:1109.2218v1 (2007).
[14] Springel, V. *et al.*, *Arepo Code*, https://arepo-code.org/about-arepo (2020).
[15] Van de Weygaert, M. and Icke, V., *Fragmenting the Universe. II - Voronoi vertices as Abell clusters*, Astron. & Astrophys. **213** (1989), 1-9.
[16] Van Genderen, A.M., Lobel, A., Nieuwenhuijzen, H., Henry, G.W., De Jager, C., Blown, E., DiScala, G. and Van Ballegoij, E.J., *Pulsations, eruptions and evolution of four yellow hypergiants*, Astron. & Astrophys. **631** (2019), A48.
[17] Voronoi, G., *Nouvelles applications des paramètres continus à la théorie des formes quadratiques. Deuxième mémoire. Recherches sur les parallélloèdres primitifs.* , J. reine angew. Math. **134** (1908), 198.

Sterrewacht Leiden, Universiteit Leiden, Niels Bohrweg 2, Leiden, 2333 CA, The Netherlands
Email: icke(at)strw(dot)leidenuniv(dot)nl
URL: https://www.strw.leidenuniv.nl/~icke/

Voronoï's Impact on Modern Science, Book 6, Volume 2
Proceedings of the Sixth International Conference on Analytic Number Theory and Spatial Tessellations

COMPUTING OPTIMAL DISTANCE BASED CLIQUE RELAXATIONS IN UNIT DISK GRAPHS

Sera Kahruman Anderoglu and Sergiy Butenko (*USA*)

Abstract. Given a simple, undirected graph G, its subset of vertices C is called an s-clique if the distance between any pair of vertices from C is at most s in G. A unit disk graph is the intersection graph of closed disks of equal diameter. This paper proposes an exact algorithm for computing a maximum s-clique in a unit disk graph. Results of numerical experiments for $s = 2$ are presented.

1. Introduction

Given a simple, undirected graph $G = (V, E)$, its subset of vertices $C \subseteq V$ is called a *clique* if $\{u, v\} \in E$ for any $u, v \in C$. Cliques have been extensively used to model tightly-knit clusters, communities, cohesive subgroups, etc., in a wide range of applications [5]. In addition, several clique relaxation models, such as s-defective clique, s-plex, s-club, and γ-quasi-clique, have been introduced in the literature, which capture some of the clique properties while relaxing others [10]. This paper focuses on a distance-based clique relaxation model, s-clique, defined next. Given a graph $G = (V, E)$, a subset of vertices $S \subseteq V$ is an *s-clique* (or *distance-s clique*) if the distance between any two vertices from S is at most s in G. Specifically, we are interested in the *maximum s-clique problem*, which is to find an s-clique of maximum cardinality in G. The maximum s-clique problem is NP-hard in general [4, 11].

In this work, the maximum s-clique problem is considered on a restricted class of graphs called *unit disk graphs* (UDGs) [3]. A UDG can be defined as the intersection graph of closed disks of equal (e.g., unit) diameter; see Figure 1 for an illustration. UDGs are often used to model wireless networks. In order to avoid the interference between different wireless nodes when they broadcast at the same time, it is important

Received July 20, 2020.
2010 *Mathematics Subject Classification.* Primary 90C27; Secondary 05C85, 52B55.
Key words and phrases. Optimization, clique relaxations, unit disk graphs, maximum s-clique problem.

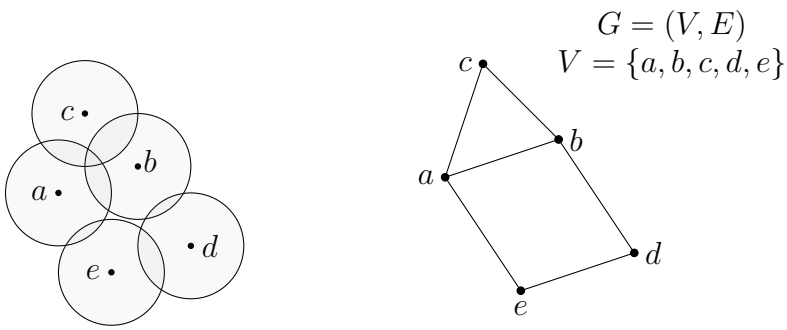

FIGURE 1. A unit disk graph.

to assign different frequencies to the nodes whose transmission ranges intersect. Thus, the clique number gives the least number of frequencies needed. Fortunately, the clique number of a unit disk graph can be computed in polynomial time [7]. However, since the unit disk graph model is only a rough approximation of the wireless network topology, clique relaxations may provide a better estimate of the number of frequencies needed. Moreover, the size of a maximum s-clique for low values of s (e.g., $s = 2$) in a UDG model of a wireless network provides a global measure of reachability between the nodes of the network.

The maximum s-clique problem in a graph G is equivalent to the maximum clique problem in its sth power graph G^s, which is obtained from G by adding edges for each pair of vertices that are distance s or less apart in G. Note that for a unit disk graph G, G^s is not necessarily a unit disk graph [8]. While the complexity of the maximum s-clique problem in unit disk graphs is unknown, we conjecture that this problem is NP-hard. To give some intuition behind this conjecture, it is worth mentioning that G^s can be shown to be an intersection graph of unit ϵ-quasi-disks for some ϵ [8], and the maximum clique problem on the class of intersection graphs of unit *ϵ-quasi-disks* is known to be NP-hard for any $\epsilon > 0$ [6]. (For $\epsilon \in [0, 1]$, a *unit ϵ-quasi-disk* is a connected compact set Q of the plane such that there exists a point P such that $D(P, 1 - \epsilon) \subseteq Q \subseteq D(P, 1)$, where $D(C, r)$ denotes the disk of radius r centered at C.)

In [9], a $\frac{1}{2}$-approximation algorithm for the maximum 2-clique problem in UDGs is proposed. We are not aware of any other work focusing on the maximum s-clique problem in UDGs.

The remainder of this paper is organized as follows. Section 2 describes the proposed exact approach to the maximum s-clique problem in a UDG. Section 3 discusses its implementation and reports the results

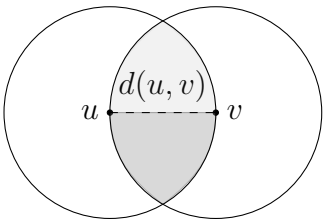

FIGURE 2. An illustration to the discussion on the maximum clique algorithm in UDG.

of preliminary computational experiments on random UDGs for $s = 2$. Section 4 concludes the paper. This paper is based on a part of Ph.D. dissertation [8] of the first author.

2. The Proposed Approach

Let $G = (V, E)$ be a UDG with unit distance d and assume the coordinates of points on the plane representing the graph's vertices are given. We define the graph G_{sd} on the same set of vertices by introducing an edge between two vertices whenever the corresponding points are distance no more than sd apart on the plane. Thus, by definition G_{sd} is a UDG, with the unit distance given by sd. Furthermore, we observe that the power graph G^s is a subgraph of G_{sd}.

Since G_{sd} is a unit disk graph, the maximum clique problem in this graph can be solved in polynomial time using a maximum matching algorithm in bipartite graphs [7] as follows.

2.1. **Maximum Clique in a UDG.** Consider a UDG $G = (V, E)$ with a maximum clique C. Let u and v be a pair of nodes in C corresponding to two farthest apart disk centers from the clique, with the Euclidean distance $d(u, v)$ between them. Then all other nodes from the clique will have their corresponding disk centers in the intersection of the disks of radius $d(u, v)$ centered at u and v, respectively; see Figure 2 for an illustration. Then the nodes corresponding to the disk centers falling within the same half of the intersection (above or below the dashed line in the figure) form a clique in the UDG. Thus, the nodes from the intersection form two cliques, C_1 and C_2, and the corresponding induced subgraph $G[C_1 \cup C_2]$ is a co-bipartite graph. Finding the maximum clique in $G[C_1 \cup C_2]$ is equivalent to finding a maximum independent set in the complement graph $\bar{G}[C_1 \cup C_2]$, which is a bipartite graph. Therefore, finding a maximum clique in a UDG reduces to solving $O(|V|^2)$ instances of the maximum independent set problem in bipartite graphs.

In order to find a maximum independent set in a bipartite graph, we first find a maximum matching in this graph. To compute a maximum matching, we use an algorithm based on augmenting paths [2]. Given a *matching* M, an *alternating path* is a path in which the edges belong alternatively to the matching and not to the matching. An *augmenting path* is an alternating path that starts from and ends on unmatched vertices. One can prove that a matching is maximum if and only if it does not have any augmenting path. Let A' and B' denote the set of vertices corresponding to the partitions of the bipartite graph $G' = (V', E')$. Since a vertex in A' can only be matched with a vertex in B', it is sufficient to search through the unmatched vertices of A' to find an augmenting path. We use breadth first search (BFS) for finding an augmenting path. As each path can be found in $O(|E'|)$ time, the running time of this algorithm is $O(|V'||E'|)$. It should be noted that we chose this implementation for its simplicity. Hopcroft-Karp algorithm [2] for the same problem has a better worst-case running time of $O(\sqrt{|V'|}|E'|)$. Given a maximum matching of G', we can find the maximum independent set of G' as follows. First we include all the unmatched vertices in the solution. It is clear that these vertices are all independent, since otherwise we would have an augmenting path and the matching we had would not be a maximum matching. For the matched vertices, we check their neighborhood and include them in the solution set if they do not have any neighbors in the current solution.

2.2. **Algorithm for the Maximum s-Clique Problem in a UDG.** The main idea of the proposed algorithm is to solve the maximum clique problem in G_{sd}, and do branching on some nodes if the found solution is not a clique in the power graph G^s. Note that since G^s is a subgraph of G_{sd} with the same set of vertices but some missing edges, there exists a pair of adjacent vertices u and v in G^s for which the intersection region of disks of radius $d(u, v) \leq sd$ centered in u and v contains the optimal solution. Hence, a maximum clique in G^s can be found by trying each pair of adjacent vertices in G^s as such u and v.

Algorithm 1 outlines the approach. We start by forming the graphs G^s and G_{sd} and applying GREEDY-s-CLIQUE(G) procedure, which is the standard greedy heuristic for the maximum clique problem in G^s, recursively adding a maximum degree vertex v_{max} in the residual graph and removing all vertices that are not in the neighborhood $N_{G^s}(v_{max})$ of v_{max} in G^s. After obtaining an initial solution C^* using the greedy heuristic, an attempt to reduce the size of the graph is made by recursively eliminating the vertices whose degree in G^s is less than $|C^*| - 1$, since

Algorithm 1 An exact algorithm for the max s-clique problem in UDG.

Input: UDG $G = (V, E)$; coordinates of the points in V; integer $s \geq 2$

Form graphs G^s and G_{sd}
$C^* \leftarrow$ GREEDY-s-CLIQUE(G)
$V \leftarrow$ PEEL$(G^s, V, |C^*| - 1)$
for each $\{u, v\} \in E(G^s)$ **do**
    $S \leftarrow \{w \in V(G) : d(w, u) \leq d(u, v)$ and $d(w, v) \leq d(u, v)\}$
    $S \leftarrow$ PEEL$(G^s, S, |C^*| - 1)$
    if $|S| > |C^*|$ **then**
        C^*_{uv}=MAX-s-CLIQUE(G, S)
        if $|C^*_{uv}| > |C^*|$ **then**
            $C^* \leftarrow C^*_{uv}$
        end if
    end if
end for
return C^*
function GREEDY-s-CLIQUE(G)
    $C \leftarrow \emptyset$
    while $V \setminus C \neq \emptyset$ **do**
        Find a vertex v_{max} of maximum degree in $G^s[V \setminus C]$
        $C \leftarrow C \cup \{v_{max}\}$; $V \leftarrow V \cap N_{G^s}(v_{max})$
    end while
    return C
end function
function PEEL(G, C, k)
    while $\exists$ a vertex v_{min} of degree $\geq k$ in $G[C]$ **do**
        $C \leftarrow C \setminus \{v_{min}\}$
    end while
    return C
end function
function MAX-s-CLIQUE(G, S)
    Find a maximum clique C in $G_{sd}[S]$
    if $\exists$ a fake edge $\{x, y\} \in E(G_{sd}[C]) \setminus E(G^s[C])$ **then**
        C_x =MAX-s-CLIQUE$(G, S \setminus \{x\})$
        C_y =MAX-s-CLIQUE$(G, S \setminus \{y\})$
    end if
    return argmax$\{|C_x|, |C_y|\}$
end function

such vertices cannot be included in an optimal solution. This procedure is referred to as *peeling* [1] and is denoted by PEEL$(G^s, V, |C^*| - 1)$ in Algorithm 1.

The **for** loop in lines 4–13 is the main loop of the algorithm. This loop iterates through all adjacent pairs of vertices to compute a maximum clique in G^s. It is important to note that this step can be improved by considering only adjacent pairs of vertices in G^s for which the distance in G is greater than $s-1$. In fact, computations only need to be performed for connected components of diameter strictly greater than $s-1$. If the diameter of a connected component is less than or equal to s, that connected component already forms an s-clique, and there is no need for further computations.

In the main loop, for each pair of adjacent vertices $\{u, v\}$ in G^s we form the subgraph induced by $S = \{w \in V(G) : d(w,u) \leq d(u,v)$ and $d(w,v) \leq d(u,v)\}$. Since G_{sd} is a UDG, the graph $G_{sd}[S]$ induced in G_{sd} by the set S is co-bipartite. Before solving the problem on this set, we check the degrees of vertices in the induced subgraph $G^s[S]$ and eliminate the ones that cannot take part in a solution better than the current best. If the cardinality of S after vertex deletions is less than the current best, there is no need to solve the problem for this set and we continue with the next pair. Otherwise, we call the function MAX-s-CLIQUE(G, S) to find a maximum s-clique C^*_{uv} in $G[S]$. This function first solves the maximum clique problem in $G_{sd}[S]$ by forming the complement graph $\bar{G}_{sd}[S]$, which is bipartite, and finding the maximum independent set in the complement using maximum matching, as discussed in Subsection 2.1 above.

Now that we have a maximum clique C in $G_{sd}[S]$, we first check if the solution is better than the current best. If it is not, there is no need for further analysis and we move on to the next pair. Otherwise, we check if this is a feasible solution for $G^s[S]$ by checking the existence of a *fake* edge in the solution, i.e. an edge in $E(G_{sd}[C]) \setminus E(G^s[C])$. If there exists a fake edge, this means that the endpoints of that edge are not adjacent in $G^s[S]$ and thus cannot be a part of the same clique. Thus, we create two branches for this problem by deleting an endpoint for each branch. Repeating the same procedure recursively leads to a branch-and-bound (B&B) tree. For each node, we fathom whenever we get a feasible solution for $G^s[S]$ or whenever we observe that it cannot give a solution better than the current best. Thus, fathoming for the B&B tree for each pair of vertices is done with respect to both the global best and also the incumbent of the current B&B tree. Whenever we get a better solution, we update C^*. In the end, C^* corresponds to a maximum clique in $G^s[S]$, which is also a maximum s-clique of G.

3. Implementation and Computational Results

The proposed algorithm was implemented using C++ and CPLEX 11.0 on a Pentium 4 computer with 3.20 GHz CPU. The CPLEX defaults, such as cut generations, presolve and node heuristics, were all turned off. The branch and bound (B&B) framework of CPLEX requires a mixed integer programming (MIP) formulation. The traditional B&B solves the linear programming (LP) relaxation in each node and updates the incumbent whenever it finds an integral solution better than the current incumbent. If an integral solution is found, the node is fathomed. Similarly, if the objective value of the LP relaxation is not better than the current best, the node is fathomed since the integral solution that it yields cannot be better than the LP relaxation. The branching is done on a variable which does not have an integral value. However, our problem has several different characteristics. First of all, we do not want to use s-clique formulation. Instead, we want to solve matching at each node, post-process the solution to obtain a maximum clique, and decide on the feasibility by the presence of *fake* edges. Also, we want to branch on endpoints of *fake* edges. This can all be done by taking advantage of the flexibility offered by CPLEX callbacks. In our implementation, we used the *incumbent callback*, the *branch callback*, and the *solve callback*.

CPLEX calls incumbent callback whenever it finds an integral solution better than the current best of the B&B tree. It enables the user to accept or reject the solution based on other user-defined factors. We used incumbent callback for checking for the presence of *fake* edges.

The branch callback enables the user to create custom branches. We used this callback to create branches on endpoints of fake edges. If there is no fake edge or the solution is not promising for further analysis, the branch callback gets a flag from the incumbent callback and fathoms the node. If there is a fake edge, it finds a vertex with the maximum number of fake edges and branches on that vertex and one of its *fake* neighbors.

Finally, the solve callback is used to compute a maximum clique in $G_{sd}[S]$ by means of solving the maximum matching problem in bipartite graphs. The solve callback enables the user to identify a solution strategy, such as which CPLEX solver to use at a particular node. The solution obtained must be in CPLEX format. Thus, when we use the bipartite matching algorithm, we need to make sure that CPLEX has some information about the solution status.

Even though our algorithm does not use an MIP formulation, one is still needed in order for CPLEX to be able to create a B&B tree and perform branching. We use the ONE-MAX model for this purpose, given

by $\max\left\{\sum_{v\in V(G')} x_v : x_v \in \{0,1\}\ \forall v \in V(G')\right\}$. Clearly, the optimal solution for this formulation is achieved when all variables are set to 1. The branching involves introducing an upper bound of 0 to the variables corresponding to the vertices that are the endpoints of a *fake* edge. At each node of the tree, we solve the above formulation with the corresponding bound changes using CPLEX LP solver. We give the solution to CPLEX since we know that the optimal solution sets all the variables to their upper bounds. Thus, CPLEX does not do any iterations and only confirms the optimality. Next, we solve the matching problem. Let $S' = \{w \in S : x^*_w = 1\}$, where x^*_w denotes the optimal value of the vertex w for the above formulation at the current node. The matching algorithm is run on the induced subgraph $\bar{G}[S']$.

We conducted preliminary experiments for the maximum s-clique problem with $s = 2$. The testbed used for the experiments consisted of 35 random UDGs. Table 1 describes the test instances used, as well as the cardinalities of the initial solution obtained using the greedy heuristic and the optimal solution found. In this table, "rn-k" denotes the kth test instance with n vertices. We created graphs with different edge densities. The columns of the table show the graph's name ("G"), number of edges ("$|E|$"), edge density ("$\rho(G)$"), the number of fake edges in G_{2d} ("$|F(G_{2d})|$"), the cardinality of the greedy heuristic solution ("$|C^*_h|$"), and the cardinality of the optimal solution found ("$|C^*|$"), respectively.

The results of experiments are shown in Table 2. We compare the performance of the proposed algorithm with and without the preprocessing on the set S (described in lines 11-15 of Algorithm 1). Since the proposed algorithm calls CPLEX for each pair that can lead a better solution, we report the number of such calls as well as the maximum number of B&B nodes over all CPLEX calls, which gives an idea about memory usage. We observed that the preprocessing procedure has a significant positive effect on the performance of the algorithm, yielding a reduction in both the number of CPLEX calls and the running time for most instances.

4. Conclusion

In this paper, we studied the maximum s-clique problem in unit disk graphs. We propose an exact solution procedure, which is a matching-based branch and bound method, taking advantage of the geometric properties of UDGs. We report the results of computational experiments on randomly generated test instances for the case of $s = 2$. The test results show the effectiveness of our algorithm, especially for sparser

TABLE 1. Description of the test instances used.

G	$\|E\|$	$\rho(G)$	$\|F(G_{2d})\|$	$\|C_h^*\|$	$\|C^*\|$
r100-1	4523	0.914	96	47	71
r100-2	4831	0.976	47	35	88
r100-3	4782	0.966	76	38	82
r100-4	4840	0.978	44	34	89
r100-5	4794	0.968	80	40	85
r100-6	1721	0.348	352	29	29
r100-7	2065	0.417	388	24	24
r100-8	2082	0.421	400	25	25
r100-9	2135	0.431	379	28	28
r100-10	2096	0.423	394	27	27
r200-1	18232	0.916	300	73	135
r200-2	18994	0.954	239	72	153
r200-3	19281	0.969	226	70	161
r200-4	19399	0.975	169	81	174
r200-5	19387	0.974	135	64	164
r200-6	7015	0.353	1182	41	41
r200-7	8249	0.415	771	49	50
r200-8	8713	0.438	828	53	55
r200-9	9032	0.454	807	60	62
r200-10	9487	0.477	770	55	56
r200-11	12754	0.641	1299	76	81
r200-12	14541	0.731	727	86	91
r200-13	15513	0.780	664	91	101
r200-14	15756	0.792	574	98	105
r200-15	15693	0.789	582	97	107
r500-1	116637	0.935	913	199	360
r500-2	119430	0.957	710	203	377
r500-3	121710	0.976	481	182	409
r500-4	122370	0.981	401	227	426
r500-5	121778	0.976	628	215	411
r500-6	49143	0.394	6158	124	124
r500-7	55019	0.441	2097	114	115
r500-8	59808	0.479	2662	118	120
r500-9	60373	0.484	3401	128	129
r500-10	58664	0.470	3249	125	125

instances. As for future work, considering a purely combinatorial implementation of the proposed approach that would not rely on CPLEX and extending the computational experiments to higher values of s could be of interest. In addition, the computational complexity of the maximum s-clique problem in unit disk graphs is still to be established. Other

TABLE 2. Performance of the algorithm with and without preprocessing set S. CPU times are in seconds.

	without preprocessing			with preprocessing		
G	CPU time	B&B nodes	CPLEX calls	CPU time	B&B nodes	CPLEX calls
r100-1	1.75	15	182	0.484	23	14
r100-2	0.266	7	20	0.031	0	0
r100-3	0.828	69	90	0.203	11	2
r100-4	0.281	5	22	0.125	0	1
r100-5	0.359	79	28	0.046	0	0
r100-6	0.156	3	9	0.016	0	0
r100-7	0.641	63	59	0.047	0	0
r100-8	0.391	11	38	0.031	0	0
r100-9	0.188	3	14	0.031	0	0
r100-10	0.266	3	20	0.031	0	0
r200-1	15.234	85	862	6.797	75	241
r200-2	7.953	29	569	3	7	97
r200-3	6.032	139	439	2.547	135	65
r200-4	2.61	13	174	1.157	3	3
r200-5	5.015	61	395	1.703	35	33
r200-6	2.562	15	252	0.453	0	5
r200-7	1.422	9	142	0.468	43	5
r200-8	1.234	13	121	0.39	9	3
r200-9	1.031	45	88	0.39	27	5
r200-10	4.969	9	439	1.125	9	19
r200-11	8.86	33	1514	2.156	323	5
r200-12	17.672	39	891	5.984	49	120
r200-13	16.219	41	886	4.657	41	110
r200-14	12.89	11	769	4.734	15	112
r200-15	15.845	117	885	5.562	67	205
r500-1	334.762	335	4793	188.966	421	1655
r500-2	305.621	1719	4810	177.779	641	1865
r500-3	164.03	25	3249	102.17	41	799
r500-4	122.749	3323	2446	70.031	3323	429
r500-5	185.247	2641	3172	102.045	3175	965
r500-6	94.718	1025	2091	37.656	1023	356
r500-7	192.185	247	4257	35.452	247	467
r500-8	399.057	117	6905	98.218	157	2050
r500-9	308.153	9	4732	49.187	41	428
r500-10	163.248	131	4100	40.609	63	448

interesting research directions include designing better approximation algorithms for the maximum s-clique problem as well as the closely related maximum s-club problem in unit disk graphs.

References

1. J. Abello, P. M. Pardalos, and M. G. C. Resende, *On maximum clique problems in very large graphs*, External memory algorithms, American Mathematical Society, Boston, MA, USA, 1999, pp. 119–130.
2. R. K. Ahuja, T.L. Magnanti, and J. B. Orlin, *Network flows: Theory, algorithms, and applications*, Prentice Hall, 1993.
3. B. Balasundaram and S. Butenko, *Optimization problems in unit-disk graphs*, Encyclopedia of Optimization (C. A. Floudas and P. M. Pardalos, eds.), Springer, 2 ed., 2009, pp. 2832–2844.
4. B. Balasundaram, S. Butenko, and S. Trukhanov, *Novel approaches for analyzing biological networks*, Journal of Combinatorial Optimization **10** (2005), 23–39.
5. I. M. Bomze, M. Budinich, P. M. Pardalos, and M. Pelillo, *The maximum clique problem*, Handbook of Combinatorial Optimization (Dordrecht, The Netherlands) (D.-Z. Du and P. M. Pardalos, eds.), Kluwer Academic Publishers, 1999, pp. 1–74.
6. S. Ceroi, *The clique number of unit quasi-disk graphs*, Rapport de recherche 4419, INRIA, March 2002.
7. B. N. Clark, C. J. Coulbourn, and D. S. Johnson, *Unit disk graphs*, Discrete Mathematics **86** (1990), 165–177.
8. S. Kahruman Anderoglu, *Optimization in geometric graphs: Complexity and approximation*, Ph.D. thesis, Texas A&M University, 2009.
9. J. Pattillo, Y. Wang, and S. Butenko, *Approximating 2-cliques in unit disk graphs*, Discrete Applied Mathematics **166** (2014), 178–187.
10. J. Pattillo, N. Youssef, and S. Butenko, *On clique relaxation models in network analysis*, European Journal of Operational Research **226** (2013), 9–18.
11. S. Shahinpour and S. Butenko, *Dinstance-based clique relaxations in networks: s-cliques and s-clubs*, Models, Algorithms, and Technologies for Network Analysis (B. I. Goldengorin, V. A. Kalyagin, and P. M. Pardalos, eds.), Springer Proceedings in Mathematics & Statistics, vol. 59, Spinger Science + Business Media, New York, 2013, pp. 149–174.

(S. Kahruman Anderoglu) Central New Mexico Community College, School of Mathematics, Science and Engineering,
Email: skahrumanander(at)cnm(dot)edu

(S. Butenko) Department of Industrial and Systems Engineering, Texas A&M University, TAMU-3131, College Station, TX 77843-3131, USA
Email: butenko(at)tamu(dot)edu
URL: http://ise.tamu.edu/people/faculty/butenko/

Voronoï's Impact on Modern Science, Book 6, Volume 2
Proceedings of the Sixth International Conference on Analytic Number Theory and Spatial Tessellations

MOLECULAR GEOMETRY AND ITS OPERATING SYSTEM: AN EMERGING APPLICATION OF VORONOI DIAGRAMS

Deok-Soo Kim (*Korea*)

Extended Abstract

The geometry of atomic arrangement underpins the structural understanding in many fields. In biology, the structure of biomolecules determines function. In chemistry, physics, and materials science, the properties of inorganic molecules result from the geometrical arrangement of their atoms. Many studies were conducted for the geometry of atomic arrangement but most studies were based on Monte Carlo, grid-counting, or approximation methods where a high-quality solution requires heavy computational resources, not to mention about its dependency on computation environment. The use of such resolution-dependent approaches is common despite their unreliable, inconsistent, and sometimes conflicting results. A general framework of mathematical/computational theory for the geometry of atomic arrangement does not exist. Here we present "Molecular Geometry (MG)" as such a theoretical framework to model molecular structure problem as a geometry problem in terms of primitive geometric terms such as area and volume of voids, tunnels, etc. and "MG Operating System (MGOS)" which consists of callable functions based on the Voronoi diagram of three-dimensional spherical atoms that implements the MG theory. MG facilitates simpler modeling of molecular structure problem in geometry-centric principle and the MGOS functions can be conveniently embedded in application programs for efficient and accurate solution of geometric queries involving atomic arrangements. MGOS is implemented using the Voronoi diagram of three-dimensional

Received June 29, 2019.

2010 *Mathematics Subject Classification.* Primary 01A23; Secondary 45B67, 89C10.

Key words and phrases. Atomic arrangement, Computational biology, Structural biology, Material design, Computational geometry.

This research was partially supported by the National Research Foundation of Korea (NRF) grant funded by the Korea government (MSIP, MSIT) (No. 2017R1A3B1023591, No, 2016K1A4A3914691).

spheres [1] and its two derivative constructs called the quasi-triangulation [4, 2] and beta-complex [3]. The architecture of MGOS has been carefully designed so that any future modifications will not require rewriting the existing code of an application program. If a molecular problem can be properly geometrized in terms of appropriate-sized spherical balls, the MG/MGOS framework can quickly provide the best possible solution. Examples include the BetaCavityWeb [5] and BetaSCPWeb [6] programs. It is expected that the MGOS engine will evolve, with new functions to be added in the future. The capability of the MGOS library suggests a transition of computation paradigm from a point-to-point to a sphere-to-sphere which would have an enormous impact on improving efficiency in computational science. The impact of math libraries of general purpose high-level programming languages to science and engineering is an appropriate metaphor of that of MGOS, which is currently, freely available at Voronoi Diagram Research Center (http://voronoi.hanyang.ac.kr) at Hanyang University, Seoul, Korea.

References

1. Deok-Soo Kim, Youngsong Cho, and Donguk Kim, *Euclidean Voronoi diagram of 3D balls and its computation via tracing edges*, Computer-Aided Design **37** (2005), no. 13, 1412–1424.
2. Deok-Soo Kim, Youngsong Cho, and Kokichi Sugihara, *Quasi-worlds and quasi-operators on quasi-triangulations*, Computer-Aided Design **42** (2010), no. 10, 874–888.
3. Deok-Soo Kim, Youngsong Cho, Kokichi Sugihara, Joonghyun Ryu, and Donguk Kim, *Three-dimensional beta-shapes and beta-complexes via quasi-triangulation*, Computer-Aided Design **42** (2010), no. 10, 911–929.
4. Deok-Soo Kim, Donguk Kim, Youngsong Cho, and Kokichi Sugihara, *Quasi-triangulation and interworld data structure in three dimensions*, Computer-Aided Design **38** (2006), no. 7, 808–819.
5. Jae-Kwan Kim, Youngsong Cho, Mokwon Lee, Roman A. Laskowski, Seong Eon Ryu, Kokichi Sugihara, and Deok-Soo Kim, *BetaCavityWeb: a webserver for molecular voids and channels*, Nucleic Acids Research **43** (2015), no. W1, W413–W418.
6. Joonghyun Ryu, Mokwon Lee, Jehyun cha, Roman A. Laskowski, Seong Eon Ryu, and Deok-Soo Kim, *BetaSCPWeb: side-chain prediction for protein structures using voronoi diagrams and geometry prioritization*, Nucleic Acids Research **44** (2016), no. W1, W416–W423.

Department of Mechanical Engineering, Hanyang University Haengdang-Dong, Sungdong-Gu, Seoul, 133-791, Korea
Email: dskim(at)hanyang(dot)ac(dot)kr
URL: https://voronoi.hanyang.ac.kr/

Voronoï's Impact on Modern Science, Book 6, Volume 2
Proceedings of the Sixth International Conference on Analytic Number Theory and Spatial Tessellations

ADVANTAGES OF ARC SPLINE REPRESENTATIONS FOR VARIOUS APPLICATIONS IN COMPUTATIONAL GEOMETRY

Bastian Weiss (*Austria*)

Abstract. Processing planar shapes defined by boundary curves is a fundamental task in computational geometry. Such a boundary curve is often a polyline obtained by approximating an input curve. We investigate the possibility of approximating an input curve by arc splines instead of polylines. One advantage is that an arc spline approximation needs less primitives to obtain the same accuracy compared to a polyline. Another one is that arc splines are potentially tangent continuous.

These advantages of the arc spline representation of planar domains have been exploited to formulate powerful algorithms for the computation of the medial axis, offsets, Voronoi diagrams of free-form sites, and convex hulls.

We recall a simple algorithm to compute an arc spline of a spline curve with accuracy ε. Furthermore, we discuss several applications of shapes defined by arc splines. These include mitered offsets and the associated skeletons, and arc fibrations of planar domains.

Introduction

Approximations of complex shapes by a series of simple primitives is a common approach in computational geometry. Those primitives may be straight line segments, (circular) arcs, biarcs, Bèzier curves and many others. We focus on algorithms that are applicable to shapes defined by circular arcs.

This section is based on the results from [3]. Since geometric shapes are often not directly accessible we recall a bisection algorithm to compute an approximation of a curve $c(t)$ using primitives b to a tolerance ε, which is linear in the number of created primitives.

Received March 25, 2019.
2010 *Mathematics Subject Classification.* Primary 68U05; Secondary 65D18.
Key words and phrases. arc spline, circular boundary, mitered offset, skeleton, arc fibration, arc domain, convex hull, medial axis.

bisect(t_0, t_1)

(1) Construct b
(2) Compute error $\delta = \delta(b, c[t_0, t_1])$
(3) If $\delta \leq \varepsilon$ then return b
(4) Else return bisect$(t_0, \frac{t_0+t_1}{2}) \cup$ bisect$(\frac{t_0+t_1}{2}, t_1)$

The first step of the above algorithm is the construction of the primitive b, which approximates $c(t)$ in the interval $t \in [t_0, t_1]$. After that, we compute the error δ, which is measured by the one-sided Hausdorff distance

$$\delta(b, s) = \max_{p \in b} \min_{q \in s} ||p - q|| .$$

If the error is less or equal the tolerance the primitive b is returned. Otherwise **bisect(·)** recursively calls itself two times using the intervals $\left[t_0, \frac{t_0+t_1}{2}\right]$ and $\left[\frac{t_0+t_1}{2}, t_1\right]$.

A curve can be approximated by a polyline using n straight line segments to the same precision as a polyline using only $\mathcal{O}(n^{2/3})$ circular arc segments. An equivalent formulation is that a circular arc polyline consisting of n arcs approximates a shape with o lower error than a polyline with the same number of primitives.

Biarcs were introduced by [4]. One biarc consists of two smoothly joined circular arcs and can be used to interpolate two points and associated tangents at those points. The joint of a biarc, i.e., the point that connects the two circular arcs is not unique. In fact, the joint can be any point, lying on the so called *joint circle*. Figure 1 shows the two points $c(t_0)$ and $c(t_1)$ and the associated tangents (black arrows). Both, the interpolated points and all joints lie on the joint circle (gray). A selection of possible biarcs are illustrated by dashed lines.

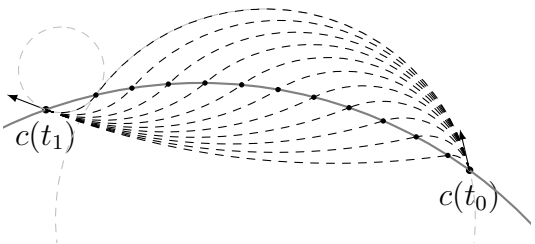

FIGURE 1. One parameter family of biarcs approximating $c(t)$ at t_0 and t_1.

The usage of biarcs as the primitives b in the above algorithm results in a tangent continuous approximation curve of $c(t)$. A tangent continuous piece-wise circular curve is an *arc spline*. An *arc domain* is a domain whose boundary curve is an arc spline.

1. Convex hull

This section is based on the results of [3]. The convex hull $CH(S)$ of a set S is the smallest convex set such that $S \subseteq CH(S)$. In its simplest form the set S consists of n points. A simple and elegant solution is given by [6] assuming that a simple polyline is given that connects those n points. Melkman's approach uses a double ended queue which represents and maintains the convex hull in each iteration. We loop over all vertices of S in the order in which they form a simple polyline. If v_i lies in the convex hull constructed in the previous step (and represented by $\mathcal{D}$) it can be deleted. Otherwise we have to restore convexity by deleting vertices from both ends of $\mathcal{D}$ until the polygon represented by $\mathcal{D}$ is convex again. The vertex v_i is then added to $\mathcal{D}$ (at both ends).

Input: Simple polyline consisting of n vertices v_i.
Output: Convex hull.

(1) initialize $\mathcal{D}$
(2) loop over polyline vertices v_i
  (a) if $v_i \in CH_{i-1}$, skip v_i.
  (b) restore convexity by deleting vertices from the bottom of $\mathcal{D}$. Insert v_i at the bottom.
  (c) restore convexity by deleting vertices from the top of $\mathcal{D}$. Insert v_i at the top.

This algorithm achieves linear complexity for two reasons. First, the polyline is simple hence the inclusion test (Item 2a) takes constant time. Second, the sum over all convexity restore steps takes linear time.

Melkman's algorithm has been generalized by [3] in a way that it computes the convex hull of a simple arc polyline.

Input: Simple arc spline consisting of n arcs b_i.
Output: Convex hull.

(1) initialize by computing $CH_2 = CH(b_1, b_2)$.
(2) loop over the b_i
  (a) If $CH(b_i) \subset CH_{i-1}$, skip b_i and set $CH_i = CH_{i-1}$

(b) Else restore convexity by deleting non convex elements of CH_{i-1} and adding b_i with tangents to CH_i.

The above algorithm is initialized by the convex hull of the first two circular arcs b_1 and b_1 of the arc polyline. If the convex hull of b_i is contained in the previous convex hull we assign $CH_i = CH_{i-1}$. Otherwise the convexity has to be restored and we add b_i to the new convex hull. The latter step however, is more involved. One must assure that the construction of the correct tangents, which connect a new arc b_i with the convex hull, only take linear time over all those steps such that a linear complexity is obtained, see [3].

2. Medial axis

This section reflects the results of [1] who computes the medial axis of a free-form shape Ω based on an arc spline approximation. They prove convergence of their approximated medial axis to the real medial axis of the free-form shape, which is not given for approximations by points or line segments.

A *maximal disk* D is a disk which is contained in Ω and there is no other disk D' such that $D' \supset D$ and $D' \subset \Omega$ holds. The upper illustration of Fig. 2 shows a maximal disk (gray). The *medial axis* of Ω is defined as the set of all maximal disks of Ω.

A divide and conquer strategy is used to compute the medial axis. Its two steps are

(1) Find an dividing disk repeat until base case. (Divide)
(2) Handle base cases and merge the results. (Conquer)

The first step is to find a *dividing disk*, i.e., a maximal disk that splits Ω into two sub-shapes of (approximately) the same size. A balanced split is crucial to obtain an optimal (randomized) run-time complexity of $\mathcal{O}(n \log n)$. Figure 2 shows Ω before (top) the division with its dividing disk and after the split (bottom). The division step is recursively repeated until one of the base cases appear for which the computation of the medial axis is trivial. For non-smooth boundaries there are nine more bases cases.

We demonstrate the well known fact that boundary approximations by points and line segments cause artificial branches of the medial axis. Consider a boundary curve (bottom, black, solid) and its medial axis (top, dashed-dotted) as in Fig. 3 (left) and approximate it by points (gray). The medial axis of the points consists then of all the dashed lines (bisectors of neighbor points). The disk (gray) indicates a maximal disk.

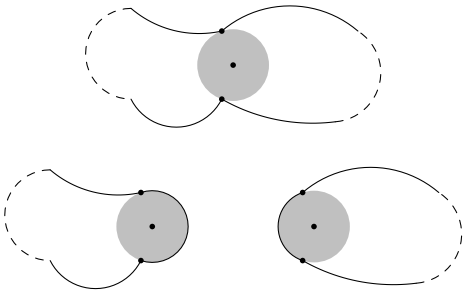

FIGURE 2. Division step

In Fig. 3 (right) the boundary is approximated by straight line segments. Again, the dashed lines are artificial branches of the medial axis. There is no convergence since a finer approximation of the boundary curve leads in both cases (point and straight line approximation) to more artificial branches.

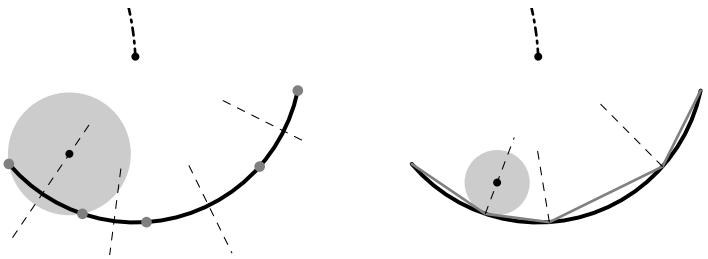

FIGURE 3. Medial axis comparison for different types of approximation primitives.

The problem of artificial branches can be avoided by using spiral biarcs as approximation primitives. Spiral biarcs preserve spirals, i.e., segments with monotone curvature.

3. Mitered offsets and skeletons

This section is based on the results of [7]. Mitered offsets and straight skeletons have been defined for planar straight subdivisions[2] (e.g. a simple polygon). An evolution process of the boundary has been employed in which all edges are shifted in a self parallel manner. Tracing the vertices of the edges during the evolution reveals the straight skeleton.

We define mitered offsets and the associated skeletons on planar subdivisions whose edges are circular arcs (A straight line segment is a circular arc with infinite radius.) by an evolution process that increase or

decrease the edge's radii. Figure 4 shows an arc polygon (black) with an untrimmed offset (gray). The offset has three self intersections and a gap (left).

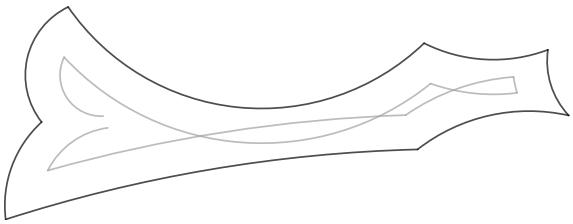

FIGURE 4. Offsetting an arc polygon without trimming.

We distinguish three types of vertices by their inner angle. A *reflex* vertex has an inner angle greater than π, *smooth* vertices have an angle of exactly π and all other vertices are said to be *convex*.

A comparison of classical (euclidean) and mitered offsets for straight line polygons as well as for arc splines can be found in Fig. 5. The main difference between classical and mitered offsets is that the latter ones preserve reflex vertices (left column). Classical offsets cause reflex vertices to be rounded (right column).

Global consistency of the offsets is ensured by handling events, which avoid the occurrence of self-intersections and gaps, during the evolution. These events can be classified into two groups. *Local events* entail only local combinatorial modifications. Topological modifications are entailed by *global events*. Figure 6 shows two local events (left) and two global events (right). We discuss those events (from left to right) starting with the vanish event: There are three edges, the one at the bottom shrinks to length zero and vanished therefore. The bubble event of an edge is also characterized by coinciding vertices of an edge, however the length of the edge does not shrink to zero, it becomes maximal, i.e. the edge becomes a circle. The third illustration shows a split event: A reflex vertex runs into an edge and splits the edge into two parts. The squeeze event is similar but do not involve any vertices. Two edges touch and both of the edges become divided into two parts.

The splice event adds an artificial edge (a semi-circle) to our shape in case the evolution causes two neighbor edges to be in tangential contact. In Fig. 7 an arc of the skeleton emerges from the reflex vertex until the contact of the edges is tangential and it splices, which creates a new edge and two new smooth vertices.

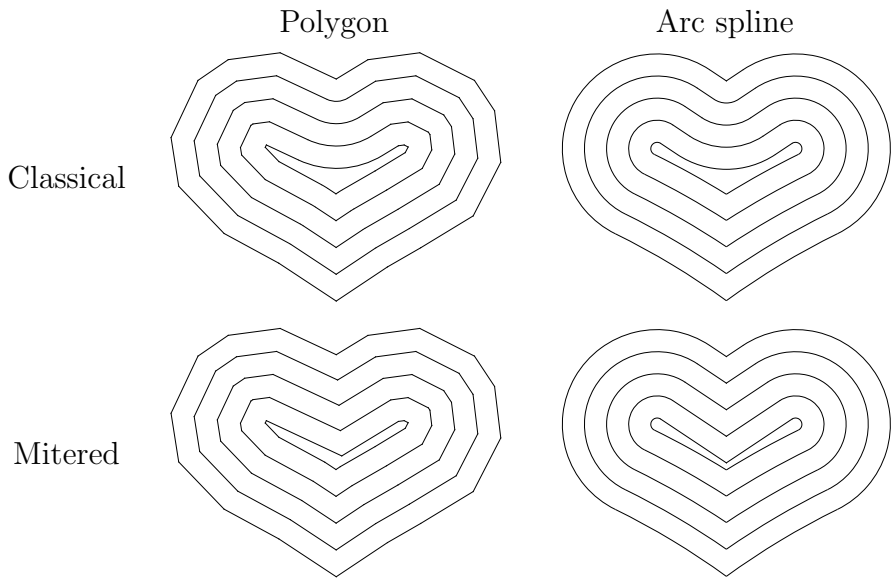

FIGURE 5. Comparison of classical and mitered offsets for polygons and arc splines.

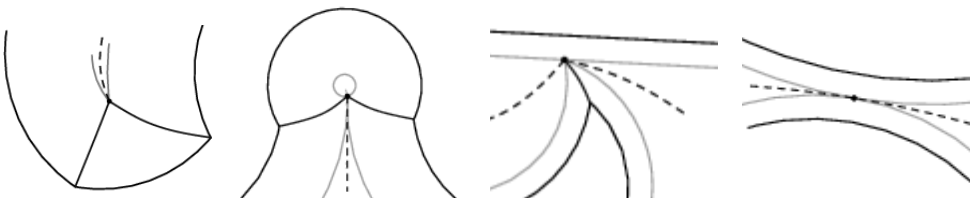

FIGURE 6. From left to right: Vanish-, bubble-, split- and squeeze event.

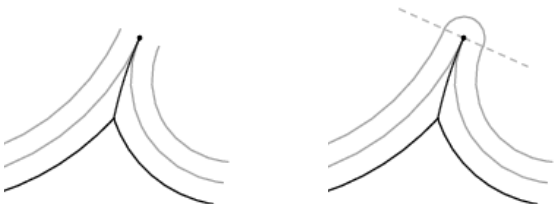

FIGURE 7. Splice event

The *skeleton* $\mathcal{S}$ of an arc spline P is defined as the path of all non-smooth vertices. This skeleton, together with the paths of smooth vertices and the arc polygon P, separates the interior of P into disjoint patches, the so called *patch decomposition* $\mathcal{P}$.

Each of these patches associated to either an edge of the patch decomposition or an edge created by a splice event. The intersection of a patch and any straight line through the center of the corresponding edge of that patch is connected. This property is known as the radial monotonicity property. The shape in Fig. 8 has three edges and four patches, the patch in the middle was created by a splice event. The radial lines in the upmost patch illustrate the radial monotonicity property.

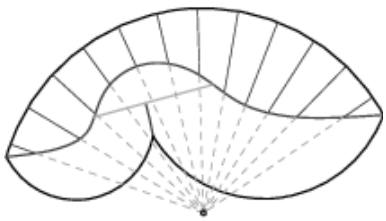

FIGURE 8. The red (radial) lines indicate the radial monotonicity property.

Mitered offsets are, in contrast to classical offsets, locally invertible: The offsetting of a shape by an offset distance $-\delta$ followed by on offset of δ yields the original shape (see Fig. 9 left) as long as there are no vanish events. This is not given for classical offsets where the same procedure (offsetting by $-\delta$ and then by δ) results in rounded corners, see Fig. 9 (right).

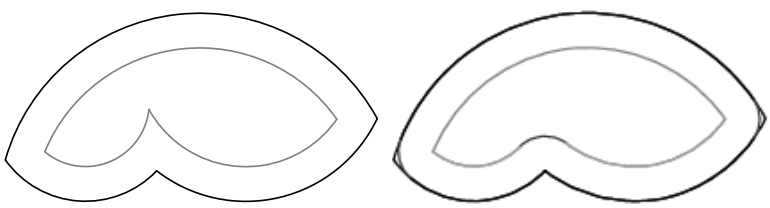

FIGURE 9. Mitered offsets are locally invertible (left) while classical offsets are not (right, red arcs).

It can be shown that the size of the patch decomposition is linear (in the number of vertices of the planar subdivision). Since each vertex of the skeleton corresponds to an events, it size can be determined by counting events. Special attention has to be paid to events that create new edges (split, squeeze and splice events).

We present an algorithm that computes the patch decomposition $\mathcal{P}$ of a circular arc polygon. Both, the skeleton and the mitered offsets, can the

obtained from $\mathcal{P}$. While computing the skeleton having $\mathcal{P}$ is trivial the computation of the mitered offsets is slightly more involved: The trick is to raise $\mathcal{P}$ into space by adding the offset distance as a third coordinate. Each patch is then a patch on a cone and we obtain the mitered offsets by intersection of a plane parallel to the planar subdivision and the cone-patches.

Our algorithm operates on the edge list E, $\mathcal{P}$ (to store the results) and an local event list Q. The local event list stores all local events sorted by the time of their occurrence.

Input: Arc Spline represented as edge list E
Output: Patch decomposition $\mathcal{P}$

(1) $Q \leftarrow \mathit{initLocalEventList}(E)$
(2) Initialize empty patch decomposition $\mathcal{P}$.
(3) while $E \neq \emptyset$
    (a) $e \leftarrow \mathit{computeNextEvent}(E)$
    (b) Grow patch decomposition $\mathcal{P}$ until event e.
    (c) $\mathit{handleEvent}(e, Q, E, \mathcal{P})$

First, we initialize the local event queue Q and the empty patch decomposition $\mathcal{P}$. We loop over the edge list of our shape as long as it is not empty. Within that loop three steps need to be processed. The next event that has to handled is either a local one, taken directly from Q, or a global event, depending on which event occurs first. The computation of the next global event is costly (up to $\mathcal{O}(n^2)$). $\mathcal{P}$ is grown until e arises. In the last step we handle the event. This means that we either have to delete edges from E (vanish events), newly connect formerly unconnected edges (bubble events) or split edges as for split- and squeeze events. In any case Q has to be updated by adding new events and delete events which refer to edges that may not exist anymore. The complexity is $\mathcal{O}(n^3)$ and memory consumption is linear. Figure 10 shows the results of our algorithm applied to a handcrafted arc polygon. The mitered offsets are shown left and on the right is the patch decomposition.

There is a slightly more general notion of splice events than the one we have introduced that closes gaps at the latest possible moment in the evolution (i.e. when neighbor edges become tangential). Since we want to permit earlier splicing we introduce σ, which is a global parameter to determine the angle at which we want a reflex vertex to splice. Figure 11 shows a curve with a reflex vertex and its offset curve (top) after an splice event occurred. However, if we splice the reflex vertex immediately at

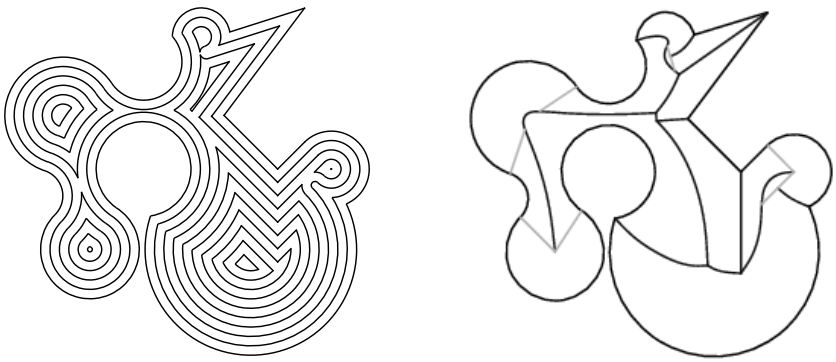

FIGURE 10. Mitered offset (left) and the associated patch decomposition (right).

the angle σ the resulting offset curve is the gray line. The dashed lines are the paths of the smooth vertices created by the σ-splice event.

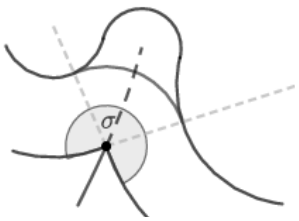

FIGURE 11. The σ-splice event

The splice parameter σ allows us to link our results to the medial axis and classical offsets. In case our planar shape consists only of straight edges and we set $\sigma = 2\pi$ the straight skeleton is obtained. If σ is exactly π the skeleton becomes the medial axis and the mitered offsets become classical offsets since every angle splices immediately.

Figure 12 shows the effect of the choice of σ on the shape and topology of the skeleton. The top left pictures shows a reflex vertex that was spliced immediately and therefore the skeleton is the medial axis. Increasing σ leads to a growing arc of the skeleton emanating from the reflex vertex. In the bottom right picture that skeleton arc connects to the remaining of the skeleton.

4. Arc fibration

This section is based on [5]. Any star-shaped domain Ω permits a polar parameterization by choosing a point of its kernel, the center of the parameterization, from which the (straight) parameter lines emanate. This

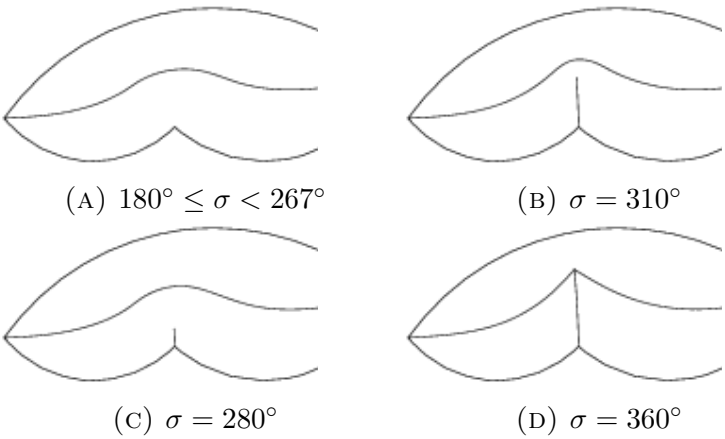

(A) $180° \leq \sigma < 267°$ (B) $\sigma = 310°$

(C) $\sigma = 280°$ (D) $\sigma = 360°$

FIGURE 12. We observe the changing skeleton (blue) for varying values of σ.

kernel's boundary consists of inflection tangents of the domain. We generalize polar parameterizations by permitting circular arcs as parameter lines, which is known as arc fibration given that it is regular.

There are two question that need to be addressed:

(1) How do we actually compute an arc fibration for a given center point?
(2) How do we find a center point that admits an arc fibration?

These questions have been discussed by [5]. First, they give a thorough analysis on the conditions under which a polar parameterization becomes an arc fibration. Second, they show that the kernel's boundary is formed by points where osculating circles touch with opposite orientation. However, this is a rather theoretical result and does not easily translate into an algorithm that computes the kernel's boundary.

We propose to discretize Ω's boundary using an arc spline approximation $c(t)$ of the boundary curve to perform the kernel computations, see Fig. 13. The arc fibration kernel of C^2 boundary curves is characterized by points where osculating circles touch with opposite orientation. Since arc splines are only C^1 smooth we introduce discretized osculating circles (*DOCs*).

A discrete osculating circle is a circle that is tangential to the boundary of Ω and changes its side from the exterior of the domain to its interior or vice versa. Therefore, the possible center points of DOCs are restricted to certain segments: In Fig. 14 (left) the upper dashed circle is a DOC while the lower one is not (it does not change its side of the boundary). For any point on the ***a****nti* ***j****oint* ***c****ircle* AJC (gray) the dashed circles touch with

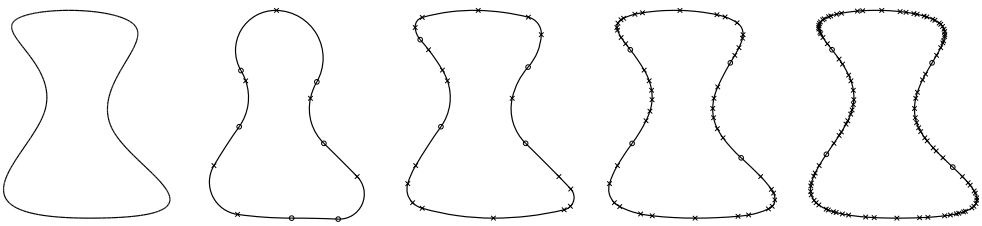

FIGURE 13. The original spline (left) is approximated by arc splines with increasing quality (from the second to the fifth illustration).

opposite orientation, which is inherited from the black solid boundary arcs. The dashed lines of the right illustration in Fig. 14 are the possible center points of DOCs. The thick arc on the anti joint circle is the region at which both DOCs fulfill their possible center constraints. The process of removing all but the thick arc on the AJC is called *trimming*.

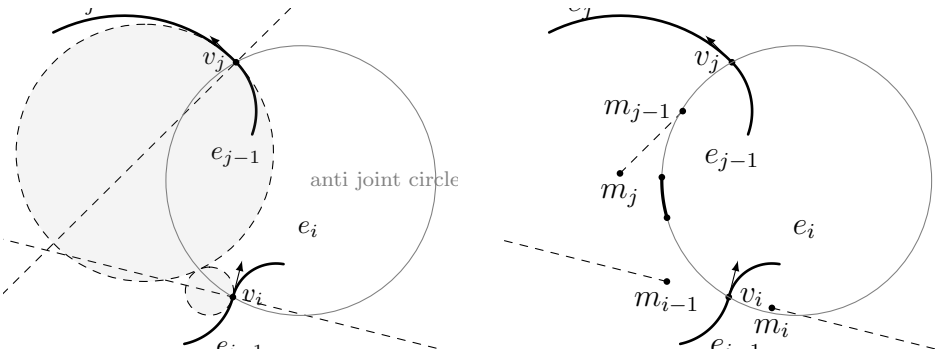

FIGURE 14. Left: Circles touch on the anti joint circle (gray). Right: Potential center points of DOCs (dashed) and the trimmed thick arc on the anti joint circle.

It can be shown that the kernel of an arc spline is bordered by DOCs, which touch with opposite orientation. For each pair of DOCs there exists a one-parameter family of points at which they touch with opposite orientation. Those touching points lie on the AJC, which is indeed a circle.

Since the DOCs inherit their orientation from the boundary curve there may be an configuration where the DOCs have non-matching orientation with respect to the boundary curve. This is illustrated in Fig. 15: The DOC arc (dashed) at v_k starts to the exterior of Ω, it ends in z where the other DOC arc (dashed) at v_ℓ touches. The orientations at v_k do not

match, the orientations at v_ℓ match. Therefore the anti joint circle arc, on which z lies, is not part of the domain's kernel and is removed. The process of detecting and removing non-matching orientations is referred to as *orientation filter*.

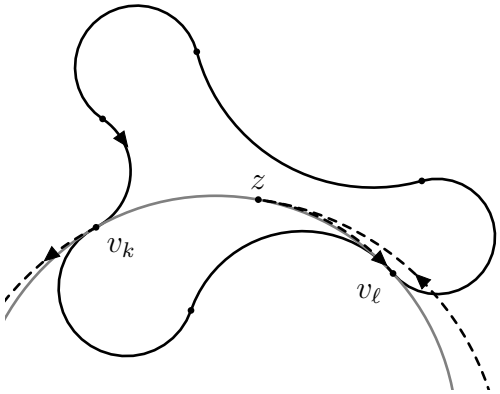

FIGURE 15. The orientation filter

The number of potential boundary elements of the kernel is further reduced by the *pear filter*: We distinguish two configurations of touching DOC arcs. In the pear case (cf. Fig. 16, left) the two DOC arcs (the one which connect z to the boundary) touch in z such that the interior of the domain (gray shaded) lies to their left and an angle of 2π at the test point z is formed. Such a test point does not lie on the boundary and will therefore be removed from the AJC arc by the pear filter.

However, in the *sting* case, an (inner) angle of 0 is formed at z, see Fig. 16 (right). The test point z does lie on the kernel's boundary and is consequently not removed by the pear filter. The rationale of the pear filter is that the test point z can be moved within a small neighborhood around itself while the boundary (via the DOC arcs) is still visible (cf. Fig. 16, left). If we move the test point z in Fig. 16 to the left the boundary is still (arc) visible. If we move z to the right of its current position the DOC arcs would need to overlap meaning that no regular parameterization is feasible for such a choice of the test point.

The following algorithm computes the arc fibration kernel of an arc domain. We initialize an empty set $\mathbf{Z}$, which stores the kernel's boundary. $\mathbf{P}$ is the set of all unordered vertex pairs of $c(t)$. For each $p \in \mathbf{P}$ three steps are performed: First, construction and trimming of the AJCs. Second, the pear and the orientation filter are applied. Finally, the remaining, potentially boundary arcs, are added to $\mathbf{Z}$.

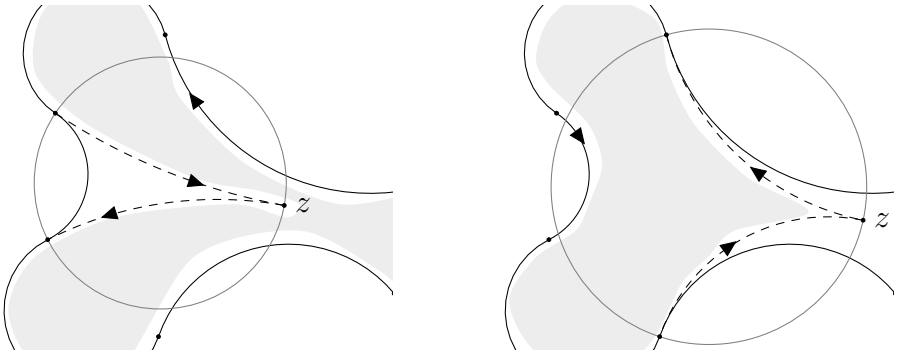

(A) Pear case (B) Sting case

FIGURE 16. The pear filter.

Input: Boundary of Ω
Output: Arc fibration kernel of Ω

(1) Initialize the empty set $\mathbf{Z}$.
(2) Initialize $\mathbf{P}$ as the set of all unordered pairs of vertices of $c(t)$.
(3) foreach $p \in \mathbf{P}$ do:
    (a) Use p to compute and trim the AJC.
    (b) Apply the pear and orientation filter.
    (c) Add ajc to $\mathbf{Z}$.

Figure 17 shows various stages of our arc fibration kernel algorithm using the HOURGLASS example. At the top left, all anti joint circles are shown and right therefrom the results after trimming. The bottom row shows the remaining anti joint circle arcs after the pear filter (left) and after the orientation filter (right) have been applied. Clearly, the kernel is the region in the middle of the illustration at the bottom right.

5. Conclusions & Future work

Circular boundary representations are beneficial since they can be computed very easily and to arbitrary precision. Circular boundary representations are potentially C^1 smooth when biarcs are employed. The number of approximation primitives is reduced to $\mathcal{O}(n^{2/3})$ (using circular arc primitives) compared to straight line primitives at the same precision.

The convex hull example shows that a well known algorithm for a simple polylines can be extended to simple arc splines while maintaining its linear complexity. We use the medial axis example to point out that

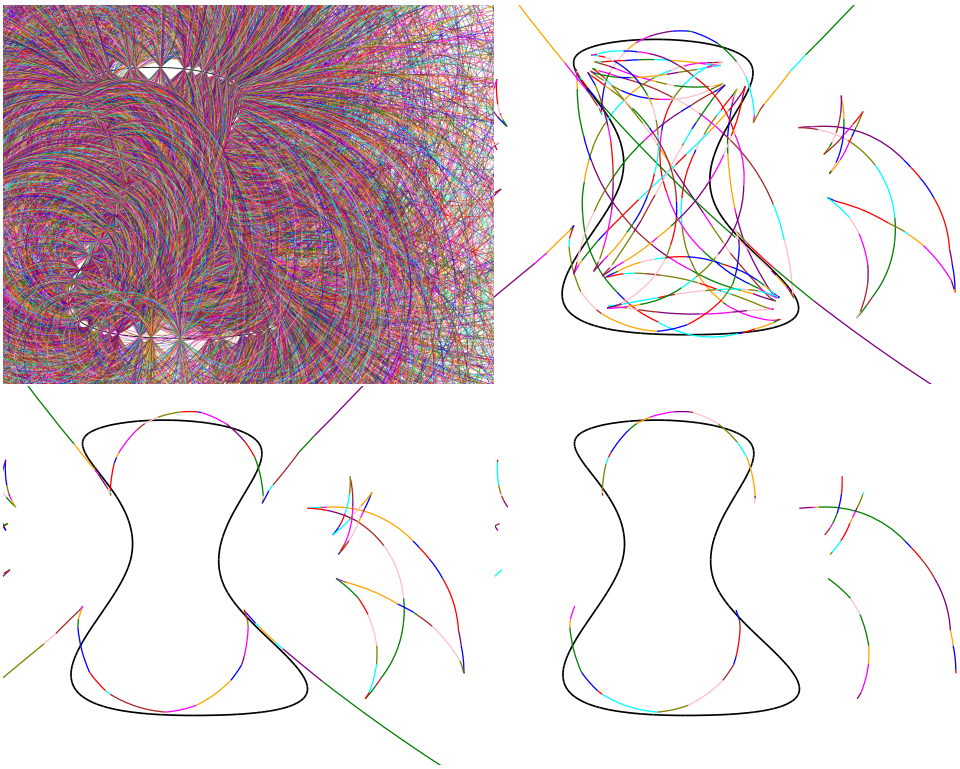

FIGURE 17. Various stages of the arc fibration kernel algorithm.

arc spline boundaries may also possess theoretical advantages over point and straight line approximations of boundary curves.

Mitered offsets and straight skeletons are generalized to arc spline boundaries by the introduction of suitable events. The size of the skeleton is linear and its patch decomposition possesses the radial monotonicity property. The extension from closed arc polygons to general planar subdivisions by circular arcs is straight forward.

Arc fibrations are a generalization of regular polar parameterizations by permitting circular arcs as parameter lines. We exemplify that the kernel's boundary of an arc domain consists of circular arcs only and outline an algorithm computing the kernel. The analysis of more general classes of parameter lines such as Bézier curves and conic section arcs is considered future work.

References

[1] Oswin Aichholzer, Wolfgang Aigner, Franz Aurenhammer, Thomas Hackl, Bert Jüttler, and Margot Rabl, *Medial axis computation for planar free–form shapes*, Computer-Aided Design **41** (2009), no. 5, 339–349.

[2] Oswin Aichholzer, Franz Aurenhammer, David Alberts, and Bernd Gärtner, *A novel type of skeleton for polygons*, J. UCS The Journal of Universal Computer Science, Springer, 1996, pp. 752–761.

[3] Oswin Aichholzer, Franz Aurenhammer, Thomas Hackl, Bert Jüttler, Margot Rabl, and Zbynek Šír, *Computational and structural advantages of circular boundary representation*, International Journal of Computational Geometry & Applications **21** (2011), no. 01, 47–69.

[4] K. M. Bolton, *Biarc curves*, Computer-Aided Design **7** (1975), no. 2, 89–92.

[5] Bert Jüttler, Sofia Maroschek, Myung-Soo Kim, and Q. Youn Hong, *Arc fibrations of planar domains*, NFN Report 80, Johannes Kepler University Linz, Geometry + Simulation.

[6] Avraham A. Melkman, *On-line construction of the convex hull of a simple polyline*, Information Processing Letters **25** (1987), no. 1, 11–12.

[7] Bastian Weiß, Bert Jüttler, and Franz Aurenhammer, *Mitered offsets and skeletons for circular arc polygons*, Manuscript.

Institute of Applied Geometry, Johannes Kepler University, Altenberger Str. 69, Linz, 4040, Austria
Email: bastian(dot)weiss(at)jku(dot)at
URL: https://www.jku.at/

Preface to Section **Voronoi Diagrams. Theoretical Aspects and Application**

Among our many distinguished compatriots, Georgy Voronoi rightfully holds an honorable place. During his short life, he published six fundamental monographs and six smaller scientific papers. However, this talented Ukrainian mathematician made numerous brilliant discoveries in number theory and the geometry of quadratic forms, which have become classical mathematical concepts and objects. He is also considered the founder of entire directions in these fields. The true significance of most of his works became clear only many years after his death, and some of the problems he addressed remain unsolved to this day. G. F. Voronoi, undeterred by difficulties, aimed to solve fundamentally important problems, and one feature of his work was the algorithmic focus of his research. In Voronoi's work, there are no published papers without algorithmically complete. One of the most famous scientific results of G. F. Voronoi is the geometric structure he studied, which was named after him: the Voronoi Diagram. It is an effective generalized algorithmic tool for solving a wide range of proximity problems and other tasks that reduce to them. This is significant because notable scientists such as R. Descartes, L. Dirichlet, A. Thiessen, and others actively engaged with the Voronoi Diagram. However, the scientific community decided to honor G. F. Voronoi by naming it after him for his substantial contribution to the study of this geometric structure. Even in ancient times, the Egyptians in the Nile Valley built their irrigation systems on an intuitive level, which were nothing other than Voronoi Diagrams. Moreover, the Voronoi Diagram is not just an abstraction created by human imagination but a reflection of the laws of nature. Today, the Voronoi Diagram has become the most popular universal tool for solving problems in various fields of science and technology. It is challenging to find an area of our lives where the Voronoi Diagram is not used at some stage. This includes creating optimally functioning communication systems, designing microchips, constructing various devices, studying processes in nature, archaeology, demography, epidemic control, astrophysics, and even in art, political, and economic dominance. At the conference dedicated to the 150th anniversary of the birth of Georgy Voronoi, an entire section, «Voronoi Diagrams. Theoretical Aspects and Applications», was devoted to the Voronoi Diagram and its applications. Five major presentations were made on the theoretical and practical aspects of applying the Voronoi Diagram to solve a wide range of problems. M. Kamarianakis presented the results of a

theoretical study on fundamental predicates for construction the 3D Additively Weighted Voronoi diagram (Apollonian Diagram). Specifically, the focus was on the algorithmic analysis of the predicate to minimize its algebraic degree. It was shown that the maximum algebraic degree required to answer any of the sub-predicates and primitives is 10, which is relatively small compared to the corresponding 2D version of the Edge-Conflict predicate. V. Tereshchenko and D. Kotsur presented an efficient method for segmenting the network of biological neurons in fluorescent microscopy images using the Voronoi Diagram. They solved the problem of outlining the contours of biological neuron networks and then constructed the skeleton of the network based on the approximate Voronoi Diagram, segmenting the main elements of individual neurons. The proposed segmentation algorithm aims to facilitate further research in biology. M. Tanemura's study focused on packings and their applications, particularly considering the Voronoi Voronoı random packing (VRP) as a new type of random sequential packing in higher-dimensional spaces. An example application of VRP could be in biology or botany: habitats for animals and plants. For instance, due to competition among individuals, the final «territory» pattern of plants may resemble the VRP pattern for asynchronous (sequential) plant colonization. A.D. Rud, I.M. Kiryan, and A.M. Lakhnik presented work on analyzing the topological properties of disordered carbon molecules modeled using the Voronoi Diagram. The paper proposes using the sphericity coefficient of Voronoi polyhedra as a topological order parameter to quantitatively assess the degree of disorder in amorphous structures. The theoretical and practical results presented in the works delve into the core principles defined by the content of the Voronoi Diagram, demonstrating their mathematical beauty. Meanwhile, the application-oriented research showcases how this geometric construct is used to address real-world problems. By celebrating the contributions of Georgy Voronoi, we honor his legacy, illustrating the breadth of his influence and the ongoing relevance of his work. The contributions on these pages are a testament to Voronoi's profound impact, providing a platform for continued innovation and discoveries inspired by his foundational ideas.

November 2018

Professor Vasyl Tereshchenko
Chair of the Section of Voronoi Diagrams.
Theoretical Aspects and Applications

Voronoï's Impact on Modern Science, Book 6, Volume 2
Proceedings of the Sixth International Conference on Analytic Number Theory and Spatial Tessellations

THE EDGECONFLICT PREDICATE IN THE 3D APOLLONIUS DIAGRAM

Manos KAMARIANAKIS (*Greece*)

ABSTRACT. In this paper we study one of the fundamental predicates required for the construction of the 3D Apollonius diagram (also known as the 3D Additively Weighted Voronoi diagram), namely the EDGECONFLICT predicate: given five sites S_i, S_j, S_k, S_l, S_m that define an edge e_{ijklm} in the 3D Apollonius diagram, and a sixth query site S_q, the predicate determines the portion of e_{ijklm} that will disappear in the Apollonius diagram of the six sites due to the insertion of S_q.

Our focus is on the algorithmic analysis of the predicate with the aim to minimize its algebraic degree. We decompose the main predicate into three sub-predicates, which are then evaluated with the aid of four additional primitive operations. We show that the maximum algebraic degree required to answer any of the sub-predicates and primitives, and, thus, our main predicate is 10.

Among the tools we use is the 3D inversion transformation. In the scope of this paper and due to space limitations, only non-degenerate configurations are considered, i.e. different Voronoi vertices are distinct and the predicates never return a "degenerate" answer. Most of our analysis is carried out in the inverted space, which is where our geometric observations and analysis is captured in algebraic terms.

1. INTRODUCTION

Voronoi diagrams have been among the most studied constructions in computational geometry since their inception [14, 9, 4, 15], due to their numerous applications, including motion planning and collision detection, communication networks, graphics, and growth of microorganisms in biology.

Received November 19, 2018.

2010 *Mathematics Subject Classification.* Primary 68U05, 65D99; Secondary 68W30, 68Q25.

Key words and phrases. computational geometry, algebraic computing, geometric predicates, Euclidean Apollonius diagram, EdgeConflict predicate.

Due to page limitations, the analysis of most subpredicates is omitted. The full version of the reviewed paper can be found at [19]. This work was supported by Onassis Foundation and Project Thales.

Despite being a central topic in research for many years, generalized Voronoi diagrams, and especially the Voronoi diagram of spheres (also known as the 3D Apollonius diagram) have not been explored sufficiently [24]; this is also pointed out by Aurenhammer et al. [5]. Moreover, due to recent scientific discoveries in biology and chemistry, 3D Apollonius diagrams are becoming increasingly important for representing and analysing the molecular 3D structure and surface [18] or the structure of the protein [23].

The methods used to calculate the Apollonius diagram usually rely on the construction of a different diagram altogether. Some methods include the intersection of cones [3] with the lifted power diagram and lower envelope calculations [29, 28, 16]. Boissonnat et al. use the convex hull to describe its construction [8, 7]. Aurenhammer's lifting method has also been implemented for two dimensions [1]. Karavelas and Yvinec [20] create the 2d Apollonius diagram from its dual, using the predicates developed in [12]. In [12], it is also reported that the Apollonius diagram can be obtained as a concrete case of the abstract Voronoi diagrams of Klein et al. [25].

Kim et al. made a major research contribution in the domain of the Voronoi diagrams of spheres including one patent [22] for the computation of 3D Voronoi diagrams. Their work provides many new algorithms related to the Voronoi diagrams including the computation of three-dimensional Voronoi diagrams [22], Euclidean Voronoi diagram of 3D balls and its computation via tracing edges [21] and the Euclidean Voronoi diagrams of 3D spheres and applications to protein structure analysis [23].

Hanniel and Elber [16] provide an algorithm for computation of the Voronoi diagrams for planes, spheres and cylinders in $\mathbb{R}^3$. Their algorithm relies on computing the lower envelope of the bisector surfaces similar to the algorithm of Will [28]. However, none of the current research efforts provide the exact method for computing the Apollonius diagram (or its dual Delaunay graph) of spheres.

In this paper, we are inspired by the the approach presented by Emiris and Karavelas in [12] for the evaluation of the 2D Apollonius diagram. In order to extend their work towards an algorithm that would incrementally construct the Apollonius diagram for 3D spheres, we develop equivalent predicates as the ones presented in their paper for the 2D case. Our main goal is to implement the most degree demanding predicate, called the EdgeConflict predicate: given five sites S_i, S_j, S_k, S_l, S_m that define a finite edge e_{ijklm} in the 3D Apollonius diagram, and a sixth query site S_q, the predicate determines the portion of e_{ijklm} that will disappear in the Apollonius diagram of the six sites due to the insertion of S_q.

In order to accomplish this task, we developed various subpredicates and primitives. The creation of these tools was made taking into consideration

the modern shift of predicate design towards lower level algorithmic issues. Specifically, a critical factor that influenced our designs was our goal to minimize the algebraic degree of the tested quantities (in terms of the input parameters) during a predicate evaluation. Such a minimization problem has become a main concern that influences algorithm design especially in geometric predicates, where zero tolerance in all intermediate computations is needed to obtain an accurate result [10, 13, 6, 27, 30] .

Our main contribution in the research area is the development of a list of subpredicates that where not implemented, either explicitly or implicitly, in the current bibliography and can be used within the scope of an incremental algorithm that constructs the 3D Apollonius diagram of a set of spheres. Our most outstanding result is the fact that all subpredicates presented in this paper along with the EdgeConflict predicate require at most 10-fold degree demanding operation (with respect to the input quantities). This is quite an unexpected result since the equivalent EdgeConflict predicate in the 2D Apollonius diagram required 16-fold operations [12, 25]. Our approach of resolving the "master" predicate and especially the observations made in the inverted plane, could also be implemented in the 2D case to yield lower algebraic degrees.

This paper is organised as follows. In Section 2, we review the preliminaries of the Apollonius diagram of 3D spheres and the orientation of hyperbolic trisectors in such a diagram. An introduction to the inversion technique is also made along with useful remarks regarding the correlation between the original and the inverted space. In Section 3, we present in detail the EdgeConflict predicate along with the assumptions made in the scope of this paper. An outline of the subpredicates developed is then provided along with the geometric properties that derive from each one. Finally, we provide the main algorithm that ultimately combines all the aforementioned tools to answer the EdgeConflict predicate. Section 4 is devoted to the implementation and algebraic analysis for each subpredicate. Finally, in Section 5, we conclude the paper.

2. Preliminaries and Definitions

Let $\mathcal{S}$ be a set of closed spheres S_n (also referred as *sites*) in $\mathbb{E}^3$, with centers $C_n = (x_n, y_n, z_n)$ and radii r_n. In this paper, we will assume that no one of these sites is contained inside another. Define the Euclidean distance $\delta(p, S)$ between a point $p \in \mathbb{E}^3$ and a sphere $S = \{C, r\}$ as $\delta(p, S) = \|p - C\| - r$, where $\|\cdot\|$ stands for the Euclidean norm. The *Apollonius diagram* is then defined as the subdivision of the plane induced by assigning each point $p \in \mathbb{E}^3$ to its nearest neighbor with respect to the distance function $\delta(\cdot, \cdot)$.

For each $i \neq j$, let $H_{ij} = \{y \in \mathbb{E}^3 : \delta(y, S_i) \leq \delta(y, S_j)\}$. Then the (closed) *Apollonius cell* V_i of S_i is defined to be $V_i = \cap_{i \neq j} H_{ij}$. The set of points that belong to exactly two Apollonius cells are called the *Apollonius faces*, whereas the connected set of points that belong to exactly three Apollonius cells are called *Apollonius edges*. Points that belong to more than three Apollonius cells are called *Apollonius vertices*; the *Apollonius diagram* $\mathcal{VD}(\mathcal{S})$ of $\mathcal{S}$ is defined as the collection of the Apollonius cells, faces, edges and vertices.

An Apollonius vertex v is a point that belongs to 4 or more Apollonius cells. Without loss of generality we may assume that an Apollonius vertex is tangent to exactly 4 sites S_i, S_j, S_k, S_l, since otherwise we may apply a pertrubation scheme to resolve the degeneracy. The sphere centered at v and tangent to S_i, S_j, S_k, S_l is either externally tangent to them, or is contained inside all 4 four sites; in the former case it is called an *external Apollonius sphere*, while in the latter an *internal Apollonius sphere*. Let T_n, $n = i, j, k, l$, be the point of tangency of the Apollonius sphere and S_n. The tetrahedron $T_iT_jT_kT_l$ can either be positively or negatively oriented, or even flat [11]. We assume below that $T_iT_jT_kT_l$ is not flat; otherwise we may employ the perturbation scheme described in [11] and, thus, consider it as non-flat. The Apollonius vertex corresponding to a positively (resp., negatively) oriented tetrahedrom $T_iT_jT_kT_l$ will be denoted v_{ijkl} (resp., v_{ikjl}). Observe that a cyclic permutation of the indices does not affect our choice of Apollonius vertex.

The *trisector* τ_{ijk} of three different sites S_i, S_j and S_k is the locus of points that are equidistant from the the three sites. In the absense of degeneracies its Hausdorff dimension is 1, and it is either (a branch of) a hyperbola, a line, an ellipse, a circle, or a parabola [29]; in this paper, due to space limitations, we focus on the cases where the trisector is an open curve, and more specifically hyperbolic or linear. An *Apollonius edge* e_{ijklm} is a connected subset of the trisector τ_{ijk} of three different sites and is defined by five sites S_i, S_j, S_k, S_l and S_m. The first three sites define the supporting trisector τ_{ijk} of the edge, whereas the last two define its endpoints v_{ijkl} and v_{ikjm}.

2.1. **Inversion.** The 3-dimensional *inversion transformation* is a mapping from $\mathbb{R}^3$ to $\mathbb{R}^3$ that maps a point $z \in \mathbb{R}^3$ to the point $W(z) = (z - z_0)/\|z - z_0\|^2$. The point z_0 is called the *pole of inversion*. Inversion maps spheres that do not pass through the pole to spheres, and spheres that pass through the pole to planes.

In the Apollonius diagram context we call $\mathcal{Z}$-space the space where the sites live. Since the Apollonius diagram does not change when we add to the radii of all spheres the same quantity, we will, most of the times, reduce the radii of the spheres S_i, S_j, S_k, S_l, S_m by the radius of one of them, the sphere S_I. The new spheres have obviously the same centers, whereas their radii

become spheres become $r_n^\star = r_n - r_I$, $n \in \{i, j, k, l, m\}$. For convience, we call the image space of this radius-reducing transformation the $\mathcal{Z}^\star$-space. We may then apply inversion, with C_I as the pole, to get a new set of spheres or planes; we call $\mathcal{W}$-space the space where the radius-reduced, inverted sites live.

Since the sites S_i, S_j, S_k, S_l, S_m are not contained inside each is tangent to another, the image of the sphere S_n in $\mathcal{W}$-space is a sphere $S_n^\star$, centered at $C_n^\star = (u_n, v_n, w_n)$ with radius ρ_n, where

$$u_n = \frac{x_n^\star}{p_n^\star}, \qquad v_n = \frac{y_n^\star}{p_n^\star}, \qquad w_n = \frac{z_n^\star}{p_n^\star}, \qquad \rho_n = \frac{r_n^\star}{p_n^\star},$$
$$x_n^\star = x_n - x_I, \quad y_n^\star = y_n - y_I, \quad z_n^\star = z_n - z_I, \quad r_n^\star = r_n - r_I,$$

and $p_n^\star = (x_n^\star)^2 + (y_n^\star)^2 + (z_n^\star)^2 - (r_n^\star)^2$. Note that $p_n^\star$ is positive due to the non-inclusion assumption. We also define the quantities

$$D_{ijk}^{\pi\theta} = \begin{vmatrix} \pi_i & \theta_i & 1 \\ \pi_j & \theta_j & 1 \\ \pi_k & \theta_k & 1 \end{vmatrix}, \quad D_{ijk}^{\pi\theta\eta} = \begin{vmatrix} \pi_i & \theta_i & \eta_i \\ \pi_j & \theta_j & \eta_j \\ \pi_k & \theta_k & \eta_k \end{vmatrix}, \quad D_{ijkl}^{\pi\theta\eta} = \begin{vmatrix} \pi_i & \theta_i & \eta_i & 1 \\ \pi_j & \theta_j & \eta_j & 1 \\ \pi_k & \theta_k & \eta_k & 1 \\ \pi_l & \theta_l & \eta_l & 1 \end{vmatrix},$$

$$D_{ijkl}^{\pi\theta\eta\zeta} = \begin{vmatrix} \pi_i & \theta_i & \eta_i & \zeta_i \\ \pi_j & \theta_j & \eta_j & \zeta_j \\ \pi_k & \theta_k & \eta_k & \zeta_k \\ \pi_l & \theta_l & \eta_l & \zeta_l \end{vmatrix}, E_{ijk}^{\pi\theta\eta} = \begin{vmatrix} \pi_i^\star & \theta_i^\star & \eta_i^\star \\ \pi_j^\star & \theta_j^\star & \eta_j^\star \\ \pi_k^\star & \theta_k^\star & \eta_k^\star \end{vmatrix}, E_{ijkl}^{\pi\theta\eta\zeta} = \begin{vmatrix} \pi_i^\star & \theta_i^\star & \eta_i^\star & \zeta_i^\star \\ \pi_j^\star & \theta_j^\star & \eta_j^\star & \zeta_j^\star \\ \pi_k^\star & \theta_k^\star & \eta_k^\star & \zeta_k^\star \\ \pi_l^\star & \theta_l^\star & \eta_l^\star & \zeta_l^\star \end{vmatrix},$$

for $\pi, \theta, \eta, \zeta \in \{x, y, z, r, u, v, w, \rho\}$, and it holds that

$$D_{ijk}^{\pi\theta} = E_{ijk}^{klp}(p_i^\star p_j^\star p_k^\star)^{-1}, \quad D_{ijk}^{\pi\theta\eta} = E_{ijk}^{klm}(p_i^\star p_j^\star p_k^\star)^{-1}$$

for $\pi, \theta \in \{u, v, w, \rho\}$ and $k, l, m \in \{x, y, z, r\}$.

2.2. **Orientation of a hyperbolic or linear trisector.** Under the assumption that the trisector τ_{ijk} of the sites S_i, S_j, S_k is a line or a hyperbola, the three centers C_i, C_j, C_k cannot be collinear [29]. A natural way of orienting τ_{ijk} is accomplished via the well-known "right-hand rule"; if we fold our right hand to follow the centers C_i, C_j and C_k (in that order), our thumb will be showing the positive "end" of τ_{ijk} (see Figure 1).

By orienting τ_{ijk}, we clearly define an ordering on the points of τ_{ijk}, which we denote by $\prec$. Let o_{ijk} be the intersection of τ_{ijk} and the plane Π_{ijk} going through the centers C_i, C_j and C_k. We can now parametrize τ_{ijk} as follows: if $o_{ijk} \prec p$ then $\zeta(p) = \delta(p, S_i) - \delta(o_{ijk}, S_i)$; otherwise $\zeta(p) = -(\delta(p, S_i) - \delta(o_{ijk}, S_i))$. The function $\zeta(\cdot)$ is a 1-1 and onto mapping from τ_{ijk} to $\mathbb{R}$. Moreover, we define $\zeta(S)$, where S is an external tangent sphere to the sites S_i, S_j and S_k, to be $\zeta(c)$, where $c \in \tau_{ijk}$ is the center of S.

We also use τ^+_{ijk} (resp. τ^-_{ijk}) to denote the positive (resp. negative) semi-trisector i.e., the set of points $p \in \tau_{ijk}$ such that $o_{ijk} \prec p$ (resp. $p \prec o_{ijk}$).

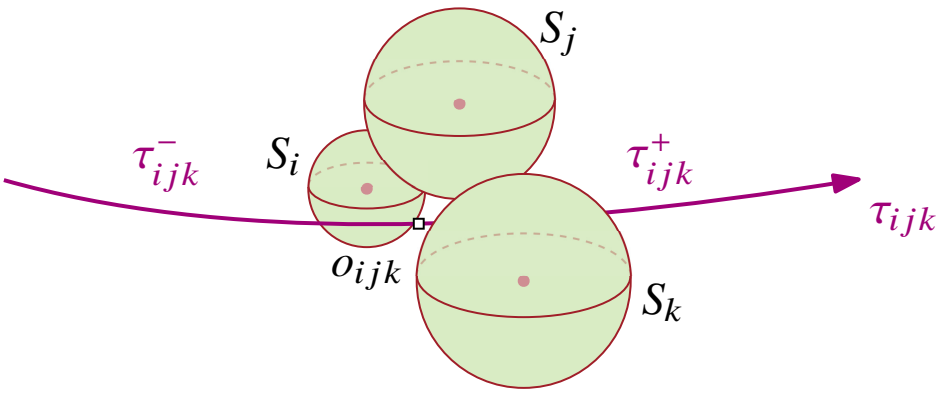

FIGURE 1. The case where the trisector τ_{ijk} of the spheres S_i, S_j and S_k is *hyperbolic*. Notice the orientation of τ_{ijk} based on the "right-hand rule". The point o_{ijk} of the trisector, which is coplanar with the centers C_i, C_j and C_k, separates the τ_{ijk} into two semi-trisectors, τ^-_{ijk} and τ^+_{ijk}.

3. Non-Degenerate Case Analysis for Hyperbolic Trisectors

3.1. **Voronoi Edges on Hyperbolic Trisectors.** In order to better understand our initial problem, more insight regarding the properties of a Voronoi diagram is required. Let us look closer at an edge e_{ijklm} (we drop the subscript for convenience) of $\mathcal{V}(\mathcal{S})$, where $\mathcal{S}$ is a set of given sites that includes S_n for $n \in \{i, j, k, l, m\}$ and does not include S_q. This edge e lies on the trisector τ_{ijk}, the locus of points that are equidistant to the sites Si, S_j and S_k. In the scope of this paper, we assume that τ_{ijk} is of Hausdorff dimension 1 and is either (a branch of) a hyperbola or a line. To ensure that the spheres Si, S_j and S_k meet this criteria, the predicate Trisector (S_i, S_j, S_k), described in Section 3.3.2 and analyzed in Section 4.2 of [19], must return "hyperbolic".

We now focus on the edge e, i.e. the open continuous subset of τ_{ijk} whose closure is bounded by the Voronoi vertices v_{ijkl} and v_{ikjm}. If $\mathcal{T}(t)$ denotes the external Apollonius sphere of the sites S_i, S_j and S_k that is centered at t, the most crucial property of a point $t \in e$ is that $\mathcal{T}(t)$ does not intersect with any other site of $\mathcal{S}$. We call this *the Empty Sphere Principle* since it is a property that derives from the empty circle principle of a generic Voronoi diagram and its basic properties.

Using this property, we can show that the left and right endpoint of e are the Apollonius vertices v_{ijkl} and v_{ikjm} respectively. To prove that the left endpoint

is indeed v_{ijkl} and not v_{ikjl}, consider a point $t \in \tau_{ijk}$ such that $t \equiv v_{ikjl}$ and move it infinitesimally on the trisector towards its positive direction. The initial Apollonius sphere $\mathcal{T}(v_{ikjl})$ was tangent to S_l, and assuming v_{ikjl} was the left endpoint of e, the sphere $\mathcal{T}(t)$ should not longer be tangent nor intersect S_l since $t \in e$ and the Empty Sphere Principle must hold. However, due to the negative orientation of the tetrahedron $T_iT_jT_kT_l$, where T_n is the tangency point of the sphere S_n and $\mathcal{T}(v_{ikjl})$ for $n = i, j, k, l$, and the orientation of τ_{ijk}, the sphere $\mathcal{T}(t)$ contains T_l and therefore intersects S_l, yielding a contradiction. Therefore, we have proven that the left point of e is necessarily v_{ijkl} and we can prove that the right endpoint is v_{ikjm} (and not v_{ijkm}) in a similar way.

3.2. **Problem Outline and Assertions.** For clarity reasons, we restate the EdgeConflict predicate, highlighting its input, output as well as the assertions we are making for the rest of this paper.

The EdgeConflict predicate, one of the fundamental predicates required for the construction of the 3D Apollonius diagram (also known as the 3D Additively Weighted Voronoi diagram), takes as input five sites S_i, S_j, S_k, S_l and S_m that define an edge e_{ijklm} in the 3D Apollonius diagram as well as a sixth query site S_q. The predicate determines the portion of e_{ijklm} (we drop the subscript for convenience) that will disappear in the Apollonius diagram of the six sites due to the insertion of S_q and therefore its output is one of the following

- NoConflict: no portion of e is destroyed by the insertion of S_q in the Apollonius diagram of the five sites.
- EntireEdge: the entire edge e is destroyed by the addition of S_q in the Apollonius diagram of the five sites.
- LeftVertex: a subsegment of e adjacent to its origin vertex (v_{ijkl}) disappears in the Apollonius diagram of the six sites.
- RightVertex: is the symmetric case of the LeftVertex case; a subsegment of e adjacent to the vertex v_{ikjm} disappears in the Apollonius diagram of the six sites.
- BothVertices: subsegments of e adjacent to its two vertices disappear in the Apollonius diagram of the five sites.
- Interior: a subsegment in the interior of e disappears in the Apollonius diagram of the five sites.

In Section 3.4, we prove that these are indeed the only possible answers to the studied predicate, under the assumption that no degeneracies occur. Specifically, all analysis presented in this paper is done under the following two major assertions:

- The trisector τ_{ijk} of the sites S_i, S_j and S_k is "hyperbolic" i.e., it is either a branch of a hyperbola or a straight line. Therefore, the spheres

must lie in *convex position*; in other words, there must exist two distinct planes commonly tangent to all three spheres.
- None of the subpredicates called during the algorithm presented in Section 3.4 returns a degenerate answer. Mainly, this is equivalent to the statement: *All of the existing Apollonius vertices defined by the sites S_i, S_j, S_k and S_n, for $n \in \{l, m, q\}$, are distinct and the respective Apollonius spheres are all finite i.e., they are not centered at infinity*. Such assertion dictates that the edge e is finite as none of its bounding vertices v_{ijkl} and v_{ikjm} can lie at infinity.

3.3. **SubPredicates and Primitives.** In this section, we describe the various subpredicates used throughout the evaluation of the EdgeConflict predicate via the main algorithm presented in Section 3.4. For convenience, only the input, output and specific geometric observations is provided in this section, whereas a detailed implementation along with a algebraic degree analysis of each subpredicate is found in Section 4 of [19].

3.3.1. *The* InSphere *predicate.* The InSphere$(S_i, S_j, S_k, S_a, S_b)$ predicate returns $-$, $+$ or 0 if and only if the sphere S_b intersects, does not intersect or is tangent to the external Apollonius sphere of the sites S_i, S_j, S_k and S_b, centered at v_{ijka}. It is assumed that v_{ijka} exists and none of the first four inputed sites are contained inside one another. In [17], it is shown that the evaluation of the InSphere predicate requires operations of maximum algebraic degree 10, whereas in [2] an implicit InSphere predicate could be evaluated via the Delaunay graph, using 6-fold degree operations (although it is not clear if we could easily distinguish if we are testing against the Apollonius sphere centered at v_{ijka} or v_{ikja}).

Since degenerate configurations are beyond the scope of this paper, the InSphere tests evaluated during the main algorithm (see Section 3.4) will always return $+$ or $-$. We should also remark that, in bibliography, the InSphere predicate is also referred to as the VertexConflict predicate to reflect the fact that a negative (resp. positive) outcome of InSphere$(S_i, S_j, S_k, S_a, S_b)$ amounts to the Apollonius vertex v_{ijka} in $\mathcal{VD}(\Sigma)$ vanishing (resp. remaining) in $\mathcal{VD}(\Sigma \cup \{S_b\})$, where Σ contains S_i, S_j, S_k and S_a but not S_b.

Lemma 1. *The* InSphere *predicate can be evaluated by determining the sign of quantities of algebraic degree at most 10 (in the input quantities).*

3.3.2. *The* InCone *and* Trisector *predicates.* Given three spheres S_a, S_b and S_c, such that S_a and S_b are not contained one inside the other, we want to determine the relative geometric position of S_c with respect to the uniquely defined closed semi-cone $\mathcal{K}(S_a, S_b b)$ that is tangent to both S_a and S_b and

includes their centers (see Figure 2). We shall call this the $\textsc{InCone}(S_a, S_b; S_c)$ predicate.

In case the radii of S_a and S_b are equal, $\mathcal{K}(a, b)$ (we drop the parenthesis for convenience) degenerates into a cylinder without this having an impact to the predicate. If S_c° is used to denote the open sphere that corresponds to S_c, then all possible answers of the predicate $\textsc{InCone}(S_a, S_b; S_c)$ are

- Outside , if at least one point of S_c is outside $\mathcal{K}$,
- Inside, if S_c° lies inside $\mathcal{K}$ and $S_c \cap \mathcal{K} = \emptyset$,
- OnePointTouch, if S_c° lies inside $\mathcal{K}$ and $S_c \cap \mathcal{K}$ is a point,
- CircleTouch, if S_c° lies inside $\mathcal{K}$ and $S_c \cap \mathcal{K}$ is a circle.

The last two answers are considered "degenerate" and therefore, we may consider that whenever InCone is called during the algorithm presented in Section 3.4, it will either return Outside or Inside.

This predicate is basic tool used in various other sub-predicates such as the Trisector, which returns the trisector type of a set of three spheres. It is known ([29]) that if the trisector τ_{abc} of S_a, S_b, S_c has Hausdorff dimension 1, it can either be a branch of a"hyperbola", a "line", an "ellipse", a "circle" or a "parabola"; these are the possible answers of the $\textsc{Trisector}(S_a, S_b, S_c)$ predicate. However, since the "line" and the "circle" type are sub-case of the "hyperbolic" and "elliptic" trisector types respectively, we can characterize a trisector as either "hyperbolic", "elliptic" or "parabolic".

During the execution of the main algorithm of Section 3.4, the Trisector (S_i, S_j, S_k) has to be evaluated. Being able to distinguish the type of the trisector τ_{ijk} is essential since all the analysis presented in this paper assumes that τ_{ijk} is hyperbolic.

The analysis followed to determine the outcome of the InCone or the Trisector predicate can be found in Sections 4.1 and 4.2 of [19] respectively, where the following lemma is proved.

Lemma 2. *The* InCone *and* Trisector *predicates can be evaluated by determining the sign of quantities of algebraic degree at most 4 (in the input quantities).*

3.3.3. *The* Distance *predicate.* When the trisector τ_{ijk} is a hyperbola or a line, there exist two distinct planes, denoted by Π^-_{ijk} and Π^+_{ijk}, such that each one is commonly tangent to the sites S_i, S_j, S_k and leave their centers on the same halfspace.

Observe that Π^-_{ijk} and Π^+_{ijk} correspond to the two Apollonius spheres *at infinity*, in the sense that they are centered at *infinity* and are cotangent to the spheres S_i, S_j and S_k. These planes are considered as oriented, and subdivide

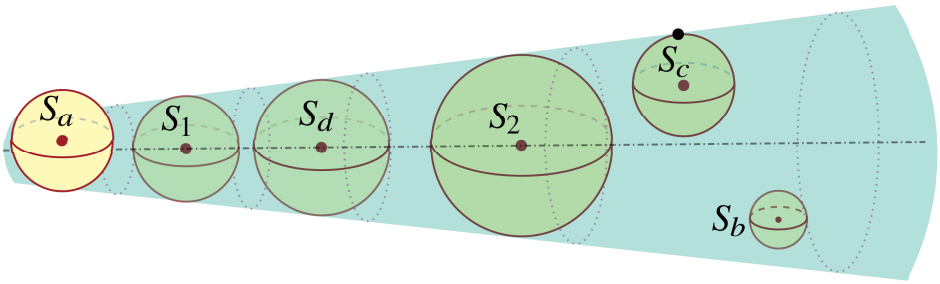

FIGURE 2. Some of the possible locations of a sphere S_n against the cone $\mathcal{K}$ defined by S_1 and S_2. The INCONE$(S_1, S_2; S_n)$ returns Outside, Inside, OnePointTouch and CircleTouch for $n = a, b, c$ and d respectively.

$\mathbb{R}^3$ into a positive and a negative halfspace, the positive being the halfspace containing the centers of the spheres.

Given a point p on τ_{ijk}, we denote by $\mathcal{T}(p)$ the tritangent Apollonius sphere of S_i, S_j and S_k centered at p. If we move p on τ_{ijk} such that $\zeta(p)$ goes towards $-\infty$ or $+\infty$, the sphere $\mathcal{T}(p)$ becomes the corresponding Apollonius sphere at infinity i.e., the plane Π^-_{ijk} or Π^+_{ijk} (see Figure 3).

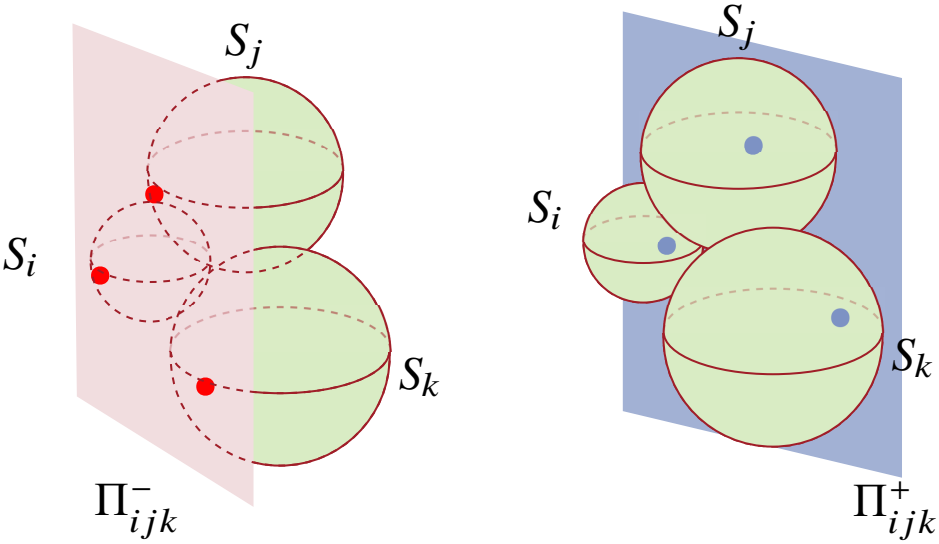

FIGURE 3. If the spheres S_i, S_j and S_k lie in a convex position there exist two distinct planes, Π^-_{ijk} and Π^+_{ijk}, cotangent to all spheres. These planes are considered as the Apollonius sphere of the sites S_i, S_j and S_k, centered at $p \in \tau_{ijk}$, as $\zeta(p)$ goes to $\pm\infty$ respectively.

Given the sites S_i, S_j, S_k and S_α, the DISTANCE $(S_i, S_j, S_k, S_\alpha)$ predicate determines whether S_α intersects, is tangent to, or does not intersect the (closed) negative halfspaces delimited by the two planes Π^-_{ijk} and Π^+_{ijk}. The "tangency" case is considered as degenerate and is beyond the scope of this paper. This predicate is used in the evaluation of the SHADOW predicate. and is equal to $\text{DISTANCE}(S_i, S_j, S_k, S_\alpha) = \big(\mathsf{sign}(\delta(S_\alpha, \Pi^-_{ijk})), \mathsf{sign}(\delta(S_\alpha, \Pi^+_{ijk}))\big)$, where $\delta(S, \Pi) = \delta(C, \Pi) - r$, and $\delta(C, \Pi)$ denotes the signed Euclidean of C from the plane Π and S is a sphere of radius r, centered at C. As for the EXISTENCE predicate, we reduce it to the computation of the signs of the two roots of a quadratic equation and prove the following lemma (see Section 4.4 of [19] for this analysis).

Lemma 3. *The* DISTANCE *predicate can be evaluated by determining the sign of quantities of algebraic degree at most 6 (in the input quantities).*

3.3.4. *The* EXISTENCE *predicate.* The next primitive operation we need for answering the EDGECONFLICT predicate is what we call the EXISTENCE predicate: given four sites S_a, S_b, S_c and S_n, we would like to determine the number of Apollonius spheres of the quadruple S_a, S_b, S_c, S_n. In general, given four sites there can be "0", "1", "2" or "infinite" Apollonius spheres (cf. [11]) including the Apollonius sphere(s) at infinity. The $\text{EXISTENCE}(S_a, S_b, S_c, S_n)$ predicate only counts the Apollonius spheres that are *not* centered at infinity and since degenerate configurations of the input sites are beyond the scope of this paper, it is safe to assume that the outcome will always be "0","1" or "2". It is also clear that in case of a "1" outcome, the corresponding Apollonius center will either be v_{abcn} or v_{acbn} but not both; the case where $v_{abcn} \equiv v_{acbn}$ is ruled out by our initial no-degeneracies assumption.

The analysis of the EXISTENCE predicate can be found in Section 4.3 of [19] where we prove the following lemma.

Lemma 4. *The* EXISTENCE *predicate can be evaluated by determining the sign of quantities of algebraic degree at most 8 (in the input quantities).*

3.3.5. *The* SHADOW *predicate.* We now come to the second major subpredicate used by the EDGECONFLICT predicate: the SHADOW predicate.

Given three sites S_i, S_j and S_k, we define the *shadow region* $\mathcal{SR}(S_\alpha)$ of a site S_α, with respect to the trisector τ_{ijk}, to be the locus of points p on τ_{ijk} such that $\delta(C_\alpha, \mathcal{T}(p)) < r_\alpha$. The shadow region of the sites S_l, S_m and S_q play an important role when answering $\text{EDGECONFLICT}(S_i, S_j, S_k, S_l, S_m, S_q)$ (see Figure 4 and Section 3.4).

The $\text{SHADOW}(S_i, S_j, S_k, S_\alpha)$ predicate returns the type of $\mathcal{SR}(S_\alpha)$ seen as an interval, or union of intervals, in $\mathbb{R}$. More precisely, the SHADOW

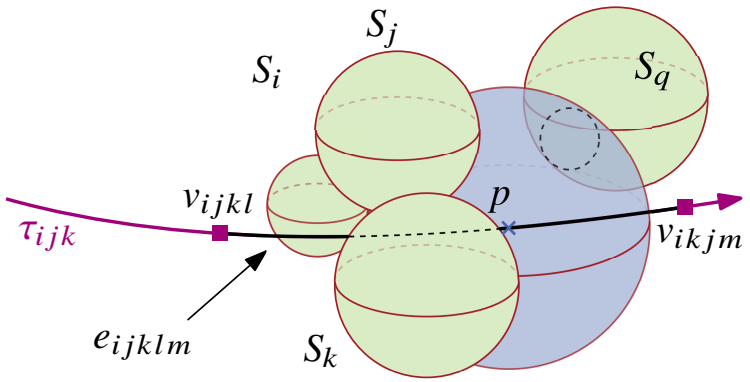

FIGURE 4. A finite edge e_{ijklm} of the Voronoi diagram $\mathcal{VD}(\mathcal{S})$ of the set $\mathcal{S} = \{S_n : n = i, j, k, l, m\}$ is the locus of points $p \in \tau_{ijk}$ such that $v_{ijkl} \prec p \prec v_{ikjm}$. Any sphere $\mathcal{T}(p)$, centered at p and cotangent to S_i, S_j and S_k does not intersect any sphere of $\mathcal{S}$ (*Empty Sphere Principle*). However, after inserting S_q in the existing Voronoi diagram, $\mathcal{T}(p)$ may intersect it. In $\mathcal{VD}(\mathcal{S} \cup \{S_q\})$, all points $p \in \mathcal{SR}(S_q)$ will no longer exist on the "updated" edge e'_{ijklm}.

predicate returns the topological structure of the set $\zeta(\mathcal{SR}(S_\alpha)) = \zeta(\{p \in \tau_{ijk} \mid \delta(C_\alpha, \mathcal{T}(p)) < r_\alpha\})$, which we denote by $SRT(S_\alpha)$.

Clearly, the boundary points of $\textsc{Shadow}(S_i, S_j, S_k, S_\alpha)$ are the points p on τ_{ijk} for which $\delta(C_\alpha, \mathcal{T}(p)) = r_\alpha$. These points are nothing but the centers of the Apollonius spheres of the four sites S_i, S_j, S_k and S_α, and, as such, there can only be 0, 1 or 2 (assuming no degeneracies). This immediately suggests that $SRT(S_\alpha)$ can have one of the following 6 types: $\emptyset$, $(-\infty, \infty) = \mathbb{R}$, $(-\infty, \phi)$, $(\chi, +\infty)$, (χ, ϕ), or $(-\infty, \phi) \cup (\chi, +\infty)$, where $\phi, \chi \neq \pm\infty$.

For convenience, we will use the $\mathcal{SR}(S_a)$ notation instead of $SRT(S_\alpha)$; for example, the statement "$\mathcal{SR}(S_a) = (-\infty, \phi)$" will be often used instead of "$\mathcal{SR}(S_a)$'s type is $(-\infty, \phi)$" or "$SRT(S_\alpha) = (-\infty, \phi)$" (see Figure 5 for an example). This notation change further highlights the fact that we are only interested in the topological structure of $\mathcal{SR}(S_a)$ rather than the actual set itself.

In Section 4.5 of [19], we prove that the evaluation of the SHADOW predicate only requires the call of the respective DISTANCE and EXISTENCE predicate, yielding the following lemma.

Lemma 5. *The* SHADOW *predicate can be evaluated by determining the sign of quantities of algebraic degree at most 8 (in the input quantities).*

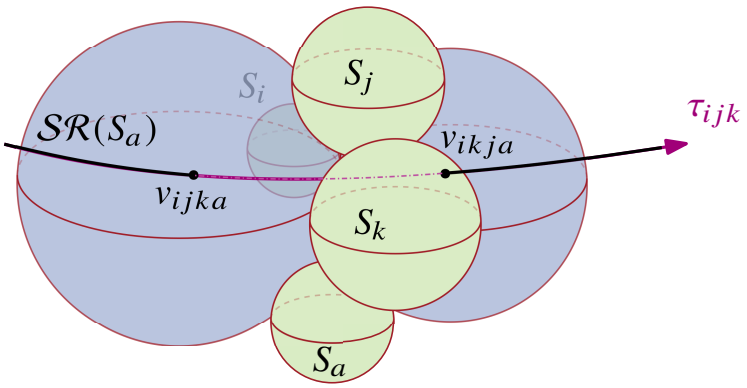

FIGURE 5. Since there are two Apollonius spheres of the sites S_n, for $n \in \{i, j, k, a\}$, centered at v_{ijka} and v_{ikja}, the $\mathcal{SR}(S_a)$ on τ_{ijk} must have two endpoints. In this specific configuration notice that, for every point p on the segments of τ_{ijk} painted black, the sphere $\mathcal{T}(p)$ will intersect S_a. Therefore, the black segments are indeed the shadow region $\mathcal{SR}(S_a)$ of the sphere S_a on the trisector τ_{ijk}.

3.3.6. *The* ORDER *predicate.* The most important sub-predicate used to evaluate the EDGECONFLICT predicate is what we call the ORDER predicate. When ORDER$(S_i, S_j, S_k, S_a, S_b)$ is called, it returns the order of appearance of any of the existing Apollonius vertices $v_{ijka}, v_{ikja}, v_{ijkb}$ and v_{ikjb} on the oriented trisector τ_{ijk}.

This sub-predicate is called during the main algorithm that answers the EDGECONFLICT$(S_i, S_j, S_k, S_l, S_m, S_q)$, for $(a, b) \in \{(l, q), (m, q)\}$, only in the case that either v_{ijkq}, v_{ikjq} or both exist. Let us also recall that, in this paper, the trisector τ_{ijk} is "hyperbolic" and that e_{ijklm} is a valid finite Apollonius edge; the Apollonius vertices v_{ijkl} and v_{ikjm} both exist on (the oriented) τ_{ijk} and $v_{ijkl} \prec v_{ikjm}$.

In order to answer the ORDER predicate, we first call the SHADOW(S_i, S_j, S_k, S_n) predicate, for $n \in \{a, b\}$, to obtain the type of $\mathcal{SR}(S_a)$ and $\mathcal{SR}(S_b)$. From the shadow region types, two pieces of information is easily obtained; firstly, we determine which of the Apollonius vertices v_{ijka}, v_{ikja} and v_{ijkb}, v_{ikjb} actually exist and secondarily, if both v_{ijkn} and v_{ikjn} exist for some $n \in \{a, b\}$, then their ordering on the oriented trisector is also retrieved. Such deductions derive from the study of the shadow region, as shown in Section 4.6.3, Lemma 15 of [19]. For example, if $\mathcal{SR}(S_a) = (\chi, \phi)$, then both v_{ijka} and v_{ikja} exist and appear on the oriented trisector in this order: $v_{ikja} \prec v_{ijka}$.

Now that the existence and partial ordering of the Apollonius vertices v_{ijka} and v_{ikja} (resp. v_{ijkb} and v_{ikjb}) is known, we must provide a way of "merging"

them into a complete ordering. For this reason, we examine all possible complete orderings of the Apollonius vertices on the oriented trisector τ_{ijk}. The study of these orderings is seen in the inverted plane $\mathcal{W}$-space. In Section 4.6.2 of [19], we present the strong geometric relationship that holds between the spheres of the original $\mathcal{Z}$-space and their images in the inverted plane. The observations we make regarding the connection of the two spaces allow us to interpret geometric configurations on one space to equivalent ones on the other. A full analysis of how we tackle all possible configurations is presented in Section 4.6 of [19].

In our analysis, we prove that the Order predicate, in the worst case, amounts to evaluate up to 4 InSphere predicates plus some auxiliary tests of lesser algebraic cost. We have therefore proven the following lemma.

Lemma 6. *The* Order *predicate can be evaluated by determining the sign of quantities of algebraic degree at most 10 (in the input quantities).*

3.4. **The main algorithm.** In this section, we describe in detail how the predicate EdgeConflict $(S_i, S_j, S_k, S_l, S_m, S_q)$ is resolved with the use of the subpredicates InCone, Trisector, Existence, Shadow and Order.

We begin by determining the type of the trisector τ_{ijk}; this is done via the call of the Trisector (S_i, S_j, S_k) predicate. Recall that in the scope of this paper, it is assumed that the τ_{ijk} is a hyperbola (or a line) and that none of the subpredicates called return a degenerate answer.

To answer the EdgeConflict predicate, one must determine which "part" of the edge e_{ijklm} remains in the Voronoi diagram after the insertion of the site S_q. This is plausible by identifying the set of points of e_{ijklm} that still remain in the updated Voronoi Diagram; each of these points must satisfy the "empty-sphere property": a sphere, centered at that point and tangent to the spheres S_i, S_j, S_k, must not intersect any other sites of the Voronoi Diagram. As an immediate result, a point p of the edge e_{ijklm} in $\mathcal{VD}(\mathcal{S})$ remains in $\mathcal{VD}(\mathcal{S} \cup \{S_q\})$ if and only if $\mathcal{T}(p)$ does not intersect S_q. Since the shadow region of the sphere S_q with respect to the trisector τ_{ijk} consists of all points p such that $\mathcal{T}(p)$ intersects S_q, it must hold that the part of the edge e_{ijklm} that no longer remains in $\mathcal{VD}(\mathcal{S} \cup \{S_q\})$ is actually $e_{ijklm} \cap \mathcal{SR}(S_q)$ (see Figure 4) . In conclusion, the result of the EdgeConflict predicate is exactly the set $e_{ijklm} \cap \mathcal{SR}(S_q)$ seen as an interval or union of intervals of $\mathbb{R}$.

To determine the intersection type of $e_{ijklm} \cap \mathcal{SR}(S_q)$, we first take into account that the finite edge e_{ijklm} consists of all points p on the oriented trisector τ_{ijk} bounded by the points v_{ijkl} and v_{ikjm} from left and right respectively (see Section 3.1). Next, we consider the type of $\mathcal{SR}(S_q)$ which can be evaluated as shown in Section 4.5 of [19] and is one of the following: $(-\infty, \phi)$, $(\chi, +\infty)$, (χ, ϕ), $(-\infty, \phi) \cup (\chi, +\infty)$, $\emptyset$ or $\mathbb{R}$.

If the edge e_{ijklm} is seen as the interval (λ_1, μ_2), evidently the intersection type of $E' = e_{ijklm} \cap \mathcal{SR}(S_q)$ must be one of the following 6 types, each corresponding to a different answers of the EdgeConflict predicate.

- If E' is of type $\emptyset$, the predicate returns NoConflict.
- If E' is of type e_{ijklm}, the predicate returns EntireEdge.
- If E' is of type (λ_1, ϕ), the predicate returns LeftVertex.
- If E' is of type (χ, μ_2), the predicate returns RightVertex.
- If E' is of type $(\lambda_1, \phi) \cup (\chi, \mu_2)$, the predicate returns BothVertices.
- If E' is of type (χ, ϕ), the predicate returns Interior.

This observation suggests that, if we provide a way to identify the type of E', we can answer the EdgeConflict predicate. Taking into consideration that

- λ_1 and μ_2 correspond to v_{ijkl} and v_{ikjm} respectively as shown in Section 3.1, and
- χ, ϕ correspond to v_{ikjq} and v_{ijkq} respectively as stated in Lemma 15 that we prove in Section 4.6.3 of [19],

it becomes apparent that if we order all Apollonius vertices v_{ijkl}, v_{ikjm} and any of the existing among v_{ijkq}, v_{ikjq}, bearing in mind the type of $\mathcal{SR}(S_q)$, we can deduce the type of E'.

For example, let us assume that $\mathcal{SR}(S_q)$ type is $(-\infty, \chi) \cup (\phi, +\infty)$. If $v_{ijkl} \prec v_{ikjq} \prec v_{ikjm} \prec v_{ijkq}$ on the oriented trisector τ_{ijk}, or equivalently $\lambda_1 < \chi < \mu_2 < \phi$, we can conclude that E' is of type (λ_1, ϕ) and the EdgeConflict predicate would return LeftVertex.

Therefore, it is essential that we are able to provide an ordering of the Apollonius vertices v_{ijkl}, v_{ikjm} and any of the existing among v_{ijkq}, v_{ikjq}. Such a task is accomplished via the call of the Order $(S_i, S_j, S_k, S_a, S_b)$ predicate $(a, b) = (l, q)$ and (m, q). The outcomes of these predicates consist of the orderings of all possible Apollonius vertices of the sites S_i, S_j, S_k, S_a and S_i, S_j, S_k, S_b on the trisector τ_{ijk}. These partial orderings can then be merged into a complete ordering, which contains the desired one. The results' combination principle is identical to the one used when we have to order a set of numbers but we can only compare two at a time.

A detailed algorithm that summarizes the analysis of this Section and can be followed to answer the EdgeConflict$(S_i, S_j, S_k, S_l, S_m; S_q)$ is described in the following steps.

Step 1: The Trisector (S_i, S_j, S_k) is called to determine the type of the trisector τ_{ijk}. In this Section, we assume that τ_{ijk} return "hyperbolic".

Step 2: We evaluate $SRT(q) =$ Shadow(S_i, S_j, S_k, S_q). If $SRT(q) = \emptyset$ or $\mathbb{R}$, we return NoConflict or EntireEdge respectively. Otherwise, we know that $SRT(q)$ has one of the forms $(-\infty, \phi)$, $(\chi, +\infty)$, (χ, ϕ)

or $(-\infty, \phi) \cup (\chi, +\infty)$, where ϕ and χ correspond to the Apollonius vertices v_{ijkq} and v_{ikjq} respectively.

Step 3: We evaluate Order $(S_i, S_j, S_k, S_l, S_q)$ and break down our analysis depending on how many of the vertices v_{ijkq} and v_{ikjq} exist; if only one vertex exist (which is equivalent to $SRT(q)$ being $(-\infty, \phi)$ or $(\chi, +\infty)$), denote it by v_q and go to Step 3a. Otherwise, if both exist, go to Step 3b.

Step 3a: If only v_{ikjq} or v_{ijkq} exist, then $SRT(q)$, which was evaluated in Step 2, is of the form $(-\infty, \phi)$ or $(\chi, +\infty)$ respectively. From the outcome of Order $(S_i, S_j, S_k, S_l, S_q)$, we know whether $v_q \prec v_{ikjl}$ or $v_{ikjl} \prec v_q$. If $v_q \prec v_{ijkl}$, and therefore $v_q \prec v_{ijkl} \prec v_{ikkm}$, the EdgeConflict predicate returns NoConflict if $SRT(q) = (-\infty, \phi)$ or EntireEdge if $SRT(q) = (\chi, +\infty)$.
If $v_{ijkl} \prec v_q$, we evaluate Order$(S_i, S_j, S_k, S_m, S_q)$ and determine whether $v_q \prec v_{ikjm}$ or $v_{ikjm} \prec v_q$. In the first case, we conclude that $v_{ijkl} \prec v_q \prec v_{ikjm}$ and the EdgeConflict predicate returns LeftVertex if $SRT(q) = (-\infty, \phi)$ or RightVertex if $SRT(q) = (\chi, +\infty)$. In the second case, we get that $v_{ijkl} \prec v_{ikjm} \prec v_q$ and the predicate returns EntireEdge if $SRT(q) = (-\infty, \phi)$ or NoConflict if $SRT(q) = (\chi, +\infty)$.

Step 3b: If both v_{ijkq} and v_{ikjq} exist, then $SRT(q)$ is of the form (χ, ϕ) or $(-\infty, \phi) \cup (\chi, +\infty)$, where ϕ and χ correspond to v_{ijkq} and v_{ikjq} respectively. We now call the Order$(S_i, S_j, S_k, S_l, S_q)$ predicate. If it returns that $v_{ijkq}, v_{ikjq} \prec v_{ijkl}$, the EdgeConflict predicate immediately returns NoConflict if $SRT(q) = (\chi, \phi)$, otherwise it returns EntireEdge.
If this is not the case, we have to call the Order$(S_i, S_j, S_k, S_m, S_q)$ predicate to acquire the ordering of v_{ijkq}, v_{ikjq} and v_{ijkm}. If $v_{ijkm} \prec v_{ijkq}, v_{ikjq}$, the EdgeConflict predicate immediately returns NoConflict if $SRT(q) = (\chi, \phi)$, otherwise it returns EntireEdge.
In any other case, we must combine the information from the two Order predicates with the fact that $v_{ikjl} \prec v_{ijkm}$, to obtain the complete ordering of v_{ikjl}, v_{ijkm}, v_{ijkq} and v_{ikjq}. The list of possible EdgeConflict predicate answers for the cases that have not been already handled is found in this list.

NoConflict: If $SRT(q) = (-\infty, \phi) \cup (\chi, +\infty)$, $v_{ikjq} \prec v_{ijkl} \prec v_{ikjm}$ and $v_{ijkl} \prec v_{ikjm} \prec v_{ijkq}$.

EntireEdge: If $SRT(q) = (\chi, \phi)$, $v_{ijkl} \prec v_{ikjm} \prec v_{ikjq}$ and $v_{ijkq} \prec v_{ijkl} \prec v_{ikjm}$.

LeftVertex: If $SRT(q) = (\chi, \phi)$, $v_{ijkl} \prec v_{ikjq} \prec v_{ikjm}$ and $v_{ijkq} \prec v_{ijkl} \prec v_{ikjm}$, or $SRT(q) = (-\infty, \phi) \cup (\chi, +\infty)$,

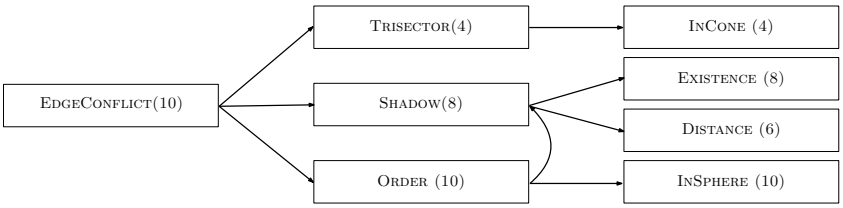

FIGURE 6. The layout of predicates and their subpredicates used to answer the EDGECONFLICT predicate. The number next to each predicate corresponds to its algebraic cost. It is assumed that every subpredicate returns a non-degenerate answer.

$v_{ijkl} \prec v_{ikjq} \prec v_{ikjm}$ and $v_{ijkl} \prec v_{ikjm} \prec v_{ijkq}$.

RightVertex: If $SRT(q) = (\chi, \phi)$ $v_{ijkl} \prec v_{ikjm} \prec v_{ikjq}$ and $v_{ijkq} \prec v_{ijkl} \prec v_{ikjm}$, or $SRT(q) = (-\infty, \phi) \cup (\chi, +\infty)$, $v_{ikjq} \prec v_{ijkl} \prec v_{ikjm}$ and $v_{ijkl} \prec v_{ijkq} \prec v_{ikjm}$.

BothVertices: If $SRT(q) = (-\infty, \phi) \cup (\chi, +\infty)$ and $v_{ijkl} \prec v_{ijkq}, v_{ikjq} \prec v_{ikjm}$

Interior: If $SRT(q) = (\chi, \phi)$ and $v_{ijkl} \prec v_{ijkq}, v_{ikjq} \prec v_{ikjm}$.

A sketch of the subpredicates used when answering the EDGECONFLICT predicate is shown in Figure 6. Since the highest algebraic degree needed in the evaluation of the subpredicates used is 10, we have proven the following theorem.

Theorem 1. *The* EDGECONFLICT *predicate can be evaluated by determining the sign of quantities of algebraic degree at most 10 (in the input quantities).*

4. Conclusion and Future Work

In this paper, we presented a clever way of combining various subpredicates in order to answer the EDGECONFLICT predicate. The design of all predicates and primitives was made in such a way that the maximum algebraic cost of answering them would be as low as possible, on the input quantities. Based on current bibliography, the resulting degree 10 of the main predicate is quite small when compared with the respective 2D version of the EDGECONFLICT predicate (16 as shown in [12] and 6 as shown in [26]). It is also remarkable that both the INSPHERE and the EDGECONFLICT predicates share the same algebraic degree under the no-degeneracies assumption.

Through our attempt to answer the master predicate, various useful primitives were also developed. These tools can also be used in the context of an incremental algorithm that evaluates the 3D Apollonius diagram of a set of spheres.

A natural extension of the work presented in this paper involves answering the EdgeConflict predicate in the case where the trisector of the first three input sphere is a parabola. One can follow a similar analysis with the hyperbolic case presented here, but several modifications have to be made for the analysis to be complete.

References

[1] Francçois Anton, Jean-Daniel Boissonnat, Darka Mioc, and Mariette Yvinec. An exact predicate for the optimal construction of the additively weighted voronoi diagram. In *Europ. Workshop Comput. Geom*, 2002.

[2] François Anton, Darka Mioc, and Marcelo Santos. Exact computation of the voronoi diagram of spheres in 3d, its topology and its geometric invariants. 28, 06 2011.

[3] Franz Aurenhammer. Power diagrams: properties, algorithms and applications. *SIAM Journal on Computing*, 16(1):78–96, 1987.

[4] Franz Aurenhammer and Rolf Klein. Voronoi diagrams. *Handbook of computational geometry*, 5:201–290, 2000.

[5] Franz Aurenhammer, Rolf Klein, and Der-Tsai Lee. *Voronoi diagrams and Delaunay triangulations*. World Scientific Publishing Company, 2013.

[6] Eric Berberich, Arno Eigenwillig, Michael Hemmer, Susan Hert, Kurt Mehlhorn, and Elmar Schömer. A computational basis for conic arcs and boolean operations on conic polygons. In *European Symposium on Algorithms*, pages 174–186. Springer, 2002.

[7] Jean-Daniel Boissonnat and Christophe Delage. Convex hull and voronoi diagram of additively weighted points. In GerthStølting Brodal and Stefano Leonardi, editors, *Algorithms – ESA 2005*, volume 3669 of *Lecture Notes in Computer Science*, pages 367–378. Springer Berlin Heidelberg, 2005.

[8] Jean-Daniel Boissonnat and Menelaos I. Karavelas. On the combinatorial complexity of euclidean voronoi cells and convex hulls of d-dimensional spheres. In *Proceedings of the Fourteenth Annual ACM-SIAM Symposium on Discrete Algorithms*, SODA '03, pages 305–312, Philadelphia, PA, USA, 2003. Society for Industrial and Applied Mathematics.

[9] Kevin Q Brown. Voronoi diagrams from convex hulls. *Information Processing Letters*, 9(5):223–228, 1979.

[10] Olivier Devillers, Alexandra Fronville, Bernard Mourrain, and Monique Teillaud. Algebraic methods and arithmetic filtering for exact predicates on circle arcs. *Computational Geometry*, 22(1-3):119–142, 2002.

[11] Olivier Devillers, Menelaos Karavelas, and Monique Teillaud. Qualitative Symbolic Perturbation: a new geometry-based perturbation framework. Rapport de recherche RR-8153, INRIA, 2012.

[12] Ioannis Z Emiris and Menelaos I Karavelas. The predicates of the Apollonius diagram: algorithmic analysis and implementation. *Computational Geometry: Theory and Applications*, 33(1-2):18–57, 1 2006. Special Issue on Robust Geometric Algorithms and their Implementations.

[13] Nicola Geismann, Michael Hemmer, and Elmar Schömer. Computing a 3-dimensional cell in an arrangement of quadrics: Exactly and actually! In *Proceedings of the seventeenth annual symposium on Computational geometry*, pages 264–273. ACM, 2001.

[14] Peter J Green and Robin Sibson. Computing dirichlet tessellations in the plane. *The computer journal*, 21(2):168–173, 1978.

[15] Leonidas J Guibas, Donald E Knuth, and Micha Sharir. Randomized incremental construction of delaunay and voronoi diagrams. In *International Colloquium on Automata, Languages, and Programming*, pages 414–431. Springer, 1990.

[16] Iddo Hanniel and Gershon Elber. Computing the voronoi cells of planes, spheres and cylinders in r 3. In *Proceedings of the 2008 ACM symposium on Solid and physical modeling*, pages 47–58. ACM, 2008.

[17] Iordan Iordanov. The Euclidean InSphere Predicate. Thesis, Department of Applied Mathematics, University of Crete, 2013.

[18] Ryu Joonghyun, Kim Donguk, Cho Youngsong, Park Rhohun, and Kim Deok-Soo. Computation of molecular surface using euclidean voronoi diagram. *Computer-Aided Design and Applications*, 2(1-4):439–448, 2005.

[19] M. N. Kamarianakis. The EdgeConflict Predicate in the 3D Apollonius Diagram. *ArXiv e-prints*, November 2018.

[20] Menelaos I Karavelas and Mariette Yvinec. Dynamic additively weighted voronoi diagrams in 2d. In *European Symposium on Algorithms*, pages 586–598. Springer, 2002.

[21] Deok-Soo Kim, Youngsong Cho, and Donguk Kim. Euclidean voronoi diagram of 3d balls and its computation via tracing edges. *Computer-Aided Design*, 37(13):1412–1424, 2005.

[22] Deok-Soo Kim, Youngsong Cho, and Donguk Kim. Calculating three-dimensional (3d) voronoi diagrams, March 16 2010. US Patent 7,679,615.

[23] Deok-Soo Kim, Youngsong Cho, Donguk Kim, Sangsoo Kim, Jonghwa Bhak, and Sung-Hoon Lee. Euclidean voronoi diagrams of 3d spheres and applications to protein structure analysis. *Japan Journal of Industrial and Applied Mathematics*, 22(2):251, 2005.

[24] Donguk Kim and Deok-Soo Kim. Region-expansion for the voronoi diagram of 3d spheres. *Computer-aided design*, 38(5):417–430, 2006.

[25] Rolf Klein, Kurt Mehlhorn, and Stefan Meiser. Randomized incremental construction of abstract voronoi diagrams. In *Informatik*, pages 283–308. Springer, 1992.

[26] David L Millman. *Degeneracy proof predicates for the additively weighted Voronoi diagram*. PhD thesis, Courant Institute of Mathematical Sciences New York, 2007.

[27] Ron Wein. High-level filtering for arrangements of conic arcs. In *European Symposium on Algorithms*, pages 884–896. Springer, 2002.

[28] Hans-Martin Will. Fast and efficient computation of additively weighted voronoi cells for applications in molecular biology. In *Scandinavian Workshop on Algorithm Theory*, pages 310–321. Springer, 1998.

[29] Hans-Martin Will. *Computation of additively weighted Voronoi cells for applications in molecular biology*. PhD thesis, Swiss Federal Institute of Technology, Zurich, 1999.

[30] Nicola Wolpert. Jacobi curves: Computing the exact topology of arrangements of non-singular algebraic curves. In *European Symposium on Algorithms*, pages 532–543. Springer, 2003.

Department of Mathematics & Applied Mathematics, University of Crete, Voutes University Campus, Heraklion, GR-70013, Greece
Email: m(dot)kamarianakis(at)gmail(dot)com
URL: https://www.tem.uoc.gr/~manosk/

Voronoï's Impact on Modern Science, Book 6, Volume 2
Proceedings of the Sixth International Conference on Analytic Number Theory and Spatial Tessellations

VORONOI-BASED SKELETON FOR SEGMENTING THE NETWORK OF BIOLOGICAL NEURONS

Dmytro Kotsur and Vasyl Tereshchenko (*Ukraine*)

Abstract. In this paper we introduce a method for segmenting the network of biological neurons in fluorescent microscopy images. Firstly, we apply image processing routines to enhance an image and extract contours of the biological neural network. Then we construct the skeleton of the network based on the approximate Voronoi diagram. Further, we employ Voronoi skeleton to identify the cellular somas and differentiate them from axons and dendrites. The proposed segmentation method facilitates further studies of biological neural networks. The graph representation of the segmented neural network allows us to apply classical graph processing algorithms and to compute the network characteristics such as the number connections between individual neurons or the shortest path of signal transduction between two neurons.

Introduction

Voronoi diagram is a powerful data structure, which can be applied to various problems in many areas [1] including computer graphics, machine vision, image processing, biology, chemistry, engineering, CAD/CAM systems, etc.. In particular, there is a wide diversity of Voronoi diagram applications in the area of biomedical image analysis. For example, segmentation of individual cells based on microscopy images [2], separating cell clumps [4, 5], segmentation of biological tissues [6] and image processing and of CT and MR images [3].

Voronoi diagram is a comprehensive data structure, since many related problems [7] are efficiently reduced to computing the Voronoi diagram (e.g., producing the Delaunay triangulation or convex hull, finding the largest empty circle or all nearest neighbors). There are many efficient algorithms for constructing the Voronoi diagram. For example, Fortune's algorithm [8] and "divide and conquer" algorithm [9] allow us to build a Voronoi diagram for the set of N points/line segments in $O(N \log N)$.

Received November 18, 2019.
Key words and phrases. Voronoi diagram, Voronoi skeleton, segmentation, image processing, convex hull, biological neural network, fluorescent image.

However, in practical problems objects are represented by more sophisticated shapes than the set of points or line segments. This in turn led to investigation and generalization of the Voronoi diagram for complex objects (parametric curves, polygons, etc..).

One approach for constructing the Voronoi diagram for curvilinear polygons was introduced by Ramamurthy and Farouki in their papers [10, 11]. The authors proposed an incremental algorithm for constructing the exact Voronoi diagram and medial axis for planar domains with curved boundaries. Their method uses approximate algorithms for computing curve-curve bisectors [12] and also Newton-Raphson iterative scheme for computing exact bifurcation points of the Voronoi diagram. It was shown that the complexity of such algorithm is $O(N^2)$, where N is a number of sites. In paper [13] authors proposed a randomized incremental method for constructing the Voronoi diagram of curved objects, which has a complexity $O(N \log N)$, where N is a number of curves. However, authors assume that some operations (e.g., finding intersection point of two curves) can be performed in $O(1)$, although in practice these operations can be time-consuming and require a sophisticated implementation.

The issues related with calculating the exact Voronoi diagram led community to study the approximate algorithms for computing the Voronoi diagram. One class of approximate methods aims to discretize a spatial domain and build Voronoi diagram based on a finite pixel grid [14], [1] (Algorithm 4.9.2) or as in case of [15] on an exponential grid. Another class of approximation algorithms is based on simplifying the representation of object's shape. For example, complex curved boundaries are approximated by a set of points and line segments. Then the Voronoi diagram for simple objects (points or line segments) is build and processed such that an approximate Voronoi diagram for curved-shaped objects is obtained [1] (Algorithm 4.9.1), [16].

The latter approximate approach is widely used to compute the skeleton of planar objects [1, 19, 17] as an intersection of the approximate Voronoi diagram with the domain of the object. However, at the discretization step such approach should take into account the spatial complexity of the geometrical object [18].

Problem description. In this paper we apply Voronoi-based skeletonization algorithm (as described in Sec. 3) for the problem of automated segmentation of biological neural networks in fluorescent microscopy images. The latter consists of nerve cells, whose bodies (somas) are connected by the long axons or short branched dendrites. The considered in this paper microscopy images were obtained by staining tubulin protein, which is present in both axons and dendrites. The Voronoi-based

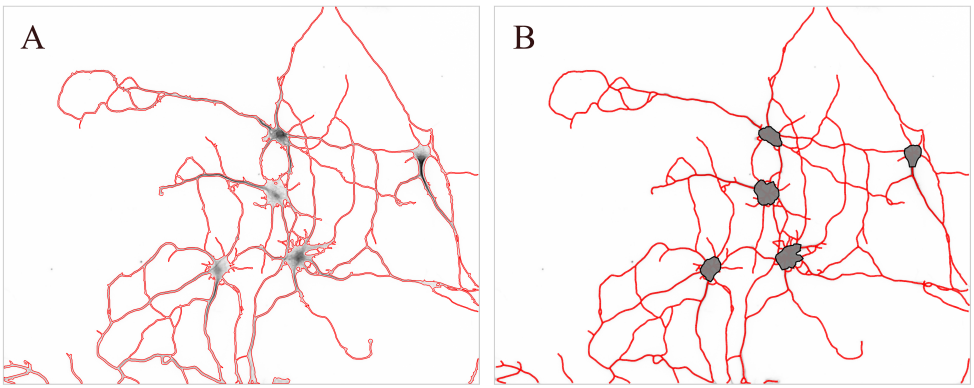

FIGURE 1. The main steps of the segmentation algorithm: (A) image processing and contours tracing; (B) computing Voronoi-based skeleton and cell bodies segmentation (gray regions)

skeletonization method allows us to represent the network of biological neurons as a graph and apply classical graph processing algorithm to study the properties of this network.

Relevance. The proposed in this paper segmentation method aims to facilitate further studies of biological neural networks and their properties. The graph-based representation allows to solve rapidly many related problems: e.g., compute the number connections between individual neurons or the shortest signaling path between two neurons.

1. Segmentation algorithm

In this section we provide a brief high-level description of the main steps of our segmentation algorithm:

(1) The fluorescence image is preprocessed as described in Sec. 2: image is enhanced and binarized, the contours of somas, axons and dendrites are extracted and interpolated using cubic splines (see Fig. 1, A);
(2) Voronoi-based skeleton of the network (which is represented by a set of parametric spline curves (contours) S) is computed as described in Sec. 3;
(3) Using the skeleton graph from Step (2) we classify points corresponding to the somas/cell bodies (see Fig. 1, B), axons and dendrites (see Sec. 4). We also localize the regions corresponding to somas;

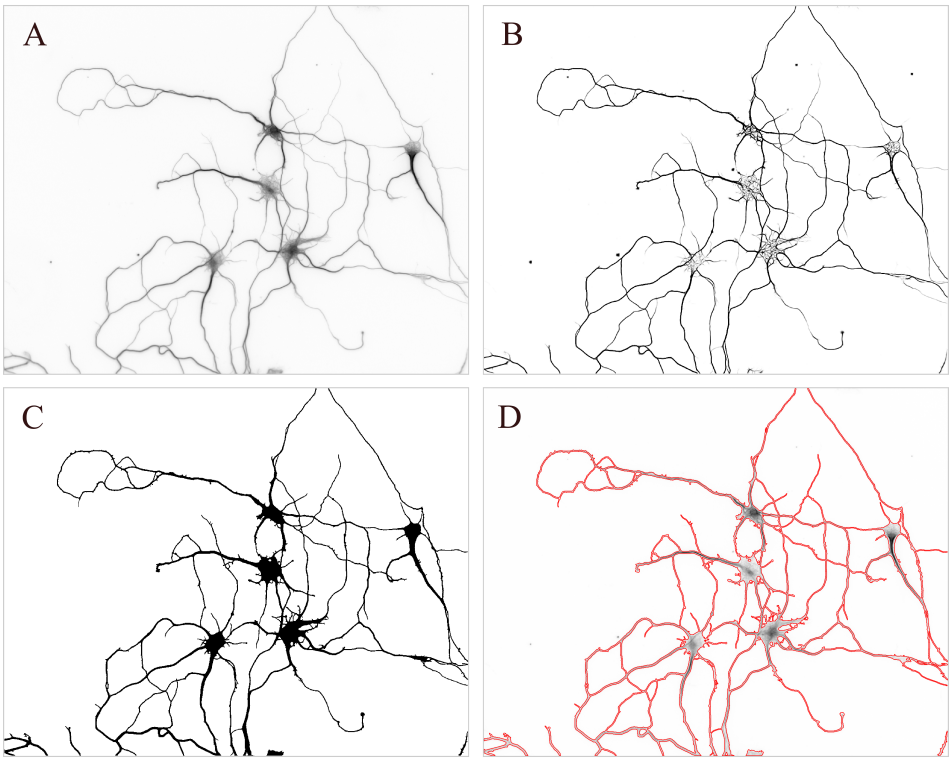

FIGURE 2. The original image (A) is processed using Frangi's ridge enhancement filter (B). The result of this procedure is used to produce the binary mask (C). Then we use obtained mask to trace the contours of biological neural network (D).

Remark 1. The image contours at Step (1) are oriented in such way that the interior of the object is always to the left from any point of a contour.

2. IMAGE PROCESSING

Fluorescent microscopy images can be exposed to the noise and/or photo bleaching, which makes it difficult to use these images in further computations (e.g., for contour tracing). In order to suppress the artifacts obtained during the image acquisition, we perform additional image enhancement steps. The comprehensive workflow of image processing routines is described below:

(1) [Optional] Original image (see Fig. 2, A) is denoised using TV-regularization [20];

(2) The brightness of dim axons and dendrites is enhanced in the image from Step (1) using Frangi's filter [21] (see Fig. 2, B);
(3) The images from Step (1, 2) are binarized using Otsu's global thresholding [22]. Then the resulting binary masks are combined using morphological union operation (see Fig. 2, C);
(4) The binary mask from Step (3) is used to trace the contours of the objects. The contours are oriented such that the interior part of the objects (where binary mask is non-zero) is always to the left from contour;
(5) Finally we interpolate each contour using the parametric cubic spline (see Fig. 2, D), which is used later for Voronoi-based skeleton construction;

3. Voronoi-based skeleton construction

In this section, we firstly recall the definition of the Voronoi diagram for curves according to [10, 13], then provide the description of skeletonization algorithm based on the approximate Voronoi diagram and finally analyze the complexity of the skeletonization algorithm.

3.1. **Definitions.** Let's denote by $\|\cdot\|$ an Euclidean norm in $\mathbb{R}^2$. The distance between a parametric curve $C(t), t \in [0,1]$ and a point $q \in \mathbb{R}^2$ is defined as follows:

$$\operatorname{dist}(q, C) = \min_{t\in[0,1]} \|q - C(t)\| \tag{1}$$

The value $t^* \in [0,1]$ which minimizes equation (1) is called *footpoint* of point q on the curve $C(t)$. Note that a curve can have more than one footpoint [10].

Let $S = \{C_1, C_2, ..., C_M\}$ be a set of M continuous parametric curves ($M \geq 0$) in $\mathbb{R}^2$. Then:

Definition 1. The **Voronoi region** $VR(C_i)$ of a curve C_i is defined by:

$$VR(C_i) := \{q \in \mathbb{R}^2 | \operatorname{dist}(q, C_i) \leq \operatorname{dist}(q, C_j), \forall j \in I_{1,M} \setminus \{i\}\} \tag{2}$$

where $I_{1,M} = \{1, ..., M\}$ is a set of indices from 1 to M.

Definition 2. The **Voronoi polygon** $VP(C_i)$ associated with a curve C_i is defined as a boundary of $VR(C_i)$.

According to [10] it is customary to call $VP(C_i)$ a 'polygon', although it has curved edges.

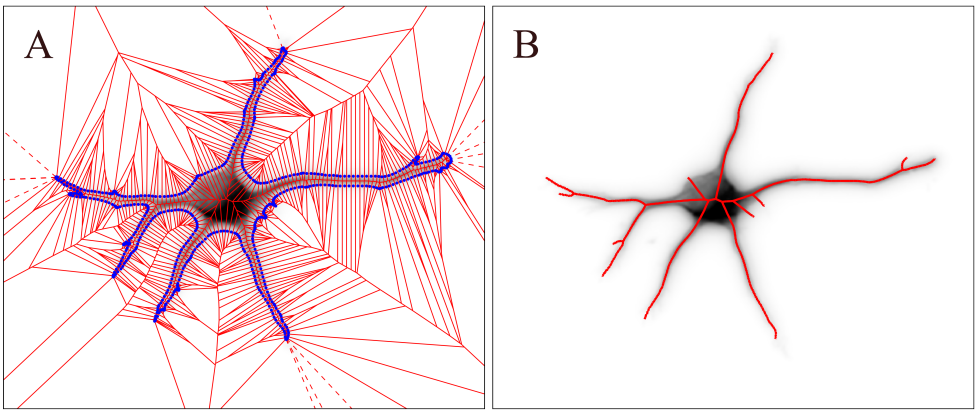

FIGURE 3. Voronoi diagram for sampled points (A) and corresponding Voronoi-based skeleton (B)

Definition 3. The **Voronoi diagram** $VD(S)$ for a set of parametric curves S is defined as follows:

$$VD(S) = \bigcup_{i=1}^{M} VP(C_i) \tag{3}$$

Definition 4. The **Bisector** of two curves $C_i(s)$ and $C_j(t)$, where $s, t \in [0, 1]$ is defined as a set of points that are equidistant from these two curves:

$$\{q|\text{dist}(q, C_i(s)) = \text{dist}(q, C_j(t))\} \tag{4}$$

Definition 5. The **Self-bisector** of a curve $C(t), t \in [0, 1]$ is defined as a set of points, which have at least two footpoints on C:

$$\{q|\text{dist}(q, C(t)) = \text{dist}(q, C(u_1)) = \text{dist}(q, C(u_2))\} \tag{5}$$

where $u_1 \neq u_2$ are two distinct footpoints of C.

Thus, Voronoi polygon $VP(C_i)$ of curve C_i consists of a subset of (possibly trimmed) bisectors between C_i and all other curves from S. It also contains self-bisectors of the curve C_i. According to [13] self-bisectors are important in order to capture the connectivity of the domain.

Definition 6. The junction point connecting three or more bisectors (incl. self-bisectors) of the Voronoi diagram is called **Voronoi vertex**.

3.2. **Algorithm description.** Steps (1-3) of the proposed method are based on Algorithm 4.9.1 from [1]. Step (3) is slightly modified in order to preserve self-bisectors and handle topological errors. The basic steps of the algorithm are described below:

1. Represent each curve $C_i(t), t \in [0,1]$ as a set of points:
$$P_{C_i} = \{C_i(t_1), C_i(t_2), ..., C_i(t_{m_i})\}, \tag{6}$$
where $0 = t_1 \leq t_2 \leq \cdots \leq t_{m_i} = 1$ (cf., Figs. 3a,b).
2. Construct Voronoi diagram for points $VD(P)$, where $P = \bigcup_{i=1}^{M} P_{C_i}$, using Fortune's algorithm [8]. Example is shown in Figure 3, A.
3. Process Voronoi diagram $VD(P)$:
   3.1. Apply depth-first search algorithm to classify all vertices of Voronoi diagram $VD(P)$ as "inner" or "outer" w.r.t. the object interior. Firstly, start DFS algorithm from "outer" vertex (outside the convex hull of P, which can be obtained from $VD(P)$). If DFS traverse is crossing the border of the object change the label of the vertex to the opposite ("inner" to "outer" and vice versa), otherwise propagate current label. The cross-check can be performed efficiently if we store in a hash-table the pairs of Voronoi vertices and corresponding to them consecutive Voronoi cells.
   3.2. Remove edges of $VD(P)$ for every pair of successive sampled points $C_i(t_j), C_i(t_{j+1})$ $\forall i, j$ on a curve. Also remove all Voronoi vertices and respective edges classified as "outer". The resulting graph is denoted as $VD'(P)$;
   3.3. Determine bifurcation points of the Voronoi-based skeleton $VD(S)$ using $VD'(P)$: traverse all vertices of Voronoi digram using breadth-first search (BFS), mark v as a bifurcation point if $\deg(v) \geq 2$.
   3.4. If a pair of neighboring bifurcation points is connected by polyline edge shorter than a give threshold value T_{merge} then the corresponding polyline edge is removed and the pair is represented by one vertex (see Fig. 3, B);
4. [Optional] Approximate edges of the processed Voronoi graph by Bezier splines using algorithm [23].

Remark 1. Step 3.2. can be performed faster if we organize data into two hash-tables. The first hash-table maps indices of sampled points to the data-structure, which consists of index of respective curve and indices of the next and previous sampled points of the corresponding curve (if applicable). The second hash-table maps indices of a curve to indices of sampled points on these curve (one point per curve is sufficient).

Remark 2. In the step 3.2. we obtain Voronoi diagram $VD'(P)$. It can possibly contain vertices of degree 1, which are isolated vertices (e.g., centers of circles), vertices of degree > 2 (bifurcation points) and also vertices of degree 2. The latter constitute the approximate polyline edge

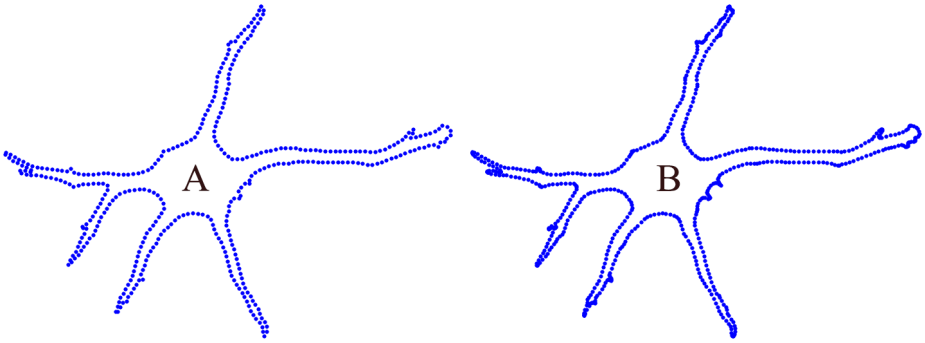

FIGURE 4. Application of different curve parameterization methods: (A) arc-length parameterization, distance between two consecutive points are constant; (B) mixed parameterization – combination of curvature-based and arc-length parameterizations; The difference between (A) and (B) is well visible around the tips of dendrites.

of the Voronoi diagram for curves. At the Step 4. we approximate these polyline edges by Bezier splines.

3.3. **Curve discretization methods.** At the Step 1. we sample points on a curve C_i using the formula (6). Note that, a sampling method has to take into account the shape of the curve, otherwise topological inconsistencies may occur [18]. Therefore, uniform parameterization $\forall j = \overline{1, m_i},\ |t_{j+1} - t_j| = const$ as well as an arc-length parameterization (cf., Fig. 4, A) of a curve $\forall j = \overline{1, m_i},\ \|C_i(t_{j+1}) - C_i(t_j)\| = const$ won't give satisfactory results [18].

In order to obtain a point set P_{C_i} representing the curve's (at least local) shape, we used a method, which is based on mixture of curvature and arc-length normalized parameterization (cf., Fig. 4, B) as described in [24] (see Eq. 8 in [24]).

In comparison to [24], where authors just averaged curvature and arc-length parameterizations, we use the following equation:

$$p(t) = l(t) + \gamma k_p(t) \frac{l(t_{n+1})}{k_p(t_{n+d+1}),} \tag{7}$$

where $\gamma \geq 0$ controls the "significance" of the curvature term (see [24] for other notations in Eq. 7). In case of $\gamma = 0$ we obtain just an arc-length parameterization.

Thus, if we parameterize curve in such way, it will behave like an arc-length parametrized curve in a "flat" regions with a small curvature ($\kappa(t) \approx 0$). However, in regions with a large curvature ($|\kappa(t)| >> 0$) , the density of the sampled points will increase (which is controlled by γ).

3.4. **Complexity analysis.** Let m_i be a number of points, which we sample on a curve C_i. $N = \sum_{i=1}^{M} m_i$ is a total number of points. In the following lemmas and theorem we analyze the complexity of each step of our algorithm from Section 2.2.

Lemma 1. *Let $C_i(t)$ be a curve represented by Bezier spline, then Step 1 of our algorithm can be computed in $O(N \log N)$ in the worst-case.*

Proof. The worst-case scenario appears when we construct bisector between a point and a curve represented by the rest $N-1$ points. Assuming that the number of control points of $C_i(t)$ is proportional to N, one point of $C_i(t)$ can be computed in $O(\log N)$. Then N points can be computed in $O(N \log N)$. □

Lemma 2. *Voronoi diagram for N points at the Step 2 of our algorithm can be computed in $O(N \log N)$.*

Proof. At the Step 2 we just apply well-known sweep-line algorithm for Voronoi diagram construction, which is described in detail in [8]. Its complexity in case of N input points is $O(N \log N)$. □

Lemma 3. *Processing of the Voronoi diagram for points at the Step 3 can be performed in $O(N)$.*

Proof. Let's analyze every operation of Step 3 in detail:

Step 3.1. The complexity of BFS is $O(N)$. At every step of BFS we check if we cross the border of the object, which is $O(1)$ due to the fact that all pairs of border vertices are stored in a hash-table. Thus, total complexity of Step 3.1 is $O(N)$.

Step 3.2. We can look through all pairs of consecutive sampled points for every curve in $O(N)$ using the hash-tables described in Remark 1 of Section 2.2. One edge can be removed in $O(1)$ just by reassigning pointers in doubly-connected edge list (DCEL). Thus, total complexity of Step 3.1 is $O(N)$.

Step 3.3. The complexity of BFS for a graph with N vertices and E edges is $O(N+E)$. In case of Voronoi diagram $E \propto N$. Thus, complexity of Step 3.2 is $O(N)$.

Step 3.4. In fact the length of Voronoi edges between two bifurcation points can be already computed in Step 3.1. Checking the condition that the length of an edge is less than T_{merge} for all edges can be done in $O(N)$.

Two Voronoi vertices can be merged into one in $O(1)$ by reassigning pointers of DCEL. Thus, the total complexity of Step 3.3 is $O(N)$.

Since the complexities of Step 3.1, 3.2, 3.3, 3.4 are $O(N)$, the total complexity of Step 3 of our algorithm is $O(N)$. □

Theorem 1. *The complexity the proposed algorithm for constructing an approximate Voronoi diagram for a set of M curves and N sampled points is $O(N \log N)$.*

Proof. Follows directly from Lemmas 1, 2, 3. □

Remark In the current analysis we didn't take into account optional Step 4. The fitting of Bezier spline is performed using the recursive "divide and conquer" procedure described in [23]. Although the author didn't specify the complexity analysis of the procedure, in the worst-case scenario (which is rare) this procedure should work in $O(N^2)$. However, it is possible to modify it (by selecting point close to the middle in "divide" step) such that an average time should be $O(N \log N)$.

4. Segmentation of biological neural networks

We employ skeleton from Step 2 to identify cellular bodies (somas). Since every Voronoi vertex is associated with the corresponding circle enclosing at least three generator points of Voronoi diagram, we can differentiate the cellular body vertex from axon/dendrite vertex by comparing the radius of the circle with a given threshold value.

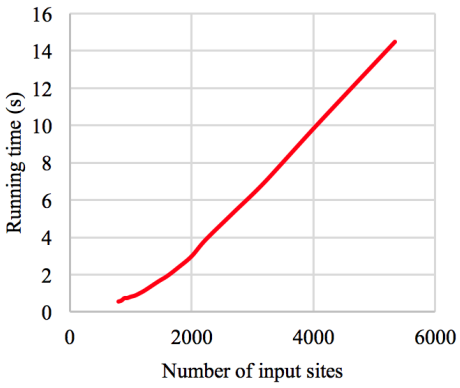

Figure 6. Average running time of the method depending on the number of contours (20 image tested)

If we consider all radii of all Voronoi vertices of the skeleton, we can apply (similar as for image binarization) Otsu's thresholding [22]. This would allow as to find an optimal value of the radius of the circle corresponding to the cellular body. Then using such procedure we can classify all Voronoi vertices as "body vertex" or "non-body vertex". Using BFS algorithm all connected "body vertices" (with no gaps between them) can be grouped into the connected components (clusters).

At the last step we build a star-shape polygon [7] for each component. This polygon would represent the body of the neuron.

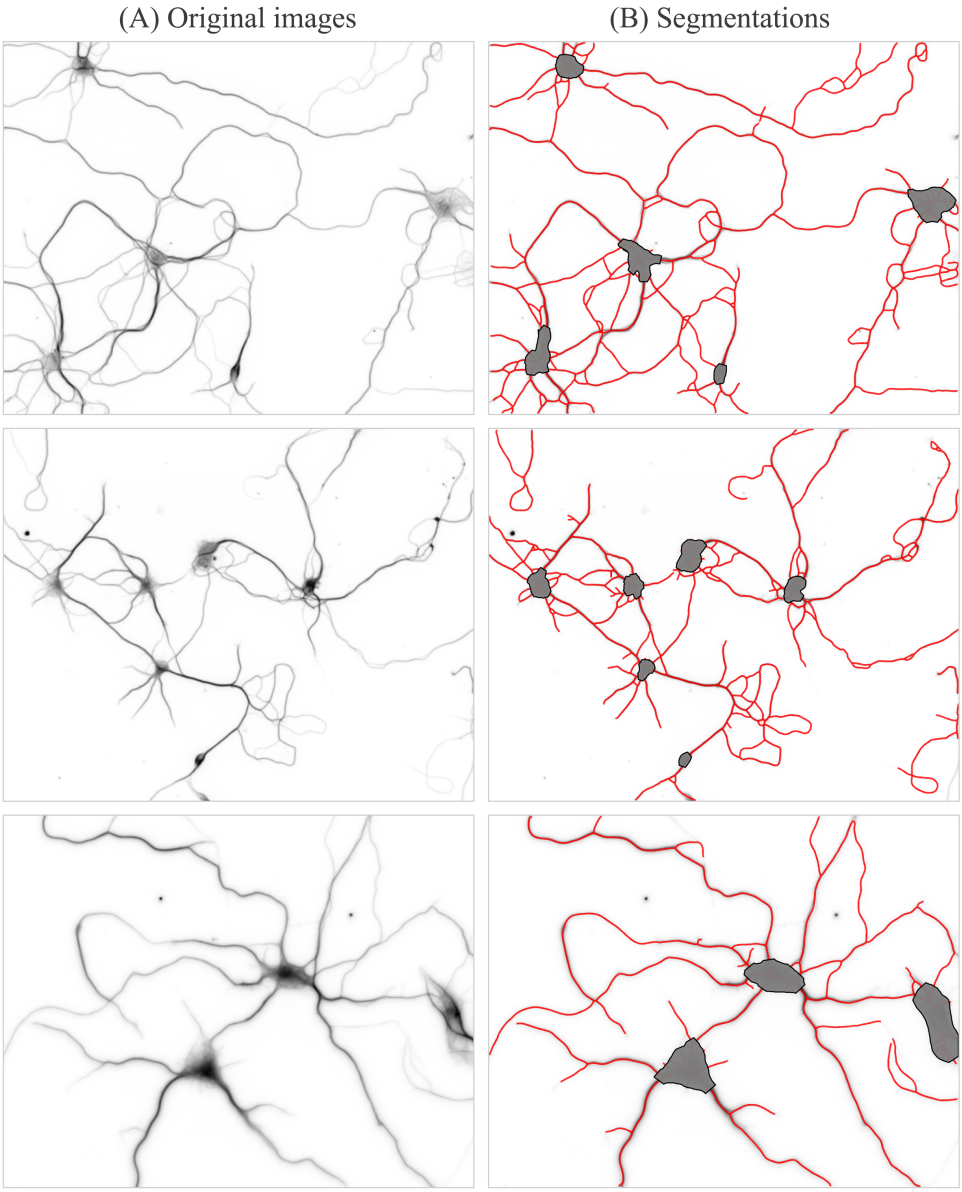

FIGURE 5. Examples of input fluorescent microscopic images (left column), nerve cells are stained in green; Segmented axons, dendrites (red lines, right column) and cell bodies (gray blobs, right columns).

Implementation. We implemented skeletonization method in C++ language and tested the performance on computer with Intel Core i7 2.2GHz and 8Gb RAM. Fig. 6 shows the running time of the method depending on the number of traced contours.

Further applications. As it was mentioned above, Voronoi diagram serves as an intermediate step bringing the graph representation of the neural network. This in turn allows us to apply such algorithms as Ford-Fulkerson [25] for finding the number of "connections" between two cells (see Fig. 7) or Dijkstra algorithm [25] to find the shortest signal transduction path.

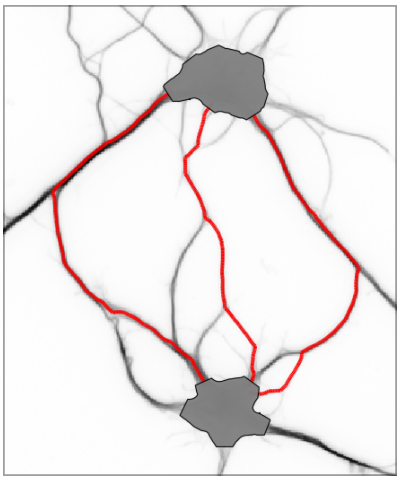

FIGURE 7. Ford-Fulkerson algorithm was applied to find the "connecting" paths between two neurons (gray blobs)

Examples. The examples of input fluorescent microscopic images (left column) and segmentation results (right column) obtained with our method are shown in Fig. 5. The processed images shown in Fig. 5 are available online at CellImageLibrary: *http://www.cellimagelibrary.org*: Dieter Brandner; Ginger Withers (2010) CIL: 8785, 10219, 10113, 10109, 10118, Rattus, multipolar neuron. CIL. Dataset.

5. Conclusion

We have presented the method, which allows us to perform automized segmentation of biological neurons in fluorescent microscopy images. The main step of the method is construction of the Voronoi-based skeleton, which can be performed in $O(N \log N)$ (according to the presented in Sec. 3.4 analysis). However, the skeleton construction requires performing the prior image processing (e.g., noise suppression, ridges enhancement) and contour tracing steps, which are described in Sec. 2. The Voronoi skeleton is employed further to localize the cellular somas and distinguish them from other components of nerve cells: axons and dendrites. The proposed segmentation algorithm aims to facilitate further investigations in the field of biology. The graph-based representation of the segmented neural network allows us to apply graph processing algorithms and compute different properties of the network (e.g., number connections between individual neurons, the shortest signal transduction path between two neurons).

References

1. A. Okabe, B. Boots, K. Sugihara, S. Chiu and D. G. Kendall. *Spatial Tessellations: Concepts and Applications of Voronoi Diagrams*, J. Wiley & Sons, 2000
2. W. Yu, K. H. Lee, S. Hariharan, W. Bu and S. Ahmed. *Evolving generalized Voronoi diagrams for accurate cellular image segmentation*, J. Cytometry: Part A, 77A (2010), no. 4, 379–386.
3. R. Xiao, J. Wu and J. Wu. *A New Medical Segmentation Method Based on Voronoi Diagrams and Region Growing*, Proc. of 2nd Int. Congress on Image and Signal Processing (2009), no. 4, 1–4.
4. D. M. Ushizima, A. G. Bianchi, and C. M. Carneiro. *Segmentation of subcellular compartments combining superpixel representation with Voronoi Diagrams*, Overlapping Cervical Cytology Image Segmentation Challenge–IEEE (2014), 1–2.
5. G. L. Ramalho, D. S. Ferreira, A. G. Bianchi, C. M. Carneiro, F. N. Medeiros, and D. M. Ushizima. *Cell reconstruction under Voronoi and enclosing ellipses from 3d microscopy*, IEEE International Symposium on Biomedical Imaging ISBI (2015).
6. A. Fakhrzadeh. *Epithelial Cell Segmentation in Histological Images of Testicular Tissue Using Graph-Cut*, Image Analysis and Processing, Springer Berlin Heidelberg (2013), 201–208
7. F. Preparata and M. Shamos. *Computational Geometry: An Introduction* Springer-Verlag, 1985
8. S. Fortune. *A sweepline algorithm for Voronoi diagrams* Algorithmica (1987), 2(1-4): 153–174
9. M. Shamos and D. Hoey. *Closest-point problems* Proc. 16th Annual Symposium on Foundations of Computer Science (1975), 131–162
10. R. Ramamurthy and R. T. Farouki. *Voronoi diagram and medial axis algorithm for planar domains with curved boundaries I. Theoretical foundations*, Journal of Computational and Applied Mathematics (1999), no. 102(1): 119–141
11. R. Ramamurthy and R. T. Farouki. *Voronoi diagram and medial axis algorithm for planar domains with curved boundaries — II: Detailed algorithm description*, Journal of Computational and Applied Mathematics (1991), no. 102(2): 253–277
12. R. T. Farouki and R. Ramamurthy. *Specified–Precision Computation of Curve/Curve Bisectors*, International Journal of Computational Geometry & Applications (1998), no. 8(5-6): 599–617
13. H. Alt, O. Cheong and A. Vigneron. *The Voronoi Diagram of Curved Objects*, Discrete & Computational Geometry (2005), no. 34(3): 439–453
14. K. Hoff, T. Culver, J. Keyser, M. Lin and D. Manocha. *Fast Computation of Generalized Voronoi Diagrams Using Graphics Hardware*, Proc. 26th Annual Conference on Computer Graphics and Interactive Techniques (1999), 277–286
15. S. Har-Peled. *Geometric Approximation Algorithms (Mathematical Surveys and Monographs)*, AMS (2011): 129–132
16. Y. Ho and J. Liu. *Collision-free curvature-bounded smooth path planning using composite Bezier curve based on Voronoi diagram*, Proc. IEEE International Symposium on Computational Intelligence in Robotics and Automation (2009)
17. O. Sharma and D. Mioc and F. Anton. *Voronoi Diagram Based Automated Skeleton Extraction from Colour Scanned Maps*, Proc. 3rd International Symposium on Voronoi Diagrams in Science and Engineering (2006), 186–195

18. J. W. Brandt and V. R. Algazi. *Continuous skeleton computation by Voronoi diagram*, CVGIP: Image Understanding (1992), no. 3(55), 329–338
19. R. Ogniewicz and M. Ilg *Voronoi skeletons: theory and applications*, Proc. IEEE Computer Society Conference on Computer Vision and Pattern Recognition (1992), 63–69
20. H.J. Kwak, S.J. Lee, Y. Lee and D.H. Lee. *Quantitative study of total variation (TV) noise reduction algorithm with chest X-Ray imaging*, Journal of Instrumentation (2018), no. 1
21. A. F. Frangi, W. J. Niessen, K. L. Vincken and M. A. Viergever. *Multiscale vessel enhancement filtering*, Proc. Medical Image Computing and Computer-Assisted Intervention (1998), 130–137
22. R. C. Gonzalez and R. E. Woods. *Digital Image Processing (3rd Edition)*, Prentice-Hall, Inc. (2006)
23. P. Schneider. *An Algorithm for Automatically Fitting Digitized Curves*. Graphics Gems, Academ. Press Prof., Inc.: 612–626
24. L. Pagani and P. J. Scott. *Curvature based sampling of curves and surfaces*, Computer Aided Geometric Design (2018), no. 59: 32–48
25. T. H. Cormen, C. Stein, R. L. Rivest and C. E. Leiserson. *Introduction to Algorithms*, McGraw-Hill Higher Education (2001)

(D. Kotsur) Faculty of Computer Science and Cybernetics, Taras Shevchenko National University of Kyiv, 4d Glushkova St., Kyiv, 03680, Ukraine
Email: dkotsur(at)gmail(dot)com
URL: http://mi.unicyb.kiev.ua/

(V. Tereshchenko) Faculty of Computer Science and Cybernetics, Taras Shevchenko National University of Kyiv, 4d Glushkova St., Kyiv, 03680, Ukraine
Email: vtereshch(at)gmail(dot)com
URL: http://tvm.unicyb.kiev.ua

TOPOLOGICAL CHARACTERISTICS OF DISORDERED CARBON

Alexander Rud, Inna Kirian, and Andrii Lakhnik (*Ukraine*)

Abstract. The Voronoi polyhedra constructed for simulated atomic configurations of ball-milled graphite have an extraordinary variety in their topological and metric characteristics and contain a lot of 5-fold faces. The analysis of VP sphericity coefficient K_{sph} enables a conclusion about changing local atomic arrangement in a structure of ball-milled carbon from graphite-like to typical for disordered tetrahedral network and random systems of points (atoms), proper for amorphous state. The sphericity coefficient is proposed to be as a parameter of the topological order to quantitative estimation of disordering degree in amorphous structures.

Introduction

Carbon based materials have a great interest through a broad spectrum of allotropic modifications depended on the degree of sp-hybridization of valence electrons. The amorphous carbon can be easily produced by either high-energy ball-milling of graphite [1] or high-voltage electric discharge treatment of hydrocarbon precursors [2]. The local atomic structure and topological characteristics of amorphous carbon produced by high-frequency electric discharge treatment of gaseous hydrocarbons and high-temperature annealing of fullerenes C_{60} [3] were investigated by X-ray, RMC and Voronoi-Delaunay methods. The goal of this paper is the systematic study of the evolution of local atomic arrangements during the quasi-continuous crystalline-amorphous transition at graphite ball-milling. Additionally, quantitative topological characteristics are estimated using RMC modeling and Voronoi analysis based on the experimental X-ray data.

Received November 4, 2019.

2010 *Mathematics Subject Classification.* PACS: 61.46.?w; 61.43.Gt; 61.05.?a; 02.70.Uu.

Key words and phrases. Voronoi polyhedra, local atomic structure, sphericity coefficient.

This research was carried out within the framework of the budgetary topics of the G.V. Kurdyumov Institute for Metal Physics.

1. Experimental and simulation details

Crystalline spectrally pure graphite powder was milled in argon gas atmosphere in the laboratory planetary ball mill Fritsch Pulverisette P-6 at the room temperature for 0.5, 1, 2, 3.5, and 10 hours, respectively. The experimental structure factors are calculated by the procedure described in [4]. Simulation of atomic configurations of graphite in initial and ball-milled state was carried out using RMCPow v.2.4 software package [5]. All configurations consist of 4000 carbon atoms placed into a configuration cell (10*10*10 unit cells in each direction). The statistical and geometrical features of the local atomic arrangements in the generated atomic configurations were established using Voronoi polyhedral (VP) analysis [6], [7] and software package developed by V. Voloshin [8].

2. Voronoi analysis

Atomic configurations were generated by RMC procedure using experimental structure factors for all specimens. The agreement between the experimental and simulated structure factors indicates adequacy of the generated atomic configurations to the real structure of the samples. The simulated atomic space is divided into VP. An individual VP is a structural unit of the amorphous state that is similar to the Wigner-Seitz cell of the crystalline state. The basic attributes used for the statistical and geometric analyzes of disordered systems are topological and metric characteristics of the Voronoi polyhedra.

The histogram distributions of the VP versus the number of faces for the ball-milled graphite are shown in Fig. 1a. It is seen that the atomic configurations in crystalline graphite can be divided into two types of polyhedra: 50% are 11-sides and the second 50% are 15-sides. After 0.5 h grinding, Voronoi polyhedra are characterized by the wide distribution of the number of faces with predominance of 15-, 16-, 19- and 20 sides. It indicates deformation of VP typical for graphite as a result of its crystalline structure destruction. Further treatment results in increasing fraction of 16 -, 17 - and 18-sided VP. The histogram after 10 hrs grinding (Fig. 1a) takes the specific for amorphous carbon nanomaterials form.

The 3-, 4-, 6- and 8-fold faces dominate in VP of the pristine graphite (Fig. 1b). Additional 5-, 7-, 9- and 10-fold those appears on VP after 0.5 hr grinding. The broad asymmetric distribution for the ball-milled materials indicates a wide variety of faces with different numbers of edges (corners) on each face. VP of disordered carbon are characterized by an increased amount of pentagonal faces.

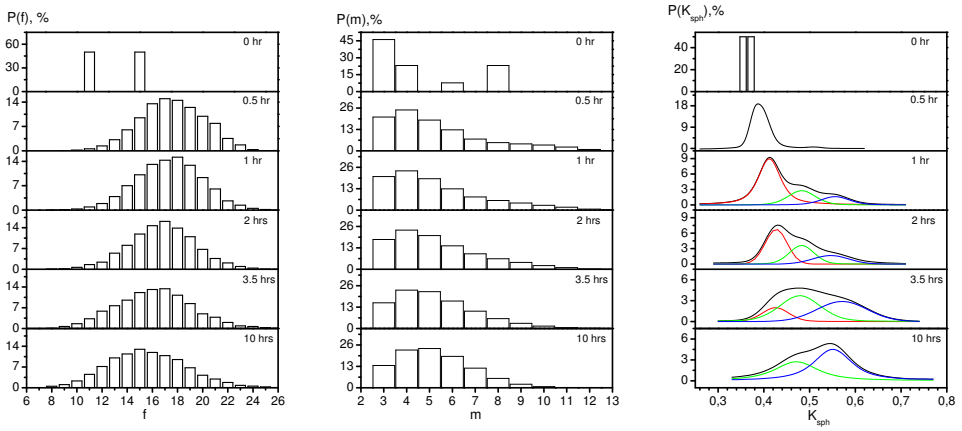

(A) (B) (C)

FIGURE 1. Face (a) and edge on the face (b) distributions of Voronoi polyhedra for pristine and ball-milled graphite and distributions of sphericity coefficient of Voronoi polyhedra for ball-milled graphite (c).

Of particular interest is the analysis of a sphericity coefficient K_{sph} of VP

$$K_{sph} = \frac{36\pi V^2}{S^3} \tag{1}$$

where V and S are polyhedral volume and area, respectively [6] or inverse its value - asphericity coefficient [9]. It is clearly seen (Fig. 1c), that a continuous transformation of K_{sph} from typical for crystalline graphite (0.35 and 0.37) to near for random system of points (0.53) takes place. Besides, the analysis of K_{sph} enables a conclusion about the change in the local structure of carbon during ball-milling. So, the powder milled to 0.5 hr possesses the graphite-like type of short-range order. After 1 hr of processing, a sphericity coefficient is characterized by a broad distribution what is decomposed on three components. The first broad sub-peak is linked with graphite-like component. Its broadening indicates a deformation of graphene sheets. The second small maximum takes the position of disordered tetrahedral network inherent to distorted diamond (0.475). The third low-intensity one appears in the position of a system of random points, peculiar to disordered arrangement of atoms. After 2 hrs of ball-milling, K_{sph} remains visually unchanged, but redistribution in intensities of its sup-components occurs. Further treatment leads to essential decreasing of graphite-like component (Fig. 1c) with growth of the second and third sub-peaks. After 10 hrs of ball-milling, K_{sph} is

characterized by a bimodal distribution. The first maximum takes the position closed to the disordered tetrahedral network, proper to amorphous diamond-like carbon, the second one is in the position of random system of points. Such behavior of the distribution of sphericity coefficient indicates the gradual structural disorder of crystalline structure of graphite and the formation of amorphous carbon with randomly arranged atomic structure after continuous ball-milling treatment.

Conclusion

Statistical analysis of VP, performed for generated by RMC method atomic configurations, has revealed that they have a wide distribution of their topological and metric characteristics that are inherited to disordered materials. We propose to apply the sphericity coefficient of the Voronoi polyhedra as a parameter of the topological order to quantitative estimation of disordering degree in amorphous structures.

References

[1] R. M. Nikonova, N. S. Larionova, V. I. Ladyanov, V. V. Aksenova, A. D. Rud and I. M. Kirian, *Changes of the structure of fullerite and graphite during their mechanical activation* J. Alloys Compd. **682** (2016), 61–69.

[2] A. D. Rud and I. M. Kiryan, *Quantitative analysis of the local atomic structure in disordered carbon*, J. Non-Cryst. Solids. **386** (2014), 1–7.

[3] A. D. Rud, I. M. Kiryan, N. M. Bilyi, R. M. Nikonova and M. A. Merzlyakova, *Dynamics of the structural state of fullerite $C_{60/70}$ in the course of high temperature annealing*, Metallofiz. Nov. Tekh. **34** (2012), 1081–1092 (in Russian).

[4] A. D. Alekseev, G. M. Zelinskaya, A. G. Ilinskii, I. G. Kaban, Yu. V. Lepeyeva, G. S. Mogilny, E. V. Ulyanova and A. P. Shpak, *Atomic structure of natural coals*, Fiz. Tekh. Vis. Davl. **3** (2008), 35–53 (in Russian).

[5] http://www.rmc-forum.org/Downloads.

[6] N. N. Medvedev, *Voronoi-Delaunay Method in Structural Studies of Noncrystalline Systems*, Russian Academy of Sciences, Novosibirsk, 2000 (in Russian).

[7] V. P. Voloshin, N. N. Medvedev, M. N. Andrews, R. R. Burri, R. Winter and A. Geiger, *Volumetric properties of hydrated peptides: Voronoi-Delaunay analysis of molecular simulation runs*, J. Phys. Chem. B **115** (2011), 14217–14228.

[8] http://www.kinetics.nsc.ru/sms/.

[9] G. Ruocco, M. Sampoli and R. Vallauri, *Analysis of the network topology in liquid water and hydrogen sulphide by computer simulation*, J. Chem. Phys. **96** (1992), 6167–6176.

Voronoï's Impact on Modern Science, Book 6, Volume 2
Proceedings of the Sixth International Conference on Analytic Number Theory and Spatial Tessellations

VORONOÏ RANDOM PACKING

Masaharu Tanemura (*Japan*)

Abstract. We present in this paper a "Voronoï random packing", a new kind of random sequential packing in the space. We first define the one-dimensional version of Voronoï random packing, and after performing computer simulations, we obtain the packing density through statistical analysis. Then, the Voronoï random packing in higher dimensional spaces are also presented. Remarks about the connection to the random sequential parking problem and its higher dimensional problems are given.

Introduction

In our daily life, we often meet random packing of objects. Car parking problem in the street is a typical example of such random packings. Figure 1 shows four independent samples of this problem. Here, rectangular cars of unit length are parked sequentially at random in a finite interval A of length x in such a manner that the first car is uniformly parked in A and, in general, having parked k cars, we park the $(k+1)$-st car uniformly at random under the condition that there is no point in common with any of k previously parked cars. In each sample of Fig.1, there is no room for a further car to be parked. One of the interesting point of this problem is how much of the interval A will be parked with cars of unit length. Rényi [2] has obtained a theoretical value of packing density c for this question, namely

$$c \equiv \lim_{x\to\infty} \frac{M(x)}{x} = \int_0^\infty \exp\left[-2\int_0^t \left(\frac{1-e^{-u}}{u}\right) du\right] dt = 0.74759\cdots$$

where $M(x)$ is the expected number of cars parked on a street of length x.

Received November 1, 2019.
2010 *Mathematics Subject Classification.* Primary 60D05.
Key words and phrases. Car parking problem, Random sequential packing, Voronoï cell, Voronoï segment.
This work is dedicated to the 150th anniversary of G.Voronoï's birth.

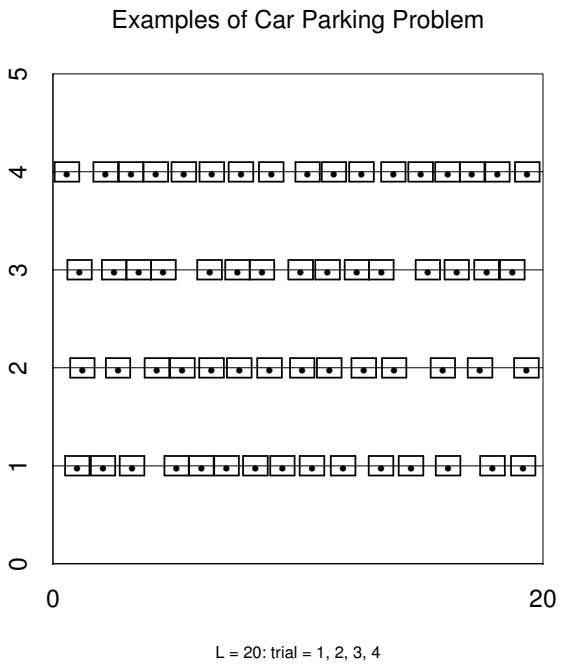

FIGURE 1. Sample patterns of car parking problem

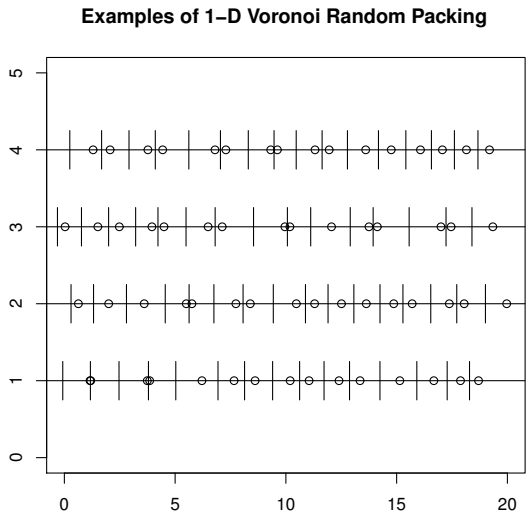

FIGURE 2. Sample patterns of 1-D Voronoï random packing

The above problem can be extended to higher dimensional space, and has many applications to material science, to medical science, and to other sciences. In two-dimensional (2-D) and three-dimensional (3-D) spaces, random packings of disks and spheres, respectively, could be considered as direct extension of Rényi's car parking problem and many researchers have concerned about this extension. The results of packing density known so far are, for disks, 0.5473 [3], 0.5471 [1] and 0.5470 [9], and for spheres, 0.381 [4] and 0.383 [9], respectively.

In this paper, however, we discuss a new class of random packing problem. Figure 2 gives four independent samples in 1-D space, which are generated by the method explained in the following section. In Section 1, we give the definition of "Voronoï random packing" and the algorithm of this packing in 1-D space. Then, the estimation of packing density for 1-D Voronoï random packing is done by applying the Complete Packing Algorithm (CPA) through computer simulations. Section 2 gives the extension of our random packing to 2-D and 3-D spaces, and the estimate of their packing densities are given. In the final Section, we remark the possible CPA for 2-D and 3-D Voronoï random packings and so on.

1. Voronoï Random Packing in 1-D Space

We suppose, in one-dimensional (1-D) space, that there is a critical size of length which is occupied by each existing point in a finite interval. We also suppose that the occupied length of a certain point is determined by the length of Voronoï cell of the corresponding point.

We call this packing a 'Voronoï random packing' (in [7], this packing was called an 'areal random packing' and was defined originally in 2-D space, but considering the extension of the model to other dimensional spaces, the terminology 'Voronoï random packing' seems suitable).

Let the whole region of the packing be an interval A of length L and let N be the number of points. We assume the critical value of the length allocated to each point be a_c.

A rough sketch of the procedure of our random packing is as follows:

(1) Put $N \leftarrow 2$, and generate N points uniformly at random inside A.
(2) Compute Voronoï division of the point pattern. If the size of any Voronoï segment is below a_c, go to Step **1**, else go to Step **3**.
(3) Generate a test particle $\mathbf{x}_t$ uniformly at random in A, and compute the Voronoï segment $V(\mathbf{x}_t)$ of the point $\mathbf{x}_t$. If the length of $V(\mathbf{x}_t)$ and the lengths of Voronoï

segments contiguous to $V(\mathbf{x}_t)$ are all bigger than a_c, then go to Step **4**, else go to Step **3**.

(4) $N \leftarrow N+1$. If a specified **Stopping Rule** is satisfied, then **Stop**, else go to Step **3**.

In the above procedure, a convenient **Stopping Rule** will be to specify the total number of test particles n_t: if a bigger n_t is used, the final value of N will become larger. It is obvious, however, how big a value is specified to n_t, the final N is limited below the value A/a_c. Then a suitable big value of n_t is needed to avoid the waste of computational effort. In our case of Fig.2 ($|A| = L = 20 : a_c = 1.0$), $n_t = 5000$ is specified and the final values of N for four samples were $15, 16, 15$ and 16 from bottom to top.

Examples of the Voronoï random packing for 1-D are given in Fig.2. In the figure, results of four independent trials are shown ($L = 20$). Vertical lines between points indicate the position of boundaries of respective Voronoï segments. From the figure, it is seen that sometimes the contiguous pair of points locate very near with each other although corresponding Voronoï segments are bigger than a_c.

1.1. **Estimation of Packing Density.** It is generally an interesting theme to estimate how much the whole area will be packed by the random packing process. The usual way of describing this estimate is to compute "packing density". In our case, the packing density ρ_A is defined as $\rho_A = N \times a_c/A$. (In Fig.2, $\rho_A = 0.75, 0.80, 0.75$ and 0.80 were obtained for the four cases.)

From the above discussions, it is obvious that our random packing is a stochastic process and that ρ_A is a random variable. Many people are often interested in the mean value of ρ_∞, $\mathrm{E}(\rho_\infty)$, the mean packing density in the limit $A \to \infty$.

In order to estimate $\mathrm{E}(\rho_\infty)$, we performed computer simulation of the Voronoï random packing for several values of L with a number of independent trials n_s for each L. The value $a_c = 1$ is chosen throughout. Regarding the **Stopping Rule** discussed above, we stated to specify the total number of test particles n_t as a convenient way. We also stated that if a bigger n_t is selected, the final value of N, the total number of points in A, will become larger. Computer simulations under this convenient Stopping Rule, by using suitably large test particles n_t, were done as a preliminary stage in order to proceed the following stage below.

1.1.1. *Random Complete Packing.* Now, we can devise a different rule in order to attain a random 'complete' packing. Here, a 'complete' packing is meant by the state where no further generating point can be added.

In the case of random packing by disks, we have presented an algorithm called CPA (Complete Packing Algorithm) [3], which substantially uses the vertices of Voronoï cells for the search of residual spaces for additional disks. In our case, in order to build the algorithm corresponding to CPA, we inspected several samples which are assumed to be near the complete packing. As a result we arrived at the following statements by which we are able to attain CPA. Let us assume the current packing state under consideration is approaching a complete packing in 1-D Voronoï random packing. Let $V(x_i)$ be the Voronoï cell of a point x_i, and let the contiguous points of x_i be x_{i-1} and x_{i+1} such that three points x_{i-1}, x_i and x_{i+1} are in ascending order.Then the following steps can find the putative 'residual space' for the further points.

Complete Packing Algorithm for 1-D Voronoï Random Packing

(1) If there is a point x_i whose Voronoï cell $V(x_i)$ is bigger than $2a_c$, then
   (a) if $|x_{i+1} - x_i| < |x_i - x_{i-1}|$ and $|x_i - x_{i-1}| > 2a_c$, then a new point x should be in the range
   $$x_{i-2} + 2a_c < x < x_{i+1} - 2a_c,$$
   (b) if $|x_{i+1} - x_i| > |x_i - x_{i-1}|$ and $|x_{i+1} - x_i| > 2a_c$, then a new point x should be in the range
   $$x_{i-1} + 2a_c < x < x_{i+2} - 2a_c.$$

(2) If there is a pair of contiguous points x_i and x_j (let $x_i < x_j$) such that $|V(x_i)| + |V(x_j)| > 3a_c$ is satisfied, then
   (a) if $|x_j - x_i| > |x_i - x_{i-1}|$, $|x_{j+1} - x_j|$ and $|x_j - x_i| > 2a_c$, then a new point x should be in the range
   $$x_{i-1} + 2a_c < x < x_{j+1} - 2a_c,$$
   (b) if $|x_i - x_{i-1}| > |x_j - x_i|$, $|x_{j+1} - x_j|$ and $|x_i - x_{i-1}| > 2a_c$, then a new point x should be in the range
   $$x_{i-2} + 2a_c < x < x_j - 2a_c,$$
   (c) if $|x_{j+1} - x_j| > |x_i - x_{i-1}|$, $|x_j - x_i|$ and $|x_{j+1} - x_j| > 2a_c$, then a new point x should be in the range
   $$x_i + 2a_c < x < x_{j+2} - 2a_c.$$

1.1.2. *Results of Computer Simulation.* We applied the above **Complete Packing Algorithm** for all preliminary simulation results. The following table is a summary of our computer simulations. In this table, $\bar{\rho}_L^{(1)}$ indicates the packing density estimated at the preliminary stage, and $\bar{\rho}_L$ corresponds to the packing density estimated after applying CPA. It is obvious that CPA gives bigger packing density for respective values of L.

L	n_t	n_s	$\bar{\rho}_L^{(1)}$	$\bar{\rho}_L$	L^{-1}
20	5×10^3	5000	0.7672	0.7717	0.05000
50	10^4	5000	0.7698	0.7712	0.02000
100	5×10^3	4000	0.7695	0.7710	0.01000
200	2×10^4	4000	0.7699	0.7711	0.00500
500	5×10^4	2000	0.7699	0.7713	0.00200
1000	10^5	500	0.7700	0.7708	0.00100
2000	2.5×10^5	200	0.7702	0.7710	0.00050
5000	5×10^5	100	0.7698	0.7709	0.00020

Table 1. Summary of simulation for 1-D Voronoï random complete packing.

We performed a weighted linear regression analysis in the form

$$\rho_L = \rho_\infty + au^{-1} + o(u^{-1}).$$

where ρ_L is represented as a linear function of $u^{-1} \equiv L^{-1}$. As a result, we obtained for the packing density $\hat{\rho}_\infty = 0.7710$ and for the regression coefficient $\hat{a} = 0.0122$. Figure 3 indicates the summary plot of simulation and the regression analysis.

Now, it is interesting to compare our result with the density of 'car parking problem' [2]. As stated in Introduction, a theoretical packing density was $c = 0.74759\cdots$. By comparing this value with our result for 1-D Voronoï random packing, we see that the density of 1-D Voronoï random packing is about three percent larger than c.

2. Voronoï Random Packings for 2-D and 3-D

It will be natural to extend the idea of Voronoï random packing to higher dimensional space. Extension of the procedure given above to these spaces are rather direct and can be described as follows.

2.1. **2-D Voronoï Random Packing.** Let the region of packing be a square $A = L \times L$, and let the critical value of accepted length be a_c.

(1) Put $N \leftarrow 3$, and generate N points uniformly at random inside A.

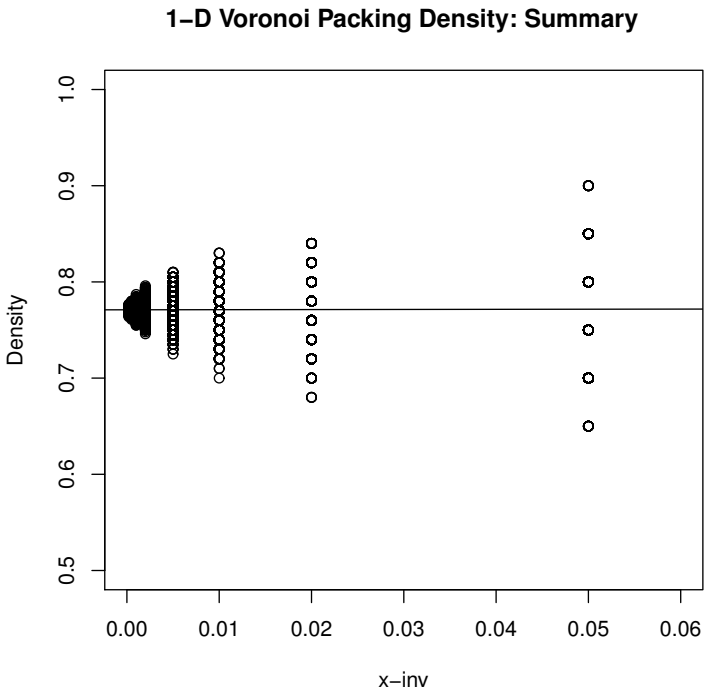

FIGURE 3. Summary plot of simulation and the linear regression analysis

(2) Compute Voronoï division of the point pattern. If the size of any Voronoï cell is below a_c, go to Step **1**, else go to Step **3**.
(3) Generate a test particle $\mathbf{x}_t$ uniformly at random in A, and compute the Voronoï cell $V(\mathbf{x}_t)$ of the point $\mathbf{x}_t$. If the size of $V(\mathbf{x}_t)$ and the sizes of contiguous Voronoï cells are all bigger than a_c, then go to Step **4**, else go to Step **3**.
(4) $N \leftarrow N+1$. If a specified **Stopping Rule** is satisfied, then **Stop**, else go to Step **3**.

As in 1-D case, in order to estimate the packing density ρ_∞ in the limit $L \to \infty$, we performed computer simulation of 2-D Voronoï random packing for several values of L by applying the same **Stopping Rule** as a preliminary stage in 1-D case (n_t: total number of test particles). The results are summarized in Table 2, where similar symbols are used as in Table 1 ($a_c = 1$ is used).

L	n_t	n_s	$\bar{\rho}_{L\times L}$	$u^{-1} = L^{-1} + L^{-1}$
5	10^4	1000	0.8343	0.40000
7	2×10^4	1000	0.8355	0.28571
10	2×10^4	500	0.8332	0.20000
15	5×10^4	500	0.8354	0.13333
20	10^5	500	0.8366	0.10000
30	1.5×10^5	500	0.8347	0.06667
40	2×10^5	200	0.8331	0.05000
50	3×10^5	200	0.8324	0.04000
70	2.5×10^5	100	0.8247	0.02857
100	4×10^5	50	0.8222	0.02000
200	2×10^6	5	0.8246	0.01000

Table 2. Summary of simulation for the 2-D Voronoï random packing.

In Table 2, $\bar{\rho}_{L\times L}$ indicates a sample mean of $\rho_{L\times L}$ and $u^{-1} \equiv X^{-1}+Y^{-1}$ is the value of the axis used for the linear regression in order to estimate $\rho_\infty = \lim_{X,Y\to\infty} \rho_{X\times Y}$ in the form

$$\rho_{X\times Y} = \rho_\infty + au^{-1} + o(u^{-1}).$$

Figure 4 is a sample of random sequential packing of disks with a Voronoï division and Figure 5 is a sample of 2-D Voronoï random packing.

Figure 6 shows the summary plot of simulation and regression analysis. The dots in Fig.6 indicate all of simulated value of density and the solid line in Fig.6 is an estimated regression line. From the regression analysis, we obtained for the limiting packing density $\hat{\rho}_\infty = 0.8335$ and for the coefficient $\hat{a} = 0.0040$.

Our results indicate that the 2-D Voronoï random packing shows a packing density of about 83 percent of the area of whole region. We point out that this packing density is rather high (about fourty percent bigger) compared with the packing density of the random packing by disks (we have obtained the value $0.5473/(\pi/\sqrt{12}) = 0.6035$ [1] for the case of disks [3]).

We can consider the high packing density of Voronoï random packing compared with the above value of identical disks might be due to the flexibility of the shape of packed objects. This fact is surmised by a

[1]Here, our packing density is considered to be a 'number' density (the ratio of total number of packed points against the number of maximally packed points for the whole region), while the value 0.5473 is the 'volume' density defined as the ratio of total 'volume' of packed disks against the 'volume' of the whole region. Therefore, 0.5473 is divided by $\pi/\sqrt{12}$ (maximal 'volume' density) to get 'number' density.

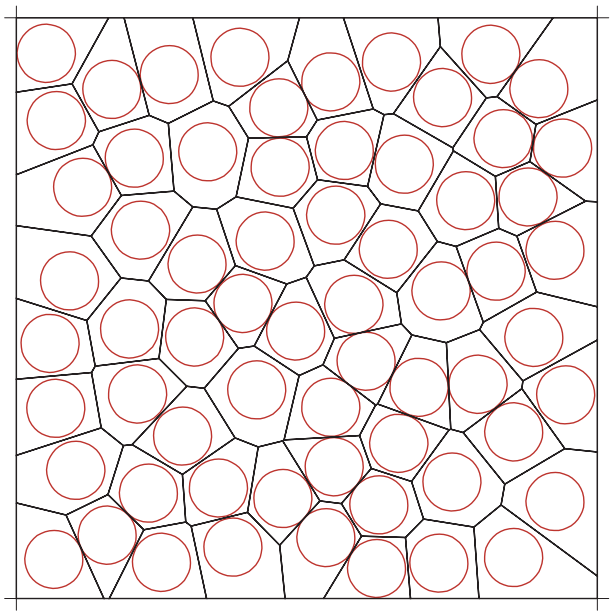

FIGURE 4. Sample pattern of random sequential packing of disks. Voronoï division is drawn.

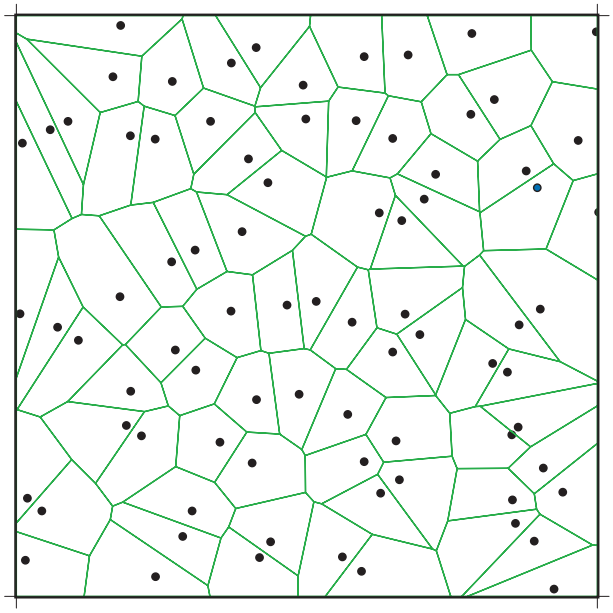

FIGURE 5. Sample pattern of 2-D Voronoï random packing

comparison of Fig.4 and Fig.5, namely, the shape of Voronoï cells for disk

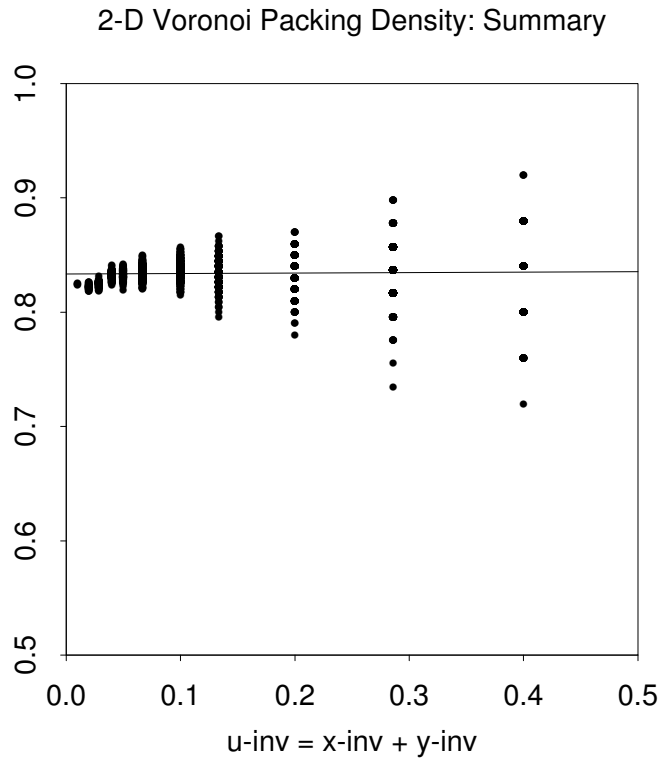

FIGURE 6. Summary plot of simulation and the linear regression analysis

packing is rather rotund, but the Voronoï cells for the Voronoï random packing are often flat, on the other.

2.2. **3-D Voronoï Random Packing.** We have also done a small scale simulation of 3-D Voronoï random packing in a finite cube L^3. Table 3 summarizes the results.

L	n_t	n_s	$\bar{\rho}_L$	L^{-1}
5	5×10^3	100	0.8130	0.0167
7	10^4	50	0.8104	0.0111

Table 3. Summary of simulation for 3-D Voronoï random packing.

These results suggest the 3-D Voronoï random packing density of $\bar{\rho} \approx 0.81$. By comparing this with the packing density for random sequential packing of spheres ($\bar{\rho} = 0.381/(\pi/\sqrt{18}) \approx 0.515$) [4], the difference of

packing density between the two packing processes seems to become more big as the dimension of space becomes large.

3. Remarks

As an application of the Voronoï random packing, we can consider the habitat of plants. It is natural to assume that an individual of plant occupies a critical size of area which is neccesary for its existence through the competition for sun light and for water or nutrition. Then, as a result of competitions among individuals, the final pattern of the plant 'territory' might look like those of the Voronoï random packing for the asynchronous (sequential) settlement of plants. As a similar model for animal territories, we have once applied the random disk packing for the asynchronous settlement [8].

Regarding the **Stopping Rule** discussed in Section 2.1, we will be able to devise a new rule in order to approach a random 'complete' packing, which was exactly done for 1-D Voronoï random packing. In 2-D case, in order to build the algorithm corresponding to CPA, we inspected several samples which are assumed to be near the complete packing. As a result we arrived at the following statements by which we are able to attain CPA in 2-D space. Let us assume the current packing state under consideration is approaching a complete packing in 2-D Voronoï random packing. Then

- If there is a point $\mathbf{x}_i$ whose Voronoï cell area $|V(\mathbf{x}_i)|$ satisfies $|V(\mathbf{x}_i)| \geq 2a_c$, then an acceptable point $\mathbf{x}$ lies near $\mathbf{x}_i$.
- If there is a contiguous pair of points $\mathbf{x}_i$ and $\mathbf{x}_j$ satisfying $|V(\mathbf{x}_i)| + |V(\mathbf{x}_j)| \geq 3a_c$, then an acceptable point $\mathbf{x}$ lies near the common edge $e(i,j) \equiv V(\mathbf{x}_i) \cap V(\mathbf{x}_j)$.
- If there is a contiguous triplet of points $\mathbf{x}_i$, $\mathbf{x}_j$ and $\mathbf{x}_k$ satisfying $|V(\mathbf{x}_i)| + |V(\mathbf{x}_j)| + |V(\mathbf{x}_k)| \geq 4a_c$, then an acceptable point x lies near the common vertex $v(i,j) \equiv V(\mathbf{x}_i) \cap V(\mathbf{x}_j) \cap V(\mathbf{x}_k)$.

By taking into consideration these statements for the algorithm, we will be able to devise a CPA as a next step of the present study, and we will get a complete packing efficiently without generating much test particles. Then the density of 2-D Voronoï random 'complete' packing will become slightly bigger than the present result. Three-dimensional version of CPA for the Voronoï random 'complete' packing will also be devised by suitably reforming the above statements.

We finally remark on the shape of Voronoï cells of our Voronoï random packing. As mentioned above, we noted a qualitative difference of the Voronoï cell shapes between the Voronoï and the disk random packings. Then, it will be an interesting problem to quantitatively compare the Voronoï cell shapes among different random processes. Regarding this, we have done an analysis of large scale computer simulation of Poisson Voronoï cells [5], [6] and presented several formula for statistical distribution of the Voronoï cell shapes. These formula will be useful for our present problem in future.

References

[1] Hinrichsen E. L., Feder J. and Jøssang T. *Geometry of random sequential adsorption.* Journal of Statistical Physics, **44**: 793–827, 1986.

[2] Rényi A. *On a one-dimensional problem concerning random space filling.* Publ. Math. Inst. Hungar. Acad. Sci., **3**: 109–127, 1958.

[3] Tanemura M. *On random complete packing by disks.* Annals of the Institute of Statistical Mathematics, **31**: 351–365, 1979.

[4] Tanemura M. *Random packing and random tessellation in relation to the dimension of space.* Journal of Microscopy, **151**: 247–255, 1988.

[5] Tanemura M. *Statistical distributions of Poisson Voronoi cells in two and three dimensions.* Forma, **18**: 221–247, 2003.

[6] Tanemura M. *Statistical distributions of the shape of Poisson Voronoï cells.* Voronoï's Impact on Modern Science (Eds. Syta, H. and Yurachkivsky, A.), Inst.Math., National Academy of Sciences of Ukraine, Book 3 (2005), 193–202.

[7] Tanemura M. *On the areal random packing.* Model. i analis inform. sistem., **20**: 134–140, 2013.

[8] Tanemura M. and Hasegawa M. *Geometrical models of territory – I. Models for synchronous and asynchronous settlement of territories.* Journal of Theoretical Biology, **82**: 477–496, 1980.

[9] Torquato S., Uche O. U. and Stillinger F. H. *Random sequential addition of hard spheres in high Euclidean dimensions.* Physical Review E, **74**: 061308, 2006.

Prof.Emer., The Institute of Statistical Mathematics, 10-3 Midori-cho, Tachikawa, Tokyo, 190-8562, Japan
Email: tanemura(at)ism(dot)ac(dot)jp

Voronoï's Impact on Modern Science, Book 6, Volume 2
Proceedings of the Sixth International Conference on Analytic Number Theory and Spatial Tessellations

ON SMALL WORLD NON-SUNADA TWINS AND CELLULAR VORONOI DIAGRAMS

Vasyl Ustimenko (*Poland*)

Abstract. Special infinite families of regular graphs of unbounded degree and of bounded diameter (small world graphs) are considered. Two families of small world graphs G_i and H_i form a family of *Non-Sunada twins* if G_i and H_i are isospectral of bounded diameter but groups $Aut(G_i)$ and $Aut(H_i)$ are nonisomorphic.

We say that a family of Non-Sunada twins is *unbalanced* if each G_i is edge-transitive but each H_i is edge-intransitive. If all G_i and H_i are edge-transitive we have a *balanced* family of small world Non-Sunada twins.

We present explicit constructions of the above defined families. Two new families of distance-regular— but not distance-transitive— graphs will be introduced.

Introduction

As everybody knows, the answer to the famous question, "Can you hear the shape of a graph?" is negative. In this paper we would like to stress that in fact we are so deaf that we are unable to recognise orchestras of large families of small world graphs. Two nonisomorphic families can produce the same symphony in absolutely identical manner.

In [1] Sunada presented a method of constructing pairs of nonisometric manifolds $\{M_1, M_2\}$ such that the eigenvalues of the Laplace operator satisfy $\lambda_i(M_1) = \lambda_i(M_2)$ for all i. His method was based on interpreting the isospectral condition in terms of finite group theory: if G is a finite group acting freely on a manifold M^G, with M_1 and M_2 quotients of M^G by subgroups H_1 and H_2 respectively, then M_1 and M_2 will be isospectral if the induced representations $(1_{H_1})^G$ and $(1_{H_2})^G$ are equivalent (here 1_X denotes the trivial representation of the group X). If Γ_1 and Γ_2 are two

Received June 12, 2019.

2010 *Mathematics Subject Classification.* Primary 05C50; Secondary 05C82, 51E24.

Key words and phrases. Laplacians, isospectral graphs, small world graphs, distance-regular graphs, Non-Sunada constructions, graph Voronoi diagram, thin Voronoi cells.

graphs, then one may define a Laplacian on them and ask whether they are isospectral. As it is written in [2] "There are many constructions of isospectral graphs which appear to have little to do with the Sunada construction, see [3] for survey. However if we imposed the condition that Γ_1 and Γ_2 are k-regular, which is a natural condition to impose from the point of view of geometry, then most of these constructions do not apply. An exception to this is the construction of Seidel switching ([3])." In fact, some other constructions of isospectral distance-regular graphs of Non-Sunada nature were already known and presented in [4]. In particular, Hemmeter's [5] and Ustimenko's [6] examples of distance-regular, but not distance-transitive, graphs via new constructions of infinite families of isospectral pairs of graphs were reflected in [4]. In fact, we now have other examples of isospectral graphs due to recent progress in Distance-Regular Graph Theory (see [7]).

The purpose of this paper is to draw attention of specialists in applied graph theory to the fact that the theory of Tits geometries over Dynkin-Coxeter diagrams B_n and C_n provides remarkable examples of infinite sequences of Non-Sunada isospectral pairs of graphs which form families of small world graphs. Note that a similar situation has occurred in Extremal Graph Theory; no earlier than seven years after Tits' initial formulation of finite regular generalised polygons [9] would Benson [8] come to observe that these objects achieve the upper bound in the Even Circuit Theorem of Erdős.

We conjecture that many other families of small world Non-Sunada twins can be defined via Borel subgroups and partitions of largest Schubert cells into special "medium" Schubert cells.

Two new families of distance-regular, but not distance-transitive, graphs are here introduced.

Finally we introduce the concept of a thin Voronoi cell connected with the notion of a Voronoi graph diagram. Nice examples of Voronoi cells of geometric nature are thin Schubert cells. It is interesting that isospectrality of small world graphs described in this paper can be easily explained via similarity of cellular Voronoi diagrams.

Two families of distance-transitive graphs defined in terms of Lie geometry form pairs of Non-Sunada twins. Let $\Gamma(B_n(q))_i$ and $\Gamma(C_n(q))_i$ be the totalities of elements of the respective geometries of Chevalley groups $B_n(q)$ and $C_n(q)$, where the subscript i (type) corresponds to the node i of the Coxeter Dynkin diagram, $i = 1, 2, \ldots, n$.

Consider the binary relations $\phi(B_n(q))$ and $\phi(C_n(q))$ whereby two distinct elements of type n are incident to a common element of type $n-1$. When q is odd, the graphs $\Gamma_n(B_n(q))$ and $\Gamma_n(C_n(q))$ are nonisomorphic

but isospectral. For $n \geq 3$, $\phi(B_n(q))$ and $\phi(C_n(q))$ are families of small world graphs. Their diameter is n, however their degrees are tending with q toward infinity.

Each family can be embedded in a larger family of small world graphs via the following scheme:
(1) Take the universal geometry of type B_n (or C_n) defined over the commutative ring K defined in section 9, compute its specialisation S which is an incidence system with partition sets $\Gamma^1(X_n)$, $\Gamma^2(X_n)$, ... , $\Gamma^n(X_n)$.
(2) Consider the graphs $\phi_S(X_n, K)$ of the binary relation of incidence of two distinct elements of $\Gamma^n(X_n)$ to some element of $\Gamma^{n-1}(X_n)$.

Note that new families of small world graphs $\phi_S(X_n, K)$ depend on the ring K and specialisation S. Graphs $\phi_S(K)$ for the chosen ring K and various S have the same sets of vertices.

So the following problem appears naturally:

Find a ring K and a pair of representations S^1 and S^2 such that nonisomorphic graphs $\phi_{S^1}(B_n, K)$ and $\phi_{S^2}(C_n, K)$ are isospectral. In the case of finite fields F_q of odd prime-power order q, such a pair S^1, S^2 actually exists.

We can consider families of distance-regular graphs $\phi(D_{n+1}(q))$ (two vertices of $\Gamma_n(D_{n+1}(q))$ are incident to some element of type $n-1$) and $\phi'(X_n(q))$ (two vertices of $\Gamma_n(X_n(q))$ are incident to some element of type $n-2$) where $X = B$ or $X = C$ and $n \geq 3$.

Note that the graphs $\phi(D_{n+1}(q))$ and $\phi'(B_n(q))$ are isomorphic, whereas $\phi'(C_n(q))$ are the Ustimenko graphs (see subject index of [4]). One can take the universal geometries of X_n over a finite commutative ring K for $X = B$, $X = C$ and $X = D$, and their specialisations.

The search for nonisomorphic isospectal pairs of graphs from the disjoint union of $\phi_{S^1}(D_{n+1}, K)$, $\phi'_{S^2}(B_n, K)$ and $\phi'_{S^3}(C_n, K)$ makes sense because of isospectrality of $\phi(D_{n+1}(q))$ and Ustimenko graphs for odd q and $n \geq 3$.

We may consider the restrictions of $\phi(D_4(q))$ and $\phi(X_3(q))$ for $X = B$ or $X = C$ on the largest Schubert cells of the corresponding geometry which are also distance-regular graphs (see section 6), and investigate restrictions of $\phi_{S^1}(D_4, K)$, $\phi'_{S^2}(B_3, K)$ and $\phi'_{S^3}(B_3, K)$ on the corresponding largest Voronoi–Schubert cells (see section 9).

The interpretation of the geometry $\Gamma(n, q)$ of the Chevalley group $X_n(q)$ as a special interpretation of the universal geometry $U(X_n, K)$ allows one to generate this object in computer memory in time $O(|\Gamma(n, q)|)$ with fast algorithm $(O(n^2))$ to check whether or not two elements of the geometry are incident. Notice that the incidence systems $U_S(X_n, K)$

where K is a finite commutative ring are "computationally equivalent" to $\Gamma(n, q)$.

The interpretation of $\Gamma(n, q)$ as $U_S(X_n, K)$ for specialisation S allows one to effectively generate small world graphs corresponding to double cosets of the form $P_i g P_i$ and more general graphs corresponding to $P_i g P_j$ such as the Double Grassman graphs of geometry $A_{2k+1}(q)$ considered in section 4 (see [31]).

The concept of Voronoi orbitals allows us to define new small world graphs in terms of specialisations of $U(X_n, K)$ which are analogues of double coset graphs.

An important geometric object is the partition of the elements of a geometry of a Chevalley group into thin Schubert cells. In the case of Projective Geometry this was investigated by D. Hilbert. We conjecture that this is a partition of vertices of incidence graphs into Voronoi cells with respect to the natural embedding of the Weyl geometry into the geometry of its corresponding Chevalley group. In the case of projective geometry over the field of complex numbers, this fact was proved by I. M. Gelfand and R. MacPherson (see [16] and further references).

For each specialisation S of the universal geometry $U(X_n, K)$, one can find the naturally embedded geometry of the Weyl group $W(X_n)$. So Voronoi–Schubert cells can be considered for each incidence graph of $U_S(X_n, K)$. We believe that properties of this partition are important for spectrum investigation of small world graph defined in terms of $U(X_n, K)$.

1. Some basic definitions from Graph Theory and Algebraic Combinatorics

1.1. **On distance in graphs and related constructions.** Let G be a finite simple graph. For vertices x and y of G, we denote by $d(x, y)$ the length of the shortest path from x to y, and set $G_i(x) = \{y : d(x, y) = i\}$. We sometimes write $G(x)$ for $G_1(x)$. Also $x \sim y$ is used to denote that $x \in G(y)$. Now fix x and y in $V(G)$ with $y \in G_i(x)$. Define $a_i = |G_i(x) \cap G_1(y)|$, $b_i = |G_{i+1}(x) \cap G_1(y)|$, $c_i = |G_{i-1}(x) \cap G_1(y)|$. If these parameters never depend on x and y, but only on i, then G is called a distance-regular graph.

One source of examples of distance-regular graphs is provided by distance-transitive graphs: a graph G is distance-transitive if for all $x_1, y_1, x_2, y_2 \in V(G)$ with $d(x_1, y_1) = d(x_2, y_2)$, there exists an automorphism σ of G with $\sigma(x_1) = x_2$ and $\sigma(x_2) = y_2$.

Let G be any graph. We define a bipartite graph G^* (called the extended bipartite double of G, cf. [4], p. 261) as follows. Let F_1 and F_2 be

disjoint sets of the same size as $V(G)$, with $f_i : V(G) \to F_i$ bijections, for $i = 1, 2$. The vertex set of G^* is defined to be $F_1 \cup F_2$. For $u, v \in V(G)$, $f_1(u) \sim f_2(v)$ in G^* if and only if either $u = v$ or $u \sim v$ in G. For $x, y \in V(G^*)$ we will write $d^*(x, y)$ for the distance from x to y. We also define $\phi : V(G^*) \to V(G)$ by $\phi|F_i = {f_i}^{-1}$.

LEMMA 1. *Let $x, y \in V(G^*)$ with $d^*(x, y) = i$. Suppose that $u = \phi(x)$ and $v = \phi(y)$ with $d(u, v) = j$. Then j is either i or $i - 1$. The diameter of G^* is greater by one than that of G.*

If a regular graph G is bipartite, it is associated with another regular graph G', defined as follows. Suppose that $V(G) = X \cup Y$ is the bipartition of G. We let $V(G') = X$, and for $x_l, x_2 \in X$ we define $x_1 \in G'(x_2)$ provided $x_1 \in G_2(x_2)$. G' is called a halved graph of G. More information on halved graphs may be found in [4].

1.2. **On Coxeter groups, Tits systems and their geometries.** An incidence system is a triple (Γ, I, t) where I is a symmetric antireflexive relation (simple graph) on the vertex set Γ, and $t : \Gamma \to N$ is a type function onto the set of types N such that $\alpha I \beta$ and $t(\alpha) = t(\beta)$ together imply $\alpha = \beta$. A flag F is a nonempty subset of Γ such that $\alpha, \beta \in F$ implies $\alpha I \beta$. We define $t(F) = \{t(x) | x \in F\}$ (see [16]).

An important example of an incidence system as described above is the so-called *group incidence system* $\Gamma(G, G_s)_{s \in S}$. Here G is the abstract group and $\{G_s\}_{s \in S}$ is the family of distinct subgroups of G. The objects of $\Gamma(G, G_s)_{s \in S}$ are the left cosets of G_s in G for all possible $s \in S$. Cosets α and β are incident precisely when $\alpha \cap \beta \neq \emptyset$. The type function is defined by $t(\alpha) = s$ where $\alpha = gG_s$ for some $s \in S$.

Let (W, S) be a Coxeter system, i.e. W is a group with a set of distinguished generators given by $S = \{s_1, s_2, \ldots, s_n\}$ and generic relations $(s_i s_j)^{m_{ij}} = 1$ for all $1 \leq i, j \leq n$. Here $M = (m_{ij})$ is a symmetric $n \times n$ matrix with $m_{ii} = 1$ and off-diagonal entries satisfying $m_{ij} \geq 2$ (allowing $m_{ij} = \infty$ as a possibility, in which case the relation $(s_i s_j)^{m_{ij}} = 1$ is omitted). Letting $W_i = \langle S - \{s_i\} \rangle$, $1 \leq i \leq n$, we obtain a group incidence system $\Gamma(W) = \Gamma(W, W_i)_{1 \leq i \leq n}$ which is called the Coxeter geometry of W. The subgroups W_i here are referred to as the *maximal standard subgroups* of W (see [32] or [16]).

Let T be the totality of all reflections, i.e. elements of the form $gs_i g^{-1}$ where $g \in W$, $i = 1, 2, \ldots, n$. We assume that elements of W and T are listed in the standard lexicographical order with respect to basis $\{s_1, s_2, \ldots, s_n\}$.

Let $l(g)$ be the length of a minimal irreducible decomposition of g into elements of S. For $\alpha \in \Gamma(W)$, we define $l(\alpha)$ as the minimal length of a representative of this coset. We introduce the set $\Delta(\alpha) = \{s \in T \mid l(s\alpha) < l(\alpha)\}$.

Let G be a group, B and N subgroups of G, and S the collection of cosets of $B \cap N$ in N. We call (G, B, N, S) a *Tits system* (or we say that G *has a* BN*-pair*) provided

(i) $G = \langle B, N\rangle$ and $B \cap N$ is normal in N,

(ii) S is a set of involutions which generates $W = N/(B \cap N)$,

(iii) sBw is a subset of $BwB \cup BswB$ for any $s \in S$ and $w \in W$,

(iv) $sBs \neq B$ for all $s \in S$.

Properties (i)-(iv) imply that (W, S) is a Coxeter system (see [32] or [16]). Whenever (G, B, N, S) is a Tits system, we call W the *Weyl group of the system*, or simply the *Weyl group of* G. The subgroups P_i of G defined by BW_iB are called the *standard maximal parabolic subgroups* of G. The group incidence system $\Gamma(G) = \Gamma(G, P_i)_{1\leq i\leq n}$ is commonly referred to as the *Lie geometry* of G (see [16], [32]). Note that the Lie geometry of G and the Coxeter geometry of the corresponding Weyl group W have the same rank n. In fact, there is a type-preserving morphism from $\Gamma(G)$ onto $\Gamma(W)$ given by $Retr : gP_i \to wW_i$, where w is determined from the equality $BgP_i = BwP_i$. This morphism $Retr$ is called a *retraction*.

Let us consider the totality $\mathcal{F}$ of conjugates of Borel subgroup B of the form $B^n = nBn^{-1}$ where $n \in N$, and their respective orbits on $\Gamma(G)$. These orbits give rise to a natural equivalence relation τ where $x\tau y$ provided x and y lie in the same orbit of each subgroup from $\mathcal{F}$. The equivalence classes are known as *thin Schubert cells* (see [16] and further references with descriptions of various applications of these equivalence classes).

1.3. **On association schemes, permutation groups and hypergroups.** The notion of an association scheme is one of the most important in all of Algebraic Combinatorics.

An association scheme Ω consists of a finite set X and a collection of binary relations R_0, R_1, ..., R_d that partitions $X \times X$, such that

(1) $R_0 = \{(x, x) \mid x \in X\}$,

(2) for each $i = 1, 2, \ldots, d$, the inverse relation

$$R_i{}^{-1} = \{(x, y) \mid (y, x) \in R_i\}$$

coincides with some R_j from the collection,

(3) for $i, j, k \in \{0, 1, 2, \ldots, d\}$, the number

$$p^k_{i,j} = p^k_{i,j}(a, b) = |\{x \in X \mid (a, x) \in R_i, (x, b) \in R_j\}|$$

does not depend on the choice of the pair $(a, b) \in R_k$.

Let (G, X) be a transitive permutation group acting on the set X. Orbitals of (G, X), i.e. orbits of the induced action of G on the set $X \times X$, are binary relations of an association scheme. Let $a \in X$, and define

$$H = \{g \in G \mid g(a) = a\}.$$

Then orbitals of (G, X) are in one-to-one correspondence with double cosets of the form HgH, $g \in G$.

For each directed graph R_i of an associative scheme we consider its adjacency matrix A_i of size $|X| \times |X|$ with entries $a(x, y) \in \{0, 1\}$ such that $a(x, y) = 1$ if and only if $(x, y) \in R_i$. It follows from the definition of matrix product that $A_i A_j = \sum p_{i,j}^k A_k$. So the vector subspace $A(\Omega) = \langle A_0, A_1, A_2, \ldots, A_d \rangle$ in $M_n(C)$, $n = |X|$ (i.e. the matrix algebra over the field C of complex numbers) is closed under matrix multiplication.

Such algebras have appeared in different areas of mathematics under different names such as *Bose-Mesner algebra*, *cellular algebra*, *centraliser algebra*, *V-Shur ring* (see [33], [34]). In the case of an association schemes of orbitals for a permutation group (G, X), we will reserve the term *Hecke algebra* (see [32]) for this algebra. The Hecke algebra $H = H(G, X)$ may be identified as the centralizer of the totality of all permutations from (G, X):

$$H = \{M \in M_n(C) \mid A_\pi M = M A_\pi \text{ for all } \pi \in G\}$$

where A_π is the $n \times n$ permutation matrix corresponding to the permutation π.

We also consider the totality $H[G]$ of formal linear combinations of the symbols a_0, a_1, $\ldots$, a_d such that the relations

$$a_i \times a_j = \sum z_{i,j}^k a_k$$

give us the definition of an associative algebra with unity a_0. This object is known in Functional Analysis as a *hypergroup* (see, [35], [36]). Note that a hypergroup is an abstract algebra with fixed basis $\{a_0, a_1, \ldots, a_d\}$ and integer structure constants $p_{i,j}^k \geq 0$.

We will refer to nonisomorphic Bose-Mesner matrix algebras with the same hypergroups as *hyper-equivalent BM algebras*.

2. Two Cartan matrices with the same Coxeter group and large families of isospectral graphs

Let us consider the Coxeter-Dynkin diagrams X_n with n nodes, where X stands for one of the letters B, C and D with $n \geq 3$. For each X_n we

denote by $W(X_n)$ and $X_n(q)$ the Weyl group and Chevalley group over the finite field F_q, respectively.

Let $\{s_1, s_2, \ldots, s_n\}$ be a set of Coxeter generators of $W = W(X_n)$ with $X = B$ or $X = C$, and let s_n correspond to the extreme right node of the diagram X_n. Let us consider the action of the group $W(X_n)$ on its left cosets by its standard subgroup W_n generated by the elements $s_1, s_2, \ldots, s_{n-1}$. One can identify the variety $(W : W_n)$ with a vector space ${F_2}^n$. The permutation group $(W, (W : W_n))$ coincides with the affine transformations $T_{A,\mathrm{b}}$ of the kind $\mathrm{x} \mapsto \mathrm{x}A + \mathrm{b}$, where A is a permutation matrix, and x and b are row vectors from ${F_2}^n$. Thus W is a semidirect product of the symmetric group S_n with the additive group of the vector space ${F_2}^n$.

Let T be the linear map on ${F_2}^n$ defined by

$$T : (x_1, x_2, \ldots, x_n) \mapsto (x_1 + x_2 + \cdots + x_n, x_2, x_3, \ldots, x_n).$$

Then the group $\langle T, s_1, s_2, \ldots, s_{n-1} \rangle$ is isomorphic to S_{n+1}. Observe that the group $W' = \langle W, T \rangle$ is isomorphic to Weyl group $W(D_{n+1})$. It is known that $W(X_n)$ preserves Hamming distance d on ${F_2}^n$ defined by the rule

$$d((x_1, x_2, \ldots, x_n), (y_1, y_2, \ldots, y_n)) = |\{i \mid x_i \neq y_i\}|.$$

Hence, orbitals of the transitive permutation group $W(X_n)$ are binary relations $\phi_i = \{(\mathrm{x}, \mathrm{y}) \mid d(\mathrm{x}, \mathrm{y}) = i\}$, $i = 0, 1, \ldots, n$. One can see that the orbitals of W' are ϕ_0 (equality relation) and $\phi_1 \cup \phi_2$, $\phi_3 \cup \phi_4$, $\ldots$, $\phi_{n-1} \cup \phi_n$ in the case of even n, and $\phi_1 \cup \phi_2$, $\phi_3 \cup \phi_4$, $\ldots$, $\phi_{n-2} \cup \phi_{n-1}$, ϕ_n in the case of odd n.

Let us consider the Chevalley group $X_n(q)$ with Borel subgroup B acting on the totality of left cosets $(X_n(q) : P_n)$ by its standard parabolic subgroup $P_n = BW_nB$ corresponding to the extreme right node of the Coxeter-Dynkin diagram. There is a natural one-to-one correspondence between orbitals of $(X_n(q), (X_n(q) : P_n))$ and orbitals of $(W(X_n), (W : W_n))$ (see [14]).

Let ϕ_i' be the orbital of $X_n(q)$ corresponding to the orbital ϕ_i of Weyl group W. Let $S(\Omega)$ be the symmetric group acting on the totality of left cosets $\Omega = (X_n(q) : P_n)$. All proper subgroups G of $S(\Omega)$ such that $X_n(q) \leq G$ are described in ([10], [11]). The proof does not use the classification of finite simple groups.

If $X = C$ then $X_n(q) < G < N(X_n(q))$, where the normaliser in $S(\Omega)$ is simply an extension of $X_n(q)$ via automorphisms of the ground field F_q. So orbitals of $N(C_n(q))$ and $C_n(q)$ are the same.

If $X = B$, then $B_n(q) < G < N(B_n(q))$ or $D_{n+1}(q) < G < N(D_{n+1}(q))$. The orbitals of groups $B_n(q)$ and $D_{n+1}(q)$ coincide with orbitals of their

respective normalisers, which are extensions of the corresponding Chevalley groups by automorphisms of the ground field F_q (see [12] for the details).

We can describe orbitals of $D_{n+1}(q)$ via special subsets of

$$N = \{1, 2, \ldots, n\}.$$

In the case of even n, we refer to $\{i, i+1\}$ $(1 \leq i \leq n/2)$ as generic subsets. In the case of odd n, our generic subsets are $\{i, i+1\}$ $(1 \leq i \leq (n-1)/2)$ and $\{n\}$. Orbitals of $D_{n+1}(q)$ are unions of ϕ'_i where i belongs to a single generic subset.

Let J be a proper subset of $N = \{1, 2, \ldots, n\}$, and let $C_J = C_J(n, q)$, $B_J = B_J(n, q)$ be graphs of binary invariant relations $\bigcup_{i \in J} \phi'_i$ of the respective permutation groups $(C_n(q), (C_n(q) : P_n))$ and $(B_n(q), (B_n(q) : P_n))$. Hecke algebras of $(B_n(q), (B_n(q) : P_n))$ and $(C_n(q), (C_n(q) : P_n))$ have the same intersectional indices (see [13] for closed formulae). This fact follows also from distance regularity of ϕ'. In fact, structure constants of the Hecke algebras of groups $B_n(q)$ and $C_n(q)$ acting on left cosets of a maximal parabolic subgroup corresponding to *any* node of the Coxeter diagram are also the same. This fact can be easily deduced from the relations in the definition of the Tits generic algebra of the Coxeter group B_n.

THEOREM 1. *Let J be a proper subset of $N = \{1, 2, \ldots, n\}$. For each $n \geq 3$, the graphs $C_J(n, q)$ and $B_J(n, q)$, where q ranges over various odd prime powers, form a family of Non-Sunada twins for which* $\mathrm{Aut}(C_J(n, q)) = N(C_n(q))$, *and* $\mathrm{Aut}(B_J(n, q)) = N(D_{n+1}(q))$ *if J is a union of generic subsets and* $\mathrm{Aut}(B_J(n, q)) = N(B_J(n+1, q))$ *in all other cases. Moreover, if J is generic set of cardinality 2 then for each $n \geq 3$ the graphs $C_J(n, q)$ and $B_J(n, q)$ form a family of unbalanced Non-Sunada twins.*

COROLLARY. *Let $n \geq 3$ be odd. If J is a singleton different from $\{n\}$, then the graphs $C_J(n, q)$ and $B_J(n, q)$ form a balanced family of Non-Sunada small world twins with respective automorphism groups $N(C_n(q))$ and $N(B_n(q))$. If $J = \{n\}$ then the graphs $C_J(n, q)$ and $B_J(n, q)$ form a balanced family of small world Non-Sunada twins with respective automorphism groups $N(C_n(q))$ and $N(D_{n+1}(q))$.*

J. Hemmeter observed that $D'(n + 1, q)$ is isomorphic to $B_{1,2}(n, q)$, and introduced the graphs $H(n, q) = C_{1,2}(n, q)^*$ [5] which are nowadays

referred to as Hemmeter graphs (see [4]).

THEOREM 2. *Let J be a proper subset of $N = \{1, 2, \ldots, n\}$. For each $n \geq 3$ the graphs $C_J(n,q)^*$ and $B_J(n,q)^*$, where q ranges over various prime powers, form a family of Non-Sunada twins with automorphism groups $\mathrm{Aut}(C_J(n,q))^* = N(C_n(q)) \times Z_2$, and $\mathrm{Aut}(B_J(n,q))^* = N(D_{n+1}(q)) \times Z_2$ if J is union of generic subsets and $\mathrm{Aut}(B_J(n,q)) = N(B_{n+1}(q)) \times Z_2$ in all other cases. Moreover, if J is a generic set of cardinality 2, then for each $n \geq 3$ the graphs $C_J(n,q)^*$ and $B_J(n,q)^*$ form a family of unbalanced Non-Sunada twins.*

3. Case of other nodes

We introduce orbitals of the Coxeter group W of type B_n (or C_n) acting on left cosets by its maximal standard subgroup

$$W_i = \langle s_1, s_2, \ldots, s_{i-1}, s_{i+1}, s_{i+2}, \ldots, s_n \rangle$$

for $i = 1, 2, \ldots, n$. The Coxeter geometry of W is the disjoint union Γ of the sets $\Gamma_i = (W : W_i)$ of left cosets of W by W_i with incidence relation I defined by $\alpha I \beta$ provided $\alpha \cap \beta \neq \emptyset$ where $\alpha \in \Gamma_i$, $\beta \in \Gamma_j$, $i \neq j$. It can be interpreted as follows (see for instance [6]): Let $N = \{1, 2, \ldots, n\}$, and consider the sets $H_i = \{(A, f) | A \in 2^N, |A| = i, f \to \{0, 1\}\}$, $i \in N$. Form the disjoint union $H = \bigcup_i H_i$ with incidence relation I defined by $(A, f) I (B, g)$ for $(A, f) \in H_i$ and $(B, g) \in H_j$ $(i \neq j)$ provided $A \subset B$ or $B \subset A$, and $f(x) = g(x)$ for all $x \in A \cap B$. The incidence system H is isomorphic to Γ. As always 2^N stands for totality of subsets of N.

The orbitals of W acting transitively on H_t, $1 \leq t \leq n$ may be described as $\phi_{r,s} = \{((A, f), (B, g)) \mid s = |A \cap B|, r = |\{x \in A \cap B \mid f(x) = g(x)\}|\}$ where $0 \leq r \leq s \leq t$.

Let us consider the action of $G = X_n(q)$ where $X \in \{B, C\}$ on the left cosets of its maximal standard parabolic subgroup $P_t = B w_t B$ where B is the standard Borel subgroup of G, $1 \leq t \leq n$. The orbitals $X_{r,s}$ of the permutation groups $(G, (G : P_t))$ are in natural one-to-one correspondence with $\phi_{r,s}$ of $(W, (W : W_t))$. Let $M(t) = \{(r, s) | 0 \leq r \leq s \leq t\}$.

THEOREM 3. *Let M be a proper subset of $M(t)$, $t < n$. Consider the action of $G = X_n(q)$ where $X \in \{B, C\}$ on the set $X(t, n, q) = (G : P_t)$ of left cosets of G by its maximal standard parabolic subgroup P_t. Assume that each $X_M(n, t, q)$ is the disjoint union of $X_{r,s}$ for all $(r, s) \in M(t)$. Then for all odd $q \geq 3$ and parameters t and n, the pairs $(B_M(n, t, q), C_M(n, t, q))$ form a family of Non-Sunada graphs with respective automorphism groups $N(B_n(q))$ and $N(C_n(q))$.*

4. Remarks on Schubert geometry, some conjectures

Let us consider the action of the group $X_n(q)$ on the geometry $\Gamma(X_n(q))$, which is the disjoint union of $X(n,t,q)$, $1 \leq t \leq n$, as well as the natural action of $X_n(q)$ on $X^2(n,t,q) = X(n,t,q) \times X(n,t,q)$. The Bruhat decomposition links these actions with the permutation representation of the Weyl group W of $X_n(q)$ acting on the elements of its geometry $\Gamma(W_n(q))$, which is the disjoint union of $W(n,t) = (W : W_t)$.

Specifically, orbits of $(X_n(q), X^2(n,t,q))$ and $(W, W(n,t))$ are in a natural one-to-one correspondence induced by the correspondence between double cosets $P_i w P_j$ and $W_i w W_j$ for $1 \leq i,j \leq t$ (see [14], [15] and further references).

The interpretation introduced above allows one to identify $W(n,t)$ with $\{(A,f)||A| = t, f \in 2^A\}$, and further identify orbits on $W(n,i) \times W(n,j)$ with the bipartite graphs $W(n,i,j,t,s) = \{((A,f),(B,g)) \in W(n,i) \times W(n,j)) \,|\, t = |A \cap B|,\ s = |\{x|f(x) = g(x)\}|\}$, where $\max(i + j - n, 0) \leq t \leq \min(i,j)$.

The orbits of $G = X_n(q)$ on $\Gamma_i(G) \times \Gamma_j(G)$ are in a natural one-to-one correspondence with $W(n,i,j,t,s)$. We use the symbol $X(n,i,j,t,s)$ to denote these orbits corresponding to $W(n,i,j,t,s)$. We define *type* $t(X(n,i,j,t,s))$ as the ordered tuple (n,i,j,t,s).

Let T be a maximal torus of $X_n(q)$. The totality of elements of $\Gamma(X_n(q))$ containing T with the restriction of the incidence relation I to this subset is isomorphic to the Weyl geometry $\Gamma(W_n(q))$. There is well defined homomorphic retraction map *Retr* from $\Gamma(X_n(q))$ onto $\Gamma(W_n(q))$ (see [16] and further references).

Without loss of generality we assume that $Retr(P_i)$ coincides with $\alpha_i = (\{1,2,\ldots,i\}, f)$, where $f(j) = 0$ for $1 \leq j \leq i$. For w a Coxeter element of Weyl group W, elements $Retr(wP_i)$ coincide with $\beta_i = (\{n, n-1, \ldots, n-i+1\}, g)$, where $g(j) = 1$ for each $n - i + 1 \leq j \leq n$. We refer to these latter elements as *Coxeter cosets of type* i.

Let $H_i = H_i^X = H_i^X(n,q)$ be the subset of elements hP_i from $\Gamma_i(X_n(q))$ such that $Retr(hP_i) = \beta_i$. We refer to the incidence system $H = H_1 \cup H_2 \cdots \cup H_t$ with the restriction I' to this set as the Schubert geometry $H = H(X_n(q))$. It is easy to check that the standard Borel subgroup B acts regularly on maximal flags of H.

Note that for $i \neq j$, the restriction of I' to $H_i \cup H_j$ is a biregular bipartite graph. We may assume that $\Gamma(W_n)$ is the subset of elements of $\Gamma(X_n(q))$ containing a maximal torus. For each element γ from $H_i(X_n(q))$ and each β_j we consider the list $L_i^j(\gamma)$ of types of orbits $\mathcal{R}$ of $(X_n(q), \Gamma_i \times \Gamma_j)$ that contain (γ, β_j). We say that γ_1, γ_2 from H_i are Weyl-equivalent

if $L_i^j(\gamma_1) = L_i^j(\gamma_2)$ for all j. By definition, Weyl-equivalence classes are unions of thin Schubert cells (see [17] and further references). In fact, each such class is a medium Schubert cell with respect to the set of Weyl elements that contain α_i and β_i $(1 \leq i \leq n)$ (see [18]).

This means that the number of Weyl-equivalence classes is bounded by a constant $c(n)$ which does *not* depend on the parameter q.

We say that two orbitals Φ_1, Φ_2 of the transitive permutation group (B, H_i) are Weyl equivalent if $(\beta_i, \gamma_1) \in \Phi_1$, $(\beta_i, \gamma_2) \in \Phi_2$ and γ_1, γ_2 are Weyl-equivalent.

We refer to unions of Weyl-equivalent orbitals as Weyl pseudo-orbitals of (B, H_i). We define type of a pseudo-orbital as a list $L_i^j(\gamma)$, $1 \leq j \leq n$, where $(\beta_i, \gamma) \in \mathcal{R}$. The partition into psudo-orbitals is defined in terms of the Coxeter matrix of the group $W(B_n) = W(C_n)$. Thus, cardinalities of pseudo-orbitals of $B(B_n(q))$ and $B(C_n(q))$ of a given type are of the same cardinality.

CONJECTURE 1. *Let Ω be the set of all types of pseudo-orbitals of (B, H_i) and let $J \neq \emptyset$ be a proper subset of Ω. For each triple (n, i, J) we consider the disjoint union $X(n, i, J, q)$ of pseudo-orbitals of type belonging to J. For $i \neq n$, the graphs $B(n, i, J, q)$ and $C(n, i, J, q)$ form a family of Non-Sunada twins with respective automorphism groups $N(B(B_n(q))$, $N(B(C_n(q))$. If n is odd then $B(n, n, J, q)$ and $C(n, n, J, q)$ form families of Non-Sunada twins with respective automorphism groups $N(B(D_{n+1}(q))$ and $N(B(C_n(q))$.*

5. New distance-regular graphs and Non-Sunada twins

For prime powers q, Pasechnik [18] constructed a distance-regular graph with intersection array $\{q^3, q^3-1, q^3-q, q^3-q^2+1, 1, q, q^2-1, q^3\}$ as a subgraph of the dual polar graph $D_4(q)$, in particular the subgraph induced on the set of vertices at maximal distance from an edge. Brouwer [18] constructed related distance-regular graphs $Z = Z_q$ with intersection array $\{q^3-1, q^3-q.q^3-q^2+1, 1, q, q^2-1\}$ as follows: Consider the vector space ${F_q}^3$ equipped with the standard cross product $\times$. The vertex set is $(F_q^3)^2$, where a pair (u, v) is adjacent to a distinct pair (u_0, v_0) if and only if $u_0 = u + v \times v_0$. The extended bipartite doubles of these graphs are the above mentioned graphs constructed by Pasechnik. In fact, Brouwer's graph is a subgraph of the dual polar graph $B_3(q)$; more precisely it is the subgraph induced on the set of vertices at maximal distance from a vertex.

For even q, the mentioned graphs have the same intersection arrays as certain Kasami graphs (see [4], Theorem. 11.2.1 and units (11),(13)). Pasini and Yoshiara [19] constructed distance-regular graphs with the same intersection array as (bipartite, diameter 4) Kasami graphs using dimensional dual hyperovals. Also the symmetric bilinear forms graphs for q even and $n = 3$ are distance-regular with the same intersection array as (diameter 3) Kasami graphs, (see [4], p. 285-286, and [20]). This shows that Z is distance-regular with the claimed parameters. The spectrum follows. The fact that the extended bipartite double is distance-regular, and has the above stated intersection array, follows from [4], Theorem 1.11.2(vi). The fact that Z_3 is strongly regular follows from [4], Proposition 4.2.17(ii), which states that this occurs when Z has eigenvalue -1. For the case $q = 2$, the graphs are (i) the folded 7-cube, (ii) the folded 8-cube, (iii) the halved folded 8-cube. All are distance-transitive. For $q > 2$, however, these graphs are not distance-transitive. When q is a power of two, the graphs Z have the same parameters as certain Kasami graphs, but for $q > 2$ they are nonisomorphic.

Observe that set $Z(q)$ of vertices of graph Z_q is a largest Schubert cell of $B_3(q)$ acting on dual polar spaces, i.e. a largest orbit of the Borel subgroup $B^3 = B^3(q)$ of $B_3(q)$. Group $D_4(q)$ is an overgroup of the permutation group $(B_3(q), B(3, q))$; the stabilizer of $Z(q)$ in $D_4(q)$ is isomorphic to the Borel subgroup $B^4 = B^4(q)$ of this group. Group $D_4(q)$ has orbitals which form a fusion scheme of the association scheme of orbitals $(B_3(q), Z(q))$. The distance in the graph Z_q defines an association scheme $\mathfrak{R}$ which is a fusion of orbital schemes of $D_4(q)$ and $B_3(q)$. For two types T_1 and T_2 of pseudo-orbitals δ_1 and δ_2 of $B_3(q)$, we write $T_1 \sim T_2$ mod (D_4) and say they are D_4-equivalent if there is an orbital ϕ of $B(D_4(q))$ such that $\phi \cap \delta_i \neq \emptyset$ for $i = 1, 2$. We refer to minimal sets of D_4-equivalent types as generic sets. Each graph of the association scheme $\mathfrak{R}$ coincides with $B(3, 3, J, q)$, where J is a union of generic sets. Note that there are four generators of this association scheme, namely z^i, $1 \leq i \leq 4$, where $z = z_q$. We consider J_1, J_2, J_3, J_4 such that $z^i = B(3, 3, J_i, q)$. It turns out that the relation $s_q^i = B(3, 3, J_i, q)$ $(1 \leq i \leq 4)$ forms an association scheme with the same intersection indices as scheme $\mathfrak{R}$. Let $s_q = s_q^1$. It is easy to see that $S_q = Z_q$ in the case of even q. In the case of odd q, the groups $\mathrm{Aut}(Z_q)$ and $\mathrm{Aut}(S_q)$ are normalisers $N_1 = N(B^4)$ and $N_2 = N(B(PSP_6(q)))$ of Borel subgroups of $D_4(q)$ and $C_3(q)$ in the corresponding symmetric groups.

THEOREM 4. *For odd q, the distance-regular graphs Z_q and S_q have the same parameters, and form a family of edge-intransitive Non-Sunada*

small world twins with respective automorphism groups $N(D_4(q))$ and $N(C_3(q))$.

PROPOSITION 1. *Let M be a nonempty proper subset of $\{1,2,3,4\}$. Then the unions $Z_q^M = \bigcup_{i\in M} z_q^i$ and $S_q^M = \bigcup_{i\in M} s_q^i$ form a family of Non-Sunada small world twins as q ranges over all odd prime powers.*

THEOREM 5. *For odd q, the extended bipartite doubles Z_q' and S_q' of Z_q and S_q, respectively, form a family of distance-regular Non-Sunada twins with respective automorphism groups $N_1 \times Z_2$ and $N_2 \times Z_2$.*

6. Case of the diagram A_n, the twisted Grassmann graphs

In [21] van Dam and Koolen constructed the first family of non-vertex-transitive distance-regular graphs with unbounded diameter. These graphs, called twisted Grassmann graphs, are denoted by $\widetilde{J}_q(2D+1, D)$ and are constructed as follows: Let q be a prime power, and let $D \geq 2$ be an integer. Let V be a $(2D+1)$-dimensional vector space over F_q, and let H be a hyperplane in V. Vertices are of two types: (i) $(D+1)$-dimensional subspaces of V that are not contained in H, and (ii) $(D-1)$-dimensional subspaces of H. Two vertices of the first type are adjacent if they intersect in a D-dimensional subspace; a vertex of the first type is adjacent to a vertex of the second type if the first contains the second; and two vertices of the second type are adjacent if they intersect in a $(D-2)$-dimensional subspace. The twisted Grassmann graph is distance-regular and has the same intersection array as the Grassmann graph $J_q(2D+1, D)$. In fact, the Grassmann graph and twisted Grassmann graph are the point graph and line graph, respectively, of the same partial linear space.

As mentioned above, the twisted Grassmann graph is not vertex-transitive (it has two orbits of vertices) and hence it is not isomorphic to the Grassmann graph. Fujisaki, Koolen, and Tagami [22] showed that the automorphism group of the twisted Grassmann graph is the subgroup of $P\Gamma L(2D+1, q)$ that fixes H. Bang, Fujisaki, and Koolen [23] determined the spectra of the local graphs, and studied in some detail their Terwilliger algebras. Remarkably, these algebras with respect to vertices in distinct orbits are not the same. The twisted Grassmann graphs are also counterexamples to two conjectures by Terwilliger ([24], p. 207-210), see [23]. Jungnickel and Tonchev [25] constructed designs that are counterexamples to Hamada's conjecture. Munemasa and Tonchev [26] showed that the twisted Grassmann graphs are isomorphic to the block graphs of these designs. Munemasa [27] showed that the twisted Grassmann graphs can also be obtained from the Grassmann graphs by

Godsil-McKay switching (cf. [28], X1.8.3]).

We say that a family of Non-Sunada twins is *strongly unbalanced* if each G_i is vertex transitive and edge-transitive but each H_i is vertex intransitive and edge-intransitive.

PROPOSITION 2. *For each $D \geq 3$ and q ranging over all prime powers, the graphs $J_q(2D+1, D)$ and $\widetilde{J}_q(2D+1, D)$ form a family of strongly unbalanced Non-Sunada graphs with respective automorphism groups $P\Gamma L(2D+1, q)$ and K, where K is the subgroup of $P\Gamma L(2D+1, q)$ fixing H.*

7. On Voronoi diagrams and cells, thin Schubert cells and isospectral graphs

The classical Voronoi diagram is a distance-based decomposition of a metric space relative to a discrete set of nodes, called the Voronoi sites. Given a set of Voronoi sites, the Voronoi decomposition leads to regions (the Voronoi regions) consisting of all nodes that are closest to a specific site. Mehlhorn [29] and Erwig [30] proposed an analogous decomposition, the *graph Voronoi Diagram*, for both undirected and directed graphs.

Definition 1. (Graph Voronoi Diagram [29], [30]). In a graph $\Gamma = (V, E, w)$, where w is weight function, the Voronoi diagram for a set $S = \{v_1, \ldots, v_s\} \subseteq V$ of nodes is a disjoint partition $\mathrm{Vor}(\Gamma, S) = V_1, V_2, \ldots, V_s$ of V such that for each node $u \in V_i$, $d(u, v_i) \leq d(u, v_j)$ for all $j \in \{1, 2, \ldots, s\}$.

In the above, the V_i are the Voronoi regions. The graph Voronoi diagram is not necessarily unique, as a node u may have the same distance to more than one Voronoi site.

We introduce the Voronoi cells as classes of the equivalence relation τ on V defined by $x\tau y$ if and only if $d(x, v_i) = d(y, v_i)$ for all $i = 1, 2, \ldots, n$. The connection with the graph Voronoi diagram is clear: Voronoi regions are disjoint unions of Voronoi cells.

Let $C(\Gamma, S)$ be the totality of Voronoi cells. We assume that the weight of each edge is 1 and that the Voronoi Diagram is unique. We consider the Voronoi-Schubert diagram $\mathrm{VorSch}(\Gamma, S)$ which is a partition of $C(\Gamma, S)$ corresponding to equivalence relation: *two Voronoi cells are in the same Voronoi region.*

For each $c \in C(\Gamma, S)$ we define its *trace* $\mathrm{tr}(c) = (d_1, d_2, \ldots, d_n)$ where $d_i = d(v_i, c) = d(v_i, x)$ for $x \in c$. If Γ is a finite graph we consider

the order $|c|$ of the Voronoi cell c which is simply the cardinality of this subsets of nodes.

We refer to (Γ, S) as a graph with selected nodes. We say that (Γ_1, S_1) and (Γ_2, S_2) are *Voronoi-equivalent* if there are bijections $\eta : S_1 \to S_2$, $\mu : C(\Gamma, S_1) \to C(\Gamma_2, S_2)$ such that $d(v_i, c) = d(\eta(v_i), \mu(c))$. We refer to the pair (η, μ) as a diagram isomorphism.

In the case of finite graphs, we say that (Γ_1, S_1) and (Γ_2, S_2) are *strongly diagram-equivalent* if they are Voronoi-equivalent and $|c| = |\mu(c)|$ for each Voronoi cell c.

Let F be a field. The Chevalley group $X_l(F)$ has a BN-pair and finite irreducible Weyl group W. Fixed points of a maximal torus T in its action on $\Gamma(X_l(F))$ form a subset of W such that the restriction of the incidence relation I to this subset is isomorphic to Weyl geometry of $W(X_l)$. So we have a natural embedding of $W(X_l)$ into $\Gamma = \Gamma(X_l(F))$. Let $I(X_l(F))$ denote the incidence relation of Γ. We are interested in studying $\mathrm{Vor}(\Gamma(G), S)$.

CONJECTURE 2. *Let $\Gamma(G)$ be the geometry of a simple group G that has a BN-pair. Let B, W and T denote a fixed Borel subgroup of G, the Weyl group of G and a maximal torus of G, respectively. Then the partition of $\Gamma(G)$, $\Gamma(W)$ into Voronoi cells coincides exactly with its partition into thin Schubert cells.*

In the case of projective geometry the above conjecture is supported by a well known theorem due to I. Gelfand and R. MacPherson (see [16] and further references).

CONJECTURE 3. *Let F be a field. Then the pairs $(I(B_n(F)), W(B_n))$ and $(I(C_n(F)), W(C_n))$ are Voronoi-equivalent. Moreover, if F is finite they are strongly diagram-equivalent.*

Let us consider a pair $(\Gamma, (a, b))$ where $(a, b) \in V^2$, and take $S = \{a, b\}$ of cardinality at most two. We say that (a_1, b_1) and (a_2, b_2) are Γ-*equivalent* if there is diagram isomorphism (η, μ) of $(\Gamma, \{a_1, b_1\})$ with $(\Gamma, \{a_2, b_2\})$ such that $\eta(a_1) = a_2$ and $\eta(b_1) = b_2$.

We refer to classes of Γ-equivalence as Γ- orbitals. We say that a partition into Γ-orbitals is transitive if there is a permutation group (G, V) such that its orbits on V^2 coincide with the Γ-orbitals.

We refer to a Voronoi-Schubert diagram of type $(\Gamma, \{a, b\})$ as a *binary VS-diagram*. We denote its trace function on Voronoi cells by tr. If the value $|c|$ is given for each cell c, we then use the term *scaled VS-diagram.*

Two graphs Γ_1 and Γ_2 are said to be Voronoi-equivalent (resp., strongly diagram-equivalent) if their orbital partitions are transitive, and their sets of binary VS-diagrams (resp., scaled VS-diagrams) coincide.

We can use technique of [31] and prove the following.

THEOREM 6. *Let F be an arbitrary field. Then the incidence graphs $\Gamma(B_n(F))$ and $\Gamma(C_n(F))$ are Voronoi-equivalent.*

THEOREM 7. *Incidence graphs of $\Gamma(B_n(q))$ and $\Gamma(C_n(q))$ are strongly diagram-equivalent.*

REMARK. *Observe that isospectrality of the graphs corresponding to the orbitals $(B_n(q), \Gamma_i(B_n(q))$ and $(C_n(q), \Gamma_i(C_n(q))$ may be deduced from this statement.*

Let us consider a partition $P = \{R_0, R_1, \ldots, R_k\}$ of the Cartesian square V^2 such that all graphs R_i are regular (recall that R_0 is the equality relation on V). The partition of V^2 into R_i orbitals coincides with some fusion of partition P. We refer to such P as a *Voronoi graph configuration.*

EXAMPLE. Let (G, V) be a transitive transformation group on V. Then each partition of V^2 into R_i orbitals will be a Voronoi graph configuration.

THEOREM 8. *Consider the groups $B_n(F)$ and $C_n(F)$ defined over an arbitrary field F, in their respective actions on totally isotropic subspaces of equal dimension. Then their Voronoi graph configurations are isomorphic.*

8. Linguistic graphs and some conjectures

We refer to a triple (V, t, I) as an *incidence system*, where V is a set, t is a type function on V which implicitly defines a partition $V = V_1 \cup V_2 \cup \cdots \cup V_n$, and I is an incidence relation (i.e. a symmetric, antireflexive binary relation) on the set V. We refer to n as the rank of the system.

A rank 2 incidence system is called an *incidence structure*, and in such case it is customary to express the partition as $V = P \cup L$ and refer to the elements of P and L as points and lines, respectively. A *flag* is a pair $\{\mathrm{x}, \mathrm{y}\}$ such that $\mathrm{x} I \mathrm{y}$, where either $\mathrm{x} \in P$, $\mathrm{y} \in L$ or $\mathrm{y} \in P$, $\mathrm{x} \in L$.

Let K be a finite commutative ring. We refer to an incidence structure with point set $P = P_{s,m} = K^{s+m}$ and line set $L = L_{r,m} = K^{r+m}$ as a

linguistic incidence structure I_m if the point

$$(\mathrm{x}) = (x_1, x_2, \ldots, x_s, x_{s+1}, x_{s+2}, \ldots, x_{s+m})$$

is incident to the line

$$[\mathrm{y}] = [y_1, y_2, \ldots, y_r, y_{r+1}, y_{r+2} \ldots, y_{r+m}]$$

if and only if the following relations hold:

$$\begin{aligned}
\xi_1 x_{s+1} + \zeta_1 y_{r+1} &= f_1(x_1, x_2, \ldots, x_s, y_1, y_2, \ldots, y_r) \\
\xi_2 x_{s+2} + \zeta_2 y_{r+2} &= f_2(x_1, x_2, \ldots, x_s, x_{s+1}, y_1, y_2, \ldots, y_r, y_{r+1}) \\
&\ldots \\
\xi_m x_{s+m} + \zeta_m y_{r+m} &= f_m(x_1, x_2, \ldots, x_{s+m-1}, y_1, y_2, \ldots, y_{r+m-1})
\end{aligned}$$

In the above, ξ_j and ζ_j, $j = 1, 2, \ldots, m$, are not zero divisors, and the functions f_j are multivariate polynomials with coefficients from K. Brackets and parenthesis allow us to distinguish points from lines (see [59]).

The colour $\rho(\mathrm{x}) = \rho((\mathrm{x}))$ of a point (x) is defined to be the projection of (x) from a free module onto its initial s coordinates. The colour $\rho(\mathrm{y}) = \rho([\mathrm{y}])$ of a line [y] is defined similarly via projection onto its initial r coordinates. In other words, point $(\mathrm{x}) = (x_1, x_2, \ldots, x_{s+m})$ has colour $\rho(\mathrm{x}) = (x_1, x_2, \ldots, x_s)$ and line $[\mathrm{y}] = [y_1, y_2, \ldots, y_{r+m}]$ has colour $\rho([\mathrm{y}]) = (y_1, y_2, \ldots, y_r)$.

From the definition of linguistic incidence structure, it follows that for each vertex of its incidence graph, there exists a unique neighbour of each chosen colour. More specifically, for each $\mathrm{b} \in K^r$ and $(\mathrm{p}) = (p_1, p_2, \ldots, p_{s+m})$ there is a unique neighbour of the point $[\mathrm{l}] = N_{\mathrm{b}}(\mathrm{p})$ with the colour b. Similarly for each $\mathrm{b} \in K^s$ and $[\mathrm{l}] = [l_1, l_2, \ldots, l_{r+m}]$ there is a unique neighbour of the line $[\mathrm{p}] = N_{\mathrm{b}}([\mathrm{l}])$ with the colour b.

We should also mention that we consider linguistic incidence structures defined by an infinite number of equations.

Let G be a group having a BN-pair, with Borel subgroup B and finite Weyl group W. We consider the action of B on the geometry $\Gamma(G)$. Orbits of this action are known as *large Schubert cells*. Let us consider the union L of two large Schubert cells S_i and S_j from $\Gamma_i(G)$ and $\Gamma_j(G)$, $i \neq j$, and assume that the restriction of incidence relation I to $S_i \cup S_j$ is nonempty. From the properties of BN-pairs, it follows that I is an edge-transitive linguistic graph, and the Borel subgroup acts regularly on its edges.

Let $S_{i,j}(G)$ be the incidence graph of the restricted geometry to the two largest Schubert cells S_i and S_j, i.e. the totality of cosets BgP_i and BgP_j where $g \in W$ is an element with maximal length $l(g)$ (a so-called

Coxeter element). We refer to $S_{i,j}(G)$ as a *Schubert graph.*

CONJECTURE 4. *Let q be an arbitrary odd power. Then the Schubert graphs $S_{i,j}(B_n(q))$ and $S_{i,j}(C_n(q))$ form families of edge-transitive Non-Sunada graphs.*

CONJECTURE 5. *Let F be an arbitrary field, Then the graphs $S_{i,j}(B_n(F))$ and $S_{i,j}(C_n(F))$ are Voronoi-equivalent.*

REMARK. *In the case of a field of odd characteristic or characteristic zero, the graphs $S_{i,j}(B_n(F))$ and $S_{i,j}(C_n(F))$ are nonisomorphic.*

9. Towards K-theory of linguistic configurations

Lingustic graphs with parameters m, s, r may be interpreted in the following way: Let Ω be a set with distinguished subsets A_1 and A_2, such that $|A_1 \cap A_2| = m$. We define a linguistic graph $L(A_1, A_2, \Omega)$ with partition sets K^{A_1} and K^{A_2} and with colour spaces $K^{A_{1,2}}$ and $K^{A_{2,1}}$, where $A_{1,2} = A_1 - (A_1 \cap A_2)$, $A_{2,1} = A_2 - (A_1 \cap A_2)$ such that $\rho(f)$, $f \in K^{A_i}$, is the restriction of f to $A_i - A_1 \cup A_2$. To do this, we may assign $A_1 \cap A_2 = \{1, 2, \ldots, m\}$, $A_1 - A_2 = \{m+1, m+2, \ldots, m+s\}$, $A_2 - A_1 = \{m+s+1, m+s+2, \ldots, m+s+r\}$ and identify (A_1, g), (A_2, h) with the tuples $(g(m+1), g(m+2), \ldots, g(m+s), g(1), g(2), g(m)) = (x_1, x_2, \ldots, x_{s+m}) =$ (x) and $[h(m+s+1), h(m+s+2), \ldots, h(m+s+r), h(1), h(2), \ldots, h(m)] = [y_1, y_2, \ldots, y_{r+m}] =$ [y] respectively. The set Ω may be chosen to be any set that contains $\{1, 2, \ldots, m+s+r\}$.

Let Γ be a simple graph with vertex set $\{1, 2, \ldots, n\}$. Let us assume that there is a set Ω and function η from $V(\Gamma)$ onto 2^{Ω}. For each edge $\{i, j\} \in \Gamma$ the linguistic graph $L_{i,j}$ is given with its $(\eta(i), \eta(j))$ interpretation. We refer to such data as a linguistic configuration with a governing triple (Γ, η, Ω) and linguistic relations $L_{i,j}$, $\{i, j\} \in E(\Gamma)$ over a commutative ring K.

For a fixed linguistic configuration, we define a linguistic blow-up $\widetilde{\Gamma}$ of the governing graph Γ which is a totality of new vertices of the kind (i, x), $x \in K^{\eta}(i)$ such that (i, x) and (j, x) are neighbours in $\widetilde{\Gamma}$ if and only if i, j are neighbours in Γ and x, y are adjacent in the linguistic graph $L_{i,j}$. For each pair (i, j) of ordered neighbouring vertices in a governing graph Γ, we consider $\Delta_{i,j} = \eta(i) - \eta(i) \cap \eta(j)$. We refer to η as a governing map, and we adopt the notation A_i for the set $\eta(i)$. For each set $A \subset \Omega$ we consider the list of all its elements $a_1, a_2, \ldots, a_m$ and the ring $K[A] = K[x_{a_1}, x_{a_2}, \ldots, x_{a_m}] = K[A]$ where x_{a_i} are formal variables.

10. On Coxeter and Lie geometries and corresponding linguistic configurations

Let $\{\alpha, \beta\}$ be a flag of cardinality 2. In the case of general linguistic configurations, $\Delta(\alpha) - \Delta(\alpha) \cap \Delta(\beta)$ will be denoted as $\Delta(\alpha, \beta)$.

Let us consider a class of *Coxeter lingustic configurations* with corresponding incidence graph I of the Coxeter geometry $\Gamma(W)$ and boolean embedding $\Delta : \alpha \to 2^T$. To define a representative from this class, we must choose a commutative ring K, and for each edge of the Coxeter geometry, a linguistic relation $L_{\alpha,\beta}$ together with its $\Delta(\alpha)$, $\Delta(\beta)$, T interpretation. Each blow-up of I corresponding to such a linguistic configuration is an incidence relation of the incidence system such that type of vertex (α, f), where $f \in K^{\Delta(\alpha)}$, is defined simply as $t(\alpha)$ for $\alpha \in \Gamma(W)$. We say that the linguistic configuration $L(\Gamma, \eta, \Omega)(K)$ defined via the choice of linguistic graphs $L_{i,j}$, iIj is bilinear if there is a bilinear product $\times$ on $L = K^\Omega$ and family of functions $l_i : \Omega \to K$, $i \in V(\Gamma)$, such that the incidence relation on each linguistic graph may be written as $x(s)l_j(s) - y(s)l_i(s) = (\mathrm{x} \times \mathrm{y})(s)$, for $x \in L_i$, $y \in L_j$ and $s \in \Delta(i) \cup \Delta(j)$.

REMARK. *We have to choose a linear ordering for each pair (i, j). In the case of a skew-symmetric bilinear product (i.e. $x \times y = -y \times x$), the order on pairs is immaterial. However, in the case of an alternative bilinear product we must speak about alternative bilinear linguistic configurations.*

Functions $\mathrm{e}_r \in K^\Omega$ such that $\mathrm{e}_r(r) = 1$ and $\mathrm{e}_r(r') = 0$ for $r \neq r'$ form a natural basis of the free module K^Ω. We say that a linguistic bilinear configuration is of normal type if there is a symmetric partial function $f(x, y)$ on $\Omega \times \Omega$ which is not defined for (r, r), $r \in \Omega$, such that the bilinear product on $L = K^\Omega$ is given by the rule $e_r \times e'_r = \lambda_{r,r'} e_{f(r,r')}$. Here, $\lambda_{r,r'} \in K$ under the assumption that $e_r \times e'_r = 0$ if (r, r') is not in the domain of f.

11. BN-pairs, their geometries as linguistic configurations

Throughout this section, (G, B, N, S) will denote a Tits system which arises in connection with a Chevalley group G or its generalisations. We write $G = X_l(K)$ to signify that G is a Chevalley group over the field K with associated Dynkin diagram X_l. We are mostly interested in the case when K is finite, and we shall write $X_l(q)$ instead of $X_l(F_q)$ in such case. So, fix a Chevalley group $G = X_l(K)$ with corresponding Weyl group W. As in the previous section, we denote by $\Gamma(W)$ and $\Gamma(G)$ the

corresponding Coxeter and Lie geometries.

PROPOSITION 3. *Let* $\Gamma = \Gamma(X_l(F))$ *be the Lie geometry of a simple Chevalley group over the field* F *of characteristic* $p > 3$ *or* 0. *Then there exists a Coxeter linguistic skew-symmetric bilinear configuration* $L(\Gamma(W), \Delta, T)(F)$ *of normal type such that its blow-up is isomorphic to* Γ.

The above statement shows that many flag-transitive algebraic incidence systems can be constructed in terms of linguistic configurations defined over a field. The proof of the statement is constructive. In fact, it is a by-product of a theorem on the embedding of a Lie Geometry into the Borel subalgebra of its corresponding Lie Algebra (see [17] and further references).

12. On universal geometries of Chevalley groups $X_n(K)$ over commutative rings

Let us consider Γ_W, Δ, T and Cartan function $f(x, y)$. For each pair $\{\alpha, \beta\}$ of incident vertices of Γ_W, we consider functions $d_{\alpha,\beta}$ and $d_{\beta,\alpha}$ mapping $\Delta(\alpha) \cap \Delta(\beta)$ to K^*, and parameters $\lambda(r, s, \alpha, \beta) \in K$ for pairs (r, s) where $r \in \Delta(\alpha)$, $s \in \Delta(\beta)$ for which $f(r, s)$ is well-defined. We consider the bilinear map $[x, y]$ from $L_\alpha \times L_\beta$ into $L_\alpha \cap L_\beta$ such that $[e_r, e_s] = \lambda^{\alpha,\beta}_{r,s} e_{f(r,s)}$ for (r, s) in the domain of f, and $[e_r, e_s] = 0$ for (r, s) outside the domain of f.

We say that $x \in L_\alpha$ and $y \in L_\beta$ are incident provided for $s \in \Delta(\alpha) \cup \Delta(\beta)$ we have $\mathrm{x}(s)d_{\beta,\alpha}(s) - \mathrm{y}(s)d_{\alpha,\beta}(s) = [\mathrm{x}, \mathrm{y}](s)$. We use term *Generalised Coxeter linguistic configuration* (GCLC) for this object. We also speak about *universal* GCLC (UGLCN), wherein for each edge α, β of the Coxeter geometry, there are functions d_α, d_β defined on $\Delta(\alpha) \cap \Delta(\beta)$ with symbolic values $d_\alpha(r) = \mathrm{x}(\alpha_r)$ and $d_\beta(r) = \mathrm{y}(\beta_r)$ (variables with values from K^*) and formal parameters $\lambda^{\alpha,\beta}_{r,s}$ (variables with all possible values from the commutative ring K).

Special cases of GCLC are Cartan-Coxeter linguistic configurations for which W is a finite irreducible Weyl group with Cartan matrix corresponding to one of the root systems A_n, B_n, C_n, D_n, E_6, E_7, E_8, F_4, G_2. To define such a configuration, we have to identify the set T with the set R of positive roots of the corresponding root system, and define $f(x, y)$ such that $f(r, s) = r + s$ if $r + s \in R$ and 0 otherwise. We assume that $\lambda^{\alpha,\beta}_{r,s} \neq 0$ if one of the roots r, s is simple.

Observe that the Universal Cartan-Coxeter linguistic configuration is uniquely determined by the choice of Cartan matrix A and commutative ring K. Let X_n denote one of the above root systems. We use symbol $UCC(X_n, A, K)$ for the universal Coxeter-Cartan linguistic configuration with Cartan matrix A defined over commutative ring K. For investigation of such algebraic objects, we use the universal geometry $UG(X_n(K))$ of the Chevalley group $X_n(K)$ for which the following parameters are taken as variables: $d(\alpha, \beta)(s) \in K^*$, $d(\beta, \alpha)(s) \in K^*$ for $s \in \Delta(\alpha) \cap \Delta(\beta)$, and $\lambda_{r,s}^{\alpha,\beta} \in K$ for $s \in \Delta(\alpha)$, $r \in \Delta(\beta)$. When values from K are prescribed for all these parameters, we speak of a *specialisation* S of the Universal Cartan-Coxeter linguistic configuration $UG_S(X_n, K)$ over K.

Proposition 3 of the previous section shows that in the case of fields, a special choice of S provides a Coxeter-Cartan linguistic configuration V_S whose blow-up is isomorphic to the geometry of the Chevalley group $X_l(F)$. Specialisations of the universal geometry $UG(X_n, K)$ form an interesting class of incidence systems which contain flag-transitive geometries of Chevalley groups when K is a field.

Computer simulation demonstrates that altering the coefficients in the generic equations of linguistic graphs of Coxeter-Cartan configurations usually changes the spectrum of the lnguistic graphs. This means that the majority of pairs of distinct specialisations provide nonisomorphic incidence systems. Representatives of this class of incidence systems share some intriguing properties. For example, from each vertex of a blow-up $\Gamma(X_n, K)$ of $UG_S(X_n, K)$ to elements of the kind $(W_i, 0)$, there is a walk whose length is restricted by a linear function $l(n)$ that does not depend on K or S. Thus the diameter of $\Gamma_S(X_n, K)$ is bounded above by $2l(n)$. In the case of a fixed n and S and family of finite rings $K = K_m$ of increasing order, the graphs $\Gamma_S(X_n, K_m)$, $m \geq 1$, form a family of small world graphs with unbounded degree (see [37] for related geometrically based constructions and further references).

The author expresses his sincere gratitude to Professor Andrew Woldar (Villanova University) for his constant support of the idea to use geometries over diagrams for applied problems and valuable advice on the improvement of this paper.

References

[1] T.Sunada, *Riemannian Coverings and Isospectral Manifolds*, Ann. Math., 121 (1985), 169-186.

[2] R. Brooks, *Non-Sunada graphs*, Annales de Institut Fourier, tome 49, no 2 (1999), p. 707-725.

[3] M. Cvetkovic, M. Doob, I. Gootman, A. Targasev, *Theory of Graph Spectra*, Ann. Disc. Math. 36, North Holland, 1988.
[4] A. E. Brouwer, A. M. Cohen and A. Neumaier, *Distance-regular Graphs*, Springer-Verlag, Berlin, 1989.
[5] J. Hemmeter, *Distance-Regular Graphs and Halved Graphs*, Europ. J. Combinatorics (1986) 7, 119-129.
[6] V. Ustimenko, *On some properties of the geometries of the Chevalley groups and their generalizations*, Investigations in Algebraic Theory of Combinatorial Objects, Kluwer, Dordrecht (1992). p. 112-119.
[7] Edwin R. van Dam, Jack H. Koolen, Hajime Tanaka, *Distance Regular Graphs*, *The Electronic Journal of Combinatorics*, Dynamic Survey, DS22, 2016
[8] C. T. Benson,*Minimal regular graphs of girths eight and twelve*, Canad. J. Math. 26 (1966), 1091-1094.
[9] J.Tits, *Sur la trialite et certains groupes qui sen deduisent*, Inst. Hautes Etudes Sci. Publ. Math. 2 (1959), 13-60.
[10] V. V. ZdanPushkin, V. A. Ustimenko, *On the maximality of certain classical transformation groups*, Voprosi teorii grupp i gomologicheskoi algebry, 1985, pp. 125–139.
[11] V.V. ZdanPushkin, V. A. Ustimenko, *Maximality of finite classical groups acting on the totally isotropic subspaces*, Selecta Mathematica Sovetica, vol. 9, no. 4, 1990, pp. 339–354.
[12] J Dieudonn, *Sur les groupes classiques*, Paris: Hermann, 1948.
[13] V. V. Zhdan-Pushkin, V.A. Ustimenko, *Classical groups and metric association schemes*, Kibernetika, 6, 1986, pp. 83-94.
[14] R. Carter, *Simple group of Lie type*, Wiley, 1989.
[15] F. Buekenhout, ed., *Handbook of incidence geometry*, Amsterdam: 1995.
[16] A, Borovik, I. Gelfand, N. White,*Combinatorial Flag Varieties*, Journal of Combinatorial Theory, Series A, 91, (2000) 111-136.
[17] V. Ustimenko, *On the varieties of parabolic subgroups, their generalisations and combinatorial applications*, Acta Applicandae Mathematicae, 52 , 1998, 223-238.
[18] A. Brouwer, D. Pasechnik, *Two distance-regular graphs*, J. Algebraic Combin., 36 (2012).
[19] A, Pasini, S. Yoshiara, *New distance regular graphs arising from dimensional dual hyperovals*, European J. Combin. 22 (2001), 547-560.
[20] A.E. Brouwer, *Corrections and additions to the book " Distance-regular Graphs"*, http://*www.win.tue.nl/ aeb/drg/BCN − ac.ps.gz* (October 2008).
[21] E. R. van Dam, J, H. Koolen, *A new family of distance-regular graphs with unbounded diameter*, Invent. Math. 162 (2005), 189-193.
[22] T Fujisaki, J. H. Koolen, M. Tagami, *Some properties of the twisted Grassmann graphs*, Innov. Incidence Geom. 3 (2006), 81-86.
[23] S. Bang, T. Fujisaki, J. H. Koolen, *The spectra of the local graphs of the twisted Grassmann graphs*, European J. Combin. 30 (2009), 638-654.
[24] P. Terwilliger, *The subconstituent algebra of an association scheme* , I, J. Algebraic Combin. 1 (1992), 363-388; II, J. Algebraic Combin. 2 (1993), 73-103; III, J. Algebraic Combin. 2 (1993), 177-210.
[25] D. Jungnickel, V. Tonchev, *Polarities, quasi-symmetric designs and Hamada's conjecture*, Des. Codes Cryptogr. 51 (2009), 131-140.

[26] A. Munemasa, V. D. Tonchev, *The twisted Grassmann graph is the block graph of a design*, Innov. Incidence Geom. 12 (2011), 16; arXiv:0906.4509.
[27] A. Munemasa, *Godsil-McKay switching and twisted Grassmann graphs*, preprint (2015); arXiv:1512.09232.
[28] A. E. Brouwer, W. H. Haemers, *Spectra of Graphs*, Springer, New York, 2012.
[29] K. Mehlhorn, *A faster approximation algorithm for the steiner problem in graphs*, Inf. Process. Lett., 1988, 27 (3), 125-128.
[30] M. Erwig, *The graph Voronoi diagram with applications*, Networks, vol. 36 (2000) no. 3, pp. 156–163.
[31] V. Ustimenko, A. Woldar, *A geometric approach to orbital recognition in Chevalley-type coherent configurations and association schemes*, Australas. J. Combin. 67 (2017), no. 2, 166–202.
[32] N. Bourbaki, *Lie Groups and Lie Algebras*, Chapters 1 - 9, Springer, 1998-2008.
[33] E. Bannai, T. Ito, Algebraic Combinatorics. 1984, 449 p.
[34] I. Faradjev M. Klin, M. Muzychuk, *Cellular Rings and Groups of Automor phisms of Graphs*, In Investigations in Algebraic Theory of Combinatorial Objects (editors: Faradzev, I.A., Ivanov, A.A., Klin, M., Woldar, A.J.), Springer, 1994, pp.1-152.
[35] E. Hewitt, K.Ross, *Abstract harmonic analysis, vol.2*, Structure and analysis for compact groups. Analysis on locally compact abelian groups, Springer, 1970, 392 p.
[36] E. Hewitt, K. Ross, *Abstract Harmonic Analysis: Volume 1*, Structure of Topological Groups., Integration Theory, Group Representations, Springer, 1994, 540 p.
[37] V. Ustimenko, Urszula Romańczuk, *Finite geometries, LDPC codes and Cryptography*, Maria Curie-Sklodowska University, Institute of Computer Science, 2012, (on line access www: informatyka.umcs.lublin.pl).
[38] T.Sunada, *Riemannian Coverings and Isospectral Manifolds*, Ann. Math., 121 (1985), 169-186.
[39] R. Brooks, *Non-Sunada graphs*, Annales de Institut Fourier, tome 49, no 2 (1999), p. 707-725.
[40] M. Cvetkovic, M. Doob, I. Gootman, A. Targasev, *Theory of Graph Spectra*, Ann. Disc. Math. 36, North Holland, 1988.
[41] A. E. Brouwer, A. M. Cohen and A. Neumaier, *Distance-regular Graphs*, Springer-Verlag, Berlin, 1989.
[42] J. Hemmeter, *Distance-Regular Graphs and Halved Graphs*, Europ. J. Combinatorics (1986) 7, 119-129.
[43] V. Ustimenko, *On some properties of the geometries of the Chevalley groups and their generalizations*, Investigations in Algebraic Theory of Combinatorial Objects, Kluwer, Dordrecht (1992). p. 112-119.
[44] Edwin R. van Dam, Jack H. Koolen, Hajime Tanaka, *Distance Regular Graphs*, *The Electronic Journal of Combinatorics*, Dynamic Survey, DS22, 2016
[45] C. T. Benson,*Minimal regular graphs of girths eight and twelve*, Canad. J. Math. 26 (1966), 1091-1094.
[46] J.Tits, *Sur la trialite et certains groupes qui sen deduisent*, Inst. Hautes Etudes Sci. Publ. Math. 2 (1959), 13-60.

[47] V. V. Zdan-Pushkin, V. A. Ustimenko, *On the maximality of certain classical transformation groups*, Voprosi teorii grupp i gomologicheskoi algebry, 1985, pp. 125–139.
[48] V.V. Zdan-Pushkin, V. A. Ustimenko, *Maximality of finite classical groups acting on the totally isotropic subspaces*, Selecta Mathematica Sovetica, vol. 9, no. 4, 1990, pp. 339–354.
[49] J Dieudonn, *Sur les groupes classiques*, Paris: Hermann, 1948.
[50] V. V. Zhdan-Pushkin, V.A. Ustimenko, *Classical groups and metric association schemes*, Kibernetika, 6, 1986, pp. 83-94.
[51] R. Carter, *Simple group of Lie type*, Wiley, 1989.
[52] F. Buekenhout, ed., *Handbook of incidence geometry*, Amsterdam: 1995.
[53] A, Borovik, I. Gelfand, N. White,*Combinatorial Flag Varieties*, Journal of Combinatorial Theory, Series A, 91, (2000) 111-136.
[54] V. Ustimenko, *On the varieties of parabolic subgroups, their generalisations and combinatorial applications*, Acta Applicandae Mathematicae, 52 , 1998, 223-238.
[55] A. Brouwer, D. Pasechnik, *Two distance-regular graphs*, J. Algebraic Combin., 36 (2012).
[56] A, Pasini, S. Yoshiara, *New distance regular graphs arising from dimensional dual hyperovals*, European J. Combin. 22 (2001), 547-560.
[57] A.E. Brouwer, *Corrections and additions to the book " Distance-regular Graphs"*, http://*www.win.tue.nl/ aeb/drg/BCN − ac.ps.gz* (October 2008).
[58] E. R. van Dam, J, H. Koolen, *A new family of distance-regular graphs with unbounded diameter*, Invent. Math. 162 (2005), 189-193.
[59] T Fujisaki, J. H. Koolen, M. Tagami, *Some properties of the twisted Grassmann graphs*, Innov. Incidence Geom. 3 (2006), 81-86.
[60] S. Bang, T. Fujisaki, J. H. Koolen, *The spectra of the local graphs of the twisted Grassmann graphs*, European J. Combin. 30 (2009), 638-654.
[61] P. Terwilliger, { The subconstituent algebra of an association scheme , I, J. Algebraic Combin. 1 (1992), 363-388; II, J. Algebraic Combin. 2 (1993), 73-103; III, J. Algebraic Combin. 2 (1993), 177-210.
[62] D. Jungnickel, V. Tonchev, *Polarities, quasi-symmetric designs and Hamada's conjecture*, Des. Codes Cryptogr. 51 (2009), 131-140.
[63] A. Munemasa, V. D. Tonchev, *The twisted Grassmann graph is the block graph of a design*, Innov. Incidence Geom. 12 (2011), 16; arXiv:0906.4509.
[64] A. Munemasa, *Godsil-McKay switching and twisted Grassmann graphs*, preprint (2015); arXiv:1512.09232.
[65] A. E. Brouwer, W. H. Haemers, *Spectra of Graphs*, Springer, New York, 2012.
[66] K. Mehlhorn, *A faster approximation algorithm for the steiner problem in graphs*, Inf. Process. Lett., 1988, 27 (3), 125-128.
[67] M. Erwig, *The graph Voronoi diagram with applications*, Networks, vol. 36 (2000) no. 3, pp. 156–163.
[68] V. Ustimenko, A. Woldar, *A geometric approach to orbital recognition in Chevalley-type coherent configurations and association schemes*, Australas. J. Combin. 67 (2017), no. 2, 166–202.
[69] N. Bourbaki, *Lie Groups and Lie Algebras*, Chapters 1–9, Springer, 1998–2008.
[70] E. Bannai, T. Ito, Algebraic Combinatorics. 1984, 449 p.

[71] I. Faradjev M. Klin, M. Muzychuk, *Cellular Rings and Groups of Automor phisms of Graphs*, In Investigations in Algebraic Theory of Combinatorial Object (editors: Faradzev, I.A., Ivanov, A.A., Klin, M., Woldar, A.J.), Springer, 1994, pp.1-152.

[72] E. Hewitt, K.Ross, *Abstract harmonic analysis, vol.2*, Structure and analysis for compact groups. Analysis on locally compact abelian groups, Springer, 1970, 392 p.

[73] Hewitt, K. Ross, *Abstract Harmonic Analysis: Volume 1*, Structure of Topological Groups., Integration Theory, Group Representations, Springer, 1994, 540 p.

[74] V, Ustimenko, Urszula Romanczuk, *Finite geometries, LDPC codes and Cryptography*, Maria Curie-Sklodowska University, Institute of Computer Science, 2012, (on line access www: informatyka.umcs.lublin.pl).

Institute of Mathematics, Maria Curie-Skłdowska University, Poland, and, Institute of Telecommunications and Global Information Space, NAS of Ukraine, Poland
Email: vasyl(at)hektor(dot)umcs(dot)lublin(dot)pl
URL: https://www.umcs.pl/

Voronoï's Impact on Modern Science, Book 6, Volume 2
Proceedings of the Sixth International Conference on Analytic Number Theory and Spatial Tessellations

VORONOI CONGRUENCES FOR BERNOULLI NUMBERS, LEOPOLDT'S ZETA FUNCTIONS AND ITS GENERALIZATIONS

Nikolaj Glazunov (*Ukraine*)

Abstract. The article is dedicated to the memory of George Voronoi. We review the results on (p-adic) zeta functions, (p-adic) L-functions, cyclotomic (p-adic) (multiple) zeta values, as well as mathematical structures related to them. Numerical examples are included.

Introduction

The present article is concerned with (p-adic) L-functions [in particular, (p-adic) zeta functions], cyclotomic (p-adic) (multiple) zeta values and includes the introduction to classical Leopoldt's zeta and L-functions. The beginning of the article contains a short summary of the results on the Bernoulli numbers associated with the studies of George Voronoi [1]. The results on multiple zeta values were obtained by D. Zagier [2], P. Deligne and A.Goncharov [4], A. Goncharov [5], F. Brown [6], C. Glanois [7], and others. A Tannakian interpretation of p-adic multiple zeta values was given by H. Furusho [9]. The short history and connections among Galois groups, fundamental groups, motives ,and arithmetic functions were presented in the talk by Y. Ihara [11]. The results on multiple zeta values, Galois groups, and geometry of modular varieties were presented by Goncharov [5]. The interesting unipotent motivic fundamental group was defined and investigated by Deligne and Goncharov [4]. S. Ünver [8, 10] investigated p-adic multiple zeta values in the depth two. The framework of (p-adic) L-functions and (p-adic) (multiple) zeta values is based on the Kubota–Leopoldt p-adic L-functions [16] and arithmetic p-adic L-functions by Iwasawa [18]. Motives and (p-adic) (multiple) zeta

Received March 31, 2019.

2010 *Mathematics Subject Classification.* Primary 14G20; Secondary 14G22, 11M32, 14C15.

Key words and phrases. p-adic interpolation; (p-adic) L-function; Eisenstein series; comparison isomorphism; crystalline Frobenius morphism; de Rham fundamental group; (p-adic) multiple zeta value; Iwasawa theory; Shimura variety; arithmetic cycles.

values, improper intersections of Kudla–Rapoport divisors and Eisenstein series were reviewed by Sankaran [42]. More fully, the content of the article can be found at the following table: Introduction. 1. Voronoi-type congruences for Bernoulli numbers. 2. Riemann zeta values. 3. On the class group of rings within the divisor theory. Imaginary quadratic and cyclotomic fields. 4. Eisenstein series. 5. Class group, class fields, and zeta functions. 6. Elements of non-Archimedean local fields and $p-$adic analysis. 7. $p-$adic interpolation of zeta and L-functions. 8. Formal groups and p-divisible groups. 9. Motives and (p-adic) (multiple) zeta values. 10. On the Eisenstein series associated with Shimura varieties. Sections 1-7 and subsection 10.1 (On some Shimura varieties and Siegel modular forms) can be considered as an elementary introduction to the results of Section 9 and Subsection 10.2 (On the improper intersections of Kudla–Rapoport divisors and Eisenstein series). Numerical examples are included.

I am grateful to J. Steuding for some helpful remarks and comments.

The subject matter of this review has deep historical roots, with contributions of many mathematiciens. I apologize for any oversights and any misrepresentations, which are not intentional, but rather due to my ignorance.

1. Voronoi-type congruences for Bernoulli numbers and generalizations

We follow [22, 1].

1.1. **Bernoulli numbers.** Bernoulli numbers B_m are determined for integers $m \geq 0$ by the expansion

$$\frac{t}{\exp(t)-1} = 1 + \sum_{m=1}^{\infty} \frac{B_m}{m!} t^m.$$

Remark 1. For $m > 0, B_{2m+1} = 0$.

$B_0 = 1, B_1 = -\frac{1}{2}, B_2 = \frac{1}{6}, B_4 = -\frac{1}{30}, B_6 = \frac{1}{42}, \ldots$
]smallskip

1.2. **Voronoi's congruences.** Let N be a natural number (the modulus), let a be coprime with N, and let $B_{2m} = \frac{P_{2m}}{Q_{2m}}$ be the Bernoulli number with coprimes P_{2m} and Q_{2m}. Then

$$(a^{2m}-1)P_{2m} \equiv 2ma^{2m-1}Q_{2m} \sum_{s=1}^{N-1} s^{2m-1} \left[\frac{sa}{N}\right] \bmod N.$$

1.3. **Kummer congruences.** If p is prime, and if $p-1$ does not divide even positive m, then the number $\frac{B_m}{m}$ is p-integer, and there is the congruence

$$\frac{B_{m+p-1}}{m+p-1} \equiv \frac{B_m}{m} \bmod p.$$

1.4. **Generalized Bernoulli numbers.** Let m be a natural number. Let χ be a primitive numerical character (Dirichlet character) modulo m. Generalized Bernoulli numbers $B_{n,\chi}$ are defined for integers $m > 0$ and a primitive Dirichlet character modulo m by the expansion

$$\sum_{a=1}^{m} \frac{\chi(a) t \exp(at)}{\exp(mt)-1} = 1 + \sum_{n=1}^{\infty} \frac{B_{n,\chi}}{n!} t^n,\ 0 \le |t| \le \frac{2\pi}{m}. \tag{1}$$

Remark 2. All the generalized Bernoulli numbers associated with the numerical character χ are contained in the extension of the field of rational numbers $\mathbb{Q}$ obtained by joining all the values of the character χ to $\mathbb{Q}$.

2. Riemann zeta, L-functions, and some their values

Here, we follow [19, 20, 21, 22].

Let $s = \sigma + it$ be a complex number, and let $\zeta(s)$ be the Riemann zeta function which is presented for $\sigma > 1$ by the series

$$\zeta(s) = \sum_{n=1}^{\infty} \frac{1}{n^s}.$$

By Euler, for $m \ge 1$, $\zeta(2m) = (-1)^{m-1} \frac{(2\pi)^{2m}}{2(2m)!} B_{2m}$, where B_{2m} are Bernoulli numbers. We recall that

$$\zeta(-n) = -\frac{B_{n+1}}{n+1}$$

for odd $n = 1, 3, 5, \ldots$, and $\zeta(1-2m) = -\frac{B_{2m}}{2m}$, if $m > 0$.

Example 1. In particular,

$$\zeta(2) = \frac{\pi^2}{6}.\ \zeta(4) = \frac{\pi^4}{90},\ \zeta(6) = \frac{\pi^6}{3^3 5 \cdot 7},$$

$$\zeta(-1) = -\frac{B_2}{2} = -\frac{1}{12}, \zeta(-3) = \frac{1}{120}.$$

Define a polylogarithm

$$L_m(z) = \sum_{n=1}^{\infty} z^n n^{-m};$$

Example 2.

$$\zeta(2) = L_2(1).$$

Remark. In 1970-1971, Yu. Manin gave courses of lectures and seminars on Algebraic Geometry and Diophantine Geometry at Moscow State University and Steklov Mathematical Institute. In his lectures and talks, Yu. Manin presented and discussed the Birch–Swinnerton–Dyer conjecture concerning the $L-$ functions of elliptic curves and Abelian varieties. In particular, Yu. Manin have proposed the modular symbols for the computation of values of the $L-$functions of elliptic curves at $s = 1$ [23, 24]. I attended the lectures and seminars of Yu. Manin. Following the kind conversation with Yu. Manin, I implemented the computer program and computed Manin's modular symbols [44] for the elliptic curve $E_{\Gamma_0(11)}$ following the Manin article [23]. It was one of the motivations of my interest in the subject of values of the zeta and $L-$functions.

3. On the class groups of rings with the divisor theory of imaginary quadratic and cyclotomic fields

The study of the class groups of rings and corresponding schemes is an actual scientific problem (see [22, 25] and references therein). For regular local rings, according to the Auslander–Buchsbaum theorem, the (divisors) class group is trivial. But the group is nontrivial in most interesting cases. The Heegner approach, together with the results of Weber, Birch, Baker and Stark, makes it possible to calculate and even to parametrize rings with a given (small) class number in some cases. Let R be a commutative ring with identity for which there exists the theory of divisors [22]. The order of the class group is calculated on the basis of the use of L-functions. We investigate one of the aspects of this problem, consisting in finding the moduli spaces of elliptic curves defined over the rings R with the given class number.

Problem. To investigate the case of elliptic curves over the rings of integers of quadratic fields (rings of integers $\mathcal{O}$ of quadratic algebraic extensions k of the field of rational numbers $\mathbb{Q}$) with a small class number, see [22].

In some cases, for instance under computer algebra computations, we have to enumerate investigated objects. Some simple parametric spaces and moduli spaces in the case of imaginary quadratic fields are presented below [45]. We present an elementary introduction to this problem and give the moduli spaces as trivial bundles over the affine part of the groups of rational points of some elliptic curves over the ring of integers $\mathbb{Z}$.

Below, we present parameter spaces and moduli for class number one and two. Let

$$E : y^2 = x^3 + ax + b,\ Disc(E) = 4a^3 + 27b^2, Disc(E) \neq 0, \quad (*)$$

be an elliptic curve over the ring $\mathcal{O}$. Let A_1 be the affine part of the group of rational points over $\mathbb{Z}$ of the Heegner elliptic curve $y^2 = 2x(x^3 + 1)$. With results by Heegner, Deuring, Birch, Baker, Stark, Kenku, and Abrashkin, we deduce

Proposition 1. *Let $\mathcal{O}$ be the ring of integers of the imaginary quadratic field with class number one. Then the parameter space of elliptic curves of the form (*) is the trivial bundle*

$$(\mathcal{O} \times \mathcal{O}/(Disc(E) = 0)) \times A_1.$$

Proposition 2. *Let k be the imaginary quadratic field with class number one. Then the moduli space of elliptic curves of the form (*) is the trivial bundle*

$$k \times A_1.$$

Let A_2 be the affine part of the group of rational points over $\mathbb{Z}$ of the elliptic curve $X^3 + 3 = -Y^2$, let A_3 be the affine part of the group for the elliptic curve $X^3 - 3 = 2Y^2$, and A_4, respectively, for $9X^4 - 1 = 2Y^2$.

Proposition 3. *Let $\mathcal{O}$ be the ring of integers of the imaginary quadratic field with class number two. Then the parameter spaces of elliptic curves of the form (*), without an exceptional case, are trivial bundles*

$$(\mathcal{O} \times \mathcal{O}/(Disc(E) = 0)) \times A_2,\ (\mathcal{O} \times \mathcal{O}/(Disc(E) = 0)) \times A_3,$$
$$(\mathcal{O} \times \mathcal{O}/(Disc(E) = 0)) \times A_4.$$

Proposition 4. *Let k be the imaginary quadratic field with class number two. Then the moduli spaces of elliptic curves of the form (*), without an exceptional case, are the trivial bundles*

$$k \times A_2,\ k \times A_3,\ k \times A_4.$$

Theorem 1. *(The Kronecker–Weber theorem) Every finite Abelian extension of $\mathbb{Q}$ is contained in a cyclotomic field.*

With the results by Heegner, Deuring, Birch, Baker, Stark, and Shafarevich, we have

Proposition 5. *Imaginary quadratic fields with class number one and with descriminants $-D = 4, 8, 3, 7, 11, 19, 43, 67, 163$ are contained, respectively, in cyclotomic fields*

$$\begin{gathered}\mathbb{Q}(\sqrt[4]{1}), \mathbb{Q}(\sqrt[8]{1}), \mathbb{Q}(\sqrt[3]{1}), \mathbb{Q}(\sqrt[7]{1}), \mathbb{Q}(\sqrt[11]{1}),\\ \mathbb{Q}(\sqrt[19]{1}), \mathbb{Q}(\sqrt[43]{1}), \mathbb{Q}(\sqrt[67]{1}), \mathbb{Q}(\sqrt[163]{1}).\end{gathered} \quad (2)$$

4. Eisenstein series

Here, we follow [19, 20, 21, 22].

Let τ belong to the modular figure of the modular group $\Gamma = \Gamma(1)$.

Definition 1. In these notations with $k > 1$, the Eisenstein series are defined as

$$c_k = \sum_{m \neq 0, k>1} \frac{1}{(n + m\tau)^{2k}}.$$

Proposition 6. *The Eisenstein series have the representation*

$$c_k = 2\zeta(2k) + \frac{2(-2\pi i)^{2k}}{(2k-1)!} \sum_{n>0, m>0} n^{2k-1} q^{nm},$$

where $q = e^{2\pi i \tau} \neq 0$.

If we will use functions of the sums of divisors σ_{2k-1}, *we obtain*

$c_k = 2\zeta(2k) + \frac{2(-2\pi i)^{2k}}{(2k-1)!} \sum_{n=1}^{\infty} \sigma_{2k-1}(n) q^n$

or, shortly,

$c_k = 2\zeta(2k) + \frac{2(-2\pi i)^{2k}}{(2k-1)!} S_{2k-1}$.

As $\zeta(2k) = (-1)^{k-1} \frac{(2\pi)^{2k}}{2(2k)!} B_{2k}$, we have

Corollary 1. $c_k = 2\zeta(2k)(1 - \frac{4k}{B_{2k}} \sum_{n=1}^{\infty} \sigma_{2k-1}(n) q^n)$.

Put $g_2 = 60c_2$, $g_3 = 140c_3$.

Proposition 7. $\Delta = g_2^3 - 27g_3^2 \neq 0$.

As $\Delta \neq 0$, it is possible to define $J = \frac{g_2^3}{\Delta}$.

Definition 2. The modular invariant of the elliptic curve $y^2 = 4x^3 - g_2 x - g_3$ is equal to $j = 2^6 3^3 J$.

Proposition 8. $j = \frac{1}{q} + u_1 q + \cdots$, *where* u_i *are integers,* $u_0 = 0$.

Let us transform c_k in such a way that the corresponding Fourier coefficients under $q^n, n \geq 1$, will be rational numbers. Dividing c_k by $2\zeta(2k)$ and denoting the obtained result as E_k, we have, by Corollary 1,

Proposition 9. $E_k = 1 - \frac{4k}{B_{2k}} \sum_{n=1}^{\infty} \sigma_{2k-1}(n) q^n$.

Example 3.

$$E_2 = 1 + 240 \sum_{n=1}^{\infty} \sigma_3(n) q^n,$$

$$E_3 = 1 - 504 \sum_{n=1}^{\infty} \sigma_5(n) q^n.$$

5. Class group, class fields, and zeta functions

Here, we follow [20, 22].

Let K be an imaginary quadratic field, and let Cl_K be its class group.

Definition 3. Let $N(\mathfrak{a})$ be the norm of the ideal $\mathfrak{a}$. The Dedekind ζ-function for K is defined for all $s > 1$ by the series

$$\zeta_K(s) = \sum \frac{1}{N(\mathfrak{a})^s},$$

where the sum is taken over all nonzero ideals $\mathfrak{a} \in \mathcal{O}_K$.

Let R be a subring ($R \neq \mathbf{Z}$) of the ring of integers $\mathcal{O}_K$ of the imaginary quadratic field K.

Let $M_1, \dots M_h$ be pairwise nonequivalent modules of K with the same ring of multipliers R.

Proposition 10. *$j(M_1), \dots, j(M_h)$ are integer algebraic numbers which are conjugate over K.*

Proposition 11. *The field $K(j(M_i))/K$ is the normal field.*

Definition 4. The field $K(j(M_i))/K$ is called the ring class field.

Following [20], it is possible to define a ray class field. As in an imaginary quadratic field there is no real infinite primes so modulus of the field is an ideal of the ring of integers of the field.

Let $\mathfrak{m}$ be a modulus of the an imaginary quadratic field K, let $Cl_K^{\mathfrak{m}}$ be the ray class group, let τ_W be a Weber function .

Let $\mathfrak{R} \in Cl_K$, and let $\mathfrak{R}^* \in Cl_K^{\mathfrak{m}}$ be the ideal class whose image in Cl_K is equal to $(\mathfrak{m})\mathfrak{R}^{-1}$.

Proposition 12. *The field $K(j(\mathfrak{R}), \tau_W(\mathfrak{R}^*))/K$ is the ray class field.*

Let C be an ideal class.

Definition 5. The ideal class zeta function is the expression

$$\zeta_C(s) = \sum_{\substack{\mathfrak{a} \in C \\ \mathfrak{a} \text{ integral}}} \frac{1}{N(\mathfrak{a})^s}, \ s = \sigma + it, \ \sigma > 1.$$

Below, we present values of the zeta and L-functions connecting with imaginary quadratic fields. Let d be a squarefree integer number, $K = \mathbb{Q}(\sqrt{d})$ a quadratic field, χ be the character of the quadratic field K. Let $L(s, \chi)$ be the $L-$series with a nonunit character χ modulo $|D|$. Here, D is the discriminant of the field K.

Proposition 13.

$$\zeta_K(s) = \zeta(s)L(s,\chi) = \zeta(s)\prod_p(1-\frac{\chi(p)}{p^s}).$$

Let m be the number of roots of unity of the imaginary quadratic field $[K:\mathbb{Q}]$.

Remark 3. $m = 4$ for $K = \mathbb{Q}(\sqrt{-1})$, $m = 6$ for $K = \mathbb{Q}(\sqrt{-3})$, $m = 2$ for all other imaginary quadratic fields.

Let h be the class number of the field K.

Proposition 14.

$$L(1,\chi) = \frac{2\pi h}{m\sqrt{|D|}}.$$

Corollary 2. *For imaginary quadratic fields with class number one ($h = 1$), we have*

$$L(1,\chi) = \begin{cases} \frac{\pi}{4}, K = \mathbb{Q}(\sqrt{-1}) \\ \frac{\pi}{3\sqrt{3}}, K = \mathbb{Q}(\sqrt{-3}) \\ \frac{\pi}{\sqrt{|D|}}, -D = 8,7,11,19,43,67,163. \end{cases}$$

6. Elements of non-Archimedean local fields and $p-$adic analysis

Here we present elements of $p-$adic local fields, their algebraic extensions, and $p-$adic interval analysis. We follow [22, 26].

6.1. **Elements of non-Archimedean local fields.** A non-Archimedean local field is a complete discrete valuation field with finite residue field. Further, for brevity, we call these fields local. In other words, a field K is called local, if it is complete in a topology determined by the valuation of the field, and if its residue field k is finite. We assume further that the valuation ν is normalized, i.e. the homomorphism of the multiplicative group of the field to the additive group of rational integers $\nu : K^* \to \mathbb{Z}$ is surjective.

The structure of such fields is known: if the field K has the characteristic zero, then it is a finite extension of the $p-$adic field $\mathbb{Q}_p$, which is the completion of the field of rational numbers with respect to the $p-$adic valuation.

If $[K:\mathbb{Q}_p] = n$, then $n = ef$, where f is the degree of classes of residues (i.e. $f = [k:\mathbb{F}_p]$), and $e = \nu_K(p)$ is the ramification index of K..

If the field K has the characteristic p, then it is isomorphic to the field $k((T))$ of formal power series, where T is a uniformizing parameter.

Let L be a finite extension of a local field K with their residue fields l and k, $p = char\ k$, and let $e_{L/K}$ be the ramification index of L over K.

An extension L/K is called unramified, if a) $e_{L/K} = 1$; b) the extension l/k is separable. An extension L/K is called tamely ramified, if a) p does not divide $e_{L/K}$; b) the extension l/k is separable.

An extension L/K is called wildly ramified, if $e_{L/K} = p^s,\ s \geq 1$.

Denote, by $Tr_{L/K}$ and by $Norm_{L/K}$, respectively, the trace and the norm of the extension L/K. We drop indices, when it is clear what kind of extension we are talking about.

Denote, by K_{nr}, the maximal unramified extension of the field K (in a fixed algebraic closure of the field K) with a residue field k_s which is the algebraic closure of a field k.

In a non-Archimedean local field K, each of its elements α has a representation $\alpha = \epsilon\pi^m$, where ϵ is a unit of the ring of integers of the field K, and π its uniformizing element, i.e. $\nu(\pi) = 1$, and m is an integer rational number. A unit is called principal if $\epsilon \equiv 1 \pmod{\pi}$.

Lemma 1. *(This result was reported to the author by O.N. Vvedenskii) If the local field contains a primitive $p-$th root ξ_p of unity, then $\nu(\xi_p - 1) = \frac{e}{p-1}$ is an integer number.*

Proof. The p-root ξ_p is the root of the equation

$$x^{p-1} + x^{p-2} + \cdots + x + 1 = 0.$$

Therefore, $\xi_p - 1$ is the root of the equation

$$(x+1)^{p-1} + (x+1)^{p-2} + \cdots + (x+1) + 1 = x^{p-1} + p(\cdots) + p.$$

The value of the $p-$adic valuation at the root of this equation is $\frac{e}{p-1} = e_1$, which proves the required. □

A complete discrete valuation field with an algebraically closed residue field is called a quasilocal field.

Corollary 3. *Let K be the quasilocal field with a residue field of characteristics p. Then the divisibility $e \neq \infty$ by $p-1$ equivalent to the existence in K of the primitive $p-$th root ξ_p of unity.*

6.2. **$p-$adic intervals and $p-$adic distributions.** Let X be a topological space. A distribution on X with values in an Abelian group A is a finitely additive function from the compact-open subsets of X to A. Let $|\ |_p$ be a $p-$adic norm.

Define $[\alpha, N]_p = \{x \in \mathbb{Q}_p || x - \alpha|_p \leq \frac{1}{p^N}\}$, $\alpha \in \mathbb{Q}_p, N \in \mathbb{N}$.

Definition 6. We call sets $[\alpha, N]_p$ the $p-$adic intervals (disks) and define, by these $p-$adic intervals, the basis of open sets on $\mathbb{Q}_p$.

It is easy to test that the axioms of open sets are satisfied.

Remark 4. $p-$adic intervals $[\alpha, N]_p$ are open and closed simultaneously.

Proof. Any union of open $p-$adic intervals is open. Intervals $[\alpha, N]_p$ are closed, because $[\alpha, N]_p$ is an addition to the union of open intervals $[\alpha', N]_p$ for all $\alpha' \in \mathbb{Q}_p$ for which $\alpha' \neg \in [\alpha, N]_p$. $\square$

Further, we call $[\alpha, N]_p$ as intervals. More generally, we will consider compact-open sets. Let X be a compact-open set. Recall that a function $f : X \to \mathbb{Q}_p$ is locally constant, iff f has a representation as a finite linear combination of characteristic functions of compact-open subsets.

Let $U = U_1 \cup U_2 \cup \cdots \cup U_n$ be a partition of $U \subset X$. Recall that the additive mapping μ of a set of compact-open subsets of X with value in $\mathbb{Q}_p$ is called the $p-$adic distribution on X:

$$\mu(U) = \mu(U_1) + \mu(U_2) + \cdots + \mu(U_n).$$

6.2.1. *Bernoulli distributions.* Let $B_m(x)$ be the $m-$Bernoulli polynomial. These polynomials are defined by the decomposition

$$\frac{te^{xt}}{e^t - 1} = \sum_{m=0}^{\infty} B_m(x)\frac{t^m}{m!}.$$

We have: $B_0(x) = 1,\ B_1(x) = x - \frac{1}{2},\ B_2(x) = x^2 - x + \frac{1}{6},\ B_3(x) = x^3 - \frac{3}{2}x^2 + \frac{1}{2}x,\ B_4(x) = x^4 - 2x^3 + x^2 - \frac{1}{30}, \ldots$

Remark 5. If we substitute $x = 0$ in the $m-$Bernoulli polynomial, we obtain $m-$Bernoulli numbers:

$$B_0(0) = 1,\ B_1(0) = -\frac{1}{2},\ B_2(0) = \frac{1}{6},\ B_3(0) = 0,\ B_4(0) = -\frac{1}{30}, \ldots$$

Let now the inequality $0 \leq \alpha \leq p^N - 1$ is satisfied for α. Define the function $\mu_{B,m}$ by the formula

$$\mu_{B,m}([\alpha, N]_p) = p^{N(m-1)}B_m(\alpha/p^N).$$

Proposition 15. *The function $\mu_{B,m}$ is expanded to the distribution on $\mathbb{Z}_p$. This distribution for the given m is called the $m-$th Bernoulli distribution.*

7. $p-$adic interpolation of zeta and L-functions

Here, we follow [12, 13, 14, 16, 17, 18, 22], but consider Leopoldt's zeta functions and Leopoldt's L-functions only.

7.1. **Leopoldt's zeta functions.** Recall that, for natural $n > 0$ and for Bernoulli numbers in pair notation,

$$\zeta(1-n) = -\frac{B_n}{n}.$$

Recall the generalization of the Kummer congruences. Let p be a prime number.

Lemma 2. *Let m, n be a pair of natural numbers such that p does not divide m, p does not divide n, and $m \equiv n \bmod (p-1)p^N$. Then*

$$(1-p^{m-1})\frac{B_m}{m} \equiv (1-p^{n-1})\frac{B_n}{n} \bmod p^{N+1}.$$

Let $p \geq 3$ be a prime number, and let P_p be the set of pairs of natural numbers $0, 2, \ldots, p-3$. For a given $P_p = \{0, 2, \ldots, p-3\}$ and $a \in P_p$, we denote, by C_a^p, the set of natural numbers m such that $m \equiv a \bmod (p-1)$.

Lemma 3. *Each C_a^p is dense in the set of $p-$adic integer numbers $\mathbb{Z}_p$.*

By Leopoldt and others, this gives possibility to expand the function

$$-(1-p^{m-1})\zeta(1-m)$$

on the ring of $p-$adic integer numbers.

Indeed, it is possible to expand the function $-(1-p^{-s})\zeta(s)$ which is defined at points $1-m, m \in C_a^p$ on all rings $\mathbb{Z}_p$. Denote these functions by $\zeta_{p,a}(s),\ s \in \mathbb{Z}_p$. We will call this expansion the $p-$adic continuation.

Proposition 16. *Let $-(1-p^{-s})\zeta(s)$ be zeta with the Euler multiplier $(1-p^{-s})$. There are $\frac{p-1}{2}$ $p-$adic continuations $\zeta_{p,a}(s)$ of the function $-(1-p^{-s})\zeta(s)$. For $a = 2, \ldots, p-3$, these continuations are $p-$adic analytic functions. For $a = 0$, this continuation $\zeta_{p,0}(s)$ is a $p-$adic meromorphic function with a single pole of the 1st order at the point $s = 1$.*

7.2. **Leopoldt's L-functions.** Let χ be the numerical character modulo $m > 1$, and let $n \geq 1$ be a natural number. Then

$$L(1-n, \chi) = -\frac{B_{n,\chi}}{n},$$

where L is the Dirichlet $L-$function, and $B_{n,\chi}$ are the generalized Bernoulli numbers (1). If we will use the Bernoulli polynomial $B_n(x)$, then

$$B_{n,\chi} = m^{n-1}\sum_{r=1}^{m}\chi(r)B_n(\frac{r}{m}).$$

Remark 6. For any integer rational c, $(c,p)=1$, the sequence $\{c^{n^p}\}$ converges in the field $\mathbb{Q}_p$. Let $\gamma=\lim_{n\to\infty}c^{n^p}$. Then $\gamma\equiv c \bmod (p)$, $\gamma^{p-1}=1$.

Proposition 17. *For any primitive numerical character χ and any prime p, there exists a $p-$adic function $L_p(1-n,\chi)$ defined at integer $p-$adic numbers s (with the exception for $s=1$ in the case of unit character $\chi=1$) with the property*

$$L_p(1-n,\chi)=-(1-\chi(p)\gamma^{-n}(p)\cdot p^{n-1})\frac{B_{n,\chi\gamma^{-n}}}{n},\ n\geq 1.$$

For the odd character χ, the function $L_p(1-n,\chi)$ is identically equal to zero.

8. Formal groups and p-divisible groups

Recall some definitions. Let K be a complete discrete variation field with the ring of integers O_K and the maximal ideal M_K. A complete discrete variation field with finite residue field is called a *local* field [29]. A complete discrete variation field K with algebraically closed residue field k is called a *quasilocal* field [31]. Below, we will suppose that the characteristic of k satisfies $p>0$. Let K be a local or quasilocal field. If K is a local field [29] and has the characteristic 0, then it is a finite extension of the field of p-adic numbers $\mathbb{Q}_p$. Let ν_K be the normalized exponential valuation of K. If $[K:\mathbb{Q}_p]=n$, then $n=e\cdot f$, where $e=\nu_K(p)$ and $f=[k:\mathbb{F}_p]$, where k is the residue field of K (always assumed perfect). If K has the characteristic $p>0$, then it isomorphic to the field $k((T))$ of formal power series, where T is a uniformizing parameter. Let L be a finite extension of a local field K, k,l their residue fields, $p=char\ k$, and $e_{L/K}$ ramification index of L over K. An extension L/K is said to be *unramified*, if $e_{L/K}=1$, and thr extension l/k is separable. An extension L/K is said to be *tamely ramified*, if p does not divide $e_{L/K}$, and the residue extension l/k is separable. An extension L/K is said to be *totally ramified*, if $e_{L/K}=[L:K]=(char\ k)^s, s\geq 1$.

Let L/K be the finite Galois extension of a quasilocal field K with Galois group G, $F(x,y)$ one-dimensional formal group low over the ring of integers O_K of the field K, $F(M_K)$ be the G-module, that is defined by the group low $F(x,y)$ on the maxilal ideal M_K of the ring O_K, and $M_K^t(t\in\mathbb{Z},t\geq 1)$, be the subgroup of t-th degrees of elements from $M_K, F_K^t:=F(M_K^t)$.

Definition 7. For $n \in \mathbb{Z}$, the function $\mu(n)$, $N_{L/K}(F_L^n) \subset F_K^{\mu(n)}$ is defined by the condition: $F_K^{\mu(n)}$ is the least of the subgroups F_K^t $(t = 1, 2, \ldots)$ containing $N_{L/K}(F_L^n)$.

Remark 7. Please do not confuse with the measure μ.

Below, we suppose that $char\ k > 3$.

8.1. **Norm Maps.** Here, we use the results on formal groups from [32, 30]. Let $F_L = F(M_L)$ be the G-module that is defined by the n-dimentional group low $F(x, y)$ on the product $(M_L)^n := M_L \times \cdots \times M_L$, ($n$ times) of maximal ideals of the ring O_L of any finite Galois extension L of the field K.

Definition 8. The norm map $N : F_L \to F_K$ of the module F_L to F_K is defined by the formula $N(a) = (((a +_F \sigma a) +_F \cdots) +_F \sigma_s a)$, where $a +_F b$ denotes the addition of points in the sense of group structure of the module F_L, $a, b \in M_L$, $G = Gal(L/K)$, $\sigma_s \in G$, $[G : 1] = s$.

Let $p := char\ k$, $e := \nu_K(p)$, ($e = +\infty$, if the characteristic of the field K is equal to p, and e is a positive integer in the opposide case), L/K be the Galois extension of the prime degree q, and $F(x, y)$ be the one-dimensional group low over O_K. Let $p := char\ k > 0$.

Lemma 4. *If* $\Pi_s \in \pi_L^s \cdot O_L$, $s \geq 1$, *then*
$N(\Pi_s) \equiv Tr(\Pi_s) + \sum_{n=1}^{\infty} c_n [Norm\ \Pi_s]^n (mod\ Tr(\pi_L^{2s} \cdot O_L))$,
where $c_n \in O_K$ *are coefficients of the p-iteration of the group low.*

Let R be a commutative ring. Let A, B, C be finite group schemes over R. The sequence

$$0 \longrightarrow A \xrightarrow{f} B \xrightarrow{g} C$$

is called exact, if $Im\ f = Ker\ g$.

Let p be a prime number, and let h be an integer, $h \geq 0$.

Recall the definition of the p-divisible group by J. Tate.

Definition 9. A p-divisible group over R of height h is an inductive system

$$G = (G_\nu, i_\nu), \nu \geq 0,$$

where
(i) G_ν is a finite group scheme over R of order $p^{\nu h}$,
(ii) for each $\nu \geq 0$,

$$0 \longrightarrow G_\nu \xrightarrow{i_\nu} G_{\nu+1} \xrightarrow{p^\nu} G_{\nu+1}$$

is exact.

Example 4. $(G_\nu = (\mathbb{Z}/p^\nu\mathbb{Z}))^h,\ G = (\mathbb{Q}_p/\mathbb{Z}_p)^h$.

9. Motives and (p-adic) (multiple) zeta values

9.1. **Multiple zeta values.**

Definition 10. Let $x_1, \dots x_p$ be natural numbers with $x_p \geq 2$. The multiple zeta value of the weight w and the depth p is called the expression of the form

$$\zeta(x_1, \dots x_p) = \sum_{0<n_1<\dots<n_r} \frac{1}{n_1^{x_1} \cdots n_p^{x_p}}, w = \sum x_i.$$

Example 5.

$$\zeta(2,2) = \sum_{0<n_1<n_2} \frac{1}{n_1^2 n_2^2}, w = \sum x_i = 4.$$

Example 6.

$$\zeta(2,2) = \frac{1}{2}(\zeta(2)\zeta(2) - \zeta(4)).$$

Let μ_N be the group of roots of unity.

Definition 11. Let $x_1, \dots x_p$ be natural numbers with $x_p \geq 2$. The multiple zeta value relative to μ_N of the weight w and the depth p is called the expression of the form

$$\zeta\left(\begin{smallmatrix} x_1,\dots x_p \\ \epsilon_1,\dots,\epsilon_p \end{smallmatrix}\right) = \sum_{0<n_1<\dots<n_p} \frac{\epsilon_1^{n_1} \dots, \epsilon_p^{n_p}}{n_1^{x_1} \cdots n_p^{x_p}}, \epsilon_i \in \mu_N,$$

$$w = \sum x_i, (x_p, \epsilon_p) \neq (1,1).$$

9.2. **Iterated integrals and (multiple) zeta values.**

Here, we follow [27, 28].

Let $\mathbb{C}$ be the complex plane, and let $f_i(z)$ be a holomorphic function on $\mathbb{C}$. Let $f_i(z)dz$ be the differential of the first kind on $\mathbb{C}$. Let S be a Riemann surface, and let w be the differential of the first kind on S. Parshin considered iterated integrals of this type on Riemann surfaces [27]. For smooth paths on a manifold M and respective path spaces, Chen [28] investegated iterated (path) integrals. For differential forms $w_1, \dots, w_r$ on M, he constructed the iterated integrals by repeating r times the integration of the path space differential forms (and their linear combinations). Chen [28] denoted the iterated integrals by $\int w_1 w_2 \cdots w_r$ and set $\int w_1 w_2 \cdots w_r = 1$, when $r = 0$, and $\int w_1 w_2 \cdots w_r = 0$, when $r < 0$.

Example 7.

$$\zeta(2) = \int_0^1 \frac{dt_1}{t_1} \int_0^{t1} \frac{dt_2}{1-t_2} = \frac{\pi^2}{6}.$$

More generally, the iterated integrals are path space differential forms which permit a further integration.

9.3. **Motives and zeta values.** Glanois in [7] presented the revised and expanded version of his Doctoral thesis [Periods of the motivic fundamental groupoid of $\mathbb{P}^1\{0,\mu_N,\infty\}$, Pierre and Marie Curie University, 2016;] written under F. Brown.

Let $k_N = \mathbb{Q}(\xi_N)$ be the cyclotomic field, $\xi_N \in \mu_N$ be a primitive Nth root of unity, and $\mathcal{O}_N$ be the ring of integers of k_N. The corresponding multiple zeta values at arguments $x_i \in \mathbb{N}, \epsilon_i \in \mu_N$ can be expressed in terms of the coefficients of a version of Drinfeld's assosiators [33] which can be expressed, in turn, in terms of periods of the corresponding motivic multiple zeta values (MMZV).

These MMZV $\zeta^{\mathfrak{m}}(\substack{x_1,\dots x_p\\ \epsilon_1,\dots,\epsilon_p})$, $\epsilon_i \in \mu_N$, $(x_p,\epsilon_p) \neq (1,1)$ relative to μ_N (of the weight $w = \sum x_i$ and the depth p), are elements of an algebra $\mathcal{H}^N$ over $\mathbb{Q}$ and span the algebra.

The algebra $\mathcal{H}^N$ carries an action of the motivic Galois group of the category of mixed Tate motives over $\mathcal{O}_N[1/N]$. The author studies the Galois action on the motivic unipotent fundumental groupoid of $\mathbb{P}^1\backslash\{0,\mu_N,\infty\}$ (or of $\mathbb{G}_m\backslash\mu_N$) for the next values of N : $N \in \{2^a3^b, a+2b \leq 3\} = \{1,2,3,4,\text{`}6\text{`},8\}$.

His results include: bases of multiple zeta values via multiple zeta values at roots of unity μ_N for the above N; more generally, construction of families of motivic iterated integrals with prescribed properties; the new proof, via the coproduct by Goncharov [34] and its extension by Brown [6], of the results by Deligne [35] that the Tannakian category of mixed Tate motives over $\mathcal{O}_N[1/N]$ 'for $N = \{2,3,4,8\}$ is spanned by the motivic fundumental groupoid of $\mathbb{P}^1\backslash\{0,\mu_N,\infty\}$ with an explicit basis'.

In [10], Unver continued his investigation of p-adic multiple zeta values[8], presenting a computation of values of the p-adic multiple polylogarithms at roots of unity. The main result of [10] (Theorem 6.4.3 with Propositions 6.4.1 and 6.3.1) is the explicit expression for the cyclotomic p-adic multizeta values $\zeta_p(s_1,s_2;i_1,i_2)$ of depth two. The result is too technical to state here.

The proof of the theorem is rather technical; it is based on rigid analytic function arguments and a long analysis of group-like elements of related algebras.

For number fields, the category of realizations was defined and investigated by Deligne [3]. Results on multiple zeta values, Galois groups, and geometry of modular varieties were presented by Goncharov [5]. An interesting unipotent motivic fundamental group was defined and investigated by Deligne and Goncharov [4]. Tannakian interpretation of p-adic multiple zeta values was given by Furusho [9].

Results obtained in [10] can be applied to the problems of the p-adic theory of higher cyclotomy.

10. On the Eisenstein series associated with Shimura varieties

The interesting classes of Shimura varieties form varieties which have an interpretation as the moduli spaces of Abelian varieties. The moduli spaces of corresponding $p-$divisible groups over perfect fields of characteristic p are used for the investigation of the local structure of such Shimura varieties.

10.1. **On some Shimura varieties and their local structure.** Let $\mathbb{C}^n$ be $n-$dimensional complex vector space, $\{e_1, \dots, e_{2n}\}$ be $2n-$linear independent vectors, and

$$\Lambda = \{e_1\mathbb{Z}, \dots, e_{2n}\mathbb{Z}\}$$

be a lattice. Then

$$\mathbb{C}^n/\Lambda$$

is a compact commutative topological group. If $\alpha \in GL_n(\mathbb{C})$ and $\Lambda_1 = \alpha\Lambda$, then

$$\mathbb{C}^n/\Lambda = \mathbb{C}^n/\Lambda_1.$$

If $n > 1$, then, not for every lattice Λ, there exists an Abelian variety.

Proposition 18. *Let $\mathbf{x}, \mathbf{y} \in \mathbb{C}^n$, and let $F(\mathbf{x}, \mathbf{y})$ be an$\mathbb{R}-$bilinear form such that*

$$(i) F(\mathbf{x}, \mathbf{y}) = -F(\mathbf{y}, \mathbf{x}),$$

(ii) $F(\mathbf{x}, i\mathbf{x})$ is the Hermitian positive defined form,
and, for
(iii) $\mathbf{x}, \mathbf{y} \in \Lambda$, it takes integer values: $F(\Lambda, \Lambda) \in \mathbb{Z}$.
Then, for this lattice Λ, there exists the Abelian variety.

Definition 12. The pair (Λ, F) is called the polarized Abelian variety.

Let $M = M(F)$ be a matrix of the form F.

Definition 13. The Abelian variety $A = (\Lambda, F)$ is called principally polarized, if the bilinear form F is unimodular or, equivalently, $det(M) = det(M(F)) = 1$.

Denote, by Π, the period matrix of the Abelian variety A. This is an $n \times 2n$ complex matrix $\Pi = (M_1, M_2)$ with nondegenerate $n \times n$ matrices M_1 and M_2.

Definition 14. The period matrix Π is called normalized, if it has the form (E_n, Z), where E_n is the unit $n \times n$ matrix and $Z \in \mathbb{H}_n$, where.

$$\mathbb{H}_n = \{n \times n \text{ matrices } Z | Z^T = Z \text{ and } ImZ > 0\},$$

is the Siegel upper half-plane. Here, Z^T is the matrix transposed to Z.

Remark 8. It is clear that the Siegel matrix $Z \in \mathbb{H}_n$ defines the normalized period matrix Π.

Let

$$J = \begin{pmatrix} 0 & E_n \\ -E_n & 0 \end{pmatrix}.$$

Definition 15. The Siegel modular group $\Gamma_n = Sp_n(\mathbb{Z})$ is the set of matrices

$$M = \begin{pmatrix} A & B \\ C & D \end{pmatrix}.$$

such that

$$M^T J M = J.$$

Definition 16. The Siegel modular group Γ_n acts on the the Siegel upper half-plane $\mathbb{H}_n$ by the formula

$$Z \mapsto (AZ + B)(CZ + D)^{-1}.$$

Proposition 19. *In the framework of Definitions 13 and 14, two Siegel matrices define isomorphic principally polarized Abelian varieties, iff one of them can be obtained from the other one by the transformation of Definition 15.*

Sometimes, we will use an equivalent notations for Siegel matrices Z: $Z = X + iY$, X, Y are real matrices, $X^T = X$, $Y^T = Y$, $Y > 0$; Y is the matrix of the positive definite quadratic form.

Definition 17. Let f be an analytic function on the Siegel upper half-plane that satisfies the equality

$$f((AZ + B)/(CZ + D)) = (CZ + D)^h f(Z)$$

and is bounded on the domains of the form

$$\{Z = X + iY,\ Z \in \mathbb{H}_n, Y \geq cE_n,\ c > 0.\}$$

Then the function f is called the Siegel modular form of the genus n and the weight k.

Remark 9. As the matrix

$$J = \begin{pmatrix} E_n & B \\ 0 & E_n \end{pmatrix}.$$

belongs to Γ_n (its determinant is equal 1) and

$$f(Z + B) = f(Z),$$

so $f(Z)$ has a representation by the Fourier series.

10.2. **On improper intersections of Kudla–Rapoport divisors and Eisenstein series by Sankaran.** Let k be an imaginary quadratic field, o_k its ring of integers, and $o_{k,p}$ be the ring of integers of the completion k_p of k at p. Sankaran [42] proves that the arithmetic degrees of Kudla–Rapoport cycles on an integral model of the Shimura variety attached to a unitary group of signature $(1, 1)$ are Fourier coefficients of the central derivative of an Eisenstein series of genus 2. The main results of the paper are Theorem 4.13 on the value of the Eisenstein series and Corollary 4.15 on the relation between the arithmetic degree of a special cycle and the Eisenstein series. These results confirm conjectures by Kudla [36] and by Kudla and Rapoport [37] on relations between the intersection numbers of special cycles and the Fourier coefficients of automorphic forms in the degenerate setting and for dimension 2. As was pointed out by Kudla [38] and others, 'these relations may be viewed as an arithmetic version of the classical Siegel–Weil formula, which identifies the Fourier coefficients of values of Siegel–Eisenstein series with representation numbers of quadratic forms'. In the paper by Kudla and Rapoport [39], 'the Shimura variety was replaced by a formal moduli space of p-divisible groups, the special arithmetic cycles were replaced by formal subvarieties, and the special values of the derivative of the Eisenstein series were replaced by the derivatives of representation densities of Hermitian forms.' Sankaran defined the local Kudla–Rapoport cycles $Z(b)$ and gave some applications of results obtained in his earlier paper [43], where he proved Theorem 3.14 on cycles $Z(b)$. He allowed 'the polarizations to be non-principal in a controlled way'. An unpolarized case of p-divisible groups with the given p^m-kernel type and with applications to their Newton polygons was considered by Harashita [40]. Sankaran's paper [42] consists of four sections. The first section presents the purpose and a short description of ideas and

results of next sections. The second section concerns with local Kudla–Rapoport cycles on the Drinfeld upper half-plane. The main result of this section is Theorem 2.14 on values of local intersection numbers of these cycles. The third section is devoted to the proof of the closed-form formula for representation densities $\alpha(S,T)$. The author specialized the explicit formula on Hermitian representation densities by Hironaka [41] to the case at hand: $F(S,T,X) \in Q[X], T \in Herm_2(o_{k,p}), ord_p det(T)$ is even, $S = diag(p,1), \alpha(S_r,T) = F(S,T,(-p)^{-r})$. In the last section, some global aspects are discussed and the main result is presented. Let $M^d_{(1,1)}$ denote the Deligne–Mumford (DM) stack over o_k of almost-principally polarized Abelian surfaces and $\mathcal{E}$ the DM stack over o_k of principally polarized elliptic curves with the multiplication by o_k. Under conditions of Subsection 4.1 in [42], the author sets $\mathcal{M} = \mathcal{E} \times_{Speco_k} M^d_{(1,1)}$ and defines, for $T \in Herm_2(o_k)$, cycles $\mathcal{Z}(T)$. Then in subsection 4.3, the author proves Theorem 4.13 and Corollary 4.15.

References

[1] Voronoi, G.F. 1952, *Collected Works*, vol. I, AN UkrSSR, Kiev.

[2] Zagier, D. 1993, "Periods of modular forms, traces of Hecke operators, and multiple $\zeta-$values", *Research into Automorphic Forms and L−functions*, Kyoto, Surikaisekikenkyusho Kokyuroku, **843**, pp. 162–170.

[3] Deligne, P. 1989, "Le groupe fondamental de la droite projective moins trois points", in: Ihara Y., et al., (Eds.), *Galois Groups over* $\mathbb{Q}$, Springer, New York, pp. 79–297.

[4] Deligne, P., Goncharov, A. 2005. "Groupes fondamentaux motiviques de Tate mixte", *Ann. Sci. Ecole Norm. Sup.*, (4), **38**, no. 1, pp. 1–56.

[5] Goncharov, A. 2000, "Multiple ζ-values, Galois groups, and geometry of modular varieties", *European Congr. of Mathematics*, **I**, Barcelona, Progr. Math., **201**, Birkh$\acute{}$auser, Basel, pp. 361–392.

[6] Brown, F. 2012, "Mixed Tate motives over Z", *Ann. of Math.*, **175**, no. 1, pp. 949–976.

[7] Glanois, C. 2016, "Motivic unipotent fundamental groupoid of $\mathbb{G}_m \backslash \mu_N$ for $N = 2,3,4,6,8$ and Galois descents", *Journal of Number Theory*, **160**, pp. 334–384.

[8] Ünver, S. 2004, "p-adic multiple zeta values", *Journal of Number Theory*, **108**, pp. 111–156.

[9] Furusho, H. 2007, "p-adic multiple zeta values II. Tannakian interpretations", *Am. J. Math.*, **129** (4), pp.1105–1144.

[10] Ünver, S. 2016, "Cyclotomic p-adic multi-zeta values in depth two", *Manuscr. Math.*, **149**, nos. 3-4, pp.405–441.

[11] Ihara, Y. 1991, "Braids, Galois Groups, and Some Arithmetic Functions", *Proc. of the ICM 90 (I)*, Springer, Berlin, pp. 99–120.

[12] Leopoldt, H.W. 1959, "Uber Klassenzahlprimteiler reeller abelschen Znhlkorper als Primteiler verallgemeinerter Bernoullischer Zahlen", *Abh. Math. Sem. Hamburg*, **23**, pp. 36–47.

[13] Leopoldt, H.W. 1960, "Ober Fermatquotienten von Kreiseinheit und Klassenzahlformeln mod p", *Rend. Circ. Mat. Palermo*, **2**, ser., 9, pp. 1–12.
[14] Leopoldt, H.W. 1962, "Zur Arithmetik in abelschen Zahlkorpern", *J. Reine Angew. Math.*, **209**, pp. 54–71.
[15] H. Hasse, 1962, "Sulla generaiizzazione di Leopoidt dei numeri di Bernoulli e sua applicazioni alia divisbilita del numero delle classi nei corpi numerici abelian", *Rend, mat. e appl.* **21**, nos. 1–2, pp. 9–27.
[16] Kubota, K. Leopoldt, H.-W. 1964, "Eine p-adische Theorie der Zetawerte". I, *J. Reine Angew. Math.*, **214/215**, pp. 328–339.
[17] Leopoldt, H.W. 1975, "Eine p-adische Theorie der Zetawerte 2", *J. Reine Angew. Math.*, **274/275**, pp. 224–247.
[18] Iwasawa, K. 2001. "Analogies between number fields and function fields". In *Collected Papers*, **II**, Springer, Tokyo, pp. 606–611.
[19] Weber, H. 1908, *Lehrbuch der Algebra*, vol. III, F. Vieweg und Sohn, Braunschweig.
[20] Hasse, H. 1931, "Zum Hauptidealsatz der komplexen Multiplikation", *Monatshefte fur Math.*, **38**, 315–322, 323–330, 331–344.
[21] Deuring, M. 1961, "Klassenkorper der komplexen Multiplikation", *Enzyklopadie der Math. Wiss.*, Bd. 12, Heft 10, Teil II, 23.
[22] Borevich, Z., Shafarevich, I. 1986, *Number Theory*, Academic Press, New York.
[23] Manin, Yu. I. 1971, "Cyclotomic fields and modular curves", *UMN*, **26:6**, pp. 7–78.
[24] Manin, Yu. I. 1972, "Parabolic points and zeta-functions of modular curves", *Math. USSR-Izv.*, **6:1**, pp. 19–64.
[25] Hashimoto, M. 2017, Equivariant class group. II: Enriched descent theorem. *Commun. Algebra* , **45**(4), pp. 1509–1532,
[26] Koblitz, N. 1997, *p-Adic Numbers, p-Adic Analysis and Zeta-Functions*, Bibphysmat, Izhevsk.
[27] Parshin, A. 1966 "A generalization of Jacobian variety ", *Izv. Akad. Nauk SSSR Ser Mat.*, **30**, pp. 175–182.
[28] Chen, K. 1977, "Iterated path integrals", *Bull. Amer. Math. Soc.* **83**, pp. 831–879.
[29] Edited by J. Cassels and A. Fröhlich, 2003, *Algebraic Number Theory*, Academic Press, London.
[30] Hazewinkel M. 1977, *Formal Groups*, Academic Press, New York.
[31] Vvedenskii O.N. 1973, " On local "class fields" of elliptic curves", *Izv. Akad. Nauk SSSR. Mat.*, **37**, no. 1, pp. 20–88.
[32] Vvedenskii O.N., 1973, *On "universal norms" of formal groups over integer ring of local fields* (In Russian), *Izv. Akad. Nauk SSSR Math.*, **37**, pp. 737–751.
[33] Drinfeld, V. 1991, "On quasi-triangular quasi-Hopf algebras and one group that is closely related to $Gal(\overline{\mathbb{Q}}/\mathbb{Q})$", *Leningrad Math. J.*, **2:4** , pp. 829–860.
[34] Goncharov, A. 2005, "Galois symmetries of fundamental groupoids and noncommutative geometry", *Duke Math. J.*, **128**, no. 2 , pp. 209 – 284.
[35] Deligne, P. 2010, "Le groupe fondamental unipotent motivique de $G_m \setminus \mu_N$ pour $N = 2, 3, 4, 6$ or 8", *Publ. Math. IHES*, **112**, no. 1, pp. 101 – 141.
[36] Kudla, K. 2004, "Special cycles and derivatives of Eisenstein series", *Math. Sci. Research Institute Publ.*, Cambridge Univ. Press, **49**. pp. 243–270.

[37] Kudla, K., Rapoport, M. 2014, "Special cycles on unitary Shimura varieties II: global theory", *J. Reine Angew. Math.*, **697**, pp. 91–157.
[38] Kudla, K., 2004 "Derivatives of Eisenstein Series and Arithmetic Geometry", *Proc. of ICM 2002*, vol. II, Higher Education Press, Beijing, pp. 173–183.
[39] Kudla, K., Rapoport, M. 2011 "Special cycles on unitary Shimura varieties I. Unramied local theory", *Invent. math.*, **184**, pp. 629–682.
[40] Harashita, S. 2009 "Geometry and analysis of automorphic forms of several variables", *Proc. Int. Symp. in honor of Takayuki Oda on the occasion of his 60th birthday*, Univ. of Tokyo, Tokyo, Japan, September 14–17, 2009, World Scientific. Series on Number Theory and its Applications, **7**, World Scientific, Hackensack, NJ, pp. 41–55.
[41] Hironaka, Y. 1998, "Local Zeta functions on Hermitian forms and its application to local densities", *Number Theory*, **71**, pp. 40–64.
[42] Sankaran, S. 2017, "Improper intersections of Kudla-Rapoport divisors and Eisenstein serie", *J. Inst. Math. Jussieu*, **16**, no. 5. pp. 899 – 945.
[43] Sankaran, S. 2013, "Unitary cycles on Shimura curves and the Shimura lift I", *Documenta Math.*, **18**, pp. 1403–1464.
[44] Glazunov, N.M. 1973, "Algorithms and programs for research in Diophantine geometry", *Preprint 73–16*, Institute of Cybernetics of the Ukrainian Academy of Sciences, Kiev, 26 p.
[45] Glazunov, N. 2018, "Class groups of rings with divisor theory, L-functions and moduli spaces", *Int. conf. 'Algebraic and geometric methods of analysis.* Book of abstracts. Institute of Mathematics, Odessa-Kiev, pp.19-20. Available at: https://www.imath.kiev.ua/ topology/conf/agma2018
[46] Glazunov, N. 2018, "Class Fields, Riemann Surfaces and (Multiple) Zeta Values", *Proc. 3-d Int.l Conf. Computer Algebra & Information Technologies*, Mechnikov National University, Odessa, pp.152–154.
[47] Glazunov, N. 2018, "p-adic L-functions and p-adic (multiple) zeta values", *Sixth Int. Conf. on Analytic Number Theory and Spatial Tessellations*, Abstracts, National Pedagogical Dragomanov University, Kyiv, pp.15–16.
[48] Glazunov, N. 2015, "Quadratic forms, algebraic groups and number theory", *Chebyshevskii Sbornik*, **16**, no. 4, pp.77–89.
[49] Glazunov, N. 2015, " Extremal forms and rigidity in arithmetic geometry and in dynamics", *Chebyshevskii Sbornik*, **16**, no. 3, pp.124–146.

Department of Electronics, National Aviation University, 1, Komarova Pr., Kyiv, 03680, Ukraine
Email: glanm(at)yahoo(dot)com
URL: https://sites.google.com/site/glazunovnm/

Preface to Section **Fractal Analysis and Fractal Geometry**

In his renowned essay, B. Mandelbrot observed that many natural spatial structures exhibit an irregular form that cannot be adequately described using classical geometry. This realisation laid the foundation for fractal geometry, which is based on the concepts of self-similarity, self-affinity, and the non-integer dimension.

Modern fractal theory, which studies objects with a fractional Hausdorff-Besicovitch dimension, consists of two main components: fractal geometry and fractal analysis. Fractal geometry investigates specific geometric figures within metric spaces, whereas fractal analysis focuses on identifying fractal properties of functions, probability distributions, dynamical systems, and related objects.

Fractal geometry offers several advantages over traditional Euclidean geometry, particularly in modelling natural phenomena and complex structures. While Euclidean geometry relies on idealised shapes such as lines, circles, squares, and triangles that rarely occur in nature, fractal geometry provides a more accurate representation of irregular and self-similar structures. This allows for a better approximation of objects such as the coastline of islands, cloud formations, mountain landscapes, galactic structures, Brownian motion trajectories, and financial process graphs. Consequently, fractal geometry and fractal analysis enable the development and examination of models that more accurately reflect real-world processes, in contrast to simplified models in Euclidean geometry.

This section explores functions and probability distributions that exhibit a complex local structure and possess fractal properties. The analysis and modelling of these objects involve a use of non-standard numeral systems such as modified continued fractions, s-adic, Q_s^*, and Q_2-representations. Employing these representations greatly facilitates the study of the aforementioned functions and reveals their intricate features.

February 2025

Dr. Dmytro Karvatskyi
Researcher at the Department of
Dynamical Systems and Fractal Analysis
of the Institute of Mathematics of NAS of Ukraine

Voronoï's Impact on Modern Science, Book 6, Volume 2
Proceedings of the Sixth International Conference on Analytic Number Theory and Spatial Tessellations

A CONSTRUCTION OF REAL FUNCTIONS DEFINED WITH QUANTITIES OF DIGITS OCCURRENCES IN THE ARGUMENT REPRESENTATION

Oleksii Panasenko and Tetiana Kyrylaschuk (*Ukraine*)

Abstract. In the present paper, we consider one type of real functions whose algebraic expressions contain quantities of digits occurrences up to every position in the s-adic argument representation. We find conditions under which these functions are well defined and investigate some properties of these functions.

Introduction

There are several approaches used to define real functions with complicated specific features. Among them, we focus our attention on the approach based on the idea of description of the relationships with digits of the argument and values (in some representation, e.g., s-adic). Many fractal continuous functions, namely, singular, nowhere differentiable, etc., can be defined in this way.

In the present paper, we analyze a construction of functions whose algebraic expression contains quantities of digits occurrences up to every position in the s-adic argument representation.

We use following notation: let $s \geq 2$ be a positive integer, let $x \in [0,1]$ and $x = \sum_{k=1}^{\infty} \frac{\alpha_k}{s^k} \equiv \Delta^s_{\alpha_1\alpha_2\ldots\alpha_k\ldots}$ be the s-adic representation of x ($\alpha_k \in \{0,1,\ldots,s-1\}$), and let $N_j(k,x)$ be the number of digits j among $\alpha_1,\ldots,\alpha_k$ of x (in the s-adic representation).

1. Definition

For given values a_j ($j = \overline{0,s-1}$), let us consider a function which maps x into the number

$$f(x) = \sum_{k=1}^{\infty} \left(\frac{\alpha_k}{s^k} \prod_{j=0}^{s-1} a_j^{N_j(k,x)} \right). \tag{1}$$

Received September 1, 2018.
2010 *Mathematics Subject Classification.* Primary 26A30.
Key words and phrases. self-affine functions, singular functions, fractal functions.

First of all, we find conditions for which this function is well defined. It is correct if for different representations of a s-adic rational number x, the corresponding values are equal.

Hence, let $\Delta^s_{\alpha_1\alpha_2\ldots\alpha_n(0)}$, $\alpha_n \neq 0$, be the representation of a s-adic rational number x and let $\Delta^s_{\alpha_1\alpha_2\ldots(\alpha_n-1)(s-1)\ldots}$ be another well-known representation of x (for the sake of convenience, we denote this representation by x'). It is necessary that $f(x) = f(x')$.

We have:

$$f(x) = \sum_{k=1}^{n-1} \left(\frac{\alpha_k}{s^k} \prod_{j=0}^{s-1} a_j^{N_j(k,x)} \right) + \frac{\alpha_n}{s^n} \prod_{j=0}^{s-1} a_j^{N_j(n,x)}.$$

and

$$f(x') = \sum_{k=1}^{n-1} \left(\frac{\alpha_k}{s^k} \prod_{j=0}^{s-1} a_j^{N_j(k,x)} \right) + \frac{\alpha_n - 1}{s^n} \prod_{j=0}^{s-1} a_j^{N_j(n,x')} + \sum_{k=n+1}^{\infty} \frac{s-1}{s^k} \prod_{j=0}^{s-1} a_j^{N_j(k,x')}.$$

But

$$N_j(n, x') = N_j(n, x) + (\alpha_n == j+1) - (\alpha_n == j)$$

for all $j \in \{0, 1, \ldots, s-1\}$ and

$$N_j(k, x') = N_j(k, x) - (\alpha_n == j) + (k-n)(j == s-1) + (\alpha_n - 1 == j)$$

for all $j \in \{0, 1, \ldots, s-1\}$ and $k > n$ (here, we use notation: $a == b$ is 1 if $a = b$, and 0, otherwise).

Thus, $f(x) = f(x')$ if and only if

$$\frac{\alpha_n}{s^n} \prod_{j=0}^{s-1} a_j^{N_j(n,x)} = \frac{\alpha_n - 1}{s^n} \prod_{j=0}^{s-1} a_j^{N_j(n,x')} + \sum_{k=n+1}^{\infty} \frac{s-1}{s^k} \prod_{j=0}^{s-1} a_j^{N_j(k,x')}.$$

The last identity can be rewritten as

$$\frac{1}{s^n} \prod_{j=0}^{s-1} a_j^{N_j(n,x)} \left(\alpha_n - (\alpha_n - 1) \cdot \prod_{j=0}^{s-1} \frac{a_j^{\alpha_n == j+1}}{a_j^{\alpha_n == j}} \right) =$$

$$= (s-1) \prod_{j=0}^{s-1} a_j^{N_j(n,x)} \cdot \sum_{k=n+1}^{\infty} \frac{1}{s^k} \prod_{j=0}^{s-1} \frac{a_j^{j==\alpha_n - 1} a_j^{(k-n)(j==s-1)}}{a_j^{j==\alpha_n}}.$$

If we denote $\alpha_n = q$, then this is equivalent to

$$\frac{1}{s^n}\prod_{j=0}^{s-1} a_j^{N_j(n,x)}\left(q-(q-1)\cdot\frac{a_{q-1}}{a_q}\right) = \\ = (s-1)\prod_{j=0}^{s-1} a_j^{N_j(n,x)}\cdot\frac{a_{q-1}}{a_q a_{s-1}^n}\cdot\sum_{k=n+1}^{\infty}\left(\frac{a_{s-1}}{s}\right)^k.$$

Let $a_{s-1} < s$. Then the sum on the right-hand side of the last equality is $\frac{(a_{s-1})^{n+1}}{(s-a_{s-1})s^n}$. Thus, after simplifying this equality, we find:

$$a_{q-1} = \frac{q(s-a_{s-1})}{(s-1)a_{s-1}+(q-1)(s-a_{s-1})}a_q. \tag{2}$$

This recurrence relation must be true for all $q = \overline{1, s-1}$. Hence, if we choose some integer $s \geq 2$ and $a_{s-1} < s$, then we get the unique function with values as in (1).

Example 1. Let $a_{s-1} = 1$. Then it is easy to verify that all a_q are equal to 1 and $f(x)$ is the identity function.

Example 2. Let $s = 2$. Then relation (2) can be rewritten as $a_0 + a_1 = 2$. In the case $a_0 = \frac{1}{2}$, $a_1 = \frac{3}{2}$, we get the strictly increasing singular function, which was described in [1].

Example 3. Let $s = 3$ and $a_2 \equiv c \in (0, 3)$. Then expression (1) can be rewritten as

$$f(x) = \sum_{k=1}^{\infty}\frac{\alpha_k}{3^k}\left(\frac{(3-c)^2}{3+c}\right)^{N_0(k,x)}\left(\frac{2c(3-c)}{3+c}\right)^{N_1(k,x)}c^{N_2(k,x)}.$$

These functions appeared and some of their properties were described in [4].

2. Some Properties

Theorem 1. *The function $f(x)$ defined by (1) with condition (2) on every a_q has following properties:*

1) $f(0) = 0$, $f(1) = \frac{(s-1)a_{s-1}}{s-a_{s-1}}$.

2) for all $i \in \{0, \ldots, s-1\}$:

$$f\left(\frac{x+i}{s}\right) = \frac{ia_i}{s} + \frac{a_i}{s}f(x).$$

3) if $a_{s-1} > 1$ then $f(x)$ is an increasing function.

Proof. The first part of theorem immediately follows from the definition of f if we set $x = \Delta^s_{(0)}$ and $x = \Delta^s_{(2)}$.

Let us prove the second part. Indeed, for every $i \in \{0, \ldots, s-1\}$ and $x = \Delta^s_{\alpha_1\alpha_2\ldots}$, we get

$$f\left(\frac{x+i}{s}\right) = f\left(\Delta^s_{i\alpha_1\alpha_2\ldots}\right) = \frac{i}{s}a_i + \sum_{k=1}^{\infty}\left(\frac{\alpha_k}{s^{k+1}}\prod_{j=0}^{s-1}a_j^{N_j\left(k+1,\frac{x+i}{s}\right)}\right) =$$

$$= \frac{i}{s}a_i + \frac{a_i}{s}\sum_{k=1}^{\infty}\left(\frac{\alpha_k}{s^k}\prod_{j=0}^{s-1}a_j^{N_j(k,x)}\right) = \frac{ia_i}{s} + \frac{a_i}{s}f(x).$$

We also note that $\frac{ia_i}{s} = f\left(\frac{i}{s}\right)$.

3) The inequality $\frac{q(s-a_{s-1})}{(s-1)a_{s-1}+(q-1)(s-a_{s-1})} < 1$ is equivalent to the inequality $a_{s-1} > 1$ and is independent of q. Hence, if $a_{s-1} > 1$, then the sequence $a_{s-1}, a_{s-2}, \ldots$ is decreasing (or $a_0, a_1, \ldots$ is increasing).

Let $x_1 < x_2$. More precisely, $x_1 = \Delta^s_{\alpha_1\ldots\alpha_n\alpha_{n+1}\ldots}$, $x_2 = \Delta^s_{\alpha_1\ldots\alpha_n\beta_{n+1}\beta_{n+2}\ldots}$, and $\beta_{n+1} > \alpha_{n+1}$. Let $x^\star = \Delta^s_{\alpha_1\ldots\alpha_n(s-1)}$ and $x^{\star\star} = \Delta^s_{\alpha_1\ldots[\alpha_n+1](0)}$. Obviously, $x^\star = x^{\star\star}$. Since $a_0, \ldots, a_{s-1}$ is increasing, we see that $f(x_1) \le f(x^\star)$ and $f(x^{\star\star}) \le f(x_2)$. Thus, $f(x_1) \le f(x_2)$ and $f(x)$ is increasing. □

As we can see from the second part of the previous theorem, our functions have certain self-affine properties. They look like self-affine functions in Kono's sense but there is a slight difference from the indicated functions (see also [5, 3]).

References

[1] Jo K., *A Construction of Strictly Increasing Continuous Singular Function*, J. Korean Soc. Math. Educ. Ser. B: Pure Appl. Math. **23** (2016), №1, 21–34.

[2] Kono N., *On self-affine functions*, Japan J. Appl. Math **3** (1986), 259–269.

[3] Калашніков А. В., Працьовитий М. В., *Самоафінні сингулярні та ніде не монотонні функції, пов'язані з Q-зображенням дійсних чисел*, Укр. мат. журн. **65** (2013), №3, 405–417.

[4] Панасенко О. Б., Тіманова А. В., *Сингулярні функції, означені в термінах частоти вживання трійкових цифр аргументу*, Матеріали Всеукраїнської конференції «Математика та інформатика у вищій школі: виклики сучасності» (2017), 51–55.

[5] Працьовитий М. В., Панасенко О. Б., *Диференціальні і фрактальні властивості одного класу самоафынних функцій*, вісник Львівського університету. Серія механіко-математична **70** (2009), 128–139.

(O. Panasenko) Faculty of Mathematics, Physics, and Technologies, Vinnytsia Mykhailo Kotsiubynskyi State Pedagogical University, 31 Ostrozhskii St., Vinnytsia, 21100, Ukraine
Email: panalbor(at)gmail(dot)com

(T. Kyrylaschuk) Faculty of Mathematics and Information Technology, Vasyl' Stus Donetsk National University, 600-richya str., 21, Vinnytsia, 21021, Ukraine
Email: ksa07750(at)gmail(dot)com

UNIFORMLY DISTRIBUTED SEQUENCES GENERATED BY SHIFT TRANSFORMATIONS IN A CLASS OF Q_s-REPRESENTATION

Mykola Pratsiovytyi, Rostyslav Kryvoshyia,
and Oleh Makarchuk (*Ukraine*)

Abstract. In this work we deepened the results of I. Niven and H. Zukerman for the Q_s^*-representations in the context of the E. Borel metric theory of normal numbers.

1. Introduction

Let $\mathbf{p}_n = (p_{0n}, \dots, p_{(s-1)n})$ be a sequence of stochastic vectors with positive coordinates such that

$$\prod_{n=1}^{\infty} \max\{p_{0n}, \dots, p_{(s-1)n}\} = 0.$$

It is known [5] that for each real number $x \in [0,1]$ there exist an infinite sequence $(\alpha_1, \alpha_2, \dots, \alpha_n, \dots)$, where $\alpha_n \in \{0, 1, \dots, s-1\}$ such that

$$x = \beta_{\alpha_1 1} + \beta_{\alpha_2 2} p_{\alpha_1 1} + \beta_{\alpha_3 3} p_{\alpha_2 2} p_{\alpha_1 1} + \cdots + \beta_{\alpha_{n+1}(n+1)} p_{\alpha_n n} \cdots p_{\alpha_1 1} + \cdots, \quad (1)$$

where

$$\begin{cases} \beta_{0n} = 0, \\ \beta_{jn} = p_{0n} + \cdots + p_{(j-1)n} \quad \text{for all } n \in \mathbb{N}. \end{cases}$$

Expression (1) is called the Q_s^*-representation of x. The number x and its Q_s^*-representation are denoted by $\Delta^{Q_s^*}_{\alpha_1\alpha_2\dots}$. If $p_{0n} = \frac{1}{s}$ for all $n \in \mathbb{N}$, then we obtain s-adic representation of x:

$$x = \sum_{n=1}^{\infty} \frac{\alpha_n}{s^n}, \ \alpha_n \in \{0, 1, \dots, s-1\}.$$

Received October 27, 2020.
2010 *Mathematics Subject Classification.* Primary 26A30.
Key words and phrases. Q_s^*-representation, normal numbers, uniformly distributed sequence, ergodic transformation, Lebesgue measure, dynamic systems.

For real numbers $\Delta^{Q_s^*}_{\alpha_1\ldots\alpha_{k-1}\alpha_k(0)}$,where $\alpha_k \neq 0$, there exist two different Q_s^*-representations:

$$\Delta^{Q_s^*}_{\alpha_1\ldots\alpha_{k-1}\alpha_k(0)} = \Delta^{Q_s^*}_{\alpha_1\ldots\alpha_{k-1}[\alpha_k-1](s-1)}.$$

The remaining numbers in $[0,1]$ have unique Q_s^*-representations.

If $\mathbf{p}_n = \mathbf{p} = (p_0,\ldots,p_{s-1})$ for all $n \in \mathbb{N}$, then the Q_s^*-representation is the Q_s-representation. The number x and its Q_s-representation are denoted by $\Delta^{Q_s}_{\alpha_1\alpha_2\ldots}$.

Definition 1. Let (x_n) be a sequence of real numbers from $[a,b]$, and let $N_n([c,d])$ be the number of elements in the set $\{x_1,x_2,\ldots,x_n\}$ that belong to $[c,d] \subset [a,b]$. Sequence (x_n) is called uniformly distributed on interval $[a,b]$ if

$$\frac{N_n([c,d])}{n} \to \frac{c-d}{b-a} \quad \text{as} \quad n \to \infty$$

for every interval $[c,d] \subset [a,b]$. Sequence (x_n) is called uniformly distributed modulo 1 if sequence $(\{x_n\})$ is uniformly distributed on $[0,1]$, where $\{t\}$ denotes the fractional part of t.

One of the most important criterion for checking uniform distribution modulo 1 is Weyl's criterion [7]:

Theorem 1. *Sequence (x_n) is uniformly distributed modulo 1 if and only if*

$$\frac{\sum\limits_{k=1}^{n} \mathrm{e}^{2\pi \mathrm{i} h x_k}}{n} \to 0 \quad \textit{as} \quad n \to \infty$$

for all $h \in Z \setminus \{0\}$, where $\mathrm{i} = \sqrt{-1}$.

In Theorem 1 it is enough to consider only natural numbers h. Indeed

$$\frac{\sum\limits_{k=1}^{n} \mathrm{e}^{2\pi i h\{x_k\}}}{n} \to 0 \quad \Leftrightarrow \frac{\sum\limits_{k=1}^{n} \cos(2\pi h\{x_k\}) + i\sum\limits_{k=1}^{n} \sin(2\pi h\{x_k\})}{n} \to 0 \quad \Leftrightarrow$$

$$\frac{\sum\limits_{k=1}^{n} \mathrm{e}^{-2\pi i h\{x_k\}}}{n} \to 0, \quad n \to \infty.$$

The concept of a uniformly distributed sequences was introduced by Weyl in 1919 in his work [7], where he established the uniform distribution of the sequence $\{n\gamma\}$ for all $\gamma \notin \mathbb{Q}$. He also proved the first criterion for uniform distribution of sequences (Theorem 1.)

Definition 2. A real number

$$x = \Delta^{s}_{\alpha_1\alpha_2\ldots\alpha_n\ldots} = \sum_{n=1}^{\infty} \frac{\alpha_n}{s^n}$$

is called normal in base s if

$$\frac{w_k}{k} \to \frac{1}{s^r} \quad \text{as} \quad k \to \infty$$

for every finite string $(c_1, c_2, \ldots, c_r)$, where w_k is the number of times a tuple $(c_1, c_2, \ldots, c_r)$ occurs as a substring in the first k elements of the sequence (α_n).

The last definition was introduced by E. Borel in [1].

In paper [3] I. Niven and H. Zukerman showed that the number x is normal in base s if and only if the sequence $s^n x$ is uniformly distributed modulo 1 (or the sequence $\{s^n x\}$ is uniformly distributed on $[0, 1]$). The last fact holds since the following theorem is correct [8].

Theorem 2. *For an arbitrary sequence $(d_n)_{n=1}^{\infty}$ of pairwise distinct integers, the sequence $(d_n x)_{n=1}^{\infty}$ is uniformly distributed modulo 1 for almost all $x \in \mathbb{R}$.*

Thus, the set of normal numbers of base s has Lebesgue measure 1. The proof of the last fact based on the Birkhoff-Khinchin theorem was first indicated by F. Riss in [4]. This was possible because the transformation $x \to \{sx\}$ is ergodic.

2. The ergodic properties of the shift operator and the uniformly distributed sequences generated by them

For Q_s-representation generated by stochastic vector $\mathbf{p} = (p_0, \ldots, p_{s-1})$, we consider the transformation

$$T\left(\Delta^{Q_s}_{\alpha_1\alpha_2\ldots}\right) = \Delta^{Q_s}_{\alpha_2\alpha_3\ldots}.$$

If number has two distinct Q_s-representations, then we will use the one with period (0).

Lemma 1. *The transformation $T(x)$ is ergodic with respect to Lebesgue measure.*

Proof. It is clear that

$$T^{-1}\left(\left[\Delta^{Q_s}_{\alpha_1\alpha_2\ldots\alpha_n(0)}; \Delta^{Q_s}_{\alpha_1\alpha_2\ldots\alpha_n(s-1)}\right]\right) =$$

$$= \bigcup_{k=0}^{s-1} \left[\Delta^{Q_s}_{k\alpha_1\alpha_2\ldots\alpha_n(0)}; \Delta^{Q_s}_{k\alpha_1\alpha_2\ldots\alpha_n(s-1)}\right].$$

$$\lambda\left(\left[\Delta^{Q_s}_{\alpha_1\alpha_2\ldots\alpha_n(0)}; \Delta^{Q_s}_{\alpha_1\alpha_2\ldots\alpha_n(s-1)}\right]\right) = \prod_{j=1}^{n} q_{\alpha_j},$$

$$\lambda\left[\Delta^{Q_s}_{k\alpha_1\alpha_2\ldots\alpha_n(0)}; \Delta^{Q_s}_{k\alpha_1\alpha_2\ldots\alpha_n(s-1)}\right] = q_k \prod_{j=1}^{n} q_{\alpha_j}.$$

Thus, we have:

$$\lambda\left(\bigcup_{k=0}^{s-1}\left[\Delta^{Q_s}_{k\alpha_1\alpha_2\ldots\alpha_n(0)}; \Delta^{Q_s}_{k\alpha_1\alpha_2\ldots\alpha_n(s-1)}\right]\right) =$$

$$= \lambda\left(\left[\Delta^{Q_s}_{\alpha_1\alpha_2\ldots\alpha_n(0)}; \Delta^{Q_s}_{\alpha_1\alpha_2\ldots\alpha_n(s-1)}\right]\right).$$

Since the set of segments

$$[\Delta^{Q_s}_{\alpha_1\alpha_2\ldots\alpha_n(0)}; \Delta^{Q_s}_{\alpha_1\alpha_2\ldots\alpha_n(s-1)}]$$

generates $B(R) \cap [0;1]$, then for each set $E \in B(R) \cap [0;1]$, we have:

$$\lambda(T^{-1}(E)) = \lambda(E).$$

Let us show that the transformation $T(x)$ is metrically transitive with respect to the Lebesgue measure, i.e. for each set $H \in B(R) \cap [0;1]$ such that $T^{-1}(H) = H$ the condition $\lambda(H) \in \{0;1\}$ is satisfied. Suppose that there exist sets U, W such that

$$U \cup W = [0;1];$$

$$U \cap W = \varnothing;$$

$$T^{-1}(U) = U;$$

$$T^{-1}(W) = W.$$

Let $u = \lambda(U) \in (0;1)$ and $X(t)$ be the characteristic function of the set U:

$$X(t) = \begin{cases} 1, t \in U \\ 0, t \notin U. \end{cases}$$

It is clear that for each

$$x = \Delta^{Q_s}_{\alpha_1\alpha_2\ldots\alpha_k\ldots} \in U$$

and for each natural number l,

$$x^{(l)} = \Delta^{Q_s}_{q_1q_2\ldots q_l\alpha_1\alpha_2\ldots\alpha_k\ldots}$$

is the inverse image of x of order l for the transformation $T(x)$.

We have:

$$X(\Delta^{Q_s}_{\alpha_1\alpha_2\ldots\alpha_k\ldots}) = X(x^{(l)}).$$

Let

$$B_l = [\Delta^{Q_s}_{a_1a_2\ldots a_l(0)}; \Delta^{Q_s}_{a_1a_2\ldots a_l(1)}],$$

we have:

$$\lambda(U \cap B_l) = \int\limits_{B_l} X(t)d\lambda =$$

$$= q_{a_1}q_{a_2}\ldots q_{a_l}\int\limits_{R} X(t)d\lambda = uq_{a_1}q_{a_2}\ldots q_{a_l}.$$

Consider a number $\varepsilon > 0$ such that $1 - u > \varepsilon$. Since the set U and its complement W to the set $[0;1]$ have positive Lebesgue measures, then by the density point theorem, there exists a density point z. Thus, for any $\varepsilon > 0$, there exists $\delta > 0$ such that

$$\frac{\lambda(U \cap \Delta)}{\lambda(\Delta)} > 1 - \varepsilon$$

for any segment Δ that contains the point z and whose Lebesgue measure is strictly less than δ.

Consider a number n_0 such that

$$(\max(q_0; q_1; ...; q_{s-1}))^{n_0} < \delta.$$

Let us denote:

$$z = \Delta^{Q_s}_{b_1b_2\ldots b_k\ldots}$$

and consider the segment

$$\Delta = B_{n_0} = [\Delta^{Q_s}_{b_1b_2\ldots b_{n_0}(0)}; \Delta^{Q_s}_{b_1b_2\ldots b_{n_0}(s-1)}].$$

We have:

$$\lambda(U \cap \Delta) = uq_{b_1}\ldots q_{b_{n_0}},$$

$$\lambda(U \cap \Delta) > (1-\varepsilon)\lambda(\Delta) = (1-\varepsilon)q_{b_1}\ldots q_{b_{n_0}},$$

$$uq_{b_1}\ldots q_{b_{n_0}} > (1-\varepsilon)q_{b_1}\ldots q_{b_{n_0}}$$

and

$$1 - u < \varepsilon.$$

We have a contradiction so the theorem is proved. □

Theorem 3. *For almost all numbers* $x = \Delta^{Q_s}_{\alpha_1\alpha_2\ldots\alpha_n\ldots}$ *a sequence*

$$x, T(x), T^2(x), \ldots, T^k(x), \ldots$$

is uniformly distributed on $[0;1]$.

Proof. Since the transformation $T(x)$ is ergodic with respect to the Lebesgue measure, then for given $h \in \mathbb{N}$ by the Birkhoff-Khinchin theorem we have

$$\frac{\sum\limits_{k=1}^{n} \cos(2\pi h T^k(x))}{n} \to \int_0^1 \cos(2\pi h x)\mathrm{d}x = 0, \quad n \to +\infty \qquad (2)$$

for almost all $x \in [0;1]$.

Denote by A_h the set of those $x \in [0;1]$, for which the condition is fulfilled (2), then $\lambda(A_h) = 1$. It is clear that

$$\lambda(A_1 \cap A_2) = \lambda(A_1) + \lambda(A_2) - \lambda(A_1 \cup A_2) = 2 - 1 = 1,$$

so by induction

$$\lambda(A_1 \cap A_2 \cap \cdots \cap A_k) = 1$$

and accordingly

$$\lambda(A_1) - \lambda\left(\bigcap_{k=1}^{+\infty} A_k\right) = \sum_{j=1}^{+\infty} \lambda(A_1 \cap \cdots \cap A_j \backslash A_1 \cap \cdots \cap A_{j+1}) = 0 \Rightarrow$$

$$\lambda(A^*) = 1,$$

where $A^* = \bigcap\limits_{k=1}^{+\infty} A_k$.

So, for arbitrary $x \in A^*$

$$\frac{\sum\limits_{k=1}^{n} \cos\left(2\pi h T^k(x)\right)}{n} \to 0, \quad n \to +\infty, \quad \forall h \in \mathbb{N}.$$

Similarly, we show that there exists a set B^* such that $\lambda(B^*) = 1$ and for arbitrary $x \in B^*$

$$\frac{\sum\limits_{k=1}^{n} \sin(2\pi h T^k(x))}{n} \to \int_0^1 \sin(2\pi h x)\mathrm{d}x = 0, \quad n \to +\infty, \ \forall h \in \mathbb{N}.$$

So, for everyone $x \in A^* \cap B^*$

$$\frac{\sum\limits_{k=1}^{n} \mathrm{e}^{2\pi i h T^k(x)}}{n} = \frac{\sum\limits_{k=1}^{n} \cos\left(2\pi h T^k(x)\right) + i \sum\limits_{k=1}^{n} \sin\left(2\pi h T^k(x)\right)}{n} \to 0,$$

$$n \to +\infty, \ \forall h \in \mathbb{N},$$

that is, the sequence $T^n(x)$ is evenly distributed on $[0;1]$. Because $\lambda(A^* \cap B^*) = 1$, we have needed. □

Theorem 4. *Let the number*

$$x = \Delta^{s}_{\alpha_1\alpha_2\ldots\alpha_n\ldots}$$

be normal in base s and let

$$\lim_{n\to\infty} q_{0n} = \tfrac{1}{s},$$

for a sequence of stochastic vectors $(q_{0n}; \ldots; q_{(s-1)n})$. Then the sequence (y_n) is a uniformly distributed on $[0,1]$, where $y_k = \Delta^{Q_s^*}_{\alpha_k\alpha_{k+1}\ldots}$ and the Q_s^*-representation of y_k defined by sequence of vectors $\mathbf{p}_n$.

Proof. Let $q_{0n} = \frac{1}{s} + S_n$ for every $n \in \mathbb{N}$. Then $\lim_{n\to\infty} S_n = 0$. Let $\varepsilon \in (0, 0.1)$ be a sufficiently small real number. Then there exists $k_0 \in \mathbb{N}$ such that

$$|S_n| < \varepsilon \quad \text{for all } n \geq k_0.$$

For arbitrary positive integers $m \geq k_0$ and l and an arbitrary binary vector $(j_1; j_2; \ldots; j_l)$ we have:

$$\tfrac{1}{s} - \varepsilon = \sqrt[l]{\left(\tfrac{1}{s} - \varepsilon\right)^l} < \sqrt[l]{q_{j_1(m+1)}q_{j_2(m+2)}\cdots q_{j_l(m+l)}} < \sqrt[l]{\left(\tfrac{1}{s} + \varepsilon\right)^l} = \tfrac{1}{s} + \varepsilon,$$

namely

$$\left|\sqrt[l]{q_{j_1(m+1)}\cdots q_{j_l(m+l)}} - \tfrac{1}{s}\right| < \varepsilon.$$

By the Lagrange theorem exists

$$z \in \left(\min\left(\tfrac{1}{s}; \sqrt[l]{q_{j_1(m+1)}\cdots q_{j_l(m+l)}}\right); \max\left(\tfrac{1}{s}; \sqrt[l]{q_{j_1(m+1)}\cdots q_{j_l(m+l)}}\right)\right)$$

that is

$$q_{j_1(m+1)}\cdots q_{j_l(m+l)} - \left(\tfrac{1}{s}\right)^l = lz^{l-1}\left(\sqrt[l]{q_{j_1(m+1)}\cdots q_{j_l(m+l)}} - \tfrac{1}{s}\right).$$

Because

$$lz^{l-1} < 0{,}51^{l-1}l,$$

then

$$\left|q_{j_1(m+1)}\cdots q_{j_l(m+l)} - \left(\tfrac{1}{s}\right)^l\right| < 0{,}51^{l-1}l\varepsilon.$$

At $m \geq k_0$ we have

$|y_m - \Delta^{s}_{\alpha_m\alpha_{m+1}\ldots\alpha_n\ldots}| \leq$

$\leq \beta_{\alpha_{m+1}(m+1)}\left|q_{\alpha_m m} - \frac{1}{s}\right| + \beta_{\alpha_{m+2}(m+2)}\left|q_{\alpha_m m}q_{\alpha_{m+1}(m+1)} - \frac{1}{s^2}\right| + \cdots < \varepsilon C,$

where

$$C = \sum_{j=1}^{+\infty} 0{,}51^{j-1}j.$$

So,

$$\lim_{n\to\infty}(y_m - \Delta^{s}_{\alpha_m\alpha_{m+1}\ldots\alpha_n\ldots}) = 0,$$

where it follows. □

References

[1] *Borel É.* Les probabiliés dénombrables et leurs applications arithmétiques. Rend. Circ. Mat. Palermo, 1909, 247–271.

[2] *Borel É.* Leçons sur la théorie des fonctions, 2nd ed. Paris: Gauthier Villars, 1914.

[3] *Niven I., Zuckerman H.S.* On the definition of normal numbers. Pacific J. Math., 1951, 1, 103–109.

[4] *Ries F.* Sur la théorie ergodique. Comment. Math. Helv., 1944/45, 17, 221–239.

[5] *Turbin A.F., Pratsiovytyi N.V.* Fractal sets, functions, distribution. Kiev: Science. opinion,1992. 208.

[6] *Titchmarsh E.* Theory of functions. Moscow: Science,1980. 464.

[7] *Weil H.* Über die Gibbs'sche Erscheinung und verwandte Konvergenzphänomene. Rend. Circ. Math.Palermo, 1910, 30, 377–407.

[8] *Weil H.* Über ein Problem aus dem Gebiete der diophantischen Approximationen. Nachr. Ges. Wiss. Göttingen, Math.-phys. Kl., 1914, 234–244.

[9] *Weil H.* Über die Gleichverteilung von Zahlen mod. Eins. Math. Ann., 1916, 77, 313–352.

(M. Pratsiovytyi) Institute of Mathematics of NAS of Ukraine, 3 Tereshchenkivska Str., Kyiv, 01004, Ukraine
Email: prats4444(at)gmail(dot)com
URL: https://www.imath.kiev.ua/people/profile.php?pid=170

(R. Kryvoshyia) Institute of Mathematics of NAS of Ukraine, 3 Tereshchenkivska Str., Kyiv, 01004, Ukraine
Email: kryvoshyia(at)imath(dot)kiev(dot)ua
URL: https://imath.kiev.ua/people/profile.php?pid=461

(O. Makarchuk) Volodymyr Vynnychenko Central Ukrainian State Pedagogical University, 1 Shevchenka Str., Kropyvnytskyi, 25000, Ukraine
Email: makolpet(at)gmail(dot)com
URL: https://cusu.edu.ua/en/kafedra-matematyky-ta-tsyfrovykhtekhnolohii/sklad-kafedri/15728-makarchuk-oleh-petrovych

STRUCTURAL AND SELF-SIMILAR PROPERTIES OF REPRESENTATIONS OF ONE CLASS OF FRACTAL FUNCTIONS AND DISTRIBUTIONS OF THEIR VALUES

Mykola Pratsiovytyi and Sofiia Ratushniak (*Ukraine*)

Abstract. We consider the Q_2-representation of numbers from the interval $[0;1]$, defined by parameters $q_0, q_1 \in (0;1)$, and expansion of an arbitrary number $x \in [0;1]$ by the series

$$x = \alpha_1 q_{1-\alpha_1} + \sum_{k=2}^{\infty} (\alpha_k q_{1-\alpha_k} \prod_{j=1}^{k-1} q_{\alpha_j}(x)) \equiv \Delta^{Q_2}_{\alpha_1\alpha_2\ldots\alpha_n\ldots},$$

where $\alpha_k \in \{0,1\} \equiv A$, $q_0 + q_1 = 1$. We study structural, local, and global topological, metric, and fractal properties of the function defined by the equality

$$f_{\overline{\varphi}}(x = \Delta^{Q_2}_{\alpha_1\alpha_2\alpha_3\ldots\alpha_n\alpha_{n+1}}) = \Delta^{Q_2}_{\varphi_1(\alpha_1,\alpha_2)\varphi_2(\alpha_2,\alpha_3)\ldots\varphi_n(\alpha_n,\alpha_{n+1})\ldots},$$

where $\overline{\varphi} = (\varphi_n)$ is a given sequence of functions $(\varphi : (0;1)^2 \to (0;1))$. For a random variable $Y = F(X)$, where X is a random variable with a given distribution, we investigate the Lebesgue structure and spectral properties.

Introduction

One of the scale-invariant continuous generalizations of the classical binary representation [3] of numbers in the interval $[0,1]$ is the two-symbol $A \equiv \{0;1\}$ multibasic Q_2^*-representation [2] that is defined by a positive infinite numerical sequence

$$(q_{0k}) = (q_{01}, q_{02}, ..., q_{0k}, ...),\ 0 < q_{0k} < 1,\ \prod_{k=1}^{\infty} \max\{q_{0k}, 1 - q_{0k}\} = 0,$$

and is given by

$$x = \alpha_1 q_{1-\alpha_1,1} + \sum_{k=2}^{\infty} (\alpha_k q_{1-\alpha_k,k} \prod_{j=1}^{k-1} q_{\alpha_j,j}) \equiv \Delta^{Q_2^*}_{\alpha_1\alpha_2\ldots\alpha_k\ldots}, \tag{1}$$

where $q_{1k} \equiv 1 - q_{0k}$, $(\alpha_k) \in L = A \times A \times ...$ (further, $\alpha_k q_{1-\alpha_k,k} \equiv \beta_{\alpha_k,k}$).

Received February 25, 2020.
2010 *Mathematics Subject Classification.* Primary 26A30.
Key words and phrases. Q_2^*-representation of numbers, Q_2-representation of numbers, fractal functions, Cantor type set.

The abbreviated (symbolic) notation $\Delta^{Q_2^*}_{\alpha_1\alpha_2\ldots\alpha_k\ldots}$ in identity (1) is called the Q_2^*-representation of x. At the same time, α_k is called the k-th digit of this representation. Most numbers in the interval $[0,1]$ have a unique Q_2^*-representation, we call them Q_2^*-*unary* numbers. And only the numbers of a countable set have two Q_2^*-representation and are called Q_2^*-*binary* numbers. Their representations have the following form: $\Delta^{Q_2^*}_{c_1c_2\ldots c_{m-1}1(0)}$ and $\Delta^{Q_2^*}_{c_1c_2\ldots c_{m-1}0(1)}$. For Q_2^*-unary numbers, the function $\alpha_k = \alpha_k(x)$ is well-defined, but for Q_2^*-binary numbers it is not so.

If $q_{0k} = q_0$ for any $k \in N$, then the Q_2^*-representation coincides with the Q_2-representation, and if $q_{0k} = \frac{1}{2}\ \forall k \in N$, then the Q_2^*-representation is the classical binary representation. The geometry of the Q_2^*-representation was described in [3] and depends on properties of its cylindrical sets.

A cylinder of rank m with base $c_1c_2\ldots c_m$ is called the set $\Delta^{Q_2^*}_{c_1c_2\ldots c_m}$ of all points $x \in [0,1]$, which have Q_2^*-representation $\Delta^{Q_2^*}_{c_1c_2\ldots c_m\alpha_{m+1}\alpha_{m+2}\ldots}$, $\alpha_{m+i} \in A$. Cylinder $\Delta^{Q_2^*}_{c_1c_2\ldots c_m}$ is the interval $[a,b]$ with endpoints

$$a = \beta_{c_1,1} + \sum_{k=2}^{\infty}(\beta_{c_k,k}\prod_{j=1}^{k-2} q_{c_j,j}), \quad b = a + \prod_{j=1}^{m} q_{c_j,j}.$$

We consider two Q_2^*-representations of numbers defined by the sequences (q_{0k}) and (g_{0k}), respectively (we will call the second G_2^*-representation), and the sequence $\overline{\varphi} \equiv (\varphi_k)$ of finite functions $\varphi_k : A \times A \to A$.

We consider the function defined by

$$f_{\overline{\varphi}}(\Delta^{Q_2^*}_{\alpha_1\alpha_2\ldots\alpha_k\ldots}) = \Delta^{G_2^*}_{\varphi_1(\alpha_1,\alpha_2)\varphi_2(\alpha_2,\alpha_3)\ldots\varphi_k(\alpha_k,\alpha_{k+1})\ldots}, \tag{2}$$

which maps $[0;1]$ onto $[0;1]$. Function $f_{\overline{\varphi}}$ is well-defined if and only if the expression (2) takes the same value for distinct Q_2^*-representations of binary numbers. It is easy to indicate an example of such sets $c_1c_2\ldots c_k$, where the inequality $f_{\overline{\varphi}}(\Delta^{Q_2^*}_{c_1c_2\ldots c_k0(1)}) \neq f_{\overline{\varphi}}(\Delta^{Q_2^*}_{c_1c_2\ldots c_k1(0)})$ holds. It is possible to ensure that the function is well-defined by agreeing to use only the representation that has period (0). Note that the number 1 has the unique Q_2^*-representation $\Delta^{Q_2^*}_{(1)}$.

There are exactly 16 distinct functions φ_k: $A \times A \to A$.

It is convenient to associate the function φ_k with a matrix $\begin{pmatrix} a_{00}^{(k)} & a_{01}^{(k)} \\ a_{10}^{(k)} & a_{11}^{(k)} \end{pmatrix}$, whose elements are either 0 or 1", namely, $a_{ij}^{(k)} = \varphi_k(i,j) \in A$. Then each

of the functions $f_{\overline{\varphi}}$ can be associated with a sequence of matrices

$$M_k = \begin{pmatrix} a_{00}^{(k)} & a_{01}^{(k)} \\ a_{10}^{(k)} & a_{11}^{(k)} \end{pmatrix}.$$

Next, we define a group operation $*$ on matrices

$$M * M' = \begin{pmatrix} a_{00} & a_{01} \\ a_{10} & a_{11} \end{pmatrix} * \begin{pmatrix} a'_{00} & a'_{01} \\ a'_{10} & a'_{11} \end{pmatrix} = \begin{pmatrix} d_{00} & d_{01} \\ d_{10} & d_{11} \end{pmatrix},$$

where $d_{ij} = |a_{ij} - a'_{ij}|$. As a result, we obtain the commutative group of matrices. Indeed, the identity element is the 2×2 zero matrix (the trivial function $f_{\overline{\varphi}} = 0$ corresponds to this matrix with a constant sequence $\overline{\varphi}$). Each function in this group is self-inverse. The operation on matrices generates a group of functions $\varphi : A \times A \to A$, and this induces a group S of functions $f_{\overline{\varphi}}$ for a constant sequence of functions $\overline{\varphi}$. At the same time, the result of the operation on a pair of dual functions φ and $\widetilde{\varphi} = 1 - \varphi$ is the trivial function $f_{\overline{\varphi}} = 1$, which corresponds to a matrix with elements equal to 1. Each function in this group is symmetric (inverse) to itself.

There are 8 pairs of dual functions among the 16 functions φ, that have at first glance "similar" properties and are determined with accuracy up to "symmetry" of digits. These are f_φ functions generated by the following functions:

$$\varphi_{[1]}(i,j) = \begin{cases} 0, \text{if } i \cdot j = 0, \\ 1, \text{if } i \cdot j \neq 0; \end{cases} \qquad \varphi_{[2]}(i,j) = \begin{cases} 0, \text{if } i(i+j) \neq 1, \\ 1, \text{if } i(i+j) = 1; \end{cases}$$

$$\varphi_{[3]}(i,j) = \begin{cases} 0, \text{if } i(i+j) = 0, \\ 1, \text{if } i(i+j) \neq 0; \end{cases} \quad \varphi_{[4]}(i,j) = \begin{cases} 0, \text{if } j(i+j) \neq 1, \\ 1, \text{if } j(i+j) = 1; \end{cases}$$

$$\varphi_{[5]}(i,j) = \begin{cases} 0, \text{if } j(i+j) = 0, \\ 1, \text{if } j(i+j) \neq 0; \end{cases} \quad \varphi_{[6]}(i,b) = \begin{cases} 0, \text{if } i = j, \\ 1, \text{if } i \neq j; \end{cases}$$

$$\varphi_{[7]}(i,j) = \begin{cases} 0, \text{if } i + j = 0, \\ 1, \text{if } i + j \neq 0; \end{cases}$$

or $\varphi_{[1]}(i,j) = i \cdot j$, $\varphi_{[2]}(i,j) = |i-j|i$, $\varphi_{[3]}(i,j) = i$, $\varphi_{[4]}(i,j) = |i-j|j$,

$\varphi_{[5]}(i,j) = j$, $\varphi_{[6]}(i,j) = |i-j|$, $\varphi_{[7]}(i,j) = i \cdot j + |i-j|$,
and their doubles.

1. Individual cases

Lemma 1. *For the function $f_{\overline{\varphi}}$ to be constant $c = \Delta^{G_2^*}_{c_1 c_2 \ldots c_n \ldots}$ it is necessary and sufficient that $\varphi_n(a,b) = c_n$ for all $n \in N$ and $(a,b) \in A_2 \times A_2$.*

Proof. Necessity. Since the equality $f_{\overline{\varphi}}(x) = \Delta^{G_2^*}_{c_1c_2\ldots c_n\ldots}$ holds for any $x \in [0,1]$, i.e.,

$$\begin{cases} \varphi_1(\alpha_1(x), \alpha_2(x)) = c_1 \text{ for } \forall(\alpha_1, \alpha_2) \in A \times A; \\ \varphi_2(\alpha_2(x), \alpha_3(x)) = c_2 \text{ for } \forall(\alpha_2, \alpha_3) \in A \times A; \\ \ldots\ldots\ldots\ldots\ldots\ldots\ldots\ldots\ldots\ldots\ldots\ldots \\ \varphi_n(\alpha_n(x), \alpha_{n+1}(x)) = c_n \text{ for } \forall(\alpha_n, \alpha_{n+1}) \in A \times A; \\ \ldots\ldots\ldots\ldots\ldots\ldots\ldots\ldots\ldots\ldots\ldots\ldots, \end{cases}$$

we get the identity $\varphi_n(a,b) = c_n$ for any $(a,b) \in A \times A$.

Sufficiency. If $\varphi_n(a,b) = c_n$ for any $n \in N$ and for each pair $(a,b) \in A \times A$, then

$$\begin{aligned} f_{\overline{\varphi}}(x = \Delta^{Q_2^*}_{\alpha_1(x)\alpha_2(x)\ldots\alpha_n(x)\ldots}) &= \Delta^{G_2^*}_{\varphi_1(\alpha_1,\alpha_2)\varphi_2(\alpha_2,\alpha_3)\ldots\varphi_n(\alpha_n,\alpha_{n+1})\ldots} = \\ &= \Delta^{G_2^*}_{c_1c_2\ldots c_n\ldots} = c. \end{aligned}$$

The sufficiency and the entire lemma are proven. □

Corollary 1. *There exists a continuum set S of continuous functions $f_{\overline{\varphi}}$ that are constants. Moreover, for any $c \in [0;1]$ there exists $f_{\overline{\varphi}} \in S$ such that $f_{\overline{\varphi}}(x) = c$.*

Definition 1. A function $f_{\overline{\varphi}}$ such that $\varphi_n(a,b) = a$ for any $n \in N$ is called quasi-identical (Q_2^*-G_2^*)-transformation of the interval $[0;1]$.

Remark 1. The argument for choosing the term «quasi-identical (Q_2^*-G_2^*)-transformation» is the fact that $f_{\overline{\varphi}}(x) = x$ provided that $G_2^* = Q_2^*$, i.e., $q_{0n} = g_{0n}$ for any $n \in N$.

Lemma 2. *If $\varphi_n(a,b) = a$ for any $n \in N$, i.e., $f_{\overline{\varphi}}(\Delta^{Q_2^*}_{\alpha_1\alpha_2\ldots\alpha_n\ldots}) = \Delta^{G_2^*}_{\alpha_1\alpha_2\ldots\alpha_n\ldots}$, then $f_{\overline{\varphi}}$ is a continuous, strictly increasing distribution function F_ξ of a random variable $\xi = \Delta^{Q_2^*}_{\xi_1\xi_2\ldots\xi_n\ldots}$. The digits (ξ_n) of its Q_2^*-representation are independent and have distributions*

$$P\{\xi_n = 0\} = g_{0n}, \quad P\{\xi_n = 1\} = g_{1n}.$$

The function F_ξ is either absolutely continuous or singular.

Indeed, the expression for the distribution function F_ξ of the random variable ξ has a G_s^*-expansion (representation). A more detailed justification can be found in the article [13], where other properties of this function, such as differential property, were also studied. The function belongs to the pure Lebesgue type, and the criteria for absolute continuity and singularity are established. In general, the differential properties of the function F_ξ are quite complex.

2. Sets of value class functions **S**

Lemma 3. *If in the sequence (φ_n) the function φ_m is a constant i, then the set of values of the function $f_{\overline{\varphi}} \in S$ is a subset of the union of m-th rank cylinders, namely,*

$$E_{f_{\overline{\varphi}}} \subset \bigcup_{c_1 \in A_2} \bigcup_{c_2 \in A_2} \dots \bigcup_{c_{m-1} \in A_2} \Delta^{G_2^*}_{c_1 c_2 \dots c_{m-1} i}. \tag{3}$$

Proof. Let (φ_n) be a sequence that satisfies the conditions of the statement, and let $f_{\overline{\varphi}}$ be its corresponding function. Since $\varphi_m(a,b) = i$ for any pair (a,b), then m-th digit is the G_2^*-representation of the values of the function $f_{\overline{\varphi}}$ is not equal to $1-i$. This implies the inclusion (3). □

Corollary 2. *If there is an infinite subsequence of constants among the functions of the sequence (φ_n), then the set of values of $f_{\overline{\varphi}}$ is a subset of a Cantor-type set $C[G_2^*, V_k]$, where*

$$V_k = \begin{cases} A_2, & \text{if } \varphi_k(a;b) - \text{is not a constant;} \\ \{j_k\}, & \text{if } \varphi_k(a,b) = j_k. \end{cases}$$

3. Continuity of functions of class S

Lemma 4. *Every function $f_{\overline{\varphi}}$ of class S is continuous on the set Q_2^*-unary numbers.*

Proof. To prove continuity at a Q_2^*-unary point $x = \Delta^{Q_2^*}_{\alpha_1\alpha_2\alpha_3\dots\alpha_n\dots}$ of the interval $[0;1]$, we must show that

$$\lim_{x' \to x} |f_{\overline{\varphi}}(x') - f_{\overline{\varphi}}(x)| = 0. \tag{4}$$

Since $x' \neq x$, there exists a number m such that $\alpha_m(x') \neq \alpha_m(x)$ and $\alpha_i(x') = \alpha_i(x)$ for all $i < m$. Then condition $x' \to x$ is equivalent to $m \to \infty$. Without loss of generality, let's assume that $\alpha_m(x) = 1$, which implies $\alpha_m(x') = 0$.

Consider the difference of the values of $f_{\overline{\varphi}}$ at points x and x':

$$\begin{aligned} f_{\overline{\varphi}}(x) - f_{\overline{\varphi}}(x') &= f_{\overline{\varphi}}(\Delta^{Q_2^*}_{\alpha_1\alpha_2\dots\alpha_{m-1}1\alpha_{m+1}\dots}) - f_{\overline{\varphi}}(\Delta^{Q_2^*}_{\alpha_1\alpha_2\dots\alpha_{m-1}0\alpha'_{m+1}\dots}) = \\ &= \Delta^{G_2^*}_{\varphi_1(\alpha_1,\alpha_2)\dots\varphi_{m-1}(\alpha_{m-1},1)\varphi_m(1,\alpha_{m+1})\dots} - \\ &- \Delta^{G_2^*}_{\varphi_1(\alpha_1,\alpha_2)\dots\varphi_{m-1}(\alpha_{m-1},0)\varphi_m(0,\alpha'_{m+1})\dots} = \prod_{j=1}^{m-2} g_{\varphi_j(\alpha_j,\alpha_{j+1}),j} \cdot A, \end{aligned}$$

where $|A| \le 1$. Then $\lim\limits_{m\to\infty} \prod\limits_{j=1}^{m-2} g_{\varphi_j(\alpha_j,\alpha_{j+1}),j} = 0$. Consequently,

$$A \prod_{j=1}^{m-2} g_{\varphi_j(\alpha_j,\alpha_{j+1}),j} \to 0,$$

as $m \to \infty$ that proves the equality $\lim\limits_{x'\to x} |f_{\overline{\varphi}}(x') - f_{\overline{\varphi}}(x)| = 0$. □

Theorem 1. *For the function $y = f_{\overline{\varphi}}(x)$ to be continuous, it is necessary and sufficient that its values at two distinct representations Q_2^*-binary numbers coincide, i.e.,*

$$f_{\overline{\varphi}}(\Delta^{Q_2^*}_{c_1\ldots c_m 0(1)}) = f_{\overline{\varphi}}(\Delta^{Q_2^*}_{c_1\ldots c_m 1(0)}), \tag{5}$$

for any sequence of digits $(c_1, ..., c_m)$ consisting of zeros and ones.

Proof. Let $x_0 = \Delta^{Q_2^*}_{c_1\ldots c_m 0(1)} = \Delta^{Q_2^*}_{c_1\ldots c_m 1(0)}$ be a Q_2^*-binary point.
1. Necessity. If a function $f_{\overline{\varphi}}$ is continuous at a point x_0, i.e.,

$$\lim_{x\to x_0} f_{\overline{\varphi}}(x) = f_{\overline{\varphi}}(x_0),$$

then it is continuous from the left and from the right at this point. Consider the sequence $x_n = \Delta^{Q_2^*}_{c_1\ldots c_m 0\underbrace{1\ldots 1}_{n}(0)} \to x_0 - 0$ $(n \to \infty)$. Then

$$\lim_{n\to\infty} f_{\overline{\varphi}}(x_n) = f_{\overline{\varphi}}(x_0) = f_{\overline{\varphi}}(\Delta^{Q_2^*}_{c_1\ldots c_m 0(1)}).$$

Now consider the sequence $\overline{x}_n = \Delta^{Q_2^*}_{c_1\ldots c_m \underbrace{0\ldots 0}_{n}1(0)} \to x_0 + 0$. Then

$$\lim_{n\to\infty} f_{\overline{\varphi}}(\overline{x}_n) = \lim_{n\to\infty} f_{\overline{\varphi}}(\Delta^{Q_2^*}_{c_1\ldots c_m \underbrace{0\ldots 0}_{n}1(0)}) = f_{\overline{\varphi}}(x_0) = f_{\overline{\varphi}}(\Delta^{Q_2^*}_{c_1\ldots c_m 1(0)}).$$

Thus, equality (5) holds.

2. Sufficiency. Now we will prove that the continuity of $f_{\overline{\varphi}}$ at the point x_0 follows from the condition

$$f_{\overline{\varphi}}(x_0) = f_{\overline{\varphi}}(\Delta^{Q_2^*}_{c_1\ldots c_m 0(1)}) = f_{\overline{\varphi}}(\Delta^{Q_2^*}_{c_1\ldots c_m 1(0)}) \tag{6}$$

First, we prove left-hand continuity at the point x_0. To do this, consider a number $x < x_0$ that is sufficiently close to x_0, spesifically $x = \Delta^{Q_2^*}_{c_1\ldots c_m 0\underbrace{1\ldots 1}_{n}\alpha_{m+n+2}\alpha_{m+n+3}\ldots}$. The modulus of the difference is

$$\delta \equiv |f_{\overline{\varphi}}(x_0) - f_{\overline{\varphi}}(x)| = A_n |\omega^{m+n+1}(f_{\overline{\varphi}}(x)) - \omega^{m+n+1}(f_{\overline{\varphi}}(x_0))|,$$

where $A_n = g_{\varphi_m(c_m,0),m} g_{\varphi_{m+1}(0,1),m+1} \prod\limits_{j=1}^{m-1} g_{\varphi_j(c_j,c_{j+1}),j} \prod\limits_{i=1}^{n} g_{\varphi_{m+1+i}(1,1),m+1+i}$.

Since $x \to x_0 \Leftrightarrow n \to \infty$ is equivalent to $n \to \infty$ and $A_n \to 0$ as $n \to \infty$, then $\delta \to \infty$. This proves the left-hand continuity of the function $f_{\overline{\varphi}}$ at the point x_0.

Similar considerations justify the right-hand continuity of the function at the point x_0. In this case, an arbitrary $x > x_0$ sufficiently close to x_0 is considered, namely: $x = \Delta^{Q_2^*}_{c_1 \ldots c_m 1 \underbrace{0 \ldots 0}_{n} \alpha_{m+n+2} \alpha_{m+n+3} \ldots}$. □

Theorem 2. *If the function $f_{\overline{\varphi}}$ is continuous at every point of the interval $[0, 1]$, then it is either an identity transformation, an inversor, or a constant.*

Proof. Since $f_{\overline{\varphi}}$ is continuous on $[0, 1]$, then according to the previous theorem, it is continuous at every Q_2^*-binary point. This means that

$$f_{\overline{\varphi}}(\Delta^{Q_2^*}_{\alpha_1 \alpha_2 \ldots \alpha_{n-1} 0(1)}) = f_{\overline{\varphi}}(\Delta^{Q_2^*}_{\alpha_1 \alpha_2 \ldots \alpha_{n-1} 1(0)}), n \in N.$$

It follows that for any $n \in N$ the equalities hold

$$\varphi_n(0,1) = \varphi_n(1,0) = \varphi_n(0,0) = \varphi_n(1,1) \text{ or}$$
$$\varphi_n(0,1) \neq \varphi_n(1,0) = \varphi_n(0,0) \neq \varphi_n(1,1).$$

In the first case, $\varphi(a, b) = Const$. In the second case, each of the functions φ_n is given by a matrix $\begin{pmatrix} i & i \\ j & j \end{pmatrix}$, where $\varphi_n(0,1) = \varphi_n(0,0) = i$, $\varphi_n(1,0) = \varphi_n(1,1) = j$, $i, j \in A$. Such functions correspond to the identity transformation $y = f_{\overline{\varphi}}(x) = x$ and $y = I(x)$. Therefore, the set of continuous functions of class S is exhausted by constants, the identity transformation, and the inversor. □

Corollary 3. *Functions of class S are continuous on the set of Q_2-unary numbers and discontinuous on the set of Q_2-binary numbers, unless they are continuous everywhere.*

4. Level sets of functions of class S

Let $q_{0k} = g_{0k} = q_0$. Recall that a level set of a function f for a given value $y_0 \in E_f$ is the set of all points of the domain that are mapped to y_0. Formally, this can be written as $f^{-1}(y_0) \equiv \{x : f(x) = y_0\}$.

Theorem 3. *The level set of functions $f_{\overline{\varphi}}$, where $\varphi_n = \varphi$ for all $n \in N$, is either a finite or continuous set. Moreover,*
1) if $E_{f_{\overline{\varphi}}} = \{i\}, i \in A$, then the set $f^{-1}_{\overline{\varphi}}(y_0)$ has cardinality continuum;
2) if $E_{f_{\overline{\varphi}}} = [0; 1]$, then the set $f^{-1}_{\overline{\varphi}}(y_0)$ is a singleton or consists of only two points x_0 and $I(x_0)$, where $I(\Delta^{Q_2}_{\alpha_1 \ldots \alpha_n \ldots}) = \Delta^{Q_2}_{[1-\alpha_1] \ldots [1-\alpha_n] \ldots}$;
3) if $E_{f_{\overline{\varphi}}} = [Q_2, V]$, then the set $f^{-1}_{\overline{\varphi}}(y_0)$ is a finite or continuum set.

Proof. We will prove this theorem case by case.

1) By the definition of the function, if $E_{f_{\overline{\varphi}}} = \{y_0\}$ then $f_{\overline{\varphi}}(x) = y_0$ for all $x \in [0,1]$. Therefore, the level set $f^{-1}_{\overline{\varphi}}(y_0)$ is the entire interval $[0;1]$, that has cardinality continuum.

2) If $E_{f_{\overline{\varphi}}} = [0;1]$, then the functions $f_{\overline{\varphi}}$ is exhausted by the identity function $f_{\overline{\varphi_{[6]}}}$, $y = x$, the left-shift operator $w(x)$ and their inversors. For the identity function $y = x$, it is obvious that every image has a unique preimage. For the left-shift operator $y = w(x)$, the function is defined as: $\forall x \in [0;1)$: $f_{\overline{\varphi}}(x = \Delta^{Q_2}_{\alpha_1\alpha_2\ldots\alpha_n\ldots}) = w(x) = y = \Delta^{Q_2}_{\alpha_2\ldots\alpha_n\ldots}$. For any given output y, the set of preimages is $f^{-1}_{\overline{\varphi}} = \{\Delta^{Q_2}_{1\alpha_2\ldots\alpha_n\ldots}, \Delta^{Q_2}_{0\alpha_2\ldots\alpha_n\ldots}\}$. Thus, the level sets of the left-shift operator consist of two points. In the case of $f_{\overline{\varphi_{[6]}}}$, due to the function's symmetry with respect to the inversor meaning that $f_{\overline{[\varphi_6]}}(x) = f_{\overline{[\varphi_6]}}(I(x))$, each Q_2-unary level consists of two points. Each Q_2-binary level consists of a single point because we exclude representations that contain an infinite sequence of 1 (i.e., we avoid representations with a repeating period (1)).

3) If $E_{f_{\overline{\varphi}}} = [Q_2, V]$, then the function defining $f_{\overline{\varphi}}$ is given by:

$$\varphi(\alpha_k, \alpha_{k+1}) = \varphi(\overline{\alpha}_k, \alpha_{k+1}) = \varphi(\overline{\alpha}_k, \overline{\alpha}_{k+1}) = i,\ \varphi(\alpha_k, \overline{\alpha}_{k+1}) = 1 - i.$$

Then for an arbitrary $y = \Delta^{Q_2}_{c_1c_2\ldots c_m\ldots} \in E_{f_{\overline{\varphi}}}$, the level set has form

$$f^{-1}_{\overline{\varphi}}(y) = \{x := \Delta^{Q_2}_{a_1a_2\ldots a_m\ldots}, \varphi(a_m, a_{m+1}) = c_m\}.$$

For every $x \in f^{-1}_{\overline{\varphi}}(y)$ we establish a correspondence to a number $z \in [0;1]$, where $z = \sum\limits_{k=1}^{\infty} \frac{z_k}{2^k}$, according to the following rule:

$$\begin{cases} z_n = 0, \text{ if for any } a_n \text{ we have } \varphi(a_n, a_{n+1}) = i, \\ z_n = 1, \text{ if only for } \overline{a}_n \text{ we have } \varphi(\overline{a}_n, a_{n+1}) = 1 - i. \end{cases}$$

In this way, the correspondence between the level set $f^{-1}_{\overline{\varphi}}$ and the unit interval $[0,1]$ is established. Therefore, the level set $f^{-1}_{\overline{\varphi}}(y)$ is continuum set. Examples of finite level sets are provided in the article [8]. The theorem is proved. □

References

[1] *Vasylenko N. A., Prasiovyyi M. V.* One family of continuous nowhere monotonic functions with fractal properties// Mykhailo Drahomanov Natl. Pedagog. Univ. Ser. 1. Phys. Math. 2013. — № 14. — P. 176—189. (in Ukrainian).

[2] *Pratsiovytyi M. V.* Random variables with independent Q_2-symbols// Asymptotic methods in the study of stochastic models, Inst. Math. Natl. Acad. Sci. Ukraine, Kyiv, 1987, pp. 92–102 (in Russian).

[3] *Pratsiovyyi M. V.* The geometry of the classical binary representation of real numbers. Mykhailo Drahomanov Natl. Pedagog. Univ. Publ., Kyiv, 2012. — 68 p.(in Ukrainian).

[4] *Pratsiovytyi M. V.* Fractal properties of distributions of random variables whose Q_2-signs form a homogeneous Markov chain // Asymptotic analysis of random evolutions. — Inst. Math. Natl. Acad. Sci. Ukraine, Kyiv, 1994 — C. 245–254. (in Ukrainian).

[5] *Pratsiovyyi M.V., Vasylenko N. A.* Probability distributions on graphs of the same class are nowhere differentiable functions // Proceedings of the IPMM of the National Academy of Sciences of Ukraine — 2013. — Том 26. — C. 159–171. (in Ukrainian).

[6] *Pratsiovytyi M. V., Panasenko O. B.* Fractal properties of one class one-parameter continuous non-differentiable functions // Mykhailo Drahomanov Natl. Pedagog. Univ. Ser. 1. Phys. Math., 2006. — №7. — P. 160–167. (in Ukrainian).

[7] *Pratsiovytyi M.V., Kalashnikov A.V.* Self-affine singular and nowhere monotone functions related to the Q-representation of real numbers, Ukrainian Math. J. 65 (2013), no. 3, 448–462.(in Ukrainian).

[8] *Pratsiovytyi M. V., Ratushniak S. P.* Distribution of values of one fractal function of a random argument // Mykhailo Drahomanov Natl. Pedagog. Univ. Ser. 1. Phys. Math., 2014. — 16(2). — P. 150–160. (in Ukrainian).

[9] *Prats'ovytyi M.V., Svynchuk O.V.* Spread of values of a Cantor-type fractal continuous nonmonotone function. // Journal of Mathematical Sciences, Vol. 240, No. 3, July, 2019 pp. 342 – 357. (in Ukrainian).

[10] *Pratsiovytyi M. V., Skrypnyk S. V.* Q_2-representation of fraction part of real numbers and inversor of their digits // Mykhailo Drahomanov Natl. Pedagog. Univ. Ser. 1. Phys. Math., 2013. — 15. — P. 134–143. (in Ukrainian).

[11] *Albeverio S., Pratsiovytyi M., Torbin G.* Fractal probability distributions and transformations preserving the Hausdorff-Besicovitch dimension // Ergod.Th. & Dynam. Sys. — 2004, 24. — P. 1–16.

[12] M. V. Pratsiovytyi, *Fractal approach to investigation of singular probability distributions*, Mykhailo Drahomanov Natl. Pedagog. Univ. Publ., Kyiv, 1998 (in Ukrainian).

[13] A. F. Turbin and M. V. Pratsiovytyi, *Fractal sets, functions, and probability distributions*, Nauk. Dumka, Kyiv, 1992 (in Russian).

(M. Pratsiovytyi) Institute of Mathematics of NAS of Ukraine, Ukraine
Email: prats4444(at)gmail(dot)com

(S. Ratushniak) Institute of Mathematics of NAS of Ukraine, Ukraine
Email: ratush404(at)gmail(dot)com

SCALE-INVARIANT FUNCTIONS GIVEN BY THE CONTINUED A_2-REPRESENTATION OF NUMBERS

Mykola Pratsiovytyi, Sofiia Ratushniak, Oxana Trebenko, and Serhii Dmytrenko (*Ukraine*)

Abstract. In this paper, we study the structural, variational, and fractal properties of a function defined on the interval $[\frac{1}{2};1]$ by

$$f(x=\cfrac{1}{a_1+\cfrac{1}{a_2+\ldots}}):=\prod_{k=1}^{\infty}\lambda_k^{\alpha_k(x)},$$

where $a_k\in\{\frac{1}{2};1\}, \alpha_k=2a_k-1$ for $k\in\mathbb{N}$, (λ_k) is a sequence of positive real numbers such that the product $\prod\limits_{k=1}^{\infty}\lambda_k$ is absolutely convergent. We also prove that f is continuous on $[\frac{1}{2};1]$ if and only if $\lambda_k=e^{\frac{c(-1)^{k-1}}{2^{k-1}}}$ for some $c\in\mathbb{R}$ and all $k\in\mathbb{N}$.

Introduction

Let $A\equiv\{0;1\}$ be an alphabet, and $L\equiv A\times A\times\ldots$ denote the space of sequences consisting of elements from the alphabet A (zeros and ones). Analogously, let $A_2\equiv\{\frac{1}{2};1\}$, and $L_2\equiv A_2\times A_2\times\ldots$.

It is known [2] that for any $x\in[\frac{1}{2};1]$ there exists a sequence $(a_k)\in L_2$ such that

$$x=\cfrac{1}{a_1+\cfrac{1}{a_2+\ldots}}\equiv[0;a_1,a_2,\ldots,a_k,\ldots]. \tag{1}$$

The infinite continued fraction (1) is termed continued A_2-fraction, and its short symbolic representation $[0;a_1,a_2,\ldots,a_k,\ldots]$ is called A_2-representation of the number x. Some numbers have two A_2-representations, since $[0;a_1,a_2,\ldots,a_m,\frac{1}{2},(\frac{1}{2},1)]=[0;a_1,a_2,\ldots,a_m,1,(1,\frac{1}{2})]$, where the

Received December 10, 2021.
2010 *Mathematics Subject Classification.* Primary 11A67; Secondary 26A30.
Key words and phrases. two-symbol encoding of numbers, continued A_2-fraction, A_2-unary and A_2-binary numbers, absolutely convergent infinite product, function with fractal properties.

parentheses mean periodicity. All other numbers have a unique A_2-representation. From now on, numbers with two representations are referred to as A-binary, while those with a unique representation are termed A-unary.

A_2-representation can be easily recoded by using alphabet A as follows:

$$x = [0; a_1, a_2, \ldots, a_k, \ldots] \equiv \Delta^A_{\alpha_1\alpha_2\ldots\alpha_k\ldots},$$

where $\alpha_k = 2a_k - 1$ for $k \in \mathbb{N}$. The new representation is known as *A-representation of number x*.

Next, we define A-cylinder of rank m, with a base $c_1 \ldots c_m$, as the set $\Delta^A_{c_1\ldots c_m} = \{x \mid x = \Delta^A_{c_1\ldots c_m\beta_1\beta_2\ldots},\ (\beta_n) \in L\}$.

The properties below follow directly from the definition of A-cylinder:

1) $\Delta^A_{c_1\ldots c_m} = \Delta^A_{c_1\ldots c_m 0} \cup \Delta^A_{c_1\ldots c_m 1}$.
2) The A-cylinder $\Delta^A_{c_1\ldots c_m}$ is a closed interval with endpoints $\Delta^A_{c_1\ldots c_m(01)}$ and $\Delta^A_{c_1\ldots c_m(10)}$, where the left or right endpoint depends on whether m is even or odd.
3) The length of $\Delta^A_{c_1\ldots c_m}$ can be calculated by the formula

$$|\Delta^A_{c_1\ldots c_m}| = \frac{1}{(q_{m-1} + q_m)(q_{m-1} + 2q_m)} \le \frac{1}{q^2_{m-1}},$$

where q_m is the denominator of the m-th rank convergent finite A_2-fraction, i.e., the denominator of the rational number given by the expression $[0; a_1, a_2, \ldots, a_m]$, which can be calculated by the recurrence relations $q_0 = 1, \quad q_1 = a_1, \quad q_{n+1} = a_{n+1}q_n + q_{n-1}$, where $a_n = \frac{c_n+1}{2}$.
4) The main metric relation takes form

$$\frac{|\Delta^A_{c_1\ldots c_m c}|}{|\Delta^A_{c_1\ldots c_m}|} = \frac{1 + a\frac{q_{m-1}}{q_m}}{2a^2 + 1 + 2a\frac{q_{m-1}}{q_m}},\ a = \frac{c+1}{2},$$

where c is an arbitrary digit. In a particular case, we have

$$\frac{|\Delta^A_{c_1\ldots c_m 0}|}{|\Delta^A_{c_1\ldots c_m}|} = \frac{2 + \frac{q_{m-1}}{q_m}}{3 + 2\frac{q_{m-1}}{q_m}}, \quad \frac{|\Delta^A_{c_1\ldots c_m 1}|}{|\Delta^A_{c_1\ldots c_m}|} = \frac{1 + \frac{q_{m-1}}{q_m}}{3 + 2\frac{q_{m-1}}{q_m}}.$$

1. One class of scale-invariant functions and their structural properties

Consider a class of functions defined by equality

$$f(x = \Delta^A_{\alpha_1\alpha_2\ldots\alpha_k\ldots}) := \prod_{k=1}^{\infty} \lambda_k^{\alpha_k(x)}, \tag{2}$$

where $\Delta^A_{\alpha_1\alpha_2\ldots\alpha_k\ldots}$ is the A-representation of number x, and (λ_k) is a predefined sequence of positive numbers such that the infinite product $P \equiv \prod\limits_{k=1}^{\infty} \lambda_k$ is absolutely convergent. Similar functions were actively studied by B. Sendov in his work [10] for the case where x is represented by its binary representation.

Let's recall that an infinite product $\prod\limits_{k=1}^{\infty} \lambda_k \equiv \lim\limits_{n\to\infty} \prod\limits_{k=1}^{n} \lambda_k$ is called *convergent*, if its sequence of partial products (P_n), where $P_n \equiv \prod\limits_{k=1}^{n} \lambda_k$, converges to a nonzero limit. Otherwise, it is called *divergent*, including the case where the product converges to zero. An infinite product $\prod\limits_{n=1}^{\infty}(1+a_n)$ is called *absolutely convergent* if the product $\prod\limits_{n=1}^{\infty}(1+|a_n|)$ is convergent. It is well known that this product is convergent if and only if $\sum\limits_{n=1}^{\infty}|a_n| < +\infty$. Throughout this article, the Lebesgue measure of a set A will be denoted by $\lambda(A)$, and the Hausdorff-Besicovitch dimension will be denoted by $\alpha_0(A)$.

Remark 1. To ensure the correctness of the definition of f given by (2), we adopt a convention to use only one of the two possible representations for A-binary numbers with period (10).

The following equalities hold:

1) $f(\Delta^A_{(0)}) = 1, f(\Delta^A_{(1)}) = P,$
$f(x = \Delta^A_{c_1\ldots c_m 1(10)}) = \lambda_1^{c_1}\lambda_2^{c_2}\ldots\lambda_m^{c_m}\lambda_{m+1}\lambda_{m+2}\ldots\lambda_{m+2k}\ldots, k \in \mathbb{N};$
2) $\dfrac{f(\Delta^A_{a_1a_2\ldots a_k\ldots})}{f(\Delta^A_{b_1b_2\ldots b_k\ldots})} = \prod\limits_{k=1}^{\infty}\lambda_k^{a_k-b_k},$

in particular, $f(\Delta^A_{\alpha_1\ldots\alpha_m c\alpha_{m+2}\ldots}) = \lambda_{m+1}^{2c-1} f(\Delta^A_{\alpha_1\ldots\alpha_m[1-c]\alpha_{m+2}\ldots})$.

Since $\lambda_k > 0$, it follows that $\lambda_k = e^{v_k}$ for some real number v_k. Therefore equality (2) can be rewritten as

$$f(x = \Delta^A_{\alpha_1\alpha_2\ldots\alpha_k\ldots}) = \prod_{k=1}^{\infty} e^{v_k\alpha_k} = e^{\sum\limits_{k=1}^{\infty} v_k\alpha_k}. \tag{3}$$

Moreover, the absolute convergence of the infinite product $\lambda_1\cdot\lambda_2\cdot\ldots\cdot\lambda_k\cdot\ldots$ implies the absolute convergence of the series $v_1 + v_2 + \ldots + v_k + \ldots$.

Since the definition of f is based on a chain of dependencies

$$[\frac{1}{2}; 1] \ni x \leftrightarrow (\alpha_n) \in L \to \varphi(x) = \sum_{i=1}^{\infty} v_i\alpha_i(x) \to f(x) = e^{\varphi}(x),$$

the following statement is evident.

Lemma 1. *The function f has a structure $f(x) = e^{\varphi(x)}$, where*

$$\varphi(x = \Delta^A_{\alpha_1\alpha_2\ldots\alpha_n\ldots}) = v_1\alpha_1(x) + v_2\alpha_2(x) + \ldots + v_n\alpha_n(x) + \ldots .$$

Corollary 1. *The set of values of the function φ, up to the a countable set, is an image of the set of subsums of a series $v_1 + v_2 + \ldots + v_n + \ldots$, consequently, it is rather a closed union of intervals, Cantor-like set or Cantorval, depending on the sequence (v_n).*

We will recall that the set of subsums of the series $v_1 + v_2 + \ldots + v_n + \ldots$ is defined as

$$E(v_n) = \{x : x = \sum_{n=1}^{\infty} \varepsilon_n v_n, \varepsilon_n \in \{0, 1\}\} = \{x : \ x = \sum_{n\in M\subset N} v_n, M \in 2^N\}.$$

It is known [4, 5] that there are only three possible topological types of the sets of subsums of an absolutely convergent series, as specified in the corollary.

According to our earlier convention, we prohibit the use of representations of A-binary numbers with period (01). As a result, from the set of subsums of the series, we generally exclude points (numbers) that are images of such A-binary points. Specifically, we remove numbers of the form $u = v_1\alpha_1 + v_2\alpha_2 + \ldots + v_m\alpha_m + s_m$, where $s_m = v_{m+3} + v_{m+5} + \ldots$, if $u \neq f(\Delta^A_{\alpha_1\ldots\alpha_m 1(10)})$ and u is not an image of an A-unary point.

Example 1. If $v_n = \frac{a}{s^n}$, $a \in \mathbb{N}$, $a < s$, then the set of values of f is a nowhere dense set with zero Lebesgue measure, and its Hausdorff–Besicovitch dimension is equal to $\log_s 2$.

In fact, the set of subsums of the geometric series $\sum\limits_{n=1}^{\infty} \frac{a}{s^n}$ is a Cantor-type set, the Hausdorff–Besicovitch dimension of which is equal to $\log_s 2$. Since the function $y = e^x$ preserves the dimension of Borel sets, the value sets of f and φ have the same dimension.

Example 2. If $v_k = \frac{(-1)^{k+1}}{2^k}$, then the set of values of the function φ is the segment $[-\frac{1}{3}; \frac{2}{3}]$. Thus, the set of values of the function f is $[e^{-\frac{1}{3}}; e^{\frac{2}{3}}]$.

In fact, the set of subsums of the series $v_1 + v_2 + \ldots$ is the segment $[-\frac{1}{3}; \frac{2}{3}]$. The prohibition against using the representation of A-binary numbers with a period (01) does not result in the loss of any points since

$$\varphi(\Delta^A_{0(01)}) = \sum_{i=1}^{\infty} \frac{1}{2^{1+2i}} = \frac{1}{6} = \frac{1}{2} - \sum_{i=1}^{\infty} \frac{1}{2^{2i}} = \varphi(\Delta^A_{1(10)}).$$

Theorem 1. *If $\lambda_k = e^{v_k}$, $v_k > r_k \equiv v_{k+1} + v_{k+2} + \ldots > 0$ for all $k \in \mathbb{N}$, then the set of values E_f of the function f, defined by equality (3), is a*

nowhere dense set with zero Lebesgue measure if and only if $\lim\limits_{k\to\infty} 2^k r_k = 0$. *Moreover, its Hausdorff–Besicovitch dimension can be calculated by the formula* $\alpha_0(E_f) = -\lim\limits_{n\to\infty} \frac{n}{\log_2 r_n}$.

Proof. Taking into account Kakeya's theorem [3], inequality $v_k \geq r_k \equiv v_{k+1} + v_{k+2} + ... > 0$ for all $k \in \mathbb{N}$ implies that the set $E(v_n)$ of subsums of the series is a perfect nowhere dense set (or Cantor-like set). As is known from [8], the Lebesgue measure of this set is calculated by the formula $\lambda(E(v_n)) = \lim\limits_{k\to\infty} 2^k r_k$.

Under the conditions of the theorem, the set of values E_φ does not coincide with the set $E(v_n)$, but rather corresponds to the difference between the latter set and the countable set of unilateral boundary points of $E(v_n)$ (not all of them). That is,

$$E_\varphi = E(v_n) \setminus \{x : x = \alpha_1 v_1 + ... + \alpha_m v_m + \sum_{i=1}^{\infty} v_{m+1+2i}\}.$$

Then the Lebesgue measures of sets E_φ and $E(v_n)$ are equal. As is known [8], for the Lebesgue measure, the following equality holds: $\lambda(E_{(v_n)}) = \lim\limits_{k\to\infty} 2^k r_k$.

Since exponential functions are absolutely continuous, that is, the image of a Lebesgue measure zero set under the action of the function is a Lebesgue measure zero set, then $\lambda(E_f) = 0$ if and only if $\lambda(E_\varphi) = 0$.

The function $y = e^x$ preserves the Hausdorff–Besicovitch dimension of Borel sets [1], therefore the dimensions of the sets E_f and E_φ are equal. The aforementioned calculation techniques can be found in [8]. □

Example 3. If $0 < p < 1$ and $v_{n+2} = pv_{n+1} - \frac{p^2}{4} v_n$ with $v_1 > 0$, $v_2 > 0$, then the conditions of the previous theorem are fulfilled and $\lambda(E_\varphi) = 0$, $\alpha_0(E_\varphi) = \frac{1}{1-\log_2 p}$ (see [6]).

2. Continuity and jump discontinuity of function

Lemma 2. *Let* $r_0 = v_1 + v_2 + \cdots + v_n + \ldots$ *be an absolutely convergent series, where* $v_n \in \mathbb{R}$. *The condition*

$$v_n + \sum_{k=1}^{\infty} v_{n+2k-1} = \sum_{k=1}^{\infty} v_{n+2k}, n \in \mathbb{N}, \tag{4}$$

is necessary and sufficient for

$$v_n = \frac{v_1(-1)^{n-1}}{2^{n-1}}, \quad n \in \mathbb{N}. \tag{5}$$

Proof. Necessity. Assume that (4) holds. We aim to establish that this condition implies (5) for all $n \in \mathbb{N}$.

For $n = 1$ equality (4) can be rewritten as $v_1+v_2-v_3+v_4-v_5+\cdots = 0$. By adding $2(v_3+v_5+\dots)$ to both sides, we obtain $r_0 = 2(v_3+v_5+\dots)$. It follows that

$$v_1 + v_2 + v_4 + \cdots = \frac{r_0}{2} = v_3 + v_5 + v_7 + \dots.$$

For $n = 2$, we have

$$v_2 + v_3 + v_5 + v_7 + \dots = v_4 + v_6 + v_8 + \dots,$$

$$v_2 + v_3 - v_4 + v_5 - v_6 + v_7 - v_8 + \dots = 0.$$

By adding $2(v_4 + v_6 + v_8 + \dots)$ to both sides, we get

$$v_2 + v_3 + v_5 + \cdots = \frac{r_1}{2} = v_4 + v_6 + v_8 + \dots.$$

From this, we deduce

$$\frac{r_0}{2} = v_1 + v_2 + \frac{r_1}{2},$$

$$\frac{r_0}{2} = v_1 + v_2 + \frac{r_0 - v_1}{2},$$

$$v_1 + v_2 - \frac{v_1}{2} = 0,$$

$$v_2 = -\frac{v_1}{2}.$$

Considering the general case, we add the right-hand side of equation (4) to both sides. This gives the following equation:

$$\sum_{k=1}^{\infty} v_{m+2k} = \frac{r_{m-1}}{2} = v_m + \sum_{k=1}^{\infty} v_{m+2k-1}.$$

For $n = m + 1$, we obtain

$$\frac{r_m}{2} = v_{m+1} + \sum_{k=1}^{\infty} v_{m+2k},$$

$$\frac{r_{m-1}}{2} = v_m + v_{m+1} + \frac{r_m}{2},$$

$$\frac{r_{m-1}}{2} = v_m + v_{m+1} + \frac{r_{m-1} - v_m}{2},$$

$$v_{m+1} = -\frac{v_m}{2}.$$

By induction, we conclude that (5) holds for all n.

Sufficiency. Directly substituting the expression $v_n = \dfrac{v_1(-1)^{n-1}}{2^{n-1}}$ into equation (4), we get

$$v_n + \sum_{k=1}^{\infty} v_{n+2k-1} = \frac{v_1(-1)^{n-1}}{2^{n-1}} + \sum_{k=1}^{\infty} v_{n+2k-1} = \sum_{k=1}^{\infty} v_{n+2k}. \qquad \square$$

Theorem 2. *The function $f(x)$ is continuous at each A-unary point and at an A-binary point $x^* = \Delta^A_{c_1\ldots c_m 0(01)} = \Delta^A_{c_1\ldots c_m 1(10)}$, if and only if*

$$v_m + \sum_{k=1}^{\infty} v_{m+2k+1} = \sum_{k=1}^{\infty} v_{m+2k}.$$

Proof. Let $x_0 = \Delta^A_{\alpha_1\alpha_2\ldots\alpha_n\ldots}$ be an arbitrary A-unary number. Consider $x = \Delta^A_{a_1\ldots a_n\ldots}$ such that $x \neq x_0$. Then there exists a suffix m such that $a_m \neq \alpha_m$, while $a_i = \alpha_i$ for all $i < m$. Moreover, $x \to x_0$ is equivalent to $m \to \infty$. Thus,

$$\frac{f(x)}{f(x_0)} = \prod_{i=1}^{m-1} \lambda_i^{a_i-\alpha_i} \cdot \lambda_m^{a_m-\alpha_m} \cdot \prod_{i=m+1}^{\infty} \lambda_i^{a_i-\alpha_i},$$

where $\prod\limits_{i=1}^{m-1} \lambda_i^{a_i-\alpha_i} = 1$, $\lim\limits_{m\to\infty} \lambda_m = 1 = \lim\limits_{m\to\infty} \prod\limits_{i=1}^{m-1} \lambda_i^{a_i-\alpha_i}$. Consequently, $\lim\limits_{x\to x_0} f(x) = f(x_0)$, i.e., the function f is continuous at the point x_0.

It is easy to prove that f is continuous at x^* if and only if the values of its two formally distinct representations, given by (3), are equal.

$$f(\Delta^A_{c_1\ldots c_{m-1}1(10)}) = e^{c_1v_1+\cdots+c_{m-1}v_{m-1}+v_m+v_{m+1}+v_{m+3}+\cdots+v_{m+2k+1}+\cdots},$$

$$f(\Delta^A_{c_1\ldots c_{m-1}0(01)}) = e^{c_1v_1+\cdots+c_{m-1}v_{m-1}+v_{m+2}+v_{m+4}+\cdots+v_{m+2k}+\cdots}.$$

Obviously, these values will be equal when

$$v_m + v_{m+1} + v_{m+3} + \cdots + v_{m+2k+1} + \cdots = v_{m+2} + v_{m+4} + \cdots + v_{m+2k} + \ldots,$$

in other words, when the equality in (4) holds. $\square$

Corollary 2. *The function f, defined by (2), is continuous on the segment $[\frac{1}{2}; 1]$ if and only if $\lambda_k = e^{\frac{c(-1)^{k-1}}{2^{k-1}}}$ for some $c \in \mathbb{R}$ and for all $k \in \mathbb{N}$.*

Lemma 3. *Let $x_0 = \Delta^A_{c_1c_2\ldots c_m1(10)} = \Delta^A_{c_1\ldots c_m0(01)}$ and*

$$\delta(x_0) \equiv \lim_{x\to x_0-0}[f(x_0) - f(x)] = \lambda_1^{c_1}\ldots\lambda_m^{c_m}(\lambda_{m+1} - \prod_{i=2}^{\infty} \lambda_{m+i}). \qquad (6)$$

If $\lambda_{m+1} \neq \lambda_{m+2} \cdot \lambda_{m+3} \cdot ...$, or equivalently, $v_{m+1} \neq v_{m+2} + v_{m+3} + ...$, then the jump discontinuity $\delta(x_0)$ of the function f at the point x_0 is given by the formula (6).

Proof. Let $x < x_0$. If x is enough close to x_0, then $x = \Delta^A_{c_1...c_m 0\underbrace{1...1}_{k}\alpha_{m+k+2}...}$, and some terms of the sequence (α_{m+2+k}) are 0. The condition $x \to x_0$ are equivalent to $k \to \infty$. As a result, we get

$$\lim_{x \to x_0} [f(x_0) - f(x)] = \lambda_1^{c_1} ... \lambda_m^{c_m} (\lambda_{m+1} - \frac{P}{\lambda_1 ... \lambda_m \lambda_{m+1}}),$$

which implies that equality (6) holds. Therefore, in the case of discontinuity of the function at the point x_0, the magnitude of its jump discontinuity can be determined by using the formula derived above. □

3. Variational properties

Lemma 4. *If there exists $m \in \mathbb{N}$ such that $\lambda_n = 1$ for all $n \geq m$, then f is a piecewise constant function, i.e., it is constant on each A-cylinder of rank m.*

Proof. Let $x \in \Delta^A_{c_1...c_m} \setminus \{\Delta^A_{c_1...c_m 1(10)}\}$. Then

$$f(x = \Delta^A_{c_1...c_m \alpha_{m+1} \alpha_{m+2}...}) = \prod_{i=1}^{m} \lambda_i^{c_i} \cdot \prod_{i=1}^{\infty} \lambda_{m+i}^{\alpha_{m+i}} = P_m \cdot 1. \qquad \square$$

Lemma 5. *The following relations hold:*

$$A_m \equiv \inf_{x \in \Delta^A_{c_1...c_m}} f(x) = \prod_{i=1}^{m} \lambda_i^{c_i} \cdot \prod_{k=m+1}^{\infty} \lambda_k^{\beta_k}, \text{ where } \beta_k = \begin{cases} 0, & \text{if } \lambda_k \geq 1, \\ 1, & \text{if } \lambda_k < 1; \end{cases}$$

$$B_m \equiv \sup_{x \in \Delta^A_{c_1...c_m}} f(x) = \prod_{i=1}^{m} \lambda_i^{c_i} \cdot \prod_{k=m+1}^{\infty} \lambda_k^{\gamma_k}, \text{ where } \gamma_k = \begin{cases} 0, & \text{if } \lambda_k < 1, \\ 1, & \text{if } \lambda_k \geq 1; \end{cases}$$

$$\lim_{m \to \infty} \frac{A_m}{B_m} = 1, \text{ that is } \lim_{m \to \infty} (A_m - B_m) = 0.$$

Proof. The first two equalities are obvious. Now, consider the fraction $\frac{A_m}{B_m} = \prod_{k=m+1}^{\infty} \lambda_k^{\beta_k - \gamma_k}$. Since $\beta_k - \gamma_k \in \{-1, 0, 1\}$ and $\lambda_k \to 1$ as $k \to \infty$, the infinite product is absolutely convergent, which proves that $\frac{A_m}{B_m} \to 1$ as $m \to \infty$. □

Lemma 6. *If $v_n > 0$ for all $n \in \mathbb{N}$, then f is nowhere monotonic.*

Proof. To prove the lemma, it suffices to show that the function f is not monotonic on any of the A-cylinders.

Let $\Delta^A_{c_1\ldots c_n}$ be an arbitrary A-cylinder, and let $\Delta^A_{c_1\ldots c_n\ldots c_m}$ be a cylinder of even rank that is contained within it. Consider the three points $x_1 = \Delta^A_{c_1\ldots c_m(0)}$, $x_2 = \Delta^A_{c_1..c_m1(0)}$, and $x_3 = \Delta^A_{c_1..c_m11(0)}$. It is clear that $x_2 < x_3 < x_1$. The values of the function at appropriate points can be expressed as:

$$\begin{aligned} f(x_1) &= \lambda_1^{c_1}\ldots\lambda_m^{c_m},\\ f(x_2) &= \lambda_1^{c_1}\ldots\lambda_m^{c_m}\lambda_{m+1},\\ f(x_3) &= \lambda_1^{c_1}\ldots\lambda_m^{c_m}\lambda_{m+1}\lambda_{m+2}. \end{aligned}$$

We observe that $\lambda_m = e^{v_m} > 1$, since $v_m > 0$. Thus,

$$f(x_3) - f(x_2) > 0, \quad f(x_3) - f(x_1) > 0.$$

Since for any interval within $[\frac{1}{2}; 1]$, we can find an embedded A-cylinder that belongs to it, it follows from the arbitrariness of the chosen cylinder that the function f is nowhere monotonic. □

Theorem 3. *If the double inequality $0 < v_n < r_n$ holds for infinitely many values of n, then the function f is nowhere monotonic.*

Proof. If $v_n < r_n$, then there exists a natural number $s = s(n)$ such that $v_n < v_{n+1} + v_{n+2} + \ldots + v_{n+s}$.

To prove the theorem, we will show that f is not monotonic on any A-cylinders. Let $\Delta^A_{c_1\ldots c_m}$ be an arbitrary A-cylinder. Consider the points $x_1 = \Delta^A_{c_1\ldots c_m\underbrace{1\ldots1}_{k}(0)}$, $x_2 = \Delta^A_{c_1..c_m\underbrace{1\ldots1}_{k-1}0\underbrace{1\ldots1}_{l}(0)}$, $x_3 = \Delta^A_{c_1..c_m\underbrace{1\ldots1}_{k-1}0\underbrace{1\ldots1}_{p}(0)}$, where $m + k$ is an even number, $l < p$, $v_{m+k} < r_{m+k}$, and $v_{m+k} < v_{m+k+1} + v_{m+k+2} + \ldots + v_{m+k+p}$.

Obviously $x_2 < x_3 < x_1$, and we have the following inequalities:

$$f(x_3) - f(x_1) = e^{(v_{m+k+1}+v_{m+k+2}+\ldots+v_{m+k+p})} - e^{v_{m+k}} > 0,$$

$$f(x_3) - f(x_2) = e^{(v_{m+l+1}+v_{m+l+2}+\ldots+v_{m+k+p})} - e^{v_{m+k}} > 0.$$

Therefore, the function f is not monotonic on the cylinder $\Delta^A_{c_1\ldots c_m}$. Due to the arbitrary choice of the cylinder, it follows that the function f is nowhere monotonic over its entire domain. □

The functions considered in this paper possess a local complex structure, similar to the functions studied in the works [9, 7], but with a fundamentally different definition.

References

1. *Albeverio S., Pratsiovytyi M., Torbin G.* Fractal probability distributions and transformations preserving the Hausdorff-Besicovitch dimension // Ergod. Th. & Dynam. Sys. – 2004. – Vol. 24, no. 1, – P. 1–16.
2. *Dmytrenko S. O., Kyurchev D. V., Pratsiovytyi M. V.* A_2-continued fraction representation of real numbers and its geometry // Ukrainian Mathematical Journal. – 2009. – Vol. 4, – P. 541–555. https://doi.org/10.1007/s11253-009-0236-7
3. *Kakeya S.* On the partial sums of an infinite series // Tohoku Science Reports. – 1914. – Vol. 3, no. 4, – P. 159–164.
4. *Markitan V. P., Pratsiovytyi M. V., Savchenko I. O.* Superfractality of the set of incomplete sums of one positive series // Ukrainian Mathematical Journal. – 2018. – Vol. 70, no. 10, – P. 1403–1416.
5. *Nymann J. E., Saenz R. A.* On the paper of Guthrie and Nymann on subsums of infinite series // Colloquium Mathematica. – 2000. – Vol. 83, no. 1. – P. 1–4.
6. *Pratsiovytyi M. V., Karvatskiy D. M.* Jacobstal-Lucas series and their applications // Algebra and Discrete Mathematics. – 2017. – Vol. 24, no. 1, – P. 169–180.
7. *Pratsiovytyi M. V., Ratushnyak S. P.* Distribution of values of one fractal function with a random argument // Naukovyi Chasopys NPU. Series 1: Physical and Mathematical Sciences. – 2014. – Vol. 16, no. 2. – P. 150–160. (in Ukrainian)
8. *Pratsiovytyi M. V.* Fractal approach in the study of singular distributions. Kyiv: Publishing House of NPU, 1998. – 296 p. (in Ukrainian)
9. *Pratsiovytyi M. V., Vasylenko N.* Fractal properties of functions defined in terms of Q-representation // International Journal of Math. Analysis. – 2013. – Vol. 7, no. 61–67, – P. 3155–3169.
10. *Sendov B. K.* Binary self-similar fractal function // Fundamental and Applied Mathematics. – 1999. – Vol. 2, – P. 589–595.

(M.Pratsiovytyi) Institute of Mathematics of NASU, Faculty of Mathematics, Informatics and Physics, National Pedagogical Dragomanov University, Kyiv, Ukraine
Email: prats4444(at)gmail(dot)com

(S.Ratushniak) Institute of Mathematics of NASU, National Pedagogical Dragomanov University, Kyiv, Ukraine
Email: ratush404(at)gmail(dot)com

(O.Trebenko) Faculty of Mathematics, Informatics and Physics, National Pedagogical Dragomanov University, Kyiv, Ukraine
Email: trebenko(at)npu(dot)edu(dot)ua

(S. Dmytrenko) NAES of Ukraine, Kyiv, Ukraine
Email: serhii(at)inlay(dot)com(dot)ua

Author Index

Airey, Dylan, 1
Antón Castro, Francesc, 5

Brukh, Roman, xi
Butenko, Sergiy, 58

Dmytrenko, Serhii, 208

Essouabri, Driss, 21

Glazunov, Nikolaj, 164
Guarnizo Cabezas, Oscar Vicente, 5

Icke, Vincent, 41

Kahruman Anderoglu, Sera, 58
Kamarianakis, Manos, 89
Karvatskyi, Dmytro, 185
Kim, Deok-Soo, 69
Kirian, Inna, 122
Kotsur, Dmytro, 108
Kryvoshyia, Rostyslav, 191
Kyrylaschuk, Tetiana, 186

Lakhnik, Andrii, 122

Makarchuk, Oleg, 191
Mance, Bill, 1

Panasenko, Oleksii, 186
Pratsiovytyi, Mykola, vii, 191, 199, 208

Ramos Cisneros, Anthony Sebastian , 5
Ratushniak, Sofiia, 199, 208
Rud, Alexander, 122

Spivakovskyi, Oleksandr, ix

Tanemura, Masaharu, 126
Tereshchenko, Vasyl, 87, 108
Trebenko, Oxana, 208

Ustimenko, Vasyl, 138

Weiß, Bastian, 71

Zhapa Camacho, Fernando Patricio, 5

Наукове видання

ВПЛИВ ВОРОНОГО НА СУЧАСНУ НАУКУ

Праці
Шостої міжнародної конференції
з аналітичної теорії чисел
і просторових мозаїк

У двох томах
том 2

Редактори Микола Працьовитий,
Дмитро Карвацький
Упорядник Галина Сита
Комп'ютерна верстка Світлана Васькевич

ВИДАВНИЦТВО
УКРАЇНСЬКОГО ДЕРЖАВНОГО УНІВЕРСИТЕТУ
імені Михайла Драгоманова

Підписано до друку 30.07.2025 р. Формат 70x108/16.
Папір офсетний. Гарнітура Computer Modern.
Умов.друк.арк. 20,48. Облік.видав.арк. 16,41
Наклад 100 прим. Зам. № 060
Віддруковано з оригіналів.

Видавництво Українського державного університету
імені Михайла Драгоманова.
01601, м. Київ-30, вул. Пирогова, 9
Свідоцтво про реєстрацію ДК 7896 від 25.07.2023.
(044) 239-30-26.